Tools and Strategies for Power Flow Management in Smart Railways

Vítor A. Morais

Supervisor: Prof. António P. Martins (FEUP)
Co-Supervisor: Prof. João L. Afonso (UMinho)

Doctoral Program in Electrical and Computer Engineering,
Faculty of Engineering, University of Porto
July 2021

Tools and Strategies for Power Flow Management in Smart Railways

Vítor A. Morais

This Thesis is submitted in partial fulfilment of the requirements of University of Porto - Faculty of Engineering for the award of Doctor of Philosophy

Doctoral Program in Electrical and Computer Engineering

Resumo

A integração de sistemas inteligentes no transporte ferroviário do futuro é uma estratégia que irá promover o aumento da mobilidade das pessoas e mercadorias, com redução dos custos desta mobilidade, trazendo vantagens ambientais para a sociedade e com potenciais benefícios para a economia e para o aumento da competitividade.

Este trabalho surge após a identificação de oportunidades de investigação, relativamente a ferramentas que permitam avaliar estratégias de otimização, e a desafios como o aumento da capacidade da infraestrutura ferroviária e o aumento da eficiência energética. O trabalho apresentado nesta tese foca-se no estudo e desenvolvimento pormenorizado de ferramentas e estratégias destinadas à gestão de fluxos de potência ativa e reativa nos sistemas ferroviários eletrificados. Deste modo, são enumeradas as seguintes linhas de investigação: (i) como estimar, com elevado grau de confiança, a informação de comboios no que concerne ao seu movimento mecânico e consumo de energia elétrica; (ii) como produzir conhecimento do estado da eletrificação do sistema ferroviário, com elevada flexibilidade, tendo em vista a avaliação do sucesso de estratégias de otimização; (iii) quais as melhorias alcançadas na capacidade da infraestrutura e na eficiência energética do sistema ferroviário, com a adoção de uma estratégia de gestão de fluxos de potência hierarquizada em duas camadas.

Em resposta às linhas de investigação consideradas, esta tese propõe três ferramentas computacionais destinadas à análise e avaliação de aspetos fundamentais em sistemas ferroviários eletrificados. Em primeiro lugar, é proposta uma ferramenta para análise, simplificação e melhoria de um modelo elétrico do sistema de alimentação ferroviário, capaz de simular com elevado grau de confiança e baixos erros (comparando com um modelo tradicional) os fluxos de potência na catenária, com recurso a um modelo de linha melhorado do tipo π. De seguida, é proposto um pacote de *software* para simulação multi-veículo capaz de estimar automaticamente, e com elevado grau de confiança, a informação de qualquer viagem de comboio no que diz respeito ao seu movimento mecânico e consumo de energia. Nesta segunda ferramenta recorre-se à comparação e validação do modelo utilizado neste simulador, fazendo uso de dados reais de operação. Fica demonstrada a capacidade do simulador multi-veículo com a simulação de 70 viagens de comboio, numa linha dupla de 50 km. A terceira ferramenta apresentada tem a designação PSSA-rail – *Power System State Analyser tool for Railways* – um pacote de *software* destinado à extração de conhecimento fazendo uso da informação sobre o estado dos comboios, tendo um elevado grau de flexibilidade e sendo capaz de avaliar o sucesso de estratégias de otimização. Esta ferramenta permite a simulação de linhas simples ou duplas, considerando a globalidade dos comboios previstos para uma dada janela temporal e produz conhecimento relativo ao estado global do sistema, bem como a pontos de interesse especificados.

Em paralelo, são propostas duas estratégias relevantes e que se encontram alinhadas com os objetivos do programa europeu *Shift2Rail*: uma para melhoria da capacidade da infraestrutura, e uma segunda para o aumento da eficiência energética destes mesmos sistemas. A primeira estratégia consiste na adoção de medidas de gestão da potência reativa hierarquizada em duas camadas. Com esta estratégia e para o caso de estudo considerado, é atingido um aumento substancial da capacidade da infraestrutura (obtendo melhorias de até 50 %), apenas com um ligeiro aumento da potência nos comboios (menos de 10 %). A segunda estratégia recorre a uma gestão hierárquica de equipamentos de armazenamento de energia com vista à melhoria da eficiência energética do sistema ferroviário. Para a sua implementação recorre-se, na camada inferior a um controlador baseado em lógica difusa e, na camada superior, é utilizado um processo de otimização suportado por algoritmos genéticos. Com esta segunda estratégia fica demonstrado, para um caso de estudo representativo, que a energia regenerada pelos comboios, e devolvida à subestação, poderá ser substancialmente reduzida pelo controlador difuso (até 22.3 %) e adicionalmente reduzida pela camada de otimização (até 6.4 %).

As ferramentas e estratégias propostas nesta tese poderão fazer parte de uma estrutura conceptual interligada de sistemas ferroviários do futuro. Os avanços tecnológicos no campo das comunicações e na digitalização destes sistemas permitirá a natural evolução da informação para conhecimento, podendo este conhecimento suportar as desejadas melhorias para este importante setor dos transportes.

Palavras-Chave

Capacidade da infraestrutura; Eficiência energética; Eletrificação ferroviária; Ferramentas de trânsito de potência; Simulação de sistemas ferroviários; Sistemas ferroviários inteligentes.

Abstract

The adoption of intelligent systems into the next-generation railway transportation is a recognized strategy towards the increase of people and goods mobility, with costs reduction, bringing environmental gains to the society and paving the way for potential economic benefits with increased competitiveness.

This work emerges after the identification of research opportunities, regarding tools targeting the assessment of optimization strategies, and challenges such as increasing infrastructure capacity and increasing energy efficiency. This work presents a detailed study and development of tools and strategies for active and reactive power flow management on railway electrification systems. Then was paved the way to address the following research opportunities: (i) how to reliably estimate the train information regarding dynamic movement and energy consumption for any journey; (ii) how to extract relevant knowledge from train energy information with high level of flexibility, targeting successfulness evaluation of optimization strategies; (iii) what are the gains in infrastructure capacity and energy efficiency with the adoption of a two-level railway power flow management strategy.

Aiming to answer the raised research questions, this thesis proposes three software tools for the analysis and evaluation of fundamental aspects regarding railway electrification systems. Firstly is proposed a tool for the analysis, simplification and enhancement of an electrical model for the railway feeding system, being this enhanced π-type line model able to simulate with high degree of certainty and with low errors (when compared to the traditional model) the catenary power flow. Then, a multi-train simulation software package is proposed to automatically perform, with high degree of confidence, the estimation of the train information regarding the dynamic movement and the energy consumption for any journey. In this tool is compared and validated the adopted train model, being used real data from field operation. To demonstrate the features of the proposed tool, 70 train journeys on a 50 km double-track line are simulated. The third presented tool, entitled PSSA-rail – Power System State Analyser tool for Railways, is a software package targeting the extraction of knowledge from train energy information state, with high level of flexibility, and being able to evaluate the successfulness of optimization strategies. This tool can simulate a single or double-track line, considering an universe of trains scheduled for a time-window, and is able to generate the knowledge relative to the global railway system state, as well as to specific points of interest.

In addition, two relevant strategies are proposed, being aligned with the objectives of Shift2Rail European program: one strategy that targets the increase of infrastructure capacity, and another that addresses the increase of energy efficiency. The first strategy consists on the adoption of actions for the management of reactive power flow with a two-level hierarchical structure. For the considered use case, this strategy achieves a substantial

increase of infrastructure capacity (up to 50 %) with a slight increase on train power consumption (less than 10 %). In the second strategy is proposed the adoption of a similar two-level structure, for the management of energy storage systems targeting the energy efficiency of the railway system. This strategy is achieved with the adoption of a fuzzy logic controller in the lower level, and an optimization process in the higher level based on a genetic algorithm. With this second strategy is demonstrated, for a representative use case, that the train regenerated energy (and returned to the substation) can be considerably reduced by the lower-level controller (up to 22.3 %), and additionally reduced by the optimization layer (up to 6.4 %).

The tools and strategies proposed in this thesis can be part of a conceptual interconnected framework for the next-generation railway systems. The technological advancements in the field of communications and on digitalization will enable the natural evolution of information into knowledge, leading this knowledge to support the desired improvements in this important transportation sector.

Keywords

Energy efficiency; Infrastructure capacity; Power flow tools; Railway electrification; Railway simulation; Smart railways.

Acknowledgements

The first acknowledgement is to my supervisor, Prof. António Pina Martins. I have no words to express my gratitude for his support, interesting discussions, knowledge, patience and above all friendship! I am also grateful to my co-supervisor, Prof. João Luiz Afonso, whose advice, knowledge and support have helped me with this journey.

To my family for being a lighthouse throughout my journey. My parents José and Helena, and my sister and brother Sandra and João.

To my girlfriend Joana Lascasas. I have no words to describe her patience during this endeavour. To my friend Valter Costa, for all the discussions, friendly ear, and sharp advises. To my friend Vítor Pinto, a strong sailor of I117.

To my laboratory current and former colleagues Jorge Pinto, Ricardo Carvalho, Vítor Lopes, Agostinho Rocha and Pedro Rodrigues.

To members of autonomous driving team whose excuse to have lunch every day has leaded to my first attendance and winning the Portuguese Robotic Cup. They are Valter Costa, Peter Cebola and Pedro Tavares.

To Prof. Adriano Carvalho, for his knowledge and continuous support. To Prof. Rui Calçada, for the opportunity in the iRail programme.

To Helder Ribeiro from NomadTech and to Marco Santos from IP - Infraestruturas de Portugal for sharing their expertise from the industry point of view.

Finally to countless people that has been part of this journey, a simple thank you.

Vítor A. Morais

Institutional Acknowledgements

The author thankfully acknowledge the funding of FCT (Fundação Ciência e Tecnologia) under grant PD/BD/128051/2016, supported by MCTES national funds and FSE funds through POCH program.

Furthermore, it is gratefully acknowledged the support by: FCT R&D Unit SYSTEC - POCI-01-0145-FEDER-006933/SYSTEC funded by FEDER funds through COMPETE2020 and by national funds through the FCT/MEC, and co-funded by FEDER, in the scope of the PT2020 Partnership Agreement.

Finally, it is thankfully acknowledged all the support by the Electrical and Computers Engineering Department and by the Faculty of Engineering of the University of Porto.

Invention is the most important
product of man's creative brain.
The ultimate purpose is the complete
mastery of mind over the material
world, the harnessing of human
nature to human needs.

Nikola Tesla

Contents

List of Figures

List of Tables

Abbreviations and Symbols

Abbreviations

5G	Fifth Generation Communication
AC	Alternating Current
ACO	Ant Colony Optimization
AP	Access Point
APQC	Active Power Quality Compensator
CEBD	Compiled Energy Billing Data
CPU	Central Processing Unit
DAO	Day Ahead Optimization
DAS	Driving Advisory Systems
DC	Direct Current
DER	Distributed Energy Resources
DOEM	Dynamic Onboard Energy Managers
EA	Evolutionary Algorithm
EC	Earth Conductance
EMS	Energy Management System
ERA	European Union Agency for Railways
ESS	Energy Storage Systems
ETH IVT	Swiss Federal Institute of Technology's Institute for Transportation Planning and Systems
EU	European Union
EV	Electric Vehicle
FA	Firefly Algorithm
FLC	Fuzzy Logic Controller
FTP	File Transfer Protocol
FTPSS	Flexible Traction Power Supply Systems
GA	Genetic Algorithm
GPS	Global Position System
GSM	Global System for Mobile communications
GSM-R	Global System for Mobile communications for Railways
H2020	2020 Horizon European Program
HESS	Hybrid Energy Storage System
HHL	Higher Hierarchical Level
HPQC	Hybrid Power Quality Compensator

HSR	High Speed Railways
IEA	International Energy Agency
IEC	International Electrotechnical Commission
IEEE	Institute of Electrical and Electronics Engineers
IGBT	Insulated Gate Bipolar Transistors
IP	Internet Protocol
IS	Initial Station
ISST	Intelligent Traction Power Substations
ITU	International Telecommunication Union
LC	Line Capacitance
LHL	Lower Hierarchical Level
LTE	Long-Term Evolution
LTE-R	Long-Term Evolution for Railways
MAE	Mean Absolute Error
MAO	Minutes Ahead Optimization
MF	Membership Functions
MMC	Modular Multilevel Converter
MTL	Multi-conductor Transmission Line
MTS	Multi-train Simulator
ns-3	discrete-event Network Simulator for Internet systems
NZ	Neutral Zone
PF	Power Factor
Ph.D	Philosophy Doctor
π-type	Line model with π topology
PID	Power Injection Devices
PoI	Point of Interest
PR	Proportional-Resonant
PSSA-rail	Power System State Analyser tool for Railways
PV	Photovoltaic generation
PWM	Pulse-Width Modulation
RAM	Random-Access Memory
RBE	Regenerative Braking Energy
RE	Rail-Earth conductance
REM-S	Railway Energy Management System
RES	Renewable Energy Sources
RESS	Railway Energy Storage Systems
rms	Root Mean Square
RMSE	Root Mean Square Error
RPC	Railway Power Conditioners
RPE	Relative Percentage Error
RQ	Research Question
RSG	Railway Smart Grid

RTO	Real-time Operation
RTS	Railway Transportation System
SG	Smart Grid
SGAM	Smart Grid Architecture Model
Shift2Rail	Shift2Rail Joint Undertaking European Program
SiC	Silicon Carbide
SNCF	*Société Nationale des Chemins de fer Français*
SoC	State of Charge
SRF-PLL	Synchronous Reference Frame Phase-Locked Loop
SVC	Static VAR Compensator
TD	Technical Demonstrator
TOM	Train Operation Model
TPS	Traction Power Substation
TSI	Technical Specifications for Interoperability
TSO/DSO	Transmission/Distribution System Operator
UDP	User Datagram Protocol
UIC	*Union Internationale des Chemins de fer* – International Union of Railways
UK	United Kingdom
UML	Unified Modeling Language
USA	United States of America
V2I	Vehicle-to-Infrastructure
VCTS	Virtual Coupling Train Sets
VSC	Voltage Source Converter
WCET	Worst-Case Execution Time
Wi-Fi	Wireless Fidelity
XML	eXtensible Markup Language

Symbols

F_a	aerodynamic resistance to motion;
F_B	maximum braking force;
F_b	braking force;
F_c	external force caused by track curve;
F_g	external force caused by track grade;
F_T	maximum traction force;
F_t	traction force;
g	gravitational acceleration;
I_s	substation current phasor;
I_t	train current phasor;
I_p	current phasor in positive conductors;
I_g	current phasor in return conductors;
M	mass of the train;
P_l	line active power;
P_s	substation active power;
P_t	train active power;
Q_l	line reactive power;
Q_s	substation reactive power;
Q_t	train reactive power;
R'	line resistance per unit of length;
R_l	line resistance;
Rv	line radius of curvature;
S_l	line apparent power;
S_s	substation apparent power;
S_t	train apparent power;
t	time;
v	train speed;
V_s	substation voltage phasor;
V_t	train voltage phasor;
V_p	voltage drop phasor in positive conductors;

V_g voltage drop phasor in return conductors;

$|V_s|$ substation voltage magnitude;

$|V_t|$ train voltage magnitude;

x position/coordinate of the vehicle;

X' line reactance per unit of length;

X_l line reactance;

$\boldsymbol{Y}_{\boxplus}$ MTL matrix admittance;

$\boldsymbol{Y}_{\pi}$ π-type matrix admittance;

$\boldsymbol{Z}_{\boxplus}$ MTL matrix impedance;

$\boldsymbol{Z}_{\pi}$ π-type matrix impedance;

Z' line impedance per unit of length;

Z_l line impedance;

Z_{ii} element of the main diagonal of series impedance matrix;

Z_{ik} element outside the main diagonal of series impedance matrix;

α angle between the railway line and the horizontal plane;

δ angle between two voltage phasors;

η train global efficiency;

μ_0 permeability of the vacuum;

μ_f relative traction force;

μ_b relative braking force;

ξ losses factor;

ϕ angle between voltage and current phasors;

ω nominal angular frequency.

CHAPTER 1

Introduction

Railway transportation systems are widespread in modern societies, paving the way to be an important part of the life of millions of people worldwide. These systems have constantly raised interest since they are considered one of the most energy-efficient modes of transportation. In fact, the rail networks carry 8 % of the world's motorized passenger movements and 7% of freight transport [1]. The transport market share in Europe is 9 % and has increased in Europe by 8.9 % between 2005 and 2015 [2]. It is efficient, since this 9 % market share only accounts for 2 % in final energy consumption, in comparison to other sectors [2]. Also, the European Commission (EC) has launched the Shift2Rail program that targets the reduction of operation costs by half, doubling the infrastructure capacity and increase in reliability and punctuality [3]. This next-generation smart railway is achieved with strong research, in particular, by bringing the concepts associated with smart grids into the railway electrification system [4]. Recognizing the global importance of the adoption of information technology tools towards a smarter railway transportation system, the scientific community presses to find tools and strategies — that will be part of an interconnected framework — for power flow management in smart railways. The research work developed in the scope of this thesis is aligned with the objectives of the Shift2Rail program.

1.1 Motivation and Scope

As mentioned, the inclusion of interconnected information technologies into railways is a necessary step to face the requirements of future smart railways. The study of the current state of the art reveals a lack integration of power flow management tools and strategies into smart railways, with the proposed solutions not considering this interconnected framework. Based on this analysis, this thesis proposes tools and strategies to be integrated into a smart railways framework, targeting increase of energy efficiency and infrastructure capacity, through power flow management.

A smart railways framework gathers concepts from the theoretical foundations of information and computers science, specifically in depending on the *data – information – knowledge* hierarchical framework [5, 6]. In this context, a smart railways framework can be illustrated in Fig. 1.1.

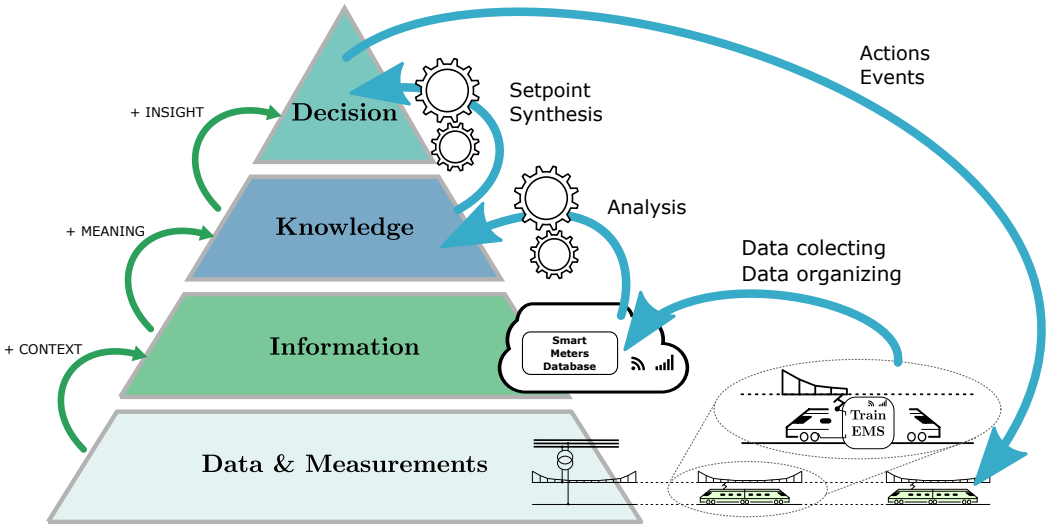

Figure 1.1: Illustration of the levels of the information in smart railways framework.

Considering the basis of this hierarchical framework composed of a universe of signals, the *data* is defined as follows:

Data *is the measurement of a universe of signals from the railway environment.* Examples of such signals are, among others, the following: i) voltage at a pantograph of one train; ii) current at a pantograph of one train; iii) absolute GPS position of one train; iv) relative train position from onboard tachometer; v) instantaneous train speed; and vi) absolute time instant.

From these measurements of signals, through computational processing, the data can be provided with **context**, which results in *information* that is defined as the following:

Information *is the result of the processing of the measurements, specifically, is a time-series database of timestamped electrical, mechanical and other physical measurements of a railway element.* For example, the standard EN 50463 [7], details onboard energy measurement systems, where the measurements are processed in an energy calculation function and a compiled energy packet is produced having among others, the following elements: i) train and energy meter identification; ii) timestamp array; iii) electrical measurements; iv) processed energy-related information; v) physical measurements such as absolute position, train speed, vi) any other journey related information. As another example, the tool presented in chapter 4 will have as output the information of train journeys.

This information can be transferred from each information producer (e.g. train onboard energy metering system) to a remote database. From a broad universe of train energy information gathered in a database, with specific computational processing, it can be provided **meaning** to the train energy information towards the generation of *knowledge*, which is defined as the following:

Knowledge *is the result of applying specific algorithms to have a global overview of the railway system state.* Such algorithms can be, for example, the **analysis** of the infrastructure power flow, as well as the **evaluation** of certain metrics and statistics. As example, in chapter 5 is presented a tool that is associated with this layer.

The produced knowledge provides **insight** to the *decision*, being defined as following:

Decision *is the layer that precedes the actions made in the railway system.* This layer is exemplified in this thesis, in chapter 6 and chapter 7, with two examples of the adaptation of railway operation, targeting increases in energy efficiency and increases in railway infrastructure capacity.

This full framework is the basis of this thesis.

1.1.1 Context

Until a few years ago, trains were not required to have an energy metering system installed onboard. In a majority of European countries, railways operators and the infrastructure managers were a single company. In 1991, the European Union (EU) promoted the liberalization of the railway sector, towards a separation of the infrastructure and the operation [8].

In order to ensure interoperability between different railways operators and infrastructure managers, the European Union Agency for Railways (ERA) proposes [9]:

- An on-ground energy data collecting system, i.e. a system to receive, store and export the Compiled Energy Billing Data (CEBD) from trains;
- An onboard energy measurement system, i.e. a system responsible for the generation of the CEBD.

In addition, this part of the Technical Specifications for Interoperability (TSI) must comply with the EN 50463 standard [7], which regulates the energy measurement on board trains.

Only in July 2020 was established the requirement for the adoption of energy meters in the EU railways [10], driving the onboard energy metering systems and the ground-level data collecting systems to be a reality nowadays.

Thus, the smart railways framework proposed in Fig. 1.1 is already framed with the objectives and directions of EU railways. The lower level of *Data & Measurements* and the *Information* level are already a reality. However, the billing purposes is the primary motivator for the current implementation of these systems.

Naturally, new tools and strategies will be proposed, implemented and evaluated, framed with the upper levels of the smart railways framework pyramid. These tools and strategies will reduce the gap between the current railways and the future smarter railways.

1.1.2 Tools and Strategies

This thesis is entitled "Tools and Strategies for Power Flow Management in Smart Railways". As presented, the next-generation for smart railways targets the increase of energy efficiency through adequate management of the railway power flow. This management depends on two nuclear and interdependent concepts: the **Tools** and the **Strategies**.

From the Cambridge online dictionary, a tool[1] can be defined as "something that helps you to do a particular activity". In the context of this thesis, the word *Tools* is defined as:

Method or simulation framework that is required for achieving objectives.

Similarly, the definition of strategy[2] can be "a long-range plan for achieving something or reaching a goal, or the skill of making such plans". Furthermore, a strategy for Power Flow Management in Smart Railways is:

Action and respective outcome of the application of tools.

The next-generation smart railways depends on tools, such as the multi-train simulator and the power system state analyser, and on strategies, like the compensation of reactive power for increase the infrastructure capacity or the intelligent management of the active power within the railway power system.

As illustrated in Fig. 1.2 the objective of the tools is to support strategies, which in turn, are conditioned and/or limited by the available or developed tools.

In this thesis, the developed tools are presented in: chapter 3 – Analysis and Parameters Estimation of Railway Electrical Line; chapter 4 – Multi-train Simulator; and chapter 5 – PSSA-rail Power System State Analyser tool.

Furthermore, the proposed strategies are clearly addressed in: chapter 6 – Reactive Power Compensation Strategy; and chapter 7 – Charging Strategy for Railway Energy Storage Systems.

[1]Definition of tool: https://dictionary.cambridge.org/dictionary/english/tool
[2]Definition of strategy: https://dictionary.cambridge.org/dictionary/english/strategy

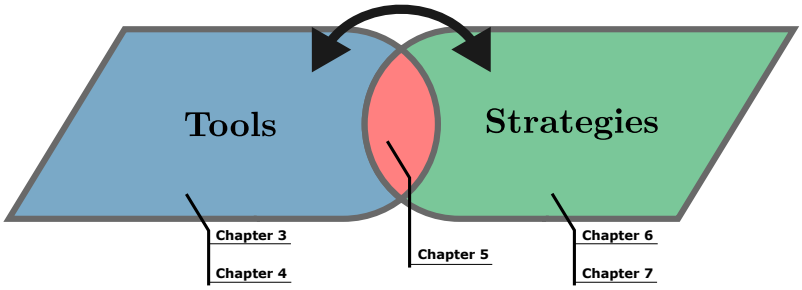

Figure 1.2: Framing of this thesis in relation to the proposed tools and strategies.

1.2 Thesis Statement and Goals

Considering the previously presented context, motivation and scope, it is defended that:

As long as there is available energy information with enough quality and quantity, the extracted knowledge can be used to enhance the railway operation.

From this statement, some main research questions arise, namely:

- **RQ1:** How to reliably estimate the train information regarding dynamic movement and energy consumption for any journey?
- **RQ2:** How to extract the relevant knowledge from train energy information with high level of flexibility, targeting successfulness evaluation of optimization strategies?
- **RQ3:** What are the gains in infrastructure capacity and energy efficiency with the adoption of a two-level railway power flow management strategy?

To answer these questions, this thesis was divided into five topics and the following objectives were established:

T1 — Railway electrification line model analysis, simplification and enhancement methodology;

> **Objective 1a:** Propose a comparison methodology to evaluate the differences between two railway line models: a complex multi-conductor transmission line model and a simplified lumped-parameters π-type line model;
>
> **Objective 1b:** Propose an enhancement methodology for the lumped-parameters π-type line model.

T2 — Multi-train tool to estimate the dynamic movement and energy consumption of any train journey;

Objective 2a: Propose a train model to estimate the dynamic movement and energy consumption, being the train model validated through measurements with a comparison methodology;

Objective 2b: Design and implementation of a multi-train simulation tool to automatically and reliably estimate train information for any journey, using the validated train model.

T3 — PSSA-rail tool to extract knowledge on power flow in railway systems;

Objective 3a: Design and implementation of PSSA-rail tool, to extract knowledge of railway electrification using train energy information;

Objective 3b: Evaluation and assessment of PSSA-rail features and limitations;

Objective 3c: Demonstrate the flexibility and capability of the PSSA-rail tool to study and evaluate strategies, with illustration for two optimization scenarios.

T4 — Strategy to increase the infrastructure capacity through mobile reactive power compensation;

Objective 4a: Propose a methodology to increase the railway infrastructure capacity with the management of the reactive power flow;

Objective 4b: Demonstrate the increase of the infrastructure capacity for deterministic scenarios;

Objective 4c: Discuss the implementation steps of this strategy, from a practical viewpoint and within the smart railways framework.

T5 — Strategy to increase energy efficiency in the charging of railway energy storage systems.

Objective 5a: Propose a methodology to increase the energy efficiency of railway energy storage systems;

Objective 5b: Demonstrate the increase of energy efficiency for a train journey case study estimated in chapter 4;

Objective 5c: Discuss the implementation steps of this strategy, from a practical viewpoint and within the smart railways framework.

This thesis follows a "Traditional-Complex" structure [11], which allows the isolated but interlinked study of the five different topics (**T1** to **T5**). Each chapter (3 to 7) contains a small introduction and a graphical abstract describing its contents, followed by the content itself.

1.3 Scientific Contributions

During the course of this thesis, the following scientific contributions were accomplished:

- Proposal of a comparison methodology to evaluate the differences between two railway line models, to support the usage of a simplified line model for power flow calculations. This will further lead to the proposal of an enhancement methodology of the lumped-parameters π-type line model.
  This contribution is fully addressed in chapter 3.

- Proposal of a multi-train simulation tool to automatically and reliably estimate train information regarding dynamic movement and energy consumption for any journey. The proposed tool uses a train model which was validated through real measurements with a comparison methodology.
  This contribution is demonstrated in chapter 4 and it was published in [12] and [13].

- Proposal of the PSSA-rail tool to extract knowledge of railway electrification using train energy information. The PSSA-rail tool features the simulation of any railway line, considering all trains moving in both directions, with the simulation valid for a broad time-window, where the electrical equivalent of the line is valid for the considered time-window, and is capable to simulate specific points of interest. The flexibility of the tool shows the capability to assess optimization strategies. The implemented PSSA-rail tool was assessed and evaluated regarding the advantages and limitations.
  This contribution is developed and discussed in chapter 5.

- Proposal of a methodology to increase the railway infrastructure capacity with the management of the reactive power flow. Demonstration of increase of the infrastructure capacity over 50 % with the injection of reactive power, only with train power consumption increase below 10 %. Discussion of the practical implementation constraints within the smart railways framework of the proposed strategy.
  This contribution is fully addressed in chapter 6 and it was published in [14].

- Proposal of a energy management strategy for railway energy storage systems capable to increase the energy efficiency. Demonstration of the advantages of a two-level

power flow management, with the highlight of the reduction of 6.4 % of the injected regenerated energy only with the automatic learning optimization algorithm. Discussion of the practical implementation constraints within the smart railways framework of the proposed strategy.
This contribution is proposed analysed and discussed in chapter 7 and it was published in [15] and [16].

From the aforementioned contributions and in the scope of this thesis, this research has resulted in the following published works:

Journal Articles:

- Vítor A. Morais, João L. Afonso, Adriano S. Carvalho, António P. Martins. New Reactive Power Compensation Strategies for Railway Infrastructure Capacity Increasing. Energies 2020, 13, 4379. DOI: 10.3390/en13174379

- Vítor A. Morais, João L. Afonso, António P. Martins. Towards Smart Railways: A Charging Strategy for Railway Energy Storage Systems. EAI Endorsed Transactions on Energy Web 2021. DOI: 10.4108/eai.14-1-2021.168136

International Conference Papers:

- Vítor A. Morais, João L. Afonso, António P. Martins. Modeling and Validation of the Dynamics and Energy Consumption for Train Simulation. 2018 International Conference on Intelligent Systems (IS), Funchal, Portugal. DOI: 10.1109/is.2018.8710569

- Vítor A. Morais, Agostinho A. Rocha, João L. Afonso, António P. Martins. Heuristic-based Speed Profile Generation for Multi-Train Simulator. 2018 International Conference on Intelligent Systems (IS), Funchal, Portugal. DOI: 10.1109/is.2018.8710483

- Vítor A. Morais, João L. Afonso, António P. Martins. Towards Smart Railways: A Charging Strategy for On-Board Energy Storage Systems. Lecture Notes of the Institute for Computer Sciences, Social Informatics and Telecommunications Engineering. DOI: 10.1007/978-3-030-45694-8_3

- Vítor A. Morais, João L. Afonso, António P. Martins. Innovative Communication System for Railways Smart Metering Towards System Efficiency Improvement. Proceedings of the 4th International Conference on Energy and Environment: bringing together Engineering and Economics.

1.4 Document Structure

This document is divided into 8 chapters, listed in Table 1.1, each of them incorporating the relevant subsections to present the subjects mentioned. Topic chapters (3, 4, 5, 6 and 7) presents a graphical abstract, in the beginning, to illustrate the contents of the chapter. Chapters 2, 3, 4, 5, 6 and 7 present also a synthesis, in the end, regarding what was discussed on its corresponding chapter.

Table 1.1: Thesis structure.

Chapter	Title
1	Introduction
2	Railway Fundamentals & Literature Review
3	Railway Electrical Line: Analysis and Parameters Estimation
4	Multi-train Simulator for Smart Railway Framework
5	PSSA-rail: Power System State Analyser Tool for Railways
6	Railway Reactive Power Compensation Strategy
7	Charging Strategy for Railway Energy Storage Systems
8	Conclusions

Chapter 1, Introduction, is divided into four sections comprising the context, motivation and scope, thesis statement and goals, scientific contributions and document structure.

Chapter 2, Railway Fundamentals & Literature Review, is divided into three parts, where the first part provides a background on the railway transportation system, with focus on electrification. Then, in the second part are covered the current state of the art on railway power flow management strategies, with an extensive literature review on the thematic. Finally, in the third part are presented specific related research on the five topics, **T1** to **T5**, with an highlight on the research opportunities.

Chapter 3, Railway Electrical Line: Analysis and Parameters Estimation, is divided in two parts and covers the study on railway electrical line. In the first part is introduced the problem of power flow analysis in railway systems, then is presented the materials and simulation framework to support the two railway line models, followed by the presentation of the comparison methodology and results. In the second part is presented the methodology to enhance the railway π-type line model, with the consideration of a compensation strategy based on pre-calculated errors, followed by the presentation of the results after the application of the enhancement methodology and then is demonstrated its application on a traditional load-flow analysis tool for multiple trains. This chapter ends with a discussion

and conclusions associated to the thematic raised in this chapter.

Chapter 4, Multi-train Simulator for Smart Railway Framework, is divided in two parts and covers the development of a multi-train simulation tool. The first part addresses the implemented train model, where the proposed model was compared with real data provided by a partner company of a main railway operator, followed by the results of the comparison and respective comparison metrics. Then, in the second part is presented a heuristic approach to estimate the dynamic movement of any journey, followed with a comparison with real data. To demonstrate the capabilities of this multi-train simulation tool, all train journeys of a railway line were simulated and the results are presented. This chapter ends with a discussion and conclusions section.

Chapter 5, PSSA-rail: Power System State Analyser Tool for Railways, is divided into two parts to present the PSSA-rail tool. The first part starts with the presentation of the requirements for the tool, followed by the model formulation (where is linked to the chapter 3), then is presented the system architecture of the tool, where is detailed the implementation steps of each of the four modules. Each module is detailed with the support of a real case-study line. The first part is finalized with the presentation of some results to illustrate the desired knowledge extraction (also, the results for a second case study line are presented in appendix E). The second part of this chapter presents the implementation and results of two optimization strategies. This chapter ends with an extensive discussion and conclusions, where is justified the rationale behind the definition of requirements for PSSA-rail tool, and is highlighted the capabilities of the proposed tool within the smart railways framework.

Chapter 6, Railway Reactive Power Compensation Strategy, is divided into two parts and covers the proposed strategy for reactive power flow management towards infrastructure capacity increase. In the first part is presented the methodology and simulation frameworks, then is addressed the algorithm and demonstration of the reactive power compensation strategy. This first part ends with the presentation of the results for the compensation in the neutral zone and for the mobile reactive power compensation in each train. Then, the second part tries to present a discussion for the system architecture to implement the mobile reactive power compensation strategy, specifically to answer the real-time limitations of the centralized compensation strategy. This chapter ends with the presentation of general discussions and conclusions (for example, one discussion is in the role of PSSA-rail in the implementation of this strategy).

Chapter 7, Charging Strategy for Railway Energy Storage Systems, is divided into two parts and covers the proposed two-level energy management strategy for railway energy storage systems. The first part starts with the presentation of the methodology and and simulation frameworks where is presented the two-level management, followed with the real-time fuzzy logic controller and the upper-level genetic algorithm optimization. Then is presented the results for one journey and a discussion on the obtained results. In the second part is discussed a practical implementation of the integration of the proposed energy management strategy within the smart railway framework, followed of a final discussion and conclusions.

Chapter 8, Conclusions, summarizes the main conclusions and findings of this thesis. Some guidelines for possible research directions are also addressed.

CHAPTER 2

Railway Fundamentals & Literature Review

This thesis is being written more than 200 years after the birth of the first steam locomotive[1], and around 125 years after the first fully electrified railway line[2].

Currently, a diversity of technologies exists in the railway sector. Mechanically, the gauge – or the distance between the rails – varies from country to country[3]. In electrified railways, the mechanical arrangement of the feeding is variable, depending on the type of electrification – AC or DC – or the type of vehicle – for metropolitan systems: overhead, third rail; for train systems: catenary wire, busbar – as examples.

The reasoning for this diversity of technologies is due to the long lifespan that railway technology is designed. Every decision in this sector is taken considering a future of several dozens of years, using the best technological evidence at the moment of the decision. From historical, geographical, political and environmental reasons, the evolution of the railway transportation systems is slow and each decision lasts for several years. From the design phase to the maintenance, each decision leads to evolution.

Despite this slow evolution, it should be highlighted in this thesis three important moments in the railway electrification:

- The 1879 Berlin Commerce Fair, where the electrified train has born, where the feeding of this first train was done in DC through a third rail system;
- The application of ohmic commutation-pole shunts to the series-wounds commutator motor in 1903, in Germany, allowing the usage of a low-frequency single-phase AC for traction (being standardized at 15 kV and 16 ⅔ Hz) [17];

[1] Pioneered by F. Trevithick in 1804, who has used Watt´s high-pressure steam engine on a rail-bound vehicle for the first time.

[2] After *Siemens & Halske* demonstrated the first electrically powered locomotive in 1879 in Berlin Commerce Fair, the first fully electrified railway main line was opened in 1895 in Baltimore, USA, in a five-kilometre city tunnel, upon a 675 V overhead system [17].

[3] The standard gauge, 1435 mm, has started to be adopted in the second half of the XIX century. However, other track gauges have been adopted, such as the Iberian track gauge (1668 mm), the Russian standard (1520 mm) and the narrow gauge (1000 mm) commonly used in metropolitan systems and also known as metro gauge.

- The usage of mercury-vapour rectifiers on 50 Hz in various German locomotives in 1936, whose technology was later studied after the end of the Second World War by French Engineering [17]. As result, this has allowed the adoption of a new standard in railway electrification, of 50 Hz @ 25 kV, mostly driven by French Railway Industry.

Nowadays, the railway systems have wide coverage in Europe, as geographically illustrated in Fig. 2.1. The historical landmarks resultant on the decisions made in the past have painted a diversity of technologies. Specifically, the three important moments listed above are one of the reasons for having diverse electrifications, as visible in Fig. 2.2. Each decision made in the railway sector lasts for dozens of years.

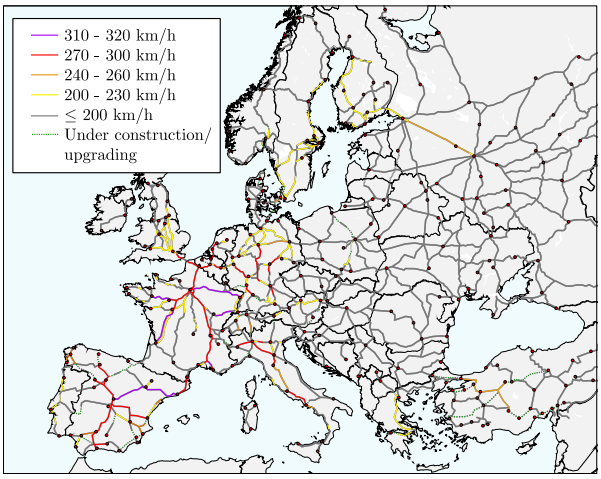

Figure 2.1: Map of Europe[4] with High Speed Rail[5].

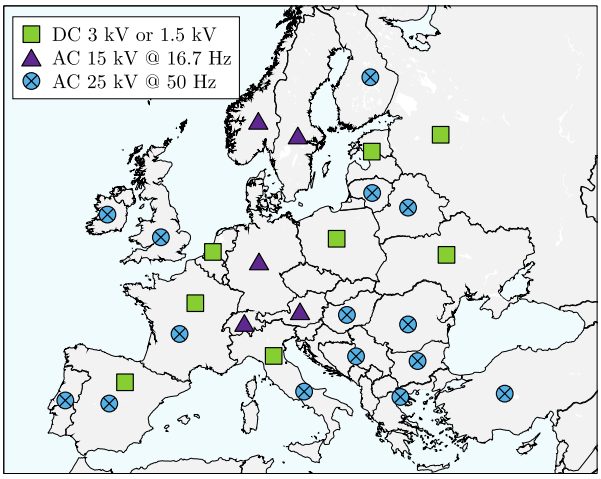

Figure 2.2: Railway main-line power supply systems in Europe[4]. Adapted from [18].

In this chapter are briefly presented concepts, system descriptions and technological solutions essential to a better understanding of the rest of this thesis. This presentation will be essentially made, in a first phase, on the railway electrification systems and on energy management on smart electrical railways. Furthermore, in the second part of this chapter is presented a literature review that leads to the research gaps that have motivated the author to write each of the six chapters of the body of this thesis.

The objectives of this chapter are:

- **Objective I**: Study the railway transportation system, with focus on electrification;
- **Objective II**: Provide a scientific literature review on railway power flow management systems;

[4]Europe map adapted from Alexrk2 and others, at Wikimedia Commons. Distributed under a CC-BY 2.0 license.

[5]2020 High Speed Railroad Map of Europe adapted from NCLY and others at Wikimedia Commons. Distributed under a CC-BY 2.0 license.

- **Objective III**: To each of the topics **T1** to **T5** of this thesis, present a specific scientific literature review.

2.1 Railway Electrification

It is unquestionable the importance of a sector like the railway transportation in modern societies. From the 2019 report produced by International Energy Agency (IEA), the rail networks carry 8 % of the world motorized passenger movements and 7 % of freight transport [1]. In Europe, not only the combined transport market share is 9 % but also this value has increased 8.9 % between 2005 and 2015 [2]. Furthermore, the railway transportation sector has a wide coverage, geographically in Europe, as illustrated in Fig. 2.1.

The electrification of the railway lines is an essential step to support the High Speed Railways (HSR) and to support this increase in demand. As presented, this electrification is based on a diversity of technology. In this section, it will be presented a brief presentation of those technological solutions.

A general rule of thumb is to define the electrification topology based on the type of railway vehicles, following the Table 2.1.

Table 2.1: Catenary topology and vehicle characteristics of different railway vehicles. Adapted from [18].

	Catenary topology		**Vehicle characteristics**	
	DC supply	**AC supply**	**Power**	**Top speed**
Tram	600 V 750 V 900 V	-	150 kW – 300 kW	50 km/h – 70 km/h
Metro	750 V 1500 V	-	350 kW–1 MW	80 km/h
Train	750 V 1500 V 3000 V	15 kV (16.7 Hz) 25 kV (50 Hz)	200 kW – 8 MW	120 km/h – 350 km/h
Locomotive	750 V 1500 V 3000 V	15 kV (16.7 Hz) 25 kV (50 Hz)	500 kW – 8 MW	100 km/h – 200 km/h

With similar functionality of the electrical grid, where a broad area of loads must be supplied with quality of service, the railway electrical power system must supply moving loads, with the functional objective of maintaining trains running in a broad area. To achieve this functional objective, the energy is supplied to trains through traction substations and through electrified conductors. The most common type of electrified conductors

is named overhead catenary system. Furthermore, throughout this thesis this system is simply called catenary.

2.1.1 Direct-Current Railway Systems

Historically being the first type of railway electrification, the DC railway electrification is usually associated with metropolitan systems. It is the commonly adopted electrification architecture in countries like Spain or Italy, where in these countries the adoption of AC 25 kV is associated to the new HSR lines.

The DC supply system depends on rectifier converters (controlled or uncontrolled) and this railway power supply topology requires several traction substations, towards the reduction of power losses in catenary due to the high value of the electric current. In Fig. 2.3 is presented the supply architecture of such lines.

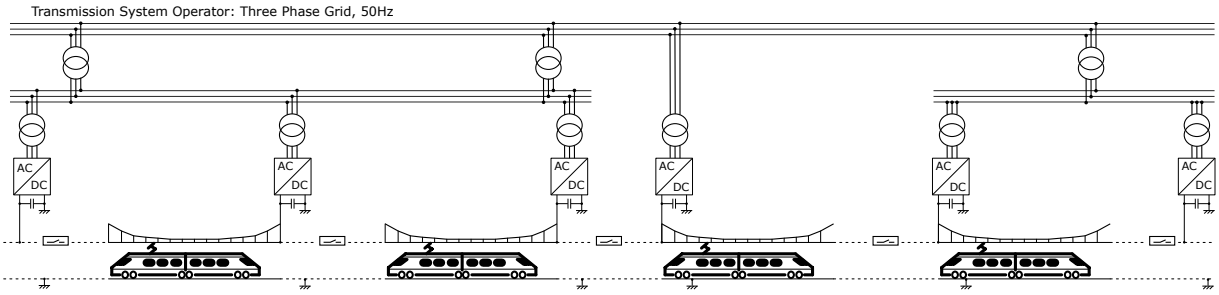

Figure 2.3: DC supply system architecture. Adapted from [18].

The DC catenary allows an almost direct connection between train power traction and inverter DC bus, as represented in Fig. 2.4.

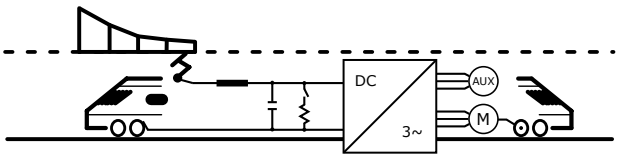

Figure 2.4: Simplified train internal power circuit of a DC supply system. Adapted from [17].

2.1.2 Single-Phase Alternating Current 15 kV 16.7 Hz Railway Systems

The first chronological AC-type train electrification system was established in the early years of XX century, introduced in central-European countries (Germany, Austria, Sweden, Switzerland and Norway [17]). This alternative setup is presented in Fig. 2.5 where a single-phase 16.7 Hz supply voltage is generated with a complete power converter.

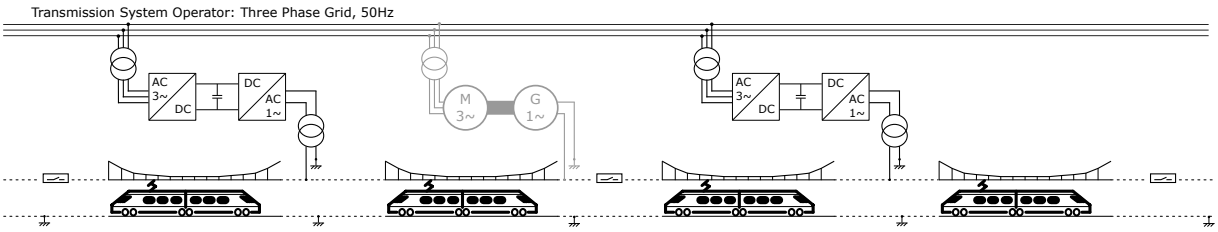

Figure 2.5: 16.7 Hz 15 kV supply system. Adapted from [18].

On the AC catenaries (16.7 Hz and 50 Hz), a single-phase transformer and a rectifier is needed to create a DC bus for traction power converters, as presented in Fig. 2.6.

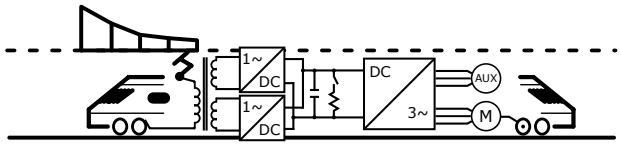

Figure 2.6: Train internal power circuit of an AC supply system. Adapted from [17].

2.1.3 Single-Phase Alternating Current 25 kV 50 Hz Railway Systems

With AC catenaries, a low frequency (50 Hz or 60 Hz) single-phase onboard transformer is required to step down the catenary voltage (25 kV or 15 kV) to the rectifier operating voltage (the rectifier is a single-phase voltage source converter, usually with bi-directional power flow).

In Fig. 2.7 are presented substation feeding arrangements of a single-phase 50 Hz catenary, as an alternative without the usage of power electronic converters, where the catenary is directly supplied with transformer arrangements (single-phase and V-V arrangements, illustrated in left and right sides of Fig. 2.7; or other alternative arrangements, like Scott, Le Blanc or modified Woodbridge [19]).

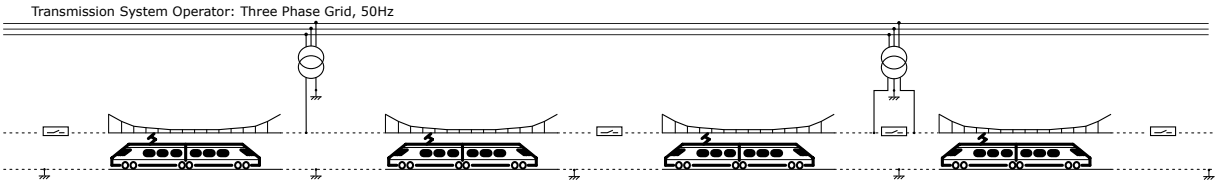

Figure 2.7: 50 Hz 1×25 kV supply system. Adapted from [18].

Furthermore, improved electrification is presented in Fig. 2.8, where the return current is made not only through the rails and parallel cables but also and mostly through the negative feeder of the auto-transformer arrangement.

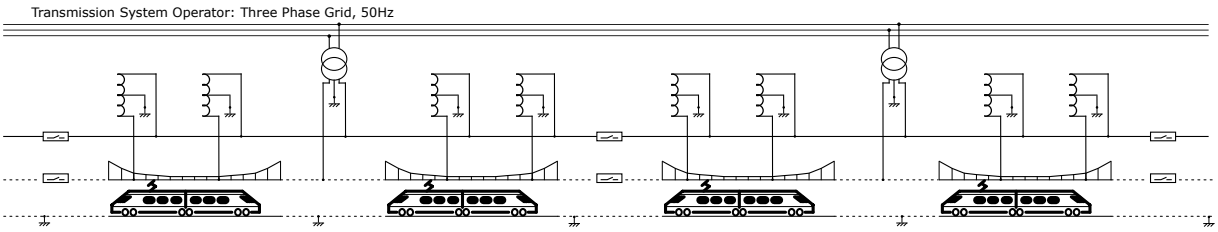

Figure 2.8: 50 Hz 2×25 kV supply system. Adapted from [18].

A brief illustration of railway transportation was presented, focusing on different electrifications. Despite this work targets the 1×25 kV electrification scheme, the tools and strategies presented in this thesis must be compatible[6] with any type of electrification.

2.2 Power Flow Management in Smart Railways

The subject of power flow management in smart railways has been researched in the past few years. It is mostly associated with the integration of the smart grid concept into the railway power system towards a better usage of the energy resources.

This section starts with a brief overview on the research of the smart grid concept, as the nuclear thematic where the topic of energy management in smart railways has emerged.

2.2.1 Smart Grid Concept

The research in the field of smart grids is enormous. As example, a search in Scopus for the mesh-term *"smart grid"* results in 60 books[7], 351 review articles[8] from an universe of 15 758 available documents[9].

The majority of the authors of the relevant works seeks for a definition of the smart grid concept. Consensually, most of them cite definitions from credited institutions, such as the following:

- **US Department of Energy** [20]: "Grid 2030 is a fully automated power delivery network that monitors and controls every customer and node, ensuring a two-way flow of electricity and information between the power plant and the appliance, and all points in between. Its distributed intelligence, coupled with broadband communications and automated control systems, enables real-time market transactions and

[6]Note: the strategy associated to the compensation of reactive power is not applicable to DC electrification systems.

[7]TITLE ("smart") AND TITLE ("grid") AND DOCTYPE (bk); retrieved in March 2021

[8]TITLE ("smart") AND TITLE ("grid") AND DOCTYPE (re); retrieved in March 2021

[9]TITLE ("smart") AND TITLE ("grid"); retrieved in March 2021

seamless interfaces among people, buildings, industrial plants, generation facilities, and electric networks".

- **European Technology Platform: Smart Grids** [21]: "SmartGrids is a new concept for electricity networks across Europe. The initiative responds to the rising challenges and opportunities, bringing benefits to all users, stakeholders and companies that perform efficiently and effectively".

- **Cisco** [22]: "A Smart Grid is a term generally used to describe the integration of all elements connected to the electrical grid with an information infrastructure, offering numerous benefits for both the providers and consumers of electricity. The Smart Grid can be considered an intelligent future electricity system that connects all supply, grid, and demand elements through an intelligent communication system. The backbone of a successful smart-grid operation is a reliable, resilient, highly secure, and manageable standards-based, open communication infrastructure that intelligently links the elements of the grid while participating in the decision making that delivers value to the utility and supply and demand entities connected to it".

- **International Electrotechnical Commission (IEC)** [23]: "The IEC Smart Grid Strategic Group defines Smart Grids as the concept of modernizing the electric grid. The Smart Grid is integrating the electrical and information technologies in between any point of generation and any point of consumption".

- **Institute of Electrical and Electronics Engineers (IEEE)** [24]: "The smart grid is a revolutionary undertaking—entailing new communications-and-control capabilities, energy sources, generation models and adherence to cross-jurisdictional regulatory structures. The successful rollout will demand objective collaboration, integration, and interoperability among a phenomenal array of disciplines, including computational and communications control systems for generation, transmission, distribution, customer, operations, markets and service provider".

In a nutshell, the smart grid concept is a generic concept for the future of the electrical grid. In the scope of this thesis, a railway smart grid aims at an increased degree of observability and controllability of a complex power system. As stated in [23] for the smart grid, this can only be achieved through increased information exchange between the individual components and subsystems of the power system.

This increased degree of observability and controllability of the railway power system is achieved through a framework for energy management in smart railways.

2.2.2 Current Research in Railway Power Flow Management Systems

The research in this thematic has the work of Hayashiya et al. [25], as one of the first references to the inclusion and demonstrative application of the smart grid concept to the railway power and energy system, within the Japan Railway Company. It was enabled the chance to integrate bi-directional communication and advanced computational features within the new components of the railway smart grid. The better usage of the Regenerative Braking Energy (RBE), as well as the availability of the Renewable Energy Sources (RES) and the Energy Storage Systems (ESS) are the drivers for the need of railway smart grids.

In the 2014 work of Pilo et al. [4], is highlighted the "vision for integration of the smart grid concept into the railway system". Each supply station of a railway track may be seen as a microgrid. The Railway Smart Grid (RSG) concept enables the potential use of RBE, ESS and RES, towards multiple benefits in the railway system. The flexibility of trains regarding the speed profiles allows the main objective of this transportation system — the transport passengers and goods according to a schedule — to be compatible with the availability of all energy resources. Therefore, new opportunities in energy optimization and cost of energy optimization are open up.

Furthermore, in 2015 work of Pilo et al. [26], is presented a practical milestone in the railway smart grid roadmap, with the presentation of a strategy to adopt power transferring devices in the neutral zones, to enable new ways of operation towards a more reliable and cost efficient railway systems. In the case study, the authors concludes that with the proposed system is able to reduce up to 31 % the manageable costs of electricity (costs associated to the power capacity, losses in transformers and losses in catenary).

Continuing on the conceptual research of railway energy management systems, in Nasr et al. and Ph.D thesis of Nasr [27, 28] is also proposed a solution based on the smart grid concept to recover the braking energy in DC lines. The excess of energy in the catenary is intelligently used to charge a hybrid storage system, where this energy is further re-used in non-railway applications. As example of those non-railway applications, the authors propose the charging of hybrid-electric buses.

Similar proposal was presented by Pankovits et al. [29], where the feasibility of implementing a RSG is analyzed. A Fuzzy Logic based Energy Management System (EMS) was proposed and implemented where the charging of the wayside ESS is defined based on the net balance of the power in the railway system. Furthermore, a long-term predictive algorithm generates an extra-input for the FLC, where this algorithm targets the reduction of the electricity bill (based on the electricity cost, RES forecast and train consumption predition). The optimization of this EMS is made with a Genetic Algorithm (GA), where the FLC membership functions are adapted.

From the outcomes of the MERLIN European project[10], an integrated energy management system was investigated, with the viability demonstrated on several publications. In the 2015 work of Khayyam et al. [30] is firstly presented the Railway Energy Management System (REM-S) concept and architecture, where the contribution is in the demonstration that the railway systems are eligible to the application of the Smart Grid (SG) concept and the Smart Grid Architecture Model (SGAM) (illustrated in Fig. 2.9).

The REM-S is further detailed in Khayyam et al. [31], where three objectives are listed:

- Optimization of the energy consumption, while keeping the fulfilment of the performance requirements;
- Optimization of the power demand, by reducing, as example, the peak power consumption (enhancing the electricity network capacity);
- Costs optimization with a more rational use of energy.

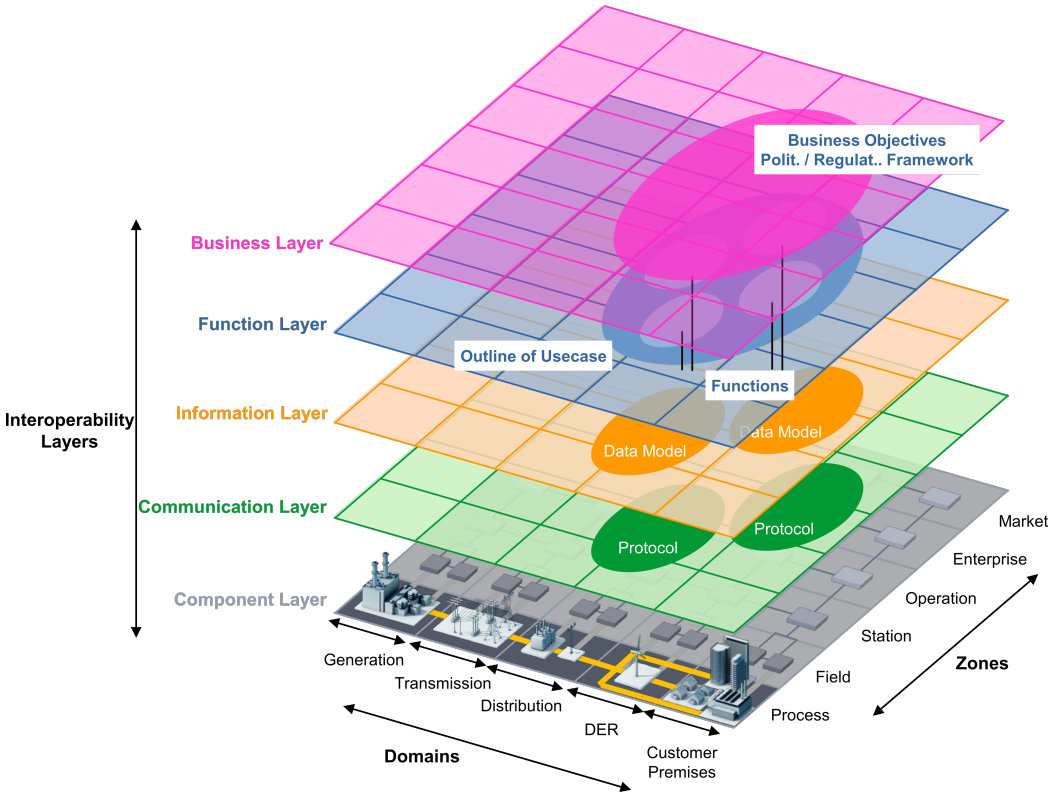

Figure 2.9: Smart Grid Architecture Model framework. Retrieved from [32].

[10] https://cordis.europa.eu/project/id/314125

The proposed automation architecture for the REM-S is an hybrid centralized-distributed architecture model. The REM-S must be based on the division of the system into different zones, mostly due to the distributed nature of the railway system as well as the size, complexity and uncertainties. In this automation architecture, each subnetwork of active entities of the system are in contact with the central controller and with the neighbouring subnetworks.

Three operational modes, defined on a time-based viewpoint, are hierarchically in the REM-S [31]:

- Day Ahead Optimization (DAO), where this architecture layer calculates the optimum behaviour of the network (power profiles, energy and power purchase, power sale, etc.) for the next time horizon (24 h).
- Minutes Ahead Optimization (MAO), where the local EMS predicts and optimizes the next 15 minutes of the subnetwork status.
- Real-time Operation (RTO), where this architecture layer fulfils the calculated MAO profiles, taking into account the real-time status and behaviour of all the components associated to this subnetwork.

In Fig. 2.10 is presented the REM-S automation architecture concept.

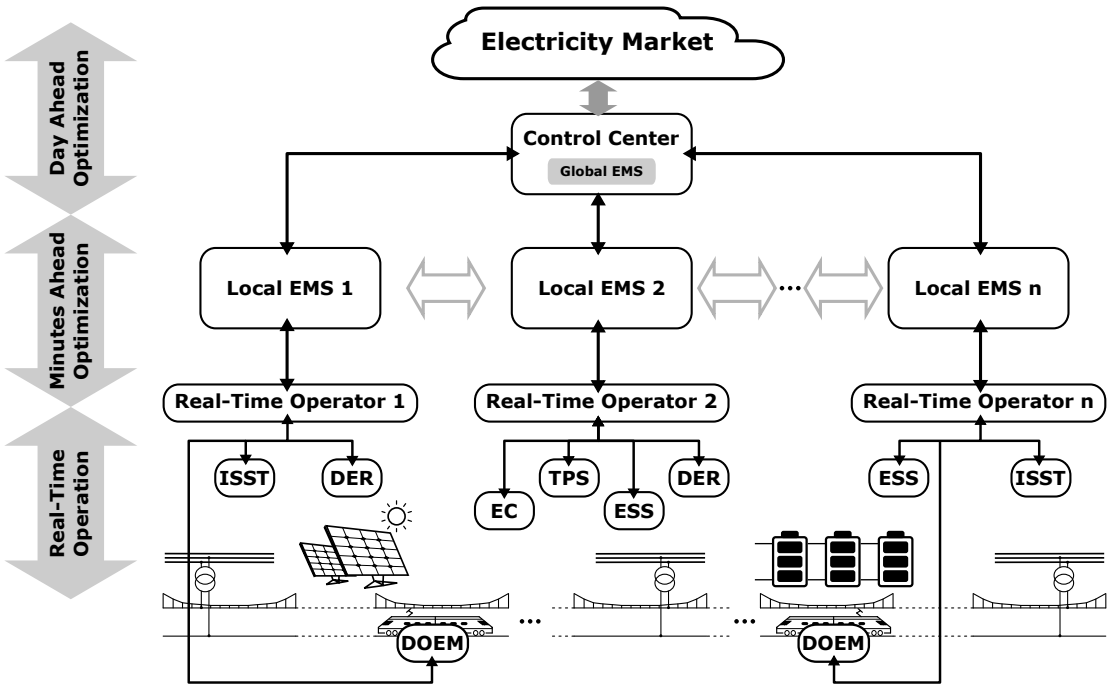

Figure 2.10: Railway Energy Management System automation architecture concept. Adapted from [31]. Note: DER – Distributed Energy Resources; DOEM – Dynamic Onboard Energy Managers; EC – External Consumers, like workshops, stations, or loads such as EV charging stations; ISST – Intelligent Traction Power Substations; TPS – Traction Power Substation.

Several works have been published based on the REM-S. In [33], is presented a proposal for the application of the REM-S in the Spanish railway, with a focus on detailing the communications infrastructure.

Flek et al. [34], focus on the presentation of the methodology for the DAO algorithm. It targets the interaction with the power grid and the participation in the energy market. Furthermore, the time intervals considered by the DAO will be compatible to the time-step in energy trading at the electricity market. The DAO algorithm proposed by Flek et al. [34] considers two steps. In the first step, the optimization objective is to find the best solution considering cost and power peak optimization criteria, using a Genetic Algorithm. Then, the Railway Energy Storage Systems (RESS) are evaluated and further optimized. The proposed algorithm was successfully applied to real scenarios of railway tracks in France and Spain.

Later in 2018, Khayyam et al. [35] further tested the real-time online operation on a Spanish railway line for a few hours. The study focus on comparing the REM-S operation in offline and online modes. Then, Razik et al. [36] specifies the prototype implementation of an advanced automation architecture designed to operate the railway electrical systems as a cyber-physical system. The algorithms for the RTO level of the REM-S are comprehensively presented.

Due to the rise of interest of the scientific community in the thematic of railway power flow management systems, multiple research directions have been reviewed in the topic of energy management for smart railway power systems.

Serrano-Jiménez et al. [37] reviews the AC and DC topologies, focusing on presenting the future directions of each configuration, and finishing with the smart railway operation of future flexible substations.

In the review paper of Steele et al. [38], the authors start to present the drivers and benefits for the railway smart grids (drivers: decrease in the reliance in fossil fuels, increase in the supply reliability, nature of the traction demand among others; benefits: attracting costumers, energy saving with Distributed Energy Resources (DER), less losses and ESS, cost benefits with the increase of the costumers, and future-proofing the supply).

Then Steele et al. [38] presents the challenges for the implementation of the RSG. Specifically, the technical challenges are divided into seven aspects: i) interfacing new equipment, towards monitoring and controllability of railway power supplies; ii) electromagnetic compatibility in the developed equipments and networks; iii) developing communications, being bi-directional, having real-time and guaranteed quality of service requirements; iv) distributed generation enabled by the rise of solar and wind systems; v) cybersecurity against active and passive threats (respectively, attacks that affect the operation,

and attacks that steal information); vi) data requirements, where multiple stakeholders will produce and have access in real-time to the data, where the consistency of the data must be ensured; vii) standardization and regulation, as the ultimate need to ensure that the technologies delivered are compatible and interoperable with the remainder of the system.

Khodaparastan et al. [39] reviews the methods and technologies proposed for regenerative braking energy recuperation (train timetable optimization, energy storage systems (onboard and wayside), and reversible substations). Essentially, such technologies needs for an Energy Management System, not only to optimize the operation of trains (with a timetable optimization strategy), but also to support the optimal operation of ESS and reversible substations. In Brenna et al. [40] is presented a comparative review on efficiency issues related to three important sectors of the transportation systems: railways, electrical vehicles, and marine. The wide analysis presented for the railway transportation sector highlights the main measures adopted in the power systems and in the train traffic control, focusing on integration of RESS.

Barros et al. [41] briefly reviews a study of different railway power systems, highlighting emerging concepts, such as regenerative braking, energy storage systems, the inclusion of renewable energy sources, bidirectional power flow and wireless power transfer.

In the recent review paper of Arboleya et al. [42], targeting 5 years in the literature, the authors present strategies for improving railway feeding infrastructures. On the topic of energy management systems, the authors concludes that the real-time operation of these systems are the critical part of a railway energy management system. It is highlighted the outcomes of the H2020 MERLIN project, specifically the REM-S system described before, and is stated the research directions for a hybrid and flexible energy management system, that can perform adjustments in real-time to the train speed, as well as the management of the energy flows needed with the integration of DER and ESS.

In the previous paragraphs, some of the review papers associated to the power flow management of railway electrification systems were presented. In addition to the research directions presented before, in following paragraphs will be presented the relevant research directions in recent years.

Starting in 2016, Novak et al. [43–45] introduced a hierarchical structure for the RSG comprising two levels: a Higher Hierarchical Level (HHL) and a Lower Hierarchical Level (LHL). Firstly, the authors [43] has presented the higher-level railway transport coordination system for trains coordination with respect to external grid conditions, routes conditions, timetable requirements and current position on the route. A practical case study was considered for a single power supply substation that comprises a local microgrid with ESS. In 2017, the authors [44] further extends the developed algorithm, where is

shown cost reductions up to 25 % for the specified scenario. In 2019 [45], the hierarchical structure was further optimized, and the developed algorithms were able to achieve up to 45 % cost reduction and 40 % reduction on energy consumption, for a case study with an actual rail route and trains of an existing commercial brand.

In 2018, an optimal scheduling approach of substation integrated RES, RBE, and hybrid ESS was proposed by Aguado et al. [46]. It was accounted the uncertainty in renewable energy resources where those were considered through a stochastic approach. The achieved costs and energy savings for a realistic case study were 33.2% and 9.6%, respectively.

Later, Sengor et al. [47] proposed a rail station energy management architecture for a railway electrification comprising ESS and Photovoltaic generation (PV), where regenerative braking takes place and where the cost of electricity is variable. Several case studies were considered to take into consideration the uncertainties in initial ESS state of energy, as well as in the uncertainties in PV generation and the impact on the variation of the number of passengers. The solution for the problem was obtained with a mixed-integer linear programming optimization strategy where a reduction of 35 % in cost of daily energy consumption is achieved when the station is able to use all the regenerative braking, ESS and PV resources.

Ciccarelli et al. [48] evaluated the feasibility of integration PV power plant and a super-capacitor ESS in a railway power system, in a real tramway electric system, having a random optimization procedure for the energy management system.

In 2019, Fernández-Rodríguez et al. [49] presents a comparison between two real metro lines, in Italy and in Spain, where the excess of energy resultant from the regenerative braking is used to charge electric vehicles. It was shown that in both case study railway lines, the regenerated energy is 98% for short interval trains (where this value decreases with the increase of the train intervals). It was estimated that between 685 and 1000 Electric Vehicles (EV) could be charged every day using the wasted braking energy for, respectively, the considered Spanish and Italian lines.

In 2020, Chen et al. [50] propose an energy management system based on a multitime-scale optimal dispatch method to improve the benefits of Flexible Traction Power Supply Systems (FTPSS). The FTPSS integrates a back-to-back converter, Hybrid Energy Storage System (HESS) and PV generation. Furthermore, the proposed algorithm is capable to compensate for the imbalance between supply and demand in short-term operation, by considering a day-ahead dispatch and an intra-day feedback correction.

The energy management system proposed by Lu et al. [51] comprises a centralized-decentralized control strategy, targeting the utilization of the regenerative braking energy and having energy storage systems, for a modified AC-fed railway system. This modified railway system comprises power quality compensator devices in the traction substation

and in the neutral zones, enabling higher degree for flexibility (either in increasing the power quality, and in managing the storage system). The centralized-decentralized control strategy benefits from the centralized operation advantages (simple control, simple operation and global optimal operation), and the decentralized operation advantages (reduced dependency on the communication and processing). Essentially, the centralized control is adopted when the communication and the processing of the central energy management system are normal. Once the communication or the processing of the central management system fails, the adopted control strategy will be the decentralized.

In the PhD thesis of David Roch Dupré [52], are proposed optimization algorithms to design the optimal installation of reversible substations and energy storage systems, in order to maximize the use of energy coming from regenerative braking.

Fletcher et al. [53] presents a tool for energy storage optimization. The proposed framework comprises a high-level design tool that integrates a versatile and configurable database-driven generic rail network model with a power supply network representative of DC electric railways. The outputs of the model were compared with data from a real railway line operation for validation of the model. Then, it is assumed the availability of ESS for further optimization with a Genetic Algorithm.

Recently in 2021, Zahedmanesh et al. [54] proposed a strategy for the optimal techno-economic operation of AC railways with DER and ESS, using a two level hierarchical management structure for the control algorithms of the energy management system. The hierarchical and sequential control algorithm starts to define the power references for the lower level, based on predictions and price of electricity, and further optimization procedure. The generated power references are further used in real-time, with the objective to reduce the negative sequence currents and increase the power quality through reactive power compensation at the traction power substation.

Not only the drivers for a better energy management in railways, such as the MERLIN project, but also the digitalization associated to the smart grids, has led to the continuous research in this field. Several other interesting publications not presented here also tried to contribute to a smarter railway.

This thesis is one more contribution towards a smarter railway. In the following section is presented some of the gaps in the scientific literature that has motivated the research opportunities in each of the topics of the chapters from chapter 3 to chapter 7.

2.3 Related Research

The objective of this third section is to briefly present a specific scientific literature review on the topics **T1** to **T5**. Then, for each of the topics, it is identified the gaps found in the state of the art that motivates the research opportunities.

2.3.1 Model Line Simplification

The chapter 3 targets the topic **T1**, where the a methodology to simplify a railway electric line is proposed. As it will be presented, the quantification of the error associated to the utilization of a simplified railway line is not clearly addressed by the scientific community.

Starting with the objective of the study of railway power system, where this study requires accurate modelling of railway electrification parameters, the first task is to identify the applications and issues addressed by the scientific community:

Harmonic distortion and resonance – where the stability of the power system is analysed, using detailed network structures and multi-transmission line models of the catenary network [55,56], having the eight port representation model as example [57];

Unbalances in three-phase electric grid – where the effect of the connection of the railway line to the Transmission/Distribution System Operator (TSO/DSO) phases are studied [58, 59];

Step/touch voltage calculation – to evaluate the hazardous effect of high currents in the rails, causing potential dangerous situations [60];

Line catenary supply fault location – where the accurate electrical conductor representation allows automatic systems to precisely locate faults [61];

Induced voltages in parallel communication lines – where the existence of high currents in the catenary causes induction of dangerous voltages in parallel communication lines due to the magnetic coupling effect [62, 63];

Optimization of catenary conductors design – as a way to evaluate improvement strategies, such as, the usage of a higher negative voltage in the feeder to increase the range/coverage of a single Traction Power Substation (TPS) [64, 65];

Load flow analysis – to obtain knowledge regarding the energy flows in the railway system and better foresee the increasing of the capacity needed in a near future.

Recognising the importance of the above reasons, the electrification model analysis of chapter 3 of this thesis is focused on the load flow analysis. The evaluation of the power

flow to increase the knowledge of power systems has been extensively researched and is an essential tool to ensure the stability of power systems [55].

In [66], is proposed the usage of a sequential linear power flow method, in railway power flow calculation, as an advantage over standard Newton-Raphson method. The reference [67] presents the forward/backward sweep load flow method, which is applied to an 2x25 kV electrification and is supported with field measurements. In [68], is presented a thevenin-equivalent-based method to solve the power flow, where the node voltage equations are converted into port-characteristic equations, before the usage of the conventional Newton-Raphson method.

2.3.1.1 Research Opportunities

For the power flow analysis, a simplified line model as later presented in chapter 3 in this work is enough. To support this claim, two line models will be tested and, later, important electrical aspects will be compared, specifically:

- At the same consumption conditions (same train active and reactive power consumption for the two line models), the voltage at train pantograph is compared;
- In similar conditions, the resultant active and reactive power at TPS is compared.

Conventional tools for power flow analysis use simple π-type models for the lines, and decoupled PQ or PV types of loads/sources. As example, with thousands of citations and many applications, the MatPower tool has been widely used [69]. This software package has different solvers for the AC power flow problem (i. the standard Newton-Raphson, two variations of the fast-decoupled and the Gauss-Seidel methods, for meshed networks; ii. the radial power flow, the current summation and the power summation methods, as specific solvers for radial distribution networks, where the railway power system is an example) [70].

Only with the adaptation of these tools, to use a multi-conductor line model, is possible to extensively simulate a railway line. Nevertheless, if the resultant errors – of the utilization of a simplified π-type line model, in contrast to the utilization of a multi-conductor line model – are available and are minimal, the extensive simulation of a railway line with traditional power flow tools is possible.

2.3.2 Train Model and Train Simulators

In chapter 4 is addressed the development of a train simulation tool capable of estimating the information regarding the train dynamic movement and the train energy consumption, targeting the topic **T2**.

This literature review, on the related research from the scientific community on the topic **T2**, is divided the thematic into three areas: i) the modelling of the longitudinal train dynamics, ii) train optimal operation and heuristic-based speed profile generation, and (iii) multi-train simulator tools.

2.3.2.1 Modelling of Longitudinal Train Dynamics

The field of train modelling has been extensively addressed in references such as the Handbook of Railway Vehicle Dynamics [71], or the references [72], [73] and [74]. In the review article of [72], the authors start to present the longitudinal train dynamics definition, as the motion of rolling stock vehicles in the direction of the track (only longitudinal movement), and the motion of the train as a whole (which includes the dynamics between coupled vehicles). Based on this definition, the authors present the research problems on longitudinal train dynamics, divided in the problem genre, force inputs and main applications. In the energy efficiency point of view, the problem genre is not addressed and the train is approximated by a single point with mass and subject to specific forces. Furthermore, the main applications listed by the authors are the energy consumption calculation and driving advisory systems (which will be further addressed in this literature research). For the modelling of the longitudinal train dynamics, the review of [72] identifies the research problems in the following aspects: the force inputs, in particular the traction force, dynamic brake force, pneumatic brake force, curving resistance, propulsion resistance and gravitational component.

Discarding the impact forces and the resonance (low frequency vibration) force, the reference [75] lists the forces affecting the train movement, (being all based on the Newton first law $\sum F(t) = 0$):

1. **Traction force**: is equal to the sum of all longitudinal traction efforts, on motorized axles of the train;
2. **Gravitational force**: is the gravitational contribution due to the slope, illustrated in Fig. 2.11, and is given by $F_g = Mg\sin(\alpha) = Mg\sin\left(\arctan\left(\frac{\Delta h}{d}\right)\right)$ where M is the total vehicle mass, g is the earth gravity acceleration, α is the angle between the railway line and the horizontal plane and depends on the ratio $\frac{\Delta h}{d}$. Furthermore, considering N discrete sections of the railway line, the gravity force can be approximated by $F_g(x) \approx -M\ g\ i(x)$ where $i(x)$ is the gradient of the railway line, as function of the position;
3. **Curving Resistive forces**: includes the resistance against the linear movement due to curves and line design, as illustrated in Fig. 2.12. These forces, in Newton per tonne of vehicle mass, are given by $F_c(x) = \frac{D}{R(x)}$ [72] where D is an empirical

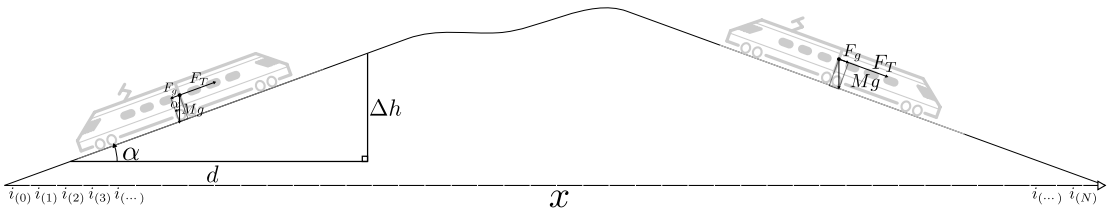

Figure 2.11: Illustration of gravity in train force calculation.

parameter that can vary with the rail flange lubrication and the train speed (the force of a stationary vehicle can be the double), and $R(x)$ is the curve radius in meters. The reference [73] proposes a constant value of $D = 6116$. Other studies [76] extends this force to be $F_c(x) = \frac{\mu(G+L)}{2\times R(x)} \times 10^6$, where μ is the wheel-to-rail adhesion coefficient, G is the track gauge in meters, L is the axial length in meters and $R(x)$ is the radius of curvature, in meters;

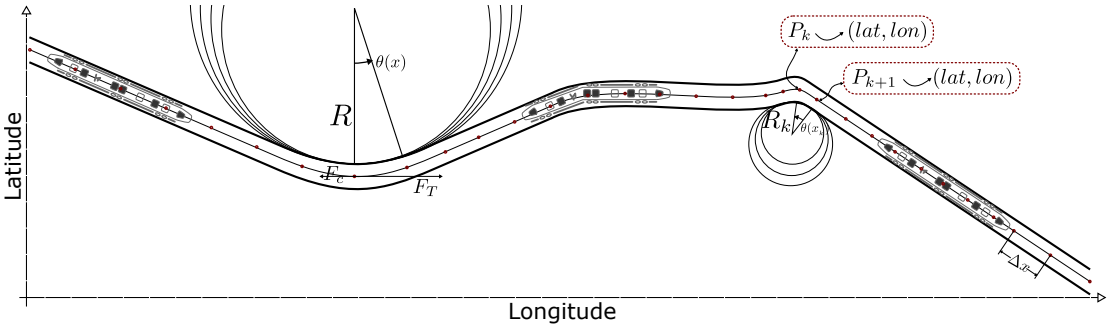

Figure 2.12: Illustration of resistive curving forces in train force calculation.

4. **Inertial term related force**: includes the inertial force due to the rotation elements (wheelsets, wheels, etc.). In the study of [76], it is considered a dynamic mass of the train-set to include this rotational kinetic energy stored in the rotating parts, and directly depends on the train mass;

5. **Propulsion resistive force**: is the force related to the rolling resistance and the aerodynamic resistive force. The reference [72] lists several resistance formulas for generic and specific trains, where it should be highlighted the Original Davis Equation, as a quadratic polynomial equation that is a function of the train speed and includes the frontal area and profile of the train as well as the mass supported per axle and the number of axles of the train. The specific train equations are mostly given by the format $F_a(v) = A + Bv + Cv^2$.

2.3.2.2 Train Optimal Operation

In the review work of Scheepmaker et al. [77] is made a comprehensive survey on train control and timetabling. It is clarified the main objective of the train optimal control: to decrease the energy consumption in the train operation. This objective, combined with more energy-efficient technologies as well as solutions to increase in the capacity (in terms of passengers per train) and measures to save energy in parked trains, will contribute to a more sustainable and profitable railway operation.

Regarding the train optimal control, the scientific community follows two lines of research [77]:

a) The extension of the optimal control theory (in particular in the Pontryagin's Maximum Principle [78, 79]) to the optimal driving strategies of a train to minimize the energy consumption;

b) The problem of finding the optimal sequence of these driving regimes (and the switching points between regimes).

The application of the outcomes of these fields of research can be used in understandable advice to train drivers in real-time with Driving Advisory Systems (DAS).

In the first line of research, targeting the estimation of optimal train speed profile, it is identified the origins in the contribution of Ph.D thesis of Milroy [80], with a rigorous mathematical treatment made by Howlett [81]. Their solutions consider a basic model where the braking phase of the train does not regenerate energy or have a cost in the optimization objective and, therefore, it addresses the diesel trains.

The main conclusion of the basic optimal train control problem is the existence of an optimal driving sequence:

(1) Maximum acceleration[11] *— (2) Coasting — (3) Maximum braking*[12].

The result of the work of Milroy [80] was a driving advisory tool — Metromiser — that searches for the early-arriving time reduction, where the trial tests have obtained a 13 % fuel reduction with an early-arriving time reduction from 28 to 10 seconds.

Mostly due to the possibility of regenerative braking, later studies [77, 82] also include other sequences:

(1) Maximum acceleration — (2) Cruising[13] *— (3) Coasting — (4) Maximum braking.*

Furthermore, as reviewed in [77], the combination of sequences for the speed profile was also proposed, as the example:

(1) Maximum acceleration — (2) Cruising 1 — (3) Coasting — (4) Cruising 2 — (5) Maximum braking.

[11] or Full Traction Force
[12] or Full Brake
[13] or Partial Power

The second line of research is supported by the existence of the optimal driving sequence and proposes do define the switching points using search algorithms. The common approach is the generation of several speed profiles and each of them will be evaluated according to objective/penalty functions. These functions are obtained by the outcomes of such speed profile, like energy consumption, punctuality, ridding comfort (or jerk), the fulfilment of the speed constraints, among others. In this second line of research, Genetic Algorithm (GA) and other meta-heuristic tools are commonly used.

It can be highlighted the work of Dominguez et al. [83] and the extension [84], that despite has based the meta-heuristic in the exhaustive simulation of all feasible speed profiles, the heuristic result uses the information of the simulation of four independent modules (automatic train operation, train engine, train dynamics and energy consumption). These works use an exhaustive search, rather than a more computational-efficient meta-heuristic such the ones used by other authors.

The authors Chang and Sim [85] firstly proposed a GA meta-heuristic to keep the punctuality while maintaining a good comfort (avoiding strong accelerations or excessive usage of brakes).

A GA meta-heuristic is also proposed in the references [86, 87]; in the reference [88] is compared the GA with the Ant Colony Optimization (ACO); the reference [89] proposes the usage of an Evolutionary Algorithm (EA); and the reference [90] also compares the GA with the Firefly Algorithm (FA).

2.3.2.3 Train and Multi-train Simulators

In 1998, Goodman et al. [91], presented a review paper on the simulation models for railway systems. The authors classified railway simulators into three categories:

- Simulation of the train movement (defined as the calculation of the speed/distance profiles when a train is travelling from one point to another);
- Simulation of the train drive systems (where simplified or detailed models will put restrictions on the train tractive effort);
- Simulation of the traction power supply (where the objective is to analyse the performance of the railway power system).

All three categories are associated to this thesis and will be discussed. The first two presented categories are directly related to the topic **T2**, whereas the simulation of the traction power supply is linked to the topic **T3**.

Furthermore, in [91] is also categorized the railway simulation tools as time-based and event-based. Time-based railway simulators are more associated with energy consumption studies and event-based ones are usually used to target timetabling and traffic control studies.

Besides, there are two types of approach in the design of such simulator systems: i) a direct matrix method; and ii) a modified load flow approach.

In the first design approach, it is performed a nodal analysis of the linearised circuit and then is coupled with the train movement objectives/restrictions. This approach was part of the University of Birmingham Multi-train Simulator to study the operational and power-supply conditions in rapid-transit railways [92] and was recently extended by [93] with the analysis of a DC railway line.

In the modified load flow approach, which was followed in the design of the chapter 4 and chapter 5, the traction power network simulator is separated from the train movement. In Fig. 2.13 is illustrated a generic structure for a train movement simulation tool.

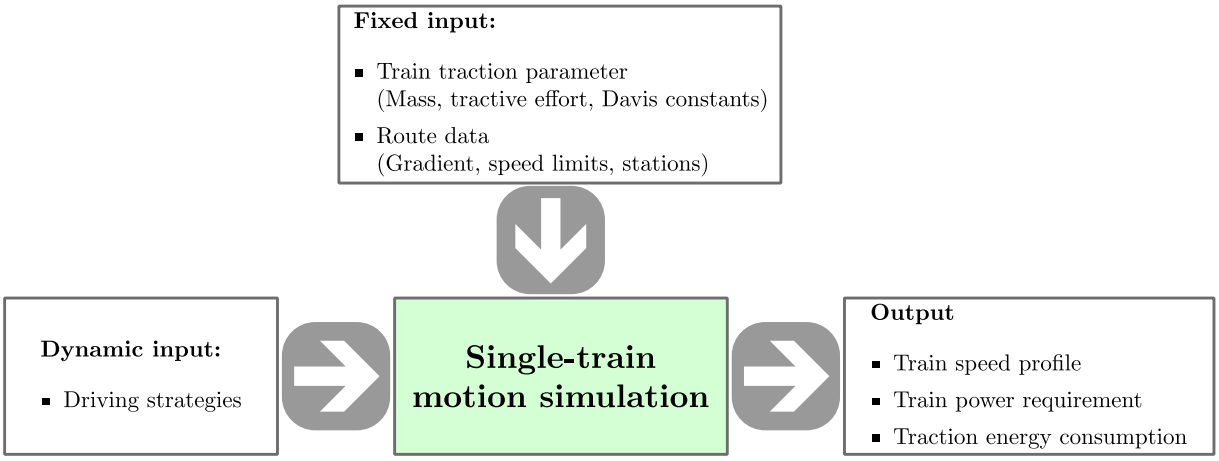

Figure 2.13: Structure of single-train simulator. Adapted from [93].

As reviewed by Khodaparastan et al. [39],the simulation of the electric rail system has been studied since late 1970, with various simulation studies and programs developed by industry and academia. Most of the programs and tools are either proprietary or commercially available.

As an example of proprietary tools, SNCF Réseau uses the Esmeralda tool [94], as one of the methods to estimate railway system losses, among other analysis. Esmeralda is capable of simulating 15 lines representative of the SNCF network.

On the commercially available tools, developed at the Swiss Federal Institute of Technology's Institute for Transportation Planning and Systems (ETH IVT), the OpenTrack is an extensive and complete simulation platform with a user-friendly interface [95]. Later in

2008, the OpenPowerNet simulation module for OpenTrack was presented [96], to complete the need for evaluation of railway power supply systems.

Siemens has the commercially available Sitras SidyTrac and Sitras EMS tools [97], featuring multi-train simulation with integrated electrical load flow calculation, as well as analysis of short-circuit, induced voltage and electric/magnetic fields on the line, among other software capabilities.

Developed by Carnegie Melon University and being implemented in several North-American railway lines[14], the commercially available tool Train Operation Model (TOM) [98] comprises three simulation modules: i) Train performance simulator; ii) Electric network simulator; and iii) Train movement simulator.

With a cloud-based development, the OlgaNG simulation tool[15] developed by Spanish EPRail company[16], allows the simulation of AC and DC railway electrification topologies, with multi-train movement simulation and having capabilities to evaluate short-circuit and line voltage analysis, as well as the power in the transformers.

Furthermore, for the simulation of DC railways, Kulworawanichpong, [99], details the implementation of a simulation tool for the Sukhumvit line of Bangkok transit system, with an highlight on the software structure of the developed tool.

The UK Rail Research and Innovation Network (UKRRIN)[17] has developed a simulator which has been used for the analysis on several aspects (signalling, virtual convoying, dynamic movement, power consumption, etc.). This RAIL-DT Engine has enabled, in a project example, a railway operator to have an digital twin of their entire operation [100]. The architecture of such simulator is presented in Fig. 2.14.

2.3.2.4 Research Opportunities

Even though the train/rail simulation tools were not extensively listed in this thesis, it is clear that the majority of studies are performed with proprietary or commercially available tools. An exception is with the Ph.D thesis of [101], where the developed software was made publicly available, for the analysis of specific objectives.

Due to the lack of availability as open-source of these simulation tools, it is of advanced interest to develop a train simulation tool with the specific objectives of this thesis. One research opportunity, that is missing in the scientific community, is on the detail on the implementation steps of a flexible train simulator and the clear comparison of the output of such simulator with real train data.

[14]List of rail transit systems who either are licensees of the TOM or have had the TOM used in their systems: http://www.railsystemscenter.com/rr.htm
[15]OlgaNG Website: https://www.olgang.com
[16]EPrail Research and Consulting Website: http://www.eprail.com/
[17]UKRRIN Website: https://www.ukrrin.org.uk

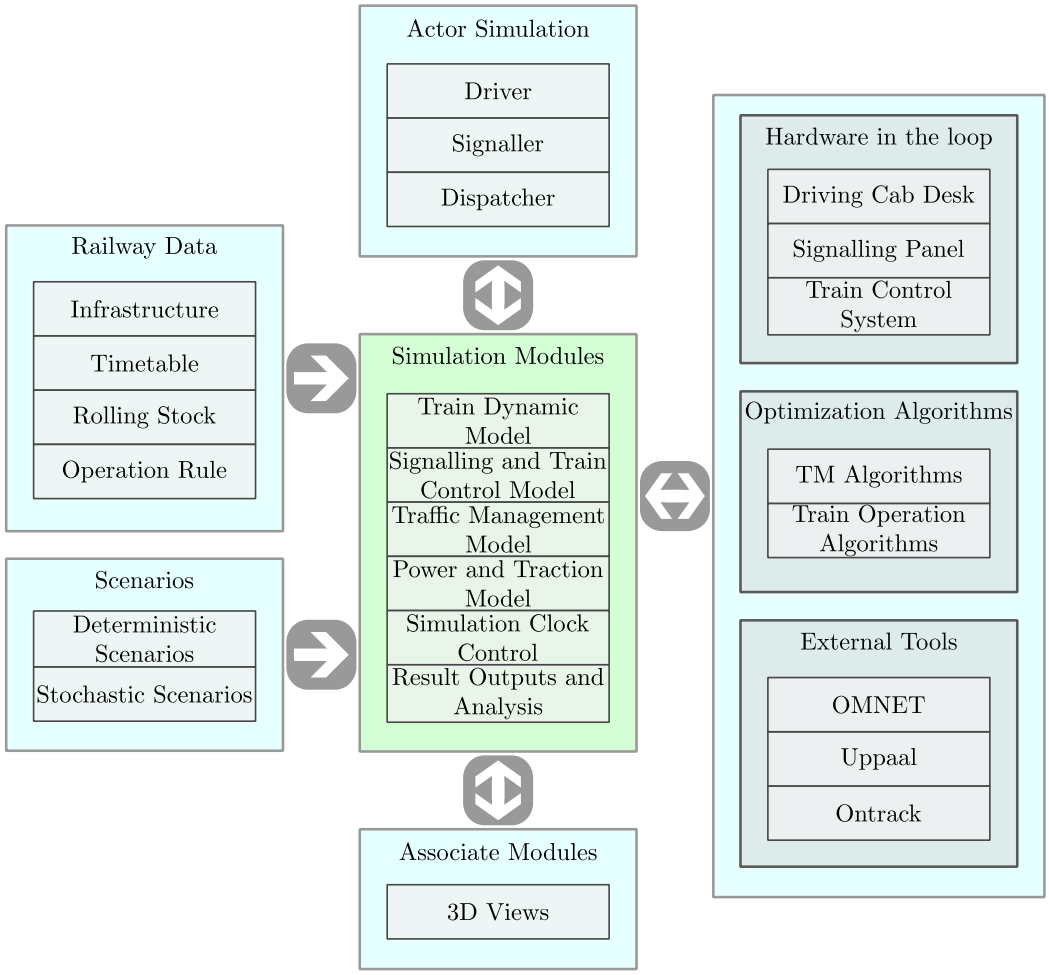

Figure 2.14: UK Rail Research and Innovation Network RAIL-DT Engine. Adapted from [100].

2.3.3 Railway Power System Simulation Tools

In chapter 5 is addressed the topic **T3**. It is proposed the PSSA-rail tool, which is a power system state analyser tool capable of the simulation of railway infrastructure.

The scientific contributions on those thematic are associated to the simulation of the traction power supply, which was covered in section 2.3.2.3. Thus, from the listed contributions of the scientific community, some research opportunities arise.

2.3.3.1 Research Opportunities

Similarly to the research opportunities that drive the development of a train simulation tool, in section 2.3.2.4, the tools for the simulation of the power system of a railway infrastructure are associated with proprietary or commercially available licenses.

Then, a research opportunity arises with the proposal of the implementation steps of

a flexible railway power system analyser tool, that can be capable of the simulation of an entire railway line, for a broad simulation time-window, and being adaptable in order to include optimization strategies.

2.3.4 Railway Reactive Power Compensation

In chapter 6 is proposed the increase of the railway infrastructure capacity with the compensation of the reactive power, which addresses the topic **T4**. This increase in the infrastructure capacity is due to the decrease of the voltage drop in the catenary line, which allows the operation of more trains in the same railway line. This section of the literature review starts with the definition of infrastructure capacity, then is presented the strategies to increase the railway infrastructure capacity with improvement on power quality.

2.3.4.1 Infrastructure Capacity

Regarding the infrastructure capacity increase, most works are focused on operational and logistics. In [102], the main concepts and methods to perform capacity analysis are reviewed. In theory, capacity is defined as the number of trains running over a line section, during a time interval, with trains running at minimum headway.

This capacity mostly depends on infrastructure constraints (signalling system, power traction constraints, single/double tracks, speed limits, braking curves, etc.), on traffic parameters (timetables, priorities, type of trains, etc.) and on operation parameters (track interruptions, train stop time, etc.). In [103], increasing the railway infrastructure capacity by increasing the speed of freight trains is proposed. Specifically, in the case of a delay, these trains are allowed to have higher maximum speeds.

2.3.4.2 Power Quality Improvement

Several works have been reported in the literature regarding strategies for power quality improvement in railways. In AC electrification, two main types of devices based on power electronics are usually implemented: voltage stabilization devices, or voltage boosters, and line current balancers [104].

The main objective of the high voltage boosters is to inject reactive power into the line, with a level adapted in real-time. Usually, this is achieved with Static VAR Compensator (SVC) [104].

Complementarily, the purpose of line current balancers is to minimize the unbalance caused in the transmission/distribution network by the railway electrification.

These two types of devices are necessary to comply with the increase in power demand. Usually, infrastructure managers adopt systems in the TPS site that can either balance

the line currents and inject reactive power.

In [105, 106], comparative studies on several Railway Power Conditioners (RPC) topologies are presented, to be employed in the TPS. Traditional RPC comprises two back-to-back converters and two isolation/coupling transformers [107, 108]. From this topology, several have been derived, such as the Active Power Quality Compensator (APQC)) which comprises a three-phase converter [109], or the Hybrid Power Quality Compensator (HPQC) in which the APQC is combined with a SVC [110, 111]; Also, Modular Multilevel Converter (MMC) topologies have been researched in current years [112].

Despite the inability to control the line current unbalances, the inclusion of voltage stabilization devices in the opposite site of the TPS (at the end of a traction section feeder: the Neutral Zone (NZ)) will strongly support this desired voltage boost. Thus, this compensation strategy allows more powerful trains without violating the standards relative to AC traction voltage levels (e.g., IEC60850 [113]). In [114, 115], strategies are presented to include compensation systems at the end of a traction section feeder. In [116], the 3 kV increase in the minimum voltage in the catenary is highlighted, with further details of this project in [117]. However, this improvement is achieved with a system occupying a very large area. The compensation scheme for Static VAR Compensator is also studied in [118], with the usage of a neural network for online operation.

In the Ph.D thesis of [101] and later in [119], an alternative to the inclusion of bulky SVCs is proposed, with the adoption of mobile reactive power compensators. This is achieved with the reactive power injection within each train. This compensation strategy is further extended with the work of [120], where the compensation scheme is based on a genetic algorithm heuristic. Later in [67], the usage of modern locomotives as mobile reactive power compensators is evaluated and compared, where they can be more efficient than SVC. However, the limitations related to the control of leading power factor as well as the need for very fast algorithms are considered that do not justify the usage of a power factor different than the unitary.

2.3.4.3 Research Opportunities

From the best knowledge of the author, the possibility of operating modern trains with variable power factor has not been actively researched in recent years. However, from the author point of view, the reason for this is not in the advantages, but in the difficulty to implement such a strategy, since it requires real-time knowledge of the state of the railway electrification.

Then, a research opportunity emerges with the study of the influence of the reactive power flow management in the railway infrastructure capacity, specifically with the adoption of mobile reactive power compensators. Despite the compensation of the reactive

power through mobile reactive power compensators is not new, it is clear a lack of research on the directions pointed by the 2003 Ph.D thesis of Kulworawanichpong [101].

Not only the technological advantages of demonstrated in recent years on communications and on computational processing power can support this real-time reactive power compensation, but also a smart railways framework is the most likely solution to achieve this goal. In fact, transition from GSM-R to next generation railway wireless communication technology has been addressed by the *Union Internationale des Chemins de fer*/International Union of Railways (UIC), highlighting this path to digital railways [121–123]. In chapter 6 is addressed this research opportunity.

From the point of view of the electrification system, the target of the Shift2Rail of doubling the infrastructure capacity [103], is closer to be achieved, with the outcomes of chapter 6.

2.3.5 Management of Railway Energy Storage Systems

In this last section of specific related research is covered the topic **T5** — proposal of a strategy to increase energy efficiency in the charging of railway energy storage systems — which is associated to chapter 7.

A charging strategy for railway ESS inherits the concepts of power management associated with the development of the railway smart grid.

In general terms and as example, the Shift2Rail program identifies this vision, through the TD3.10 technical demonstrator, where "the detailed mapping of energy consumption of a railway system is mandatory for energy efficiency analysis and management" where the knowledge of the power flow will enable "global system load prediction, peak shaving and energy cost optimisation" highlighting "the most effective actions that could be implemented to give energy savings" [3].

Furthermore, the energy management in railways is a vastly research topic by the scientific community, as previously reviewed in section 2.2 of this chapter.

The centralized-distributed aspects, where the example of Railway Energy Management System (REM-S) is key [30,31], are essential in this management. As reviewed in 2.2, two-level hierarchical EMS were proposed in [29], [43–45], [50] and [54]. Also, generic optimization strategies for railway EMS were also proposed in [46], [47], [48], [49], [51] and in the Ph.D thesis of [52].

Besides to the literature review made in section 2.2, it is needed to address specific literature review on the wayside and onboard energy storage systems as well as optimal charging strategies. This review will be made as follows.

2.3.5.1 Wayside and Onboard Railway Energy Storage Systems

Ideally, when it is not possible to inject the regenerated energy into the main grid, the most effective way to increase the global efficiency of traction systems is to use the regenerative braking energy to feed another train in traction mode (and absorbing the totality of the braking energy) [124]. However, this solution requires an excellent synchronism and a small distance between "in traction mode" and "in braking mode" trains.

Therefore, in the occurrence of small delays, the regenerative energy might not be used by another train: it and can be dissipated in the train rheostatic system or, if possible, can be returned to the TSO/DSO [125].

The usage of regenerative braking energy to charge ESS is one effective way to increase the global efficiency of traction systems [125, 126]. However, due to the high cost of ESSs, alternatives such as reversible TPS result in a higher cost-effective solution [127].

Nevertheless, onboard ESS are the most commonly used solution for a catenary-free system [128]. Besides, the majority of studies considers the total acquisition cost of infrastructure for wayside ESS, for feasibility of the solution analysis, without considering the possibility of not including batteries (or other storage technology).

As exception works, in the work [49] is evaluated the number of electric vehicles that can be fully charged using the excess of regenerative energy. Also, in [27, 28] is considered the use of excess of energy for non-railway loads, where the hybrid-electric buses are the example for storage.

2.3.5.2 Optimal Charging Strategy of ESS

The management of ESS charging system is a research topic in smart grids. Usually, the optimal charging strategy is based on the scheduling of charging profiles, using the knowledge of a predicted load profile [129].

However, due to the fast dynamics associated with the train power flow, the scheduling of the charging profile might not be an option. The prediction of train power consumption will be affected by large prediction errors which will not support the scheduling.

Then, the non-scheduling strategies for optimal management of energy storage systems should be considered for railways. Besides, solutions where this management is made in real-time using a multiple-input controller are essential.

Based on the energy management of ESS within a microgrid architecture [130], there are two possible objectives for the charging strategy:

- the financial objective function, purely based on the cost of buying/selling energy in different times;
- the battery stress level, to represent the physical degradation of the battery.

The works proposed in [131] and extended in [130] and in [132] target the usage of FLC to achieve this real-time ESS charging management. Furthermore, in these works, the fuzzy rule weights and the membership functions profile can be subject of optimization algorithms where those parameters are tuned, achieving the desired optimization.

2.3.5.3 Research Opportunities

The usage of a strong framework for smart energy management in railways is a key to achieving the optimality of the railway operation. Several energy management architectures have been proposed in the literature. However, the target application (for example, if there is available onboard or wayside storage, or if trains can regenerate energy when braking) motivates for a diversity of management architectures.

Several infrastructure solutions for the railway energy storage systems has been researched either for wayside and for onboard. Then, it would be worth to follow the research directions proposed in the works of [27, 28, 49], where is considered the usage of storage devices like hybrid-electric buses or electric vehicles. The integration of diversified energy storage systems into future railways will be expected.

It is essential to consider non-scheduling strategies for the railway ESS power flow management, not only due to the fast-dynamics of the train power flow, but also due to the predictability of the train movement: as example, a moving train eventually needs to stop, with uncertainty in time when this braking phase will occur.

Considering the works of [130–132], which addresses charging of generic storage systems, it might be worth to look at this two-level strategy for railway storage systems. The search space of the optimization algorithm (upper-level) can automatically adapt the lower-level FLC weight rules and membership functions. It should also be considered that this automatic searching algorithm must be efficient. It should be also considered the outcomes of [133], in which is referred that the FLC performance is more dependent on the rule weights rather than on MF parameters.

From the outcomes of [130], the objectives for the charging of railway ESS can be defined with a multi-objective approach: it could be worth to look at either the minimization of energy regenerating while minimizing the gradients of power, which can minimize the degradation.

By combining these research directions, it is opened the opportunity to study a strategy for power flow management in the railway energy storage systems.

2.4 Summary

This chapter presented some useful concepts and definitions to better understand the content of this thesis.

It starts with a brief historical and technical presentation of the railway transportation and electrification systems.

Furthermore, the nuclear thematic of this thesis – the railway energy management systems — is presented and extensively reviewed.

Finally, in the third section is sequentially presented a review on the five topics covered in this document. After the presentation of the relevant contributions from the scientific community on each topic, a small effort was made to identify the research opportunities.

CHAPTER 3

Railway Electrical Line: Analysis and Parameters Estimation

The topic **T1** — analysis, simplification and enhancement of the railway line model — is addressed in this chapter. This topic will contribute to achieve the challenge of this thesis: the need to develop tools and strategies for smart railways.

To achieve the challenges of this thesis, it is necessary to develop an evaluation tool for the railway electrification. This evaluation tool is essential to support the knowledge generation, which was defined as being the result of applying specific algorithms to have a global overview of the railway system state. One specific algorithm is the analysis of the infrastructure power flow. For this analysis, it is required to have an accurate railway electrification line model. However, this analysis must occur in quasi-real-time, as previously highlighted as the requirements for a smart railway framework. In this chapter, the railway electrification line model is comprehensively studied.

From this study, it is proposed a comparison methodology to evaluate the error associated with the usage of a simplified lumped parameters π-type line model, when compared to the usage of a complex Multi-conductor Transmission Line (MTL) model (which is used for advanced studies, as listed in the related research in chapter 2 associated to topic **T1**). Later, several different parameters are evaluated, in which the results are used to enhance the simplified lumped parameters π-type line model. Then, the application of this enhanced model into a traditional power flow analysis tool is clarified and demonstrated.

With this, the line model is accurately and correctly simulated with a lumped-parameter power flow analysis tool and with an enhancement procedure, as illustrated in the graphical abstract in Fig. 3.1.

The objectives of this chapter are:

- **Objective 1a:** Propose a comparison methodology to evaluate the differences between two railway line models: a complex multi-conductor transmission line model and a simplified lumped-parameters π-type line model;
- **Objective 1b:** Propose an enhancement methodology for the lumped-parameters π-type line model;

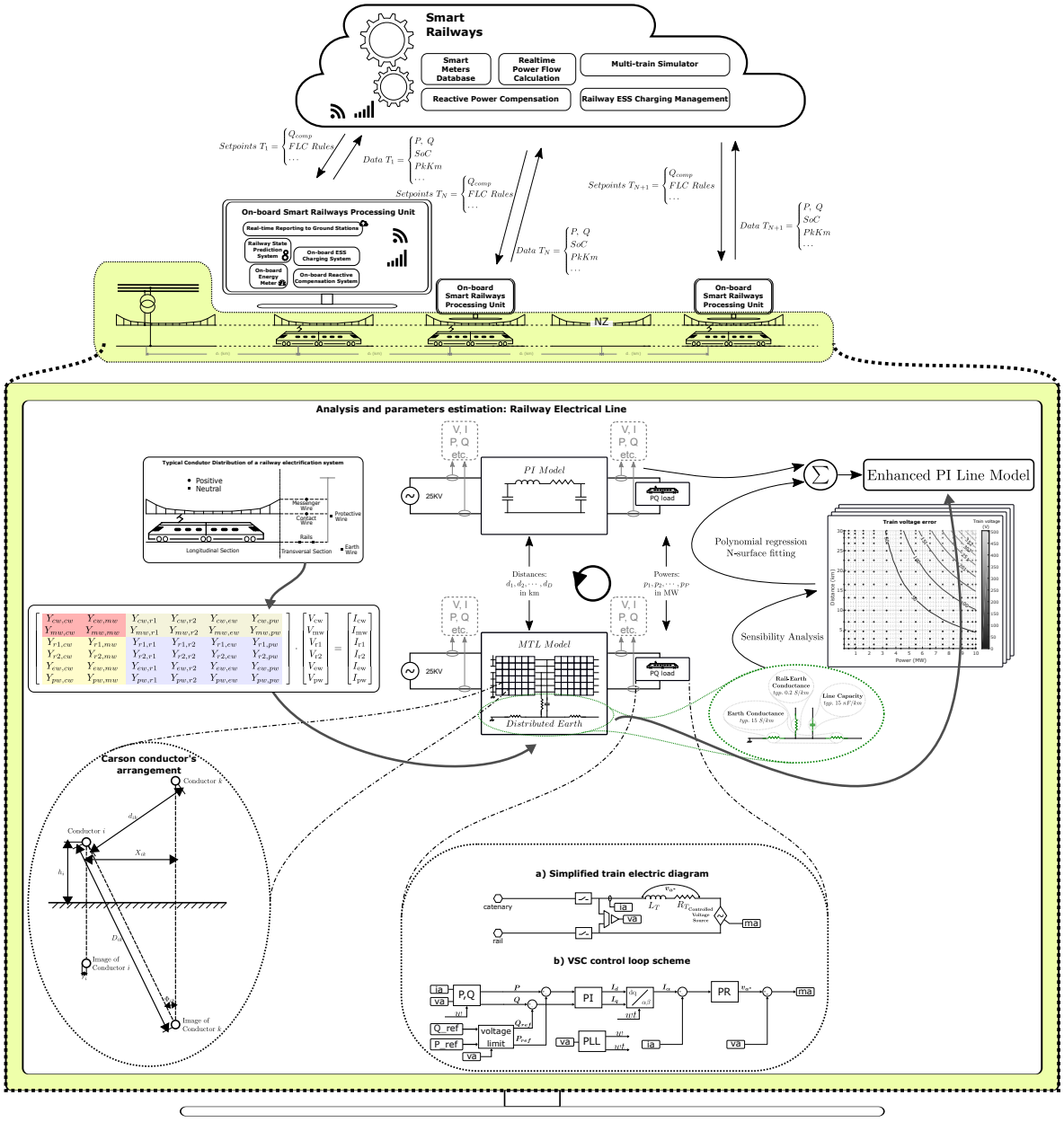

Figure 3.1: Graphical abstract of chapter 3 — Analysis and parameters estimation of the railway electrical line for smart railways.

3.1 Introduction

The knowledge of the power flow in the railway system is of advanced interest to evaluate possible improvements in this transportation sector. Examples of those improvements are, among others, peak power shaving, catenary voltage regulation and unbalance current/voltage minimization.

The desired knowledge extraction algorithm will enable and support strategies for a better management of the energy resources. From the listed research opportunities associated to the topic **T1** presented in chapter 2, it is clear the scientific community paths on the usage of line models for power flow management. One way is to propose specific power flow solver algorithms for the railway electrification, for this knowledge extraction task. Another approach is with the modelling of the catenary as a lumped-parameters π-type line model and the usage of traditional power flow solvers to perform the same knowledge extraction task.

The advantages of the utilization of traditional power flow solvers lies on the ease of implementation of those tools, in which the continuous active support and development of tools like MatPower [69] ensures the solutions to be future-proof. Furthermore and in the particular case of MatPower [69], this solution is also implemented in docker[1], enabling the scalability of the desired applications [134], in which is desirable for the smart railways framework proposed in this thesis.

Being clear the advantages of the usage of a lumped-parameters π-type line model together with a tool for power flow analysis like MatPower, the arising question is if exists a methodology to compare the knowledge produced by the two approaches. To the best knowledge of the author, in respect to the objective of obtaining the power flow knowledge, there is no comparison methodology for the two railway electrification line models.

3.1.1 Non-linear Problem in Load Flow Analysis

The power flow analysis is a non-linear mathematical problem. Considering the Fig. 3.2, the train, V_t, is supplied through the catenary line, Z_l, from a 25 kV TPS, V_s.

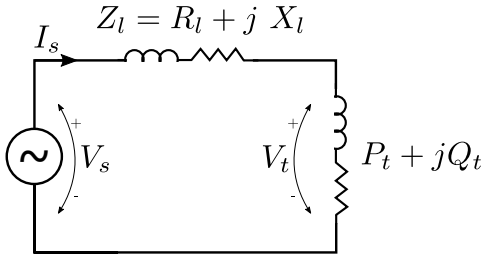

Figure 3.2: Simplified steady state equivalent circuit.

The apparent, active and reactive power flows (S_s, P_s and Q_s, respectively) in the TPS can be obtained from the following expressions:

$$\begin{aligned} S_s &= V_s\ I_s^* \\ &= P_s + jQ_s \end{aligned} \tag{3.1}$$

[1]MatPower docker image: https://hub.docker.com/r/matpower/matpower-desktop

The current in the branch can be expressed as:

$$I_s = \frac{|V_s| - |V_t|\ \cos(\delta) - j|V_t|\ \sin(\delta)}{R_l + jX_l} \tag{3.2}$$

where $V_s = |V_s|\angle 0$ and $V_t = |V_t|\angle\delta$. Thus, replacing the expression in (3.1),

$$\begin{aligned} P_s &= \frac{|V_s|^2 R_l - |V_s|\ |V_t|\ R_l\ \cos(\delta) - |V_s|\ |V_t|\ X_l\ \sin(\delta)}{R_l^2 + X_l^2} \\ Q_s &= \frac{|V_s|^2 X_l + |V_s|\ |V_t|\ R_l\ \sin(\delta) - |V_s|\ |V_t|\ X_l\ \cos(\delta)}{R_l^2 + X_l^2} \end{aligned} \tag{3.3}$$

It can be seen that the active and reactive power flow in the TPS is dependent on the magnitude and phase of the train voltage, as well as on the line characteristics.

Supported by the expression in (3.3), let's consider a variation of the train voltage magnitude (from 15 kV to 30 kV) and the train voltage phase (between $-\pi/4$ to $\pi/4$). Assuming a 1×25 kV electrification of a 30 km line distance and $X/R = 3$, which is common in railway electrification, Fig. 3.3 shows the TPS active and reactive power as a function of the train voltage and phase.

The lines in Fig. 3.3 show the equipotential lines where the power flow at TPS is the same. In particular, in each figure, the lines having, respectively, 0 MW for Fig. 3.3a and 0 MVAr for Fig. 3.3b is highlighted.

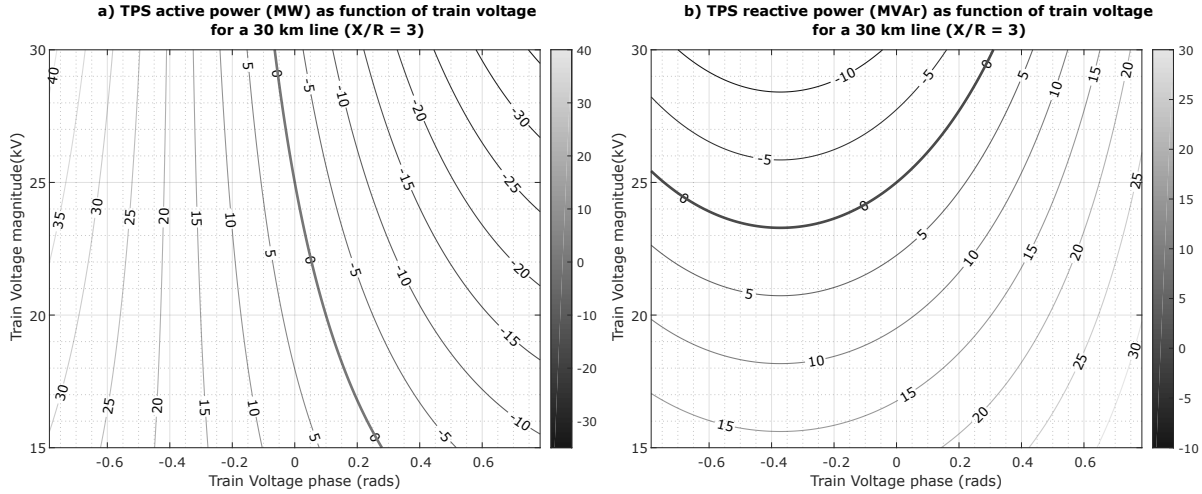

Figure 3.3: Sensibility analysis for different conditions of train voltage and phase: (**a**) Active power flow at TPS; (**b**) Reactive power flow at TPS.

From the analysis of Fig. 3.3a, it is possible to view that a variation on the phase of the train will considerably affect the active power flow in the TPS (the variation of the train voltage is barely related to a variation on active power flow at TPS).

Regarding Fig. 3.3b, it is visible that, for a train voltage phase angle of, around, -0.4 radians, the reactive power only depends on the train voltage.

If the train active and reactive power is obtained from the application of previous sensibility analysis, it is possible to perform a correlation of TPS power flow and train power flow. Specifically, train power is given by:

$$P_t + jQ_t = V_t \; I_s^* \tag{3.4}$$

Replacing the I_s^* by expression in (3.2), it is obtained for P_t and Q_t the following:

$$\begin{aligned} P_t &= \frac{|V_t| \; |V_s| \; R_l \; \cos(\delta) + |V_t| \; |V_s| \; X_l \; \sin(\delta) - |V_t|^2 \; R_l \; \cos(2\delta) - |V_t|^2 \; X_l \; \sin(2\delta)}{R_l^2 + X_l^2} \\ Q_t &= \frac{|V_t| \; |V_s| \; R_l \; \sin(\delta) - |V_t|^2 \; R_l \; \sin(2\delta) + |V_t|^2 \; X_l \; \cos(2\delta) - |V_t| \; |V_s| \; X_l \; \cos(\delta)}{R_l^2 + X_l^2} \end{aligned} \tag{3.5}$$

The TPS active and reactive power can be related to the train power, through a variable change. However, considering the expressions in (3.3) and (3.5), there is no simple mathematical solution that results in the TPS power as a function of the train power.

A simple procedure (to conduct a variable change of the train voltage and phase, to obtain the TPS power, from expression (3.3), and the train power, from expression (3.5)), towards an evaluation of the dependence of TPS power from the train voltage, is considered. The result of this evaluation can be analysed graphically, in Fig. 3.4.

Fig. 3.4a presents equipotential curves of active power at TPS, as a function on the train active and reactive power. In particular, in this result and as expected, it is visible that TPS active power is more dependent on train active power. In Fig.3.4b, the dependence of TPS reactive power is more dependent on the train reactive power.

To conclude, in the previous analysis, a dependence on TPS reactive power and train voltage magnitude are visible. Specifically, by having an inductive reactive power flow in the TPS, the train voltage magnitude will reduce, as visible in Fig. 3.3a. Besides, by changing the train reactive power value, this results in an adaptation of the reactive power in the TPS.

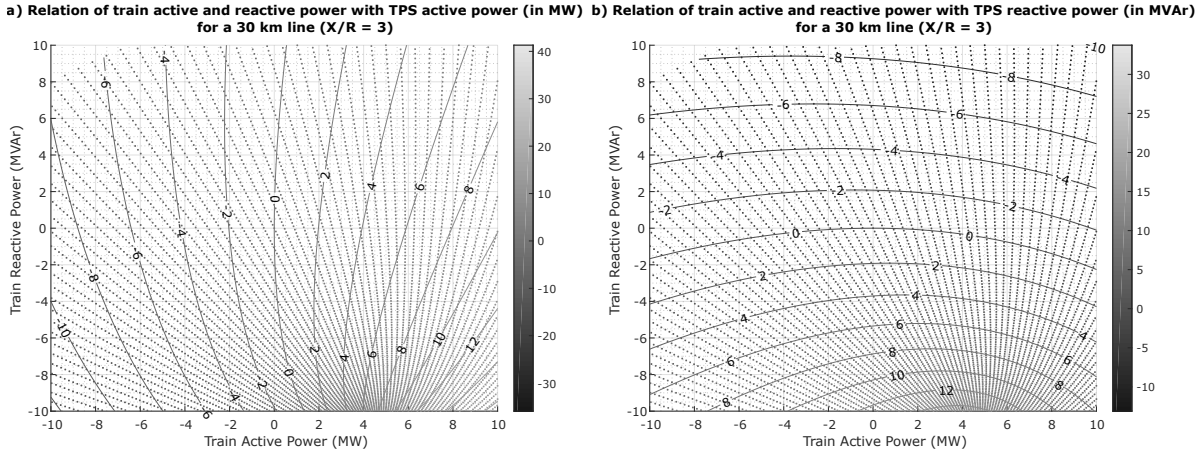

Figure 3.4: Sensibility analysis for different conditions of train power: (**a**) Active power flow at TPS; (**b**) Reactive power flow at TPS.

3.1.2 Need for Iterative-based Solver for Load Flow Analysis

Since there is no simple mathematical solution that results in the TPS power as a function of the train power, this problem needs the usage of iterative-based load flow analysis solvers.

The evaluation of the power flow to increase the knowledge of power systems has been extensively researched and is an essential tool to ensure the stability of power systems [55].

In [66], is proposed the usage of a sequential linear power flow method, in railway power flow calculation, as an advantage over standard Newton-Raphson method. The reference [67] presents the forward/backward sweep load flow method, which is applied to a 2x25 kV electrification system and is supported with field measurements. In [68], is presented a Thevenin-equivalent-based method to solve the power flow, where the node voltage equations are converted into port-characteristic equations, before the usage of the conventional Newton-Raphson method.

For the power flow analysis, a simplified lumped parameters π-type line model is enough. To support this claim, two line models will be tested and, later, important electrical aspects will be compared.

3.1.3 Objective of this Chapter

As presented, the main objective of the first part of this chapter is to compare two models of a railway electric line. This comparison is made through an extensive simulation of parameters and the evaluation of the model differences. Those set of parameters ($\boldsymbol{SP}$) are input parameters of a load-flow analysis tool, presented by the expression in (3.6).

$$\text{Set of parameters: } \boldsymbol{SP} = \begin{cases} \textit{Line distance} & \boldsymbol{d}_L & (\textit{input}) \\ \textit{Train Power} & \boldsymbol{P}_T & (\textit{input}) \\ \textit{Train Power Factor} & \boldsymbol{PF}_T & (\textit{input}) \end{cases} \tag{3.6}$$

The result of the load-flow analysis tool for the $\boldsymbol{SP}$ will be given by the expression in (3.7).

$$\text{Set of results: } \boldsymbol{SR} = \begin{cases} \textit{Train voltage} & \boldsymbol{V}_T & (\textit{output}) \\ \textit{Train current} & \boldsymbol{I}_T & (\textit{output}) \\ \textit{TPS active power} & \boldsymbol{P}_{TPS} & (\textit{output}) \\ \textit{TPS reactive power} & \boldsymbol{Q}_{TPS} & (\textit{output}) \end{cases} \tag{3.7}$$

To better evaluate the model, these parameters can be spawned across a surface of possible parameters $\boldsymbol{S}(\boldsymbol{L}_d, \boldsymbol{P}_T, \boldsymbol{PF}_T) \in \mathbb{R}^3$, where $\boldsymbol{d}_L \in]0 \;\; d_{max}]$, $\boldsymbol{P}_T \in [P_{min} \;\; P_{max}]$ and $\boldsymbol{PF}_T \in [0 \;\; 1]$. The surface of possible parameters has infinite possible solutions.

The result of the first part of this chapter will be the comparison of the four output variables of the load-flow analysis tool, for different input variables. Therefore, since there are an infinite number of solutions for the universe of possible parameters, the strategy for the comparison is to have discrete values for train distances, $\boldsymbol{d}_L$ and train power consumptions, $\boldsymbol{P}_T$. Also, a fixed value for the train power factor ($\boldsymbol{PF}_T = 0.9$ *ind.*) was considered to ease the comparison computational requirements.

In the second part of this chapter, three additional line parameters were considered, as in expression (3.8).

$$\text{Set of parameters: } \boldsymbol{SP} = \begin{cases} \textit{Line distance} \\ \textit{Train Power} \\ \textit{Train Power Factor} \\ \textit{Earth Conductance} \\ \textit{Rail} - \textit{Earth Conductance} \\ \textit{Line Capacitance} \end{cases} \tag{3.8}$$

A sensibility analysis of the errors will be presented. Also, a proposal to reduce the error by compensating the result of the lumped-parameters π-type model simulation. This compensation will be made through the usage of a regression multivariate polynomial surface, which was obtained from the generated comparison errors.

This second part will contribute to a more accurate model for the load-flow analysis. This chapter will be completed with the demonstration and application of the enhanced lumped-parameters π-type line model into a traditional power flow analysis tool.

3.2 Materials and Simulation Frameworks

The railway overhead line will supply the trains, as moving loads. A simple scheme is illustrated in Fig. 3.5, where two sections of the railway line are supplied by two TPS, with single-phase transformers.

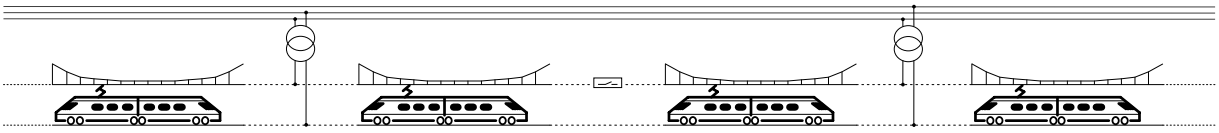

Figure 3.5: Simplified architecture of railway supply overhead line.

In this electrification system, the supply is a radial transmission line, where there is no normal interconnection between sections[2].

In Fig. 3.6 is presented the transversal and longitudinal sections of an overhead catenary system for a single-track railway electrification system.

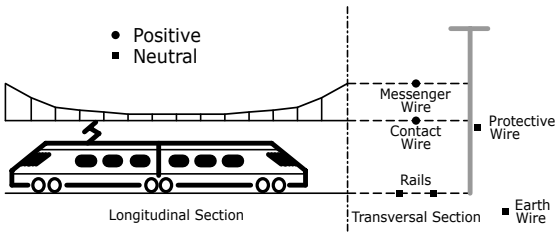

Figure 3.6: Typical conductor distribution of a railway electrification system.

The catenary can be defined as the set of conductors needed to install in an electrified railway line and is composed by all conductors responsible for the energy transport: the positive voltage conductors, the neutral/earth conductors and the negative voltage conductors (in the case of 2x25 kV). The catenary is, therefore, a transmission line.

A transmission line can be characterized by four distributed electric parameters: (i) the series resistance, that depends on the physical construction of the conductor; (ii) the series inductance, that depends on the geometrical arrangement of the cables and is due to the existence of magnetic fields in the conductors' neighbourhood; (iii) shunt capacitance, that also depends on the geometrical arrangement of the cables and is due to the existence of electric fields in the conductors' neighbourhood; and (iv) shunt conductance, that is due to leakage currents from the conductors to the air, soil, isolators, etc.

Due to the very low value of the leakage current (in comparison to the nominal current) and due to the low length of a railway overhead line (considerably less than 80 km), in

[2]Except for degraded operation modes, in which the supply is still radial.

most low-frequency power flow analysis, the shunt capacitance and the shunt conductance can be removed from the model [135, 136].

The series impedance can be transformed into equivalent conductor models since all conductors of the same voltage level are replaced by one equivalent conductor (as the example of messenger and the contact wires in the Fig. 3.6 that can be equivalent to a single positive supply conductor). Besides, assuming that the grounded conductor results in zero voltage[3], the equivalent ground conductor can be eliminated, [55]. This will be defined as the line model with the implicit neutral conductor.

In this section, is presented the details of the implemented models to be later simulated. Initially, the line models are extensively detailed. Later, the train model is presented, where it fulfils decoupled (P, Q) load requirements, with voltage invariance under normal conditions.

3.2.1 Overview of Simulation Models

In Fig. 3.7 is presented an overview of the two models considered in this chapter. Both simulation models have a traction substation, modelled as a simple sinusoidal voltage source of 25 kV rms, 50 Hz. Also, both simulation models consider the train as a constant PQ load, having the model detailed in appendix A, for time domain analysis.

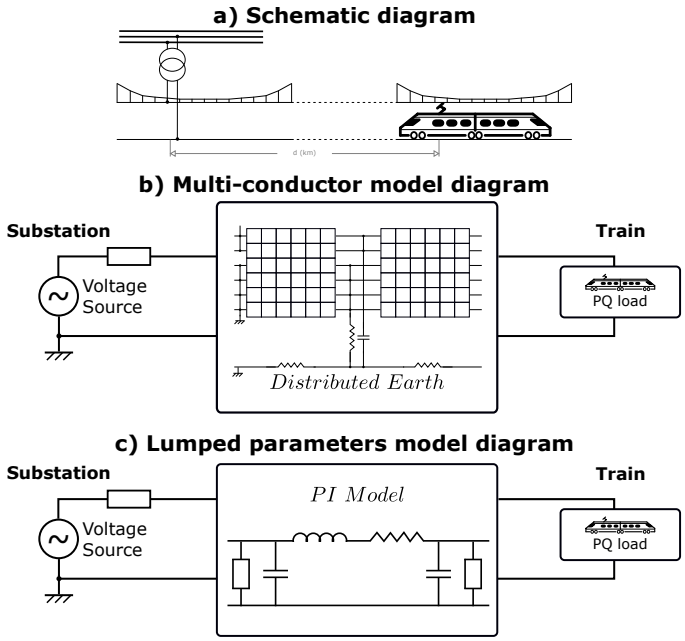

Figure 3.7: Model representation of the 1x25 kV feeding system: a) Illustration of physical representation; b) Multi-conductor model diagram; c) Reduced π-type model diagram.

[3]Which assumption is acceptable: for security reasons, the rail-earth voltages should be minimal [55].

The Multi-conductor Transmission Line (MTL) model is commonly used in railways, where the impedance of the catenary and the rail conductors are much different among them (either mechanically and in terms of the number of cables with different electrical properties, where the positive supply can be made through the catenary and the message wires, and the return of supply is commonly done with the two rails, the buried parallel cable and the aerial earth connection).

Considering a line composed of infinitesimal elements having the equivalent circuit of Fig. 3.8, a line section is a continuous distributed parameter system described by a set of partial differential equations, (3.9) and (3.10).

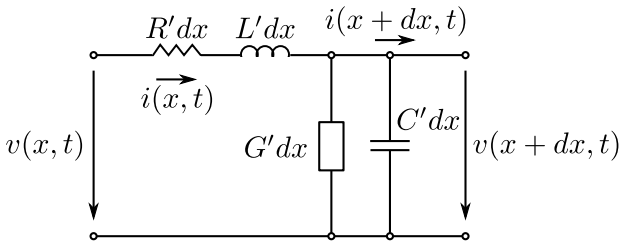

Figure 3.8: Equivalent circuit of a line section of infinitesimal length dx. Adapted from [137].

$$-\frac{dv}{dx} = R'i + L'\frac{di}{dt} \tag{3.9}$$

$$-\frac{di}{dx} = G'v + C'\frac{dv}{dt} \tag{3.10}$$

Where the R', L', G' and C' are non-constant line parameters (dependent on the frequency).

Being the lumped parameters of a overhead catenary line represented by the line series impedance, for the desired simplification, the capacitance and conductance can be discarded.

Considering the typical conductor distribution of a 1x25 kV electrification system, presented in Fig. 3.6, for this single-phase line in steady-state alternating current, the voltage drop is given by (3.11), where $[V]$ and $[I]$ are the vector of phasors of the voltages from catenary to ground and the vector of phasors of the currents flowing in the conductor, respectively, considering the earth to be a node on which all voltages are referred.

$$-\left[\frac{dV}{dx}\right] = [Z']\,[I] \tag{3.11}$$

The matrix $[Z']$ is the series impedance matrix (complex and symmetrical). On the matrix main diagonal, the elements correspond to the impedance, per unit length, of the ring formed by the ith conductor and earth return, Z'_{ii}. Outside of the diagonal, the elements are equal to the mutual impedance, per unit length, between the ith and the kth conductor Z'_{ik}. These values determine the induced voltage in k if a current flows in conductor i and vice versa [138].

To obtain the Z'_{ii} and Z'_{ik}, the approach is to use the Carson formulas, with reference to Fig. 3.9:

$$Z'_{ii} = \left(R'_{i-int} + \Delta R'_{ii}\right) + j\left(\omega\frac{\mu_0}{2\pi}\ln\frac{2h_i}{r_i} + X'_{i-int} + \Delta X'_{ii}\right) \tag{3.12}$$

$$Z'_{ik} = Z'_{ki} = \Delta R'_{ik} + j\left(\omega\frac{\mu_0}{2\pi}\ln\frac{D_{ik}}{d_{ik}} + \Delta X'_{ik}\right) \tag{3.13}$$

Having the description of adopted symbols as following:

μ_0 the permeability of the vacuum;

R'_{i-int} the internal resistance value of the ith conductor in the alternating current;

X'_{i-int} the internal reactance value of the ith conductor;

h_i the average height value of the ith conductor, from the ground;

r_i the radius of the ith conductor;

d_{ik} the distance separating the ith conductor and the kth conductor;

D_{ik} the distance separating the ith conductor and the imaginary kth conductor;

ω nominal angular frequency;

$\Delta R'_{ii}$ and $\Delta X'_{ii}$ are the Carson correction factors for Z'_{ii} terms (proposed in [139], with railway application in [55]);

$\Delta R'_{ik}$ and $\Delta X'_{ik}$ are the Carson correction factors for Z'_{ik} terms (proposed in [139], with railway application in [55]);

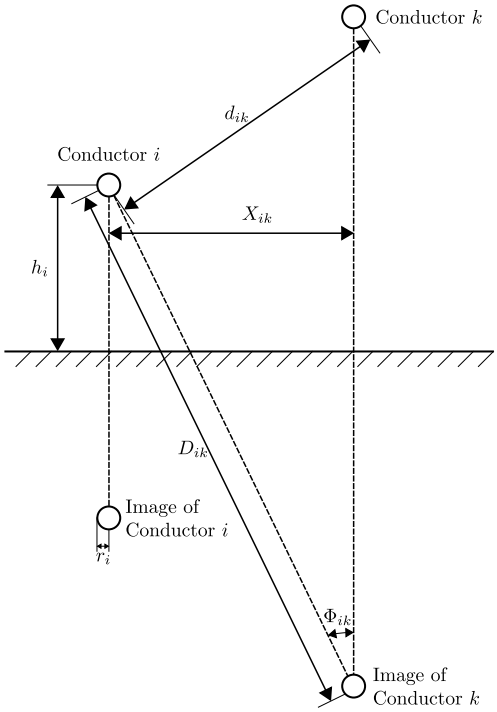

Figure 3.9: Graphical representation of Carson conductor's arrangement [139].

3.2.2 Multi-conductor Model for 1x25 kV Electrification

From (3.11), for the 1x25 kV scheme in Fig. 3.6, the voltage drop in the catenary is given by:

$$\begin{bmatrix} V_{cw} \\ V_{mw} \\ V_{r1} \\ V_{r2} \\ V_{ew} \\ V_{pw} \end{bmatrix} = \begin{bmatrix} Z_{cw,cw} & Z_{cw,mw} & Z_{cw,r1} & Z_{cw,r2} & Z_{cw,ew} & Z_{cw,pw} \\ Z_{mw,cw} & Z_{mw,mw} & Z_{mw,r1} & Z_{mw,r2} & Z_{mw,ew} & Z_{mw,pw} \\ Z_{r1,cw} & Z_{r1,mw} & Z_{r1,r1} & Z_{r1,r2} & Z_{r1,ew} & Z_{r1,pw} \\ Z_{r2,cw} & Z_{r2,mw} & Z_{r2,r1} & Z_{r2,r2} & Z_{r2,ew} & Z_{r2,pw} \\ Z_{ew,cw} & Z_{ew,mw} & Z_{ew,r1} & Z_{ew,r2} & Z_{ew,ew} & Z_{ew,pw} \\ Z_{pw,cw} & Z_{pw,mw} & Z_{pw,r1} & Z_{pw,r2} & Z_{pw,ew} & Z_{pw,pw} \end{bmatrix} \cdot \begin{bmatrix} I_{cw} \\ I_{mw} \\ I_{r1} \\ I_{r2} \\ I_{ew} \\ I_{pw} \end{bmatrix} \tag{3.14}$$

where the description of the symbols and typical examples are as following:

cw is the contact wire (example: copper alloy of 107 mm^2);

mw is the messenger wire (example: brass alloy of 65 mm^2);

$r1$, $r2$ are the rails (example: steel alloy, UIC 54 kg/m);

ew is the buried earth wire (example: copper alloy of 48 mm^2);

pw is the protective aerial earth wire (example: aluminium alloy of 93 mm^2);

As previously presented, the 1x25 kV railway electrification is composed of a positive supply and a return system. To reduce the system of equations in (3.14) to a 2x2 impedance matrix, one approach is to convert the matrix $\mathbf{Z}$ to a matrix of admittances $\mathbf{Y}$, then calculate the reduction as extensively illustrated in [55] and later, convert back the resulting matrix of admittances to a 2x2 matrix of impedances.

Since the admittance matrix is given by the inversion of the impedance matrix, then

$$\begin{bmatrix} Y_{cw,cw} & Y_{cw,mw} & Y_{cw,r1} & Y_{cw,r2} & Y_{cw,ew} & Y_{cw,pw} \\ Y_{mw,cw} & Y_{mw,mw} & Y_{mw,r1} & Y_{mw,r2} & Y_{mw,ew} & Y_{mw,pw} \\ Y_{r1,cw} & Y_{r1,mw} & Y_{r1,r1} & Y_{r1,r2} & Y_{r1,ew} & Y_{r1,pw} \\ Y_{r2,cw} & Y_{r2,mw} & Y_{r2,r1} & Y_{r2,r2} & Y_{r2,ew} & Y_{r2,pw} \\ Y_{ew,cw} & Y_{ew,mw} & Y_{ew,r1} & Y_{ew,r2} & Y_{ew,ew} & Y_{ew,pw} \\ Y_{pw,cw} & Y_{pw,mw} & Y_{pw,r1} & Y_{pw,r2} & Y_{pw,ew} & Y_{pw,pw} \end{bmatrix} \cdot \begin{bmatrix} V_{\mathrm{cw}} \\ V_{\mathrm{mw}} \\ V_{\mathrm{r1}} \\ V_{\mathrm{r2}} \\ V_{\mathrm{ew}} \\ V_{\mathrm{pw}} \end{bmatrix} = \begin{bmatrix} I_{\mathrm{cw}} \\ I_{\mathrm{mw}} \\ I_{\mathrm{r1}} \\ I_{\mathrm{r2}} \\ I_{\mathrm{ew}} \\ I_{\mathrm{pw}} \end{bmatrix} \tag{3.15}$$

The reduction of the matrix to a 2x2 matrix is given by the sum of the admittances of the same group as identified in (3.15) and giving the result in (3.16):

$$Y_{\boxplus} = \begin{bmatrix} \sum_{m=cw}^{mw} \sum_{n=cw}^{mw} Y_{m,n} & \sum_{m=cw}^{mw} \sum_{n=r1}^{pw} Y_{m,n} \\ \sum_{m=r1}^{pw} \sum_{n=cw}^{mw} Y_{m,n} & \sum_{m=r1}^{pw} \sum_{n=r1}^{pw} Y_{m,n} \end{bmatrix} \tag{3.16}$$

Finally, the inversion of the admittance matrix will result in the impedance matrix, achieving (3.17).

$$\begin{bmatrix} V_{\mathrm{p}} \\ V_{\mathrm{g}} \end{bmatrix} = \begin{bmatrix} Z_{pp} & Z_{pg} \\ Z_{gp} & Z_{gg} \end{bmatrix} \cdot \begin{bmatrix} I_{\mathrm{p}} \\ I_{\mathrm{g}} \end{bmatrix} \tag{3.17}$$

Where I_p is the current in the positive wires (cw and mw) and I_g is the current in the ground return wires ($r1$, $r2$, ew and pw). The final reduction is shown in Fig. 3.10.

Considering the multi-conductor model diagram in Fig. 3.10, one important assumption is to consider that the supply positive current, I_p, is equal in absolute value to the return ground current, I_g. Therefore, this can be reduced to one single conductor, considering the magnetic coupling as a series-opposing inductor [140]. The π-type model parameters, Fig. 3.7c), are obtained from the multi-conductor model in equation (3.17), with the application of the reduction in (3.18).

$$Z_{\pi} = Z_{pp} + Z_{gg} - 2\ Z_{pg} \tag{3.18}$$

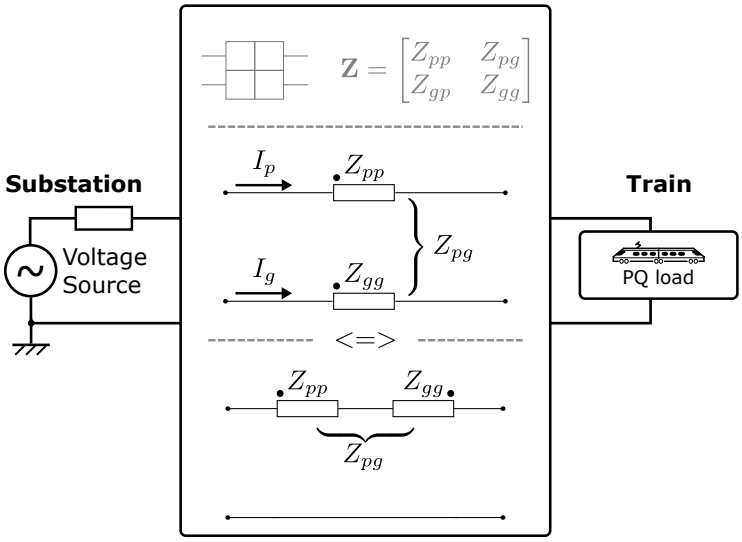

Figure 3.10: Reduced multi-conductor model of the 1x25 kV feeding system.

Previously, the steps to obtain the $\boldsymbol{Z}_{\boxplus}$ and the $\boldsymbol{Z}_{\pi}$ impedance line models were detailed.

To achieve the objectives of this chapter, it was developed a time-domain simulation model, in Simulink, that considers the MTL line model of Fig. 3.7 for the catenary. This Simulink simulation model is divided into three parts: the substation (modelled as a 25 kV voltage source), the catenary line and the train load (described in appendix A).

In the following section, the comparison methodology is presented.

3.3 Comparison Methodology

The objective for this section is to present a comparison methodology to evaluate two line models. The complex MTL line model was implemented in Simulink; the lumped-parameters π-type line model was used by the Newton-Raphson solver of MatPower.

3.3.1 Models Comparison Strategy

In the model validation section of appendix A, the two cases tested have one specific active power reference (10 MW) and two specific distances (10 km and 40 km). To properly compare the two catenary line models, several different distance values and train power consumption values will be tested, following the surface of expression in (3.6). As already referred, due to computational power constraints, the power factor was fixed. Therefore, the used testing surface, $\boldsymbol{TS}$, is expressed in (3.19) and illustrated in Fig. 3.11.

$$\boldsymbol{TS} = \begin{cases} \boldsymbol{L}_d & [d_1 \ \cdots \ d_D] \ \ (in \text{ km}) \\ \boldsymbol{P}_T & [p_1 \ \cdots \ p_P] \ \ (in \text{ MW}) \\ \boldsymbol{PF}_T & fixed: \ 0.9 \quad \text{ind.} \end{cases} \tag{3.19}$$

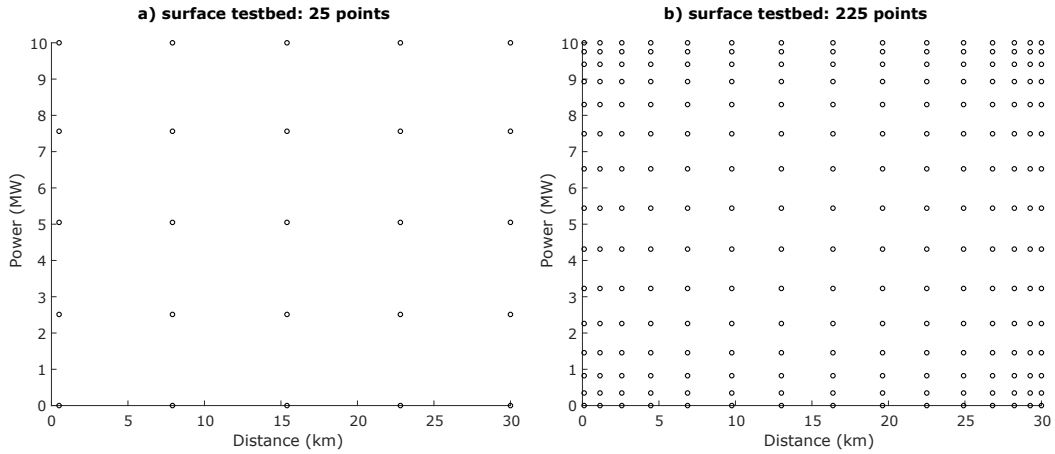

Figure 3.11: Illustration of the tested (power, distance) points: a) [5,5]; b) [15,15].

The comparison methodology considers the repetitive simulation of the two models, by covering the defined testbed surface, as illustrated in Fig. 3.12.

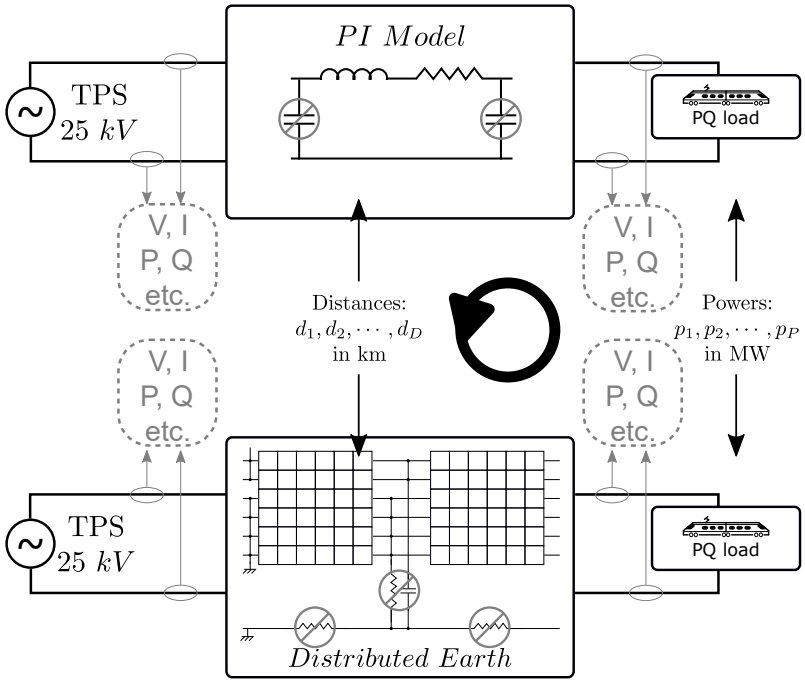

Figure 3.12: Methodology for the models comparison.

In Fig. 3.12, the power flow analysis of the π-type line model is obtained using the Newton-Raphson solver of the MatPower. The MTL line was simulated in Simulink, with a 6x6 impedance matrix, without considering the line capacitance, rail-earth conductance and earth conductance.

This methodology produces a matrix of results $\boldsymbol{RS}$, given by the expression in (3.20), which is illustrated in the following section.

$$\boldsymbol{RS} = \begin{cases} \textit{Train voltage} & \boldsymbol{V}_T \\ \textit{Train current} & \boldsymbol{I}_T \\ \textit{TPS active power} & \boldsymbol{P}_{TPS} \\ \textit{TPS reactive power} & \boldsymbol{Q}_{TPS} \end{cases} \tag{3.20}$$

3.4 Comparison Results and Validation

In the following figures are presented four result surfaces to illustrate the differences between models. Later, in this section, for each of the results, are generated a set of metrics and a histogram to better illustrate the comparison metrics.

The first result is the train voltage, visible in Fig. 3.13.

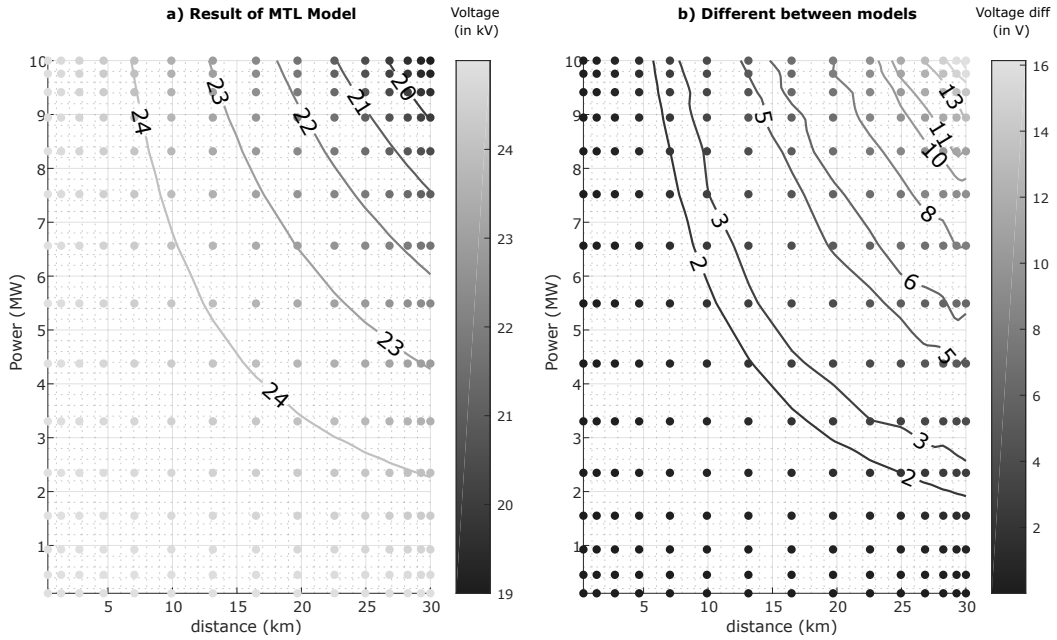

Figure 3.13: Model comparison results for a 15x15 example $\boldsymbol{TS}$ surface: a) Train voltage for multi-conductor model ($\mathbf{RS}_{\boxplus,voltage}$); b) Absolute difference of the two models, ($\mathbf{RS}_{\boxplus,voltage} - \mathbf{RS}_{\pi,voltage}$). Note: the equipotential lines in the graphs represents the values with same level.

In the result of this metric, for the considered ***TS*** surface and for a power factor of 0.9 ind., the rms voltage values seen by the train (each point of Fig. 3.13a)) varies between a minimum of 19 kV and a maximum of 25 kV. The global rms value (obtained from all points of Fig. 3.13a)) for the surface is 23.6 kV. When compared, for a higher catenary voltage drop, the error between models will increase reaching a maximum value of 16.1 V.

Regarding the train current, the results are presented in Fig. 3.14.

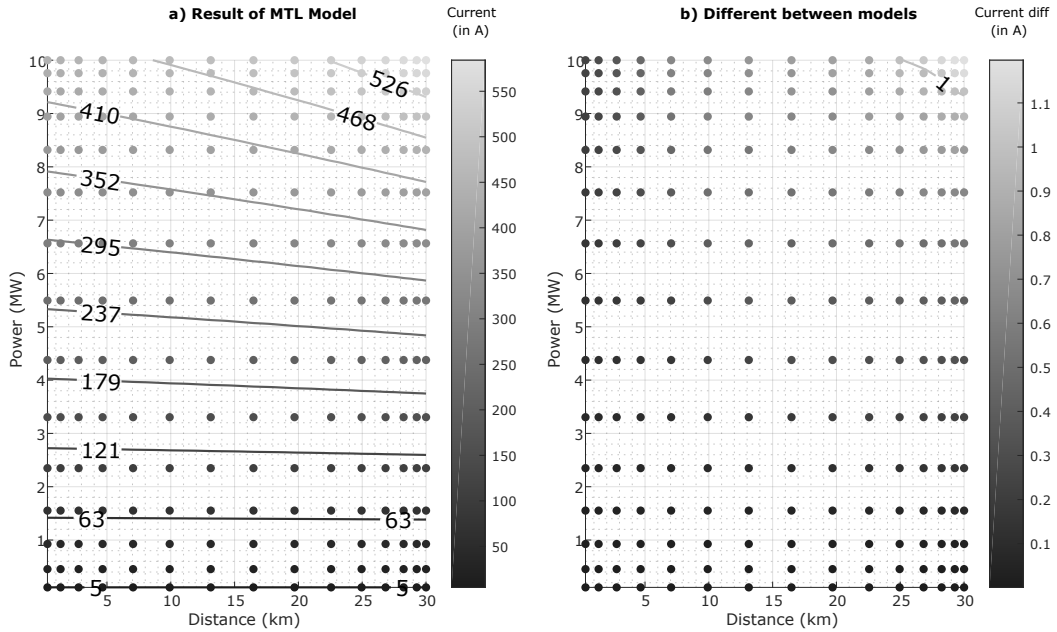

Figure 3.14: Model comparison results for a 15x15 example ***TS*** surface: a) Train current for multi-conductor model ($\mathbf{RS}_{\boxplus,current}$); b) Absolute difference of the two models, ($\mathbf{RS}_{\boxplus,voltage} - \mathbf{RS}_{\pi,current}$).

Here the minimum and maximum current at the train varies approximately between 5 A and 584 A, having an rms value of 312.8 A, resulting in a maximum error between models in the rms current of 1.2 A.

On the TPS side, the important results for a power flow analysis tool are the active and reactive power. Therefore, the result surface for the TPS active power is illustrated in Fig. 3.15.

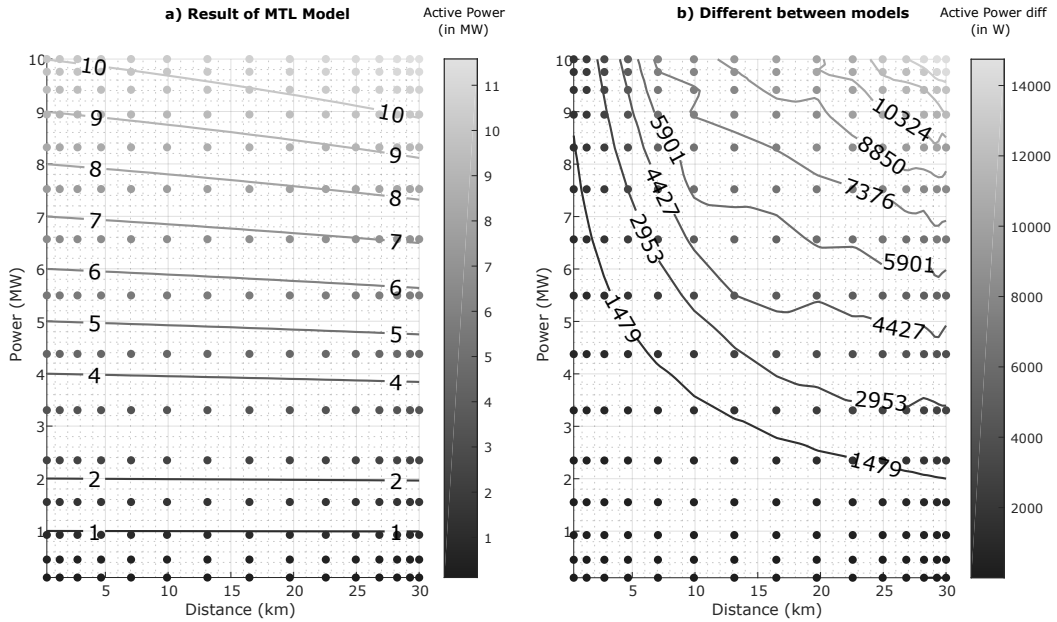

Figure 3.15: Model comparison results for a 15x15 example ***TS*** surface: a) TPS active power for multi-conductor model ($\mathbf{RS}_{\boxplus,TPS_P}$); b) Absolute difference of the two models, ($\mathbf{RS}_{\boxplus,TPS_P} - \mathbf{RS}_{\pi,TPS_P}$).

The TPS active power reaches a maximum 11.6 MW value and a minimum of 112 kW, which results in a maximum error between models of 14.7 kW for the longest distance and the maximum train power. The TPS reactive power results are presented in Fig. 3.16.

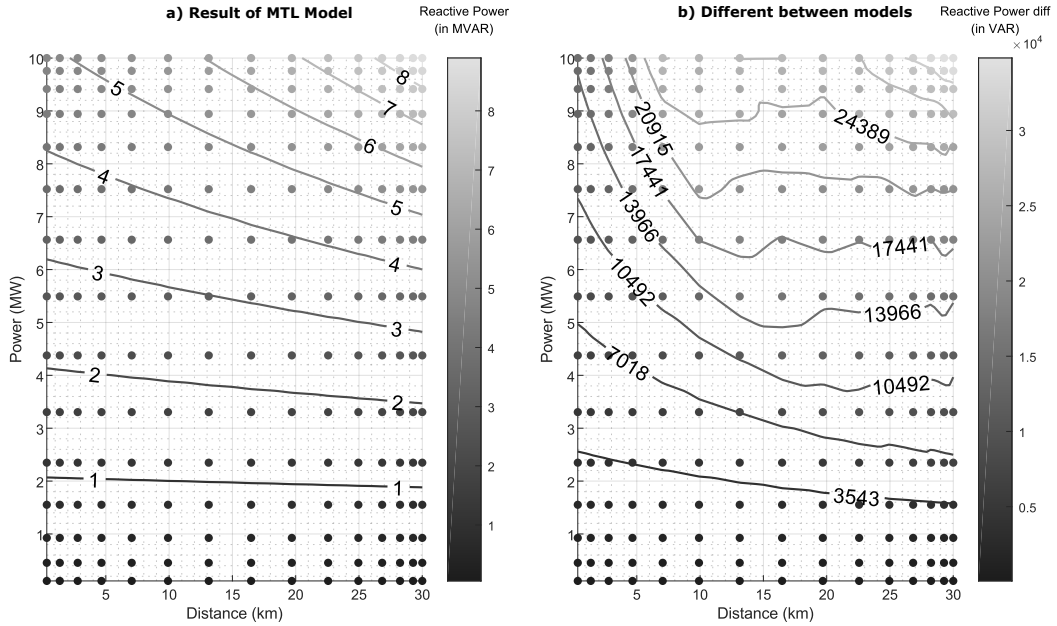

Figure 3.16: Model comparison results for a 15x15 example ***TS*** surface: a) TPS reactive power for multi-conductor model ($\mathbf{RS}_{\boxplus,TPS_Q}$); b) Absolute difference of the two models, ($\mathbf{RS}_{\boxplus,TPS_Q} - \mathbf{RS}_{\pi,TPS_Q}$).

The reactive power at TPS reaches a maximum value of 8.89 MVAr, resulting, at this point, in a maximum difference between models of around 34.8 kVAr.

3.4.1 Comparison Metrics

From the previous errors, the next step is to generate comparison metrics, specifically, the maximum and minimum errors, the Mean Absolute Error (MAE) and the Root Mean Square Error (RMSE), presented in the following expressions:

$$MAX = max(\mathbf{RS}_{\boxplus} - \mathbf{RS}_{\pi}) \tag{3.21}$$

$$MIN = min(\mathbf{RS}_{\boxplus} - \mathbf{RS}_{\pi}) \tag{3.22}$$

$$MAE = \frac{1}{P \cdot D} \sum_{p=1}^{P} \sum_{d=1}^{D} |\mathbf{RS}_{\boxplus}[p,d] - \mathbf{RS}_{\pi}[p,d]| \tag{3.23}$$

$$RMSE = \sqrt{\frac{1}{P \cdot D} \sum_{p=1}^{P} \sum_{d=1}^{D} (\mathbf{RS}_{\boxplus}[p,d] - \mathbf{RS}_{\pi}[p,d])^2} \tag{3.24}$$

These comparison metrics are absolute metrics. A relative metric will consider the rms value of the result matrix, $RMS(\mathbf{RS}_{\boxplus})$ and the RMSE value from expression in 3.24. This Relative Percentage Error (RPE) is given in the expression in (3.25).

$$RPE = \frac{RMSE}{RMS(\mathbf{RS}_{\boxplus})} \tag{3.25}$$

In Table 3.1 is presented the results for the models comparison. The first six rows of the table present a summary from the figures of the model comparison results (Fig. 3.13 to Fig. 3.16).

Table 3.1: Results for the model comparison.

	TRAIN		TPS	
	voltage	current	active power	reactive power
MAX($\mathbf{RS}_{\boxplus}$)	25.0 kV	584 A	11.6 MW	8.89 MVAr
MIN($\mathbf{RS}_{\boxplus}$)	19.0 kV	4.97 A	112 kW	54.1 kVAr
RMS($\mathbf{RS}_{\boxplus}$)	23.6 kV	312.8 A	6.69 MW	4.04 MVAr
MAX($\mathbf{RS}_{\pi}$)	25.0 kV	585 A	11.6 MW	8.93 MVAr
MIN($\mathbf{RS}_{\pi}$)	19.0 kV	4.97 A	112 kW	54.2 kVAr
RMS($\mathbf{RS}_{\pi}$)	23.7 kV	313.2 A	6.70 MW	4.06 MVAr
MIN (3.22)	2.94 mV	-1.20 A	-14.7 kW	-34.8 kVAr
MAX (3.21)	16.1 V	-0.75 mA	6.44 W	-69.0 VAr
MAE (3.23)	3.40 V	-0.342 A	-4.05 kW	-12.9 kVAr
RMSE (3.24)	5.32 V	0.465 A	5.72 kW	16.4 kVAr
RPE (3.25)	0.02 %	0.15 %	0.09 %	0.41 %

Regarding the metrics, the MIN and the MAX metrics gives an overview if the resultant error is positive or negative. Is visible a near-zero value for the minimum train voltage and the maximum train current and TPS power. This is better illustrated in the histogram graph of Fig. 3.17.

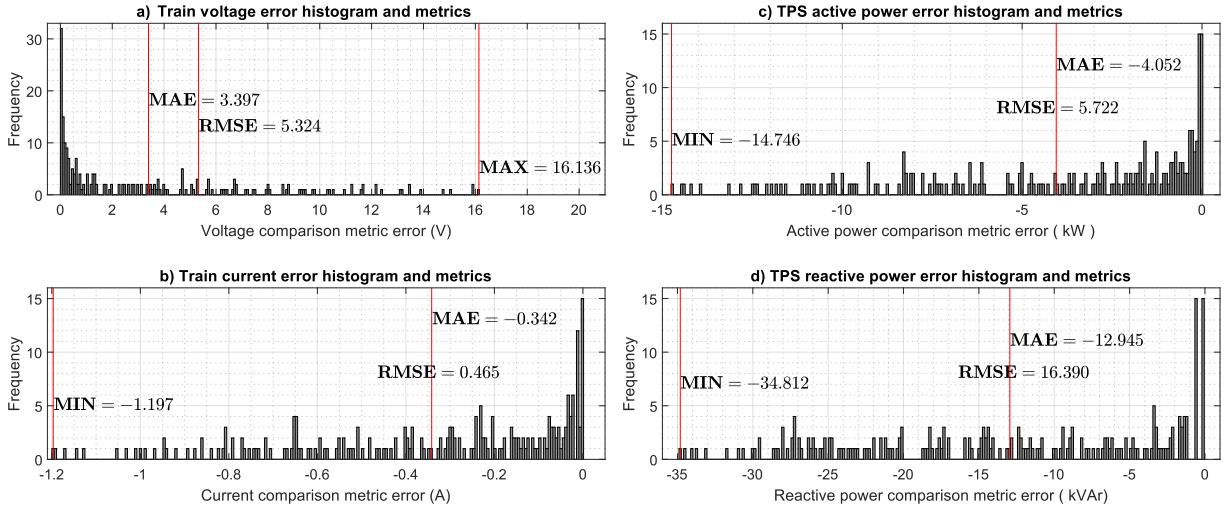

Figure 3.17: Histogram graphs for the result surfaces and respective metrics.

The RPE values show that the line models in the study are similar, with a maximum RPE of 0.41 % for the **TS** in 3.19.

In this part of this chapter were presented the steps to compare a rail line model, without considering the transversal admittances (line capacitance, rail-earth conductance, earth conductance).

In the following part, these transversal admittances will be considered, a methodology to estimate the error through a polynomial fitting is proposed, and the application of this enhanced model in a tradition power flow tool will be clarified and demonstrated.

3.5 Methodology for Enhanced Railway π-type Line Model

The methodology for this part is essentially based on the outcomes of the first part, in Fig. 3.12, considering now a sensibility analysis on line transversal admittances. Specifically, in Fig. 3.18 is illustrated the proposed enhancement of the railway π-type line model, by having adjustment based on the results of the sensibility analysis.

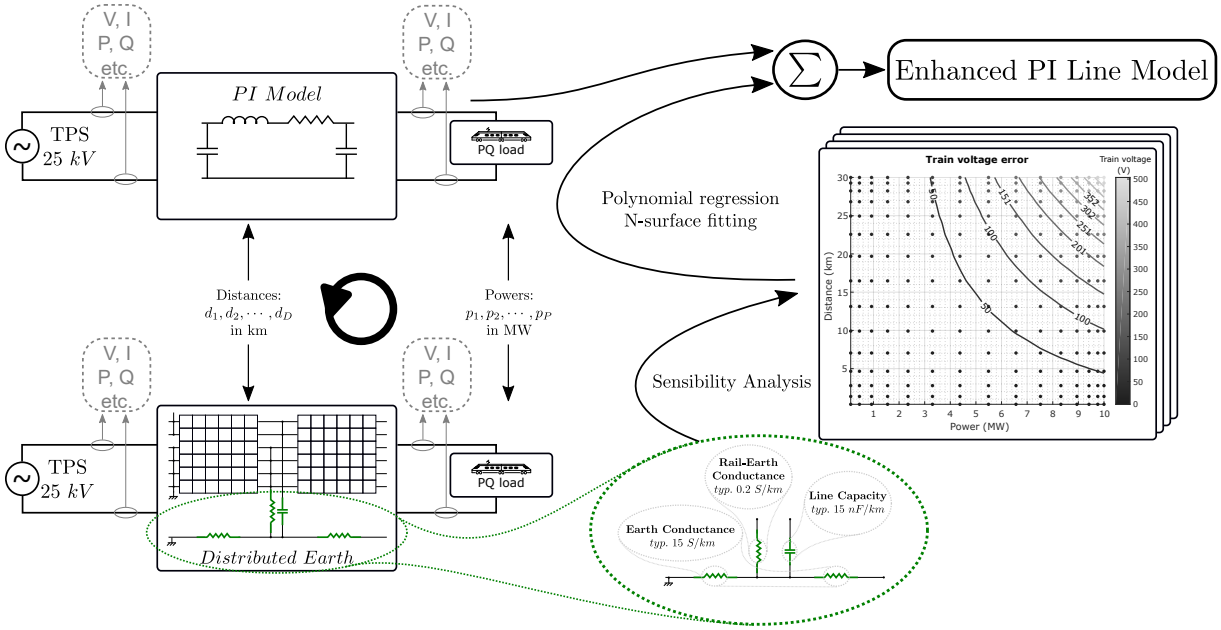

Figure 3.18: Methodology to obtain the Enhanced π-type Line Model.

This enhancement is based on two steps: i) a sensibility analysis on the line transversal admittances, and ii) a fitting of the N^{th} dimensional surface error through a polynomial regression function.

From the literature, there are three parameters for the sensibility analysis step to consider the effect of having the electrical circuit in close contact to the earth: a) the longitudinal earth conductance, that considers the longitudinal current flow through the earth; b) the transversal rail-earth conductance, that describes the current flow from the rails to the earth through the ballast; and c) the catenary-ground capacitance, that represents the capacitive effect of the conductors parallel to a ground surface.

According to [141], the Earth Conductance (EC) can vary from 10 S/km and 20 S/km, being around 1 S/km for the ground of sand-filled tunnels (the higher the ground conductance, the better the grounding). The used Earth conductance parameters are visible in Table 3.2.

Regarding the Rail-Earth conductance (RE), this value depends on the ageing of the rails and the ballast as described in [141], where a recently constructed at the time of the publication Italian high-speed rail has very low rail-earth conductance (between 0.02 S/km and 0.05 S/km). The ageing of the rubber pads (between rail and ballast) increase the conductance, as well as the environmental factors (soil moisture, etc.). Therefore, typical values for these conductances are 0.2 S/km and the worst case is 1 S/km. Contrarily to the EC, the higher the RE conductance, the poorer the quality of the line. In Table 3.2 is presented the used parameters.

The Line Capacitance (LC) matrix can be obtained from the method of the images, by assuming soil and ballast as a perfect ground, with experimental data showing variations bellow 10 % [142]. Thus, the capacitance matrix can be reduced to a single equivalent parameter. In [17] are referred the values 11 nF/km to 14 nF/km in single track and 18 nF/km to 20 nF/km in double track. In a typical 16.7 Hz electrification is referred 20 nF/km [143] and [144]. In Table 3.2 is presented the used parameters.

Table 3.2: Discretization of parameters for the sensibility analysis. In bold is highlighted the typical values.

	range	unit
Earth Conductance	[40 30 20 **15** 10 5 1 0.5]	S/km
Rail-Earth Conductance	[0.01 0.02 0.05 0.1 **0.2** 0.5 1 2]	S/km
Line Capacitance	[0.2 2 5 10 12.5 **15** 17.5 20 30]	nF/km

The first step in this second part methodology is to test and compare the models for different parameters, through a sensibility analysis, resulting in surfaces of errors. The second step is to generate a fitting of the N^{th} dimensional surface errors through a polynomial regression function.

To achieve the goals of the second step, it was used a multivariate polynomial regression tool developed in [145], and applied in [146, 147]. This tool extracts the k^{th} degree polynomial coefficients from a N^{th} dimensional multivariate surface. Specifically, in this work, the polynomial function will have $k = 6$ and for a maximum $N = 3$, this assumes the form:

$$
\begin{aligned}
f(x_1, x_2, x_3) = k_0 \; + \\
& k_1 \; x_1 + \cdots + k_{..} \; {x_1}^6 \; + \\
& k_{..} \; x_2 + k_{..} \; x_1 \; x_2 + \cdots + k_{..} \; x_1^5 \; x_2 \; + \\
& + \cdots + \\
& k_{..} \; (x_3)^5 \; x_1 + k_{..} \; (x_3)^5 \; x_2 \; + \\
& k_{..} \; (x_3)^6
\end{aligned}
\tag{3.26}
$$

In the following section are presented the results of the sensibility analysis, together with the coefficients of the multivariate polynomial regression curve, to be later used to enhance the π-type line model.

3.6 Results of Enhanced Railway π-type Line Model

The surface of testing parameters to perform the desired enhanced railway π-type line model are given by the expression in 3.27.

$$
\boldsymbol{TS}_{\infty} = \begin{cases}
\boldsymbol{L_d} & [d_1 \; \cdots \; \cdots \; \cdots \; \cdots \; d_D] \quad (in \text{ km}) \\
\boldsymbol{P}_T & [p_1 \; \cdots \; \cdots \; \cdots \; \cdots \; p_P] \quad (in \text{ MW}) \\
\boldsymbol{PF}_T & [PF_{ind.} \; \cdots \; 1 \; \cdots \; PF_{cap.}] \\
\boldsymbol{EC} & [40 \; \cdots \; \cdots \; \cdots \; \cdots \; 0.5] \quad (in \; S/\text{km}) \\
\boldsymbol{RE} & [0.01 \; \cdots \; \cdots \; \cdots \; \cdots \; 2] \quad (in \; S/\text{km}) \\
\boldsymbol{LC} & [0.2 \; \cdots \; \cdots \; \cdots \; \cdots \; 30] \quad (in \; nF/\text{km})
\end{cases}
\tag{3.27}
$$

The coverage of all possible results of this testing surface are in the universe $\mathbb{R}^6$. For an easy evaluation of the results, first the power factor is fixed, similarly to the results of Part A. Later, each of the line transversal admittances are evaluated independently.

3.6.1 Baseline

As a preliminary result, the baseline will consider the evaluation of the testing surface given by the expression in 3.28, where $\boldsymbol{TS}_0 \in \mathbb{R}^2$.

$$\boldsymbol{TS}_0 = \begin{cases} \boldsymbol{L}_d & [d_1 \ \cdots \ \cdots \ \cdots \ \cdots \ d_D] \quad (in \text{ km}) \\ \boldsymbol{P}_T & [p_1 \ \cdots \ \cdots \ \cdots \ \cdots \ p_P] \quad (in \text{ MW}) \\ \boldsymbol{PF}_T & fixed: \ 0.9 \ ind. \\ \boldsymbol{EC} & fixed: \ 15 \quad (in \ S/\text{km}) \\ \boldsymbol{RE} & fixed: \ 0.2 \quad (in \ S/\text{km}) \\ \boldsymbol{LC} & fixed: \ 15 \quad (in \ nF/\text{km}) \end{cases} \tag{3.28}$$

The application of the proposed $\boldsymbol{TS}_0$ will result in the Fig. 3.19.

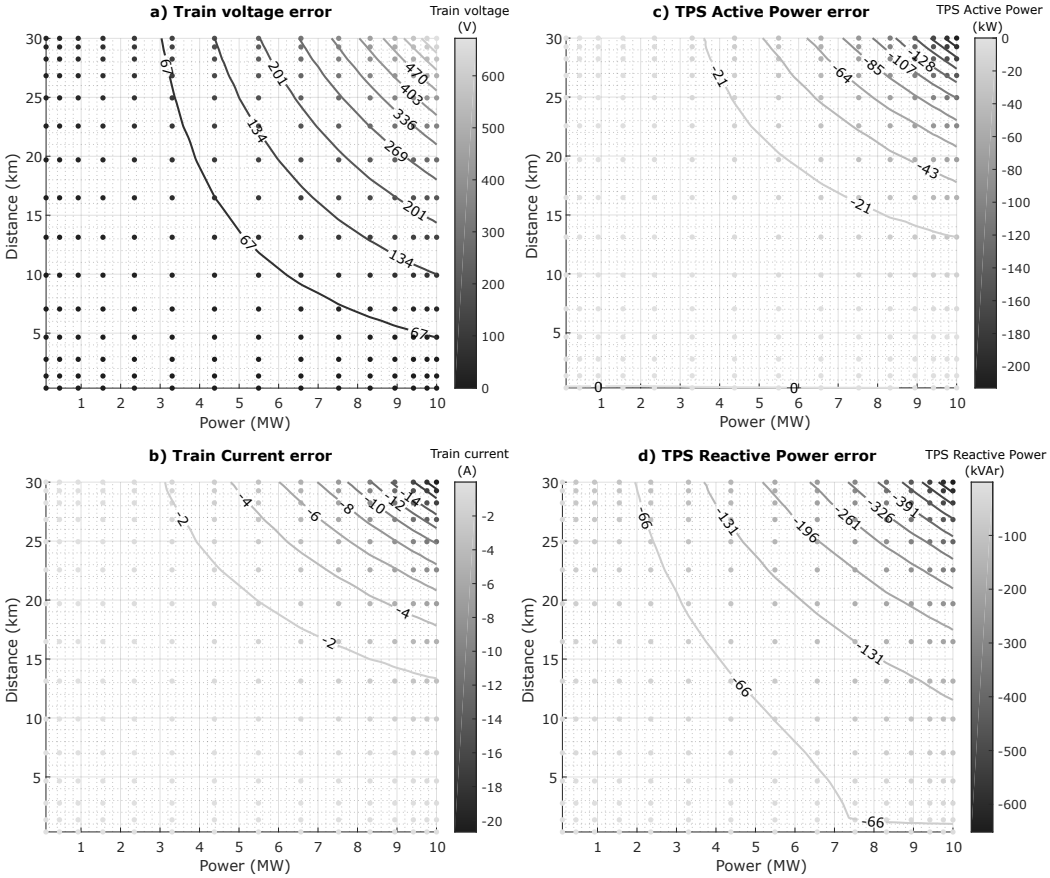

Figure 3.19: Model comparison results for the $\boldsymbol{TS}_0$ surface: a) Train voltage error; b) Train current error; c) TPS active power error; d) TPS reactive power error.

Then, the metrics are present in Table 3.3.

Table 3.3: Result metrics for the model comparison for the $\boldsymbol{TS}_0$.

	TRAIN		TPS	
	voltage	current	active power	reactive power
MAX($\mathbf{RS}_{\boxplus}$)	25.0 kV	585.3 A	11.6 MW	8.93 MVAr
MIN($\mathbf{RS}_{\boxplus}$)	19.0 kV	4.97 A	112 kW	54.2 kVAr
RMS($\mathbf{RS}_{\boxplus}$)	23.7 kV	313.2 A	6.70 MW	4.06 MVAr
MAX($\mathbf{RS}_{\pi}$)	25.0 kV	564.6 A	11.4 MW	8.27 MVAr
MIN($\mathbf{RS}_{\pi}$)	19.7 kV	4.97 A	112 kW	3.67 kVAr
RMS($\mathbf{RS}_{\pi}$)	23.8 kV	309.5 A	6.66 MW	3.90 MVAr
MIN (3.22)	-672 V	74 mA	-8.5 W	1.06 kVAr
MAX (3.21)	0.5 V	20.7 A	213 W	651 kVAr
MAE (3.23)	119 V	2.57 A	26.1 kW	123 kVAr
RMSE (3.24)	198 V	4.97 A	51.5 kW	184 kVAr
RPE (3.25)	0.84 %	1.59 %	0.77 %	4.53 %

The inclusion of typical values for the capacitance and conductance will affect negatively the metrics where, for example, the TPS reactive power is now 4.53 % (without this inclusion, the error was 0.41 %).

In Fig. 3.20 is presented the histogram errors before and after the enhancement application of the π-type line model.

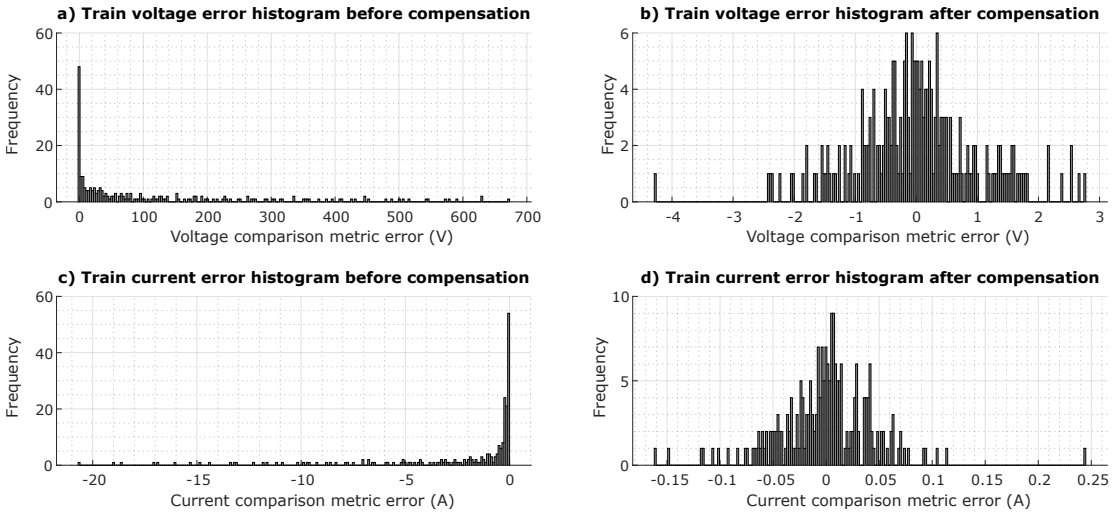

Figure 3.20: Histogram of the errors before and after the application of the methodology for the $\boldsymbol{TS}_0$ surface. (Continued on next page).

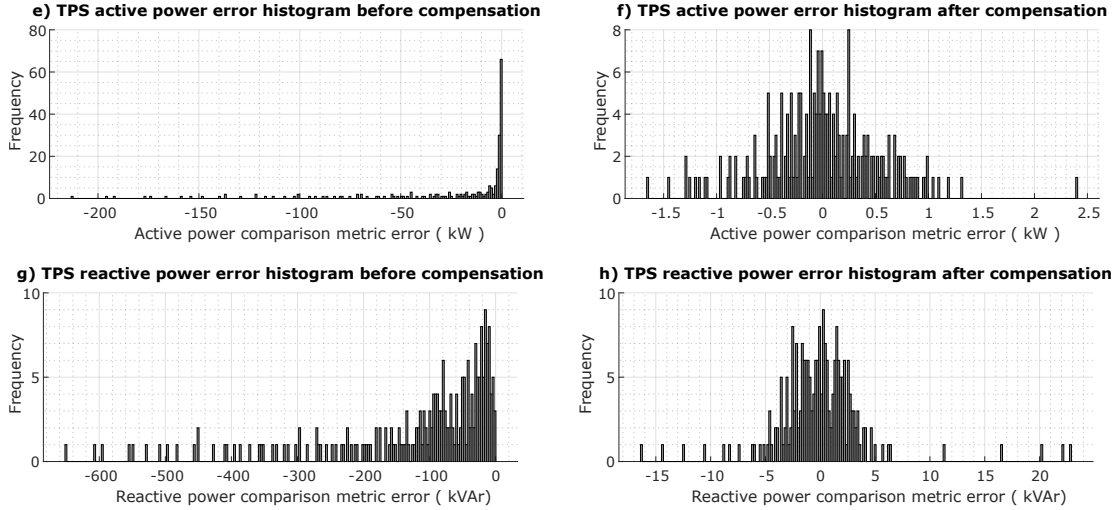

Figure 3.20: Histogram of the errors before and after the application of the methodology for the $\boldsymbol{TS}_0$ surface. (Continued from previous page).

The visible drastic reduction in the errors of each power flow value is made with the application of the function $f(\boldsymbol{P}_T, \boldsymbol{L}_d)$, where the coefficients are presented in Table 3.4.

Table 3.4: List of generated coefficients, for the $\boldsymbol{TS}_0$ surface.

	TRAIN		TPS	
	voltage	current	active power	reactive power
$(\boldsymbol{L}_d)$	-1.60857E+00	1.00375E-01	4.56987E+02	4.32744E+02
$(\boldsymbol{L}_d)^2$	2.29615E-01	-1.71796E-02	1.69142E+01	-7.46801E+02
$(\boldsymbol{L}_d)^3$	-7.92918E-03	1.44390E-03	-1.12000E+01	8.16610E+01
$(\boldsymbol{L}_d)^4$	-1.15965E-04	-6.76095E-05	9.36166E-01	-4.61993E+00
$(\boldsymbol{L}_d)^5$	1.28734E-05	1.67775E-06	-3.04046E-02	1.37461E-01
$(\boldsymbol{P}_T)$	-5.75200E+00	3.62436E-01	3.53759E+03	-4.32039E+03
$(\boldsymbol{P}_T) * (\boldsymbol{L}_d)$	1.78956E+00	-1.38335E-01	-1.33497E+03	-3.56577E+03
$(\boldsymbol{P}_T) * (\boldsymbol{L}_d)^2$	-4.79286E-02	1.31125E-02	1.30364E+02	2.46360E+02
$(\boldsymbol{P}_T) * (\boldsymbol{L}_d)^3$	-4.35064E-04	-4.84781E-04	-5.11902E+00	-9.98079E+00
$(\boldsymbol{P}_T) * (\boldsymbol{L}_d)^4$	9.33866E-05	6.66315E-06	8.31798E-02	-3.75197E-02
$(\boldsymbol{P}_T) * (\boldsymbol{L}_d)^5$	-1.66814E-06	-1.49811E-08	-4.19536E-04	2.91275E-03
$(\boldsymbol{P}_T)^2$	3.37183E+00	-2.32193E-01	-2.24747E+03	9.02271E+03
$(\boldsymbol{P}_T)^2 * (\boldsymbol{L}_d)$	-8.67164E-01	5.41955E-02	5.40906E+02	1.83751E+03
$(\boldsymbol{P}_T)^2 * (\boldsymbol{L}_d)^2$	6.65939E-02	-3.99051E-03	-4.11322E+01	-6.83170E+01
$(\boldsymbol{P}_T)^2 * (\boldsymbol{L}_d)^3$	-1.85088E-03	1.08032E-04	1.12340E+00	3.21431E+00
$(\boldsymbol{P}_T)^2 * (\boldsymbol{L}_d)^4$	1.79642E-05	-1.00017E-06	-1.04825E-02	-2.80985E-02
$(\boldsymbol{P}_T)^3$	-8.44914E-01	6.11423E-02	5.91521E+02	-5.21831E+03
$(\boldsymbol{P}_T)^3 * (\boldsymbol{L}_d)$	1.20217E-01	-8.14097E-03	-7.83445E+01	-4.20281E+02
$(\boldsymbol{P}_T)^3 * (\boldsymbol{L}_d)^2$	-5.51220E-03	3.45221E-04	3.42144E+00	3.22464E+00
$(\boldsymbol{P}_T)^3 * (\boldsymbol{L}_d)^3$	7.83892E-05	-4.47849E-06	-4.46540E-02	-1.33187E-01
$(\boldsymbol{P}_T)^4$	1.11341E-01	-8.27556E-03	-8.05884E+01	1.18759E+03
$(\boldsymbol{P}_T)^4 * (\boldsymbol{L}_d)$	-7.51877E-03	5.42811E-04	5.16824E+00	4.41434E+01
$(\boldsymbol{P}_T)^4 * (\boldsymbol{L}_d)^2$	1.58967E-04	-1.10357E-05	-1.09302E-01	-2.09867E-03
$(\boldsymbol{P}_T)^5$	-7.53368E-03	5.66542E-04	5.56136E+00	-1.17627E+02
$(\boldsymbol{P}_T)^5 * (\boldsymbol{L}_d)$	1.73699E-04	-1.31401E-05	-1.22081E-01	-1.71915E+00
$\boldsymbol{X}0$	2.75632E+00	-1.66032E-01	-1.28562E+03	-2.34121E+03
$(\boldsymbol{P}_T)^6$	2.06625E-04	-1.55869E-05	-1.54470E-01	4.23781E+00
$(\boldsymbol{L}_d)^6$	-2.01233E-07	-1.69814E-08	3.50401E-04	-1.59941E-03

3.6.2 Earth Conductance

The first sensibility analysis is made with different values for the earth conductance. The testing surface for this analysis is given by the expression 3.29, where $\boldsymbol{TS}_{ec} \in \mathbb{R}^3$.

$$\boldsymbol{TS}_{ec} = \begin{cases} \boldsymbol{L}_d & [d_1 \ \cdots \ \cdots \ \cdots \ \cdots \ d_D] \quad (in \text{ km}) \\ \boldsymbol{P}_T & [p_1 \ \cdots \ \cdots \ \cdots \ \cdots \ p_P] \quad (in \text{ MW}) \\ \boldsymbol{PF}_T & fixed: \ 0.9 \ ind. \\ \boldsymbol{EC} & [40 \ \ 30 \ \ 20 \ \ \mathbf{15} \ \ 10 \ \ 5 \ \ 1 \ \ 0.5] \quad (in \ S/\text{km}) \\ \boldsymbol{RE} & fixed: \ 0.2 \quad (in \ S/\text{km}) \\ \boldsymbol{LC} & fixed: \ 15 \quad (in \ nF/\text{km}) \end{cases} \tag{3.29}$$

For example, in Fig. 3.21 is presented the voltage errors for different values of the earth conductance.

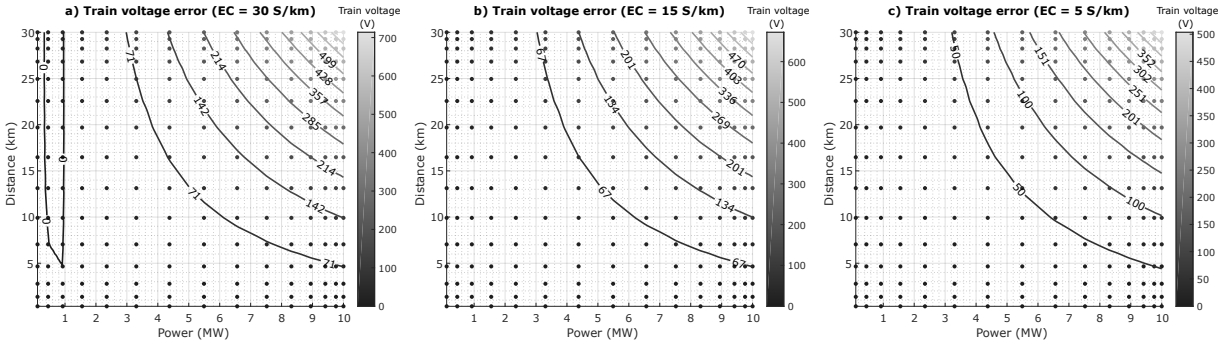

Figure 3.21: Model comparison results the $\boldsymbol{TS}_{ec}$ surface.

From the results of Fig. 3.21, it can be concluded that the higher the ground conductance, the higher the error of the voltage. In Table 3.5 and in Table 3.6 are presented the result metrics, respectively, for the RMSE and the RPE.

Table 3.5: RMSE metrics for different earth-conductance values, according to the $\boldsymbol{TS}_{ec}$.

	TRAIN RMSE				TPS RMSE			
	voltage		current		active power		reactive power	
40 S/km	215.1	V	5.35	A	60.2	kW	187.3	kVAr
30 S/km	211.8	V	5.27	A	58.5	kW	186.7	kVAr
20 S/km	205.2	V	5.13	A	55.0	kW	185.3	kVAr
15 S/km	198.4	V	4.97	A	51.5	kW	183.6	kVAr
10 S/km	184.8	V	4.66	A	44.8	kW	179.9	kVAr
5 S/km	145.4	V	3.76	A	27.4	kW	165.8	kVAr
1 S/km	26.87	V	0.93	A	7.50	kW	96.20	kVAr
0.5 S/km	13.79	V	0.60	A	4.81	kW	79.50	kVAr

Table 3.6: RPE metrics for different earth-conductance values, according to the $\boldsymbol{TS}_{ec}$.

	TRAIN RMSE		TPS RMSE	
	voltage	current	active power	reactive power
40 S/km	0.91 %	1.71 %	0.90 %	4.62 %
30 S/km	0.90 %	1.68 %	0.87 %	4.60 %
20 S/km	0.87 %	1.64 %	0.82 %	4.57 %
15 S/km	0.84 %	1.59 %	0.77 %	4.53 %
10 S/km	0.78 %	1.49 %	0.67 %	4.43 %
5 S/km	0.61 %	1.20 %	0.41 %	4.09 %
1 S/km	0.11 %	0.30 %	0.11 %	2.37 %
0.5 S/km	0.06 %	0.19 %	0.07 %	1.96 %

These results are expected since with high values of ground conductance, the distribution of the return current will occur more through the earth and not in the return conductors (rails, buried ground conductor, aerial protection cable), which results in a better grounding. Considering the standard variation between 10 S/km and 20 S/km, the RPE difference is at maximum 0.15 % (from 1.49 % to 1.64 % in the current RPE or from 0.67 % to 0.82 % in the active power RPE).

In Fig. B.1 is presented the histogram errors from the $\boldsymbol{TS}_{ec}$ surface before and after the enhancement application of the π-type line model.

Similarly to the baseline case, it visible the drastic reduction in the errors of each power flow value. This reduction is made with the application of the function $f(\boldsymbol{P}_T, \boldsymbol{L}_d, \boldsymbol{EC})$, now with a third variable $\boldsymbol{EC}$, where the coefficients of this function are presented in Table B.1 and Table B.2 (located at appendix B).

3.6.3 Rail-Earth Conductance

The second sensibility analysis presented is the rail-earth conductance, where the testing surface given by the expression 3.30, having $\boldsymbol{TS}_{re} \in \mathbb{R}^3$.

$$\boldsymbol{TS}_{re} = \begin{cases} \boldsymbol{L}_d & [d_1 \ \cdots \ \cdots \ \cdots \ \cdots \ d_D] \quad (in \text{ km}) \\ \boldsymbol{P}_T & [p_1 \ \cdots \ \cdots \ \cdots \ \cdots \ p_P] \quad (in \text{ MW}) \\ \boldsymbol{PF}_T & fixed: \ 0.9 \ ind. \\ \boldsymbol{EC} & fixed: \ 15 \quad (in \ S/\text{km}) \\ \boldsymbol{RE} & [0.01 \ 0.02 \ 0.05 \ 0.1 \ \mathbf{0.2} \ 0.5 \ 1 \ 2] \quad (in \ S/\text{km}) \\ \boldsymbol{LC} & fixed: \ 15 \quad (in \ nF/\text{km}) \end{cases} \tag{3.30}$$

Similarly and for example, in Fig. 3.22 is presented the error for the train voltage.

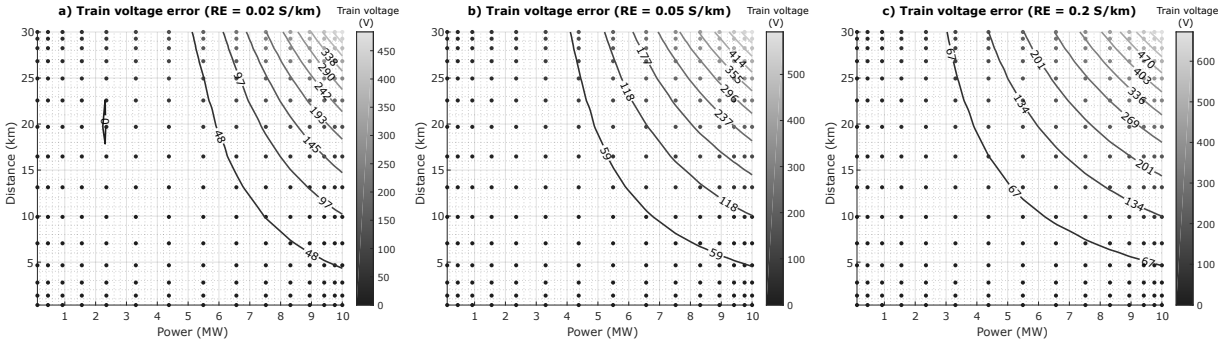

Figure 3.22: Model comparison results for the $\boldsymbol{TS}_{re}$ surface.

It is visible that the increase of the rail-earth conductance, the more current flows from the rails to the earth (and not through the rails and the return conductors) and then, the higher the error between models.

In Table 3.7 and Table 3.8 are presented respectively, the metrics for the RMSE and for the RPE.

Table 3.7: RMSE metrics for different rail-earth conductance values.

	TRAIN RMSE				TPS RMSE			
	voltage		current		active power		reactive power	
0.01 S/km	85.92	V	2.38	A	9.59	kW	133.1	kVAr
0.02 S/km	129.2	V	3.40	A	24.0	kW	155.2	kVAr
0.05 S/km	167.9	V	4.29	A	39.0	kW	172.0	kVAr
0.1 S/km	186.2	V	4.70	A	46.4	kW	179.2	kVAr
0.2 S/km	198.4	V	4.97	A	51.5	kW	183.6	kVAr
0.5 S/km	207.8	V	5.18	A	55.6	kW	186.6	kVAr
1 S/km	211.4	V	5.25	A	57.3	kW	187.6	kVAr
2 S/km	213.3	V	5.29	A	58.2	kW	188.1	kVAr

Table 3.8: RPE metrics for different rail-earth conductance values.

	TRAIN RMSE		TPS RMSE	
	voltage	current	active power	reactive power
0.01 S/km	0.36 %	0.76 %	0.14 %	3.28 %
0.02 S/km	0.55 %	1.09 %	0.36 %	3.83 %
0.05 S/km	0.71 %	1.37 %	0.58 %	4.24 %
0.1 S/km	0.79 %	1.50 %	0.69 %	4.42 %
0.2 S/km	0.84 %	1.59 %	0.77 %	4.53 %
0.5 S/km	0.88 %	1.65 %	0.83 %	4.60 %
1 S/km	0.89 %	1.68 %	0.86 %	4.63 %
2 S/km	0.90 %	1.69 %	0.87 %	4.64 %

The increase of rail-earth conductance from 0.05 S/km to 0.5 S/km (values around standard parameters) will result in a maximum increase of the RPE of 0.36 % (for the reactive power, from 4.24 % to 4.60 %).

The histogram errors for the $\boldsymbol{TS}_{re}$ surface, for this analysis, are presented in the appendix B, in Fig. B.2, where is visible the reduction of the error after the enhancement application of the π-type line model.

Similarly, these results are obtained with the application of the function $f(\boldsymbol{P}_T, \boldsymbol{L}_d, \boldsymbol{RE})$, with the the coefficients of this function being presented in Table B.3 and Table B.4 (located at appendix B).

3.6.4 Line Capacitance

The final analysis is on the line capacitance, with the testing surface given by the expression 3.31, where $\boldsymbol{TS}_{lc} \in \mathbb{R}^3$.

$$\boldsymbol{TS}_{lc} = \begin{cases} \boldsymbol{L}_d & [d_1 \ \cdots \ \cdots \ \cdots \ \cdots \ d_D] \quad (in \text{ km}) \\ \boldsymbol{P}_T & [p_1 \ \cdots \ \cdots \ \cdots \ \cdots \ p_P] \quad (in \text{ MW}) \\ \boldsymbol{PF}_T & fixed: \ 0.9 \ ind. \\ \boldsymbol{EC} & fixed: \ 15 \quad (in \ S/\text{km}) \\ \boldsymbol{RE} & fixed: \ 0.2 \quad (in \ S/\text{km}) \\ \boldsymbol{LC} & [0.2 \ 2 \ 5 \ 10 \ 12.5 \ \mathbf{15} \ 17.5 \ 20 \ 30] \quad (in \ nF/\text{km}) \end{cases} \tag{3.31}$$

A small variation of the train voltage error is presented in Fig. 3.23.

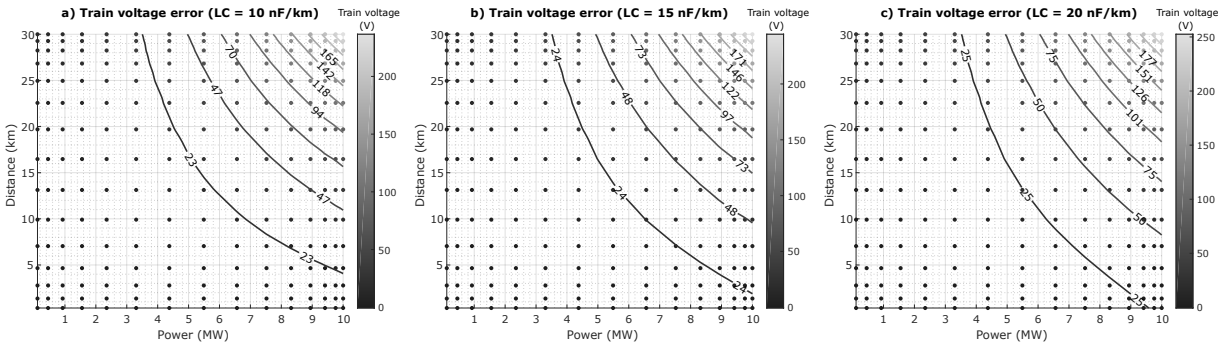

Figure 3.23: Model comparison results for the example $\boldsymbol{TS}_{lc}$ surface.

For higher values of the line capacitance, the higher the error. However, this is more visible in the reactive power, as illustrated in Table 3.9 and Table 3.10, than the other three metrics.

Table 3.9: RMSE metrics for different line capacitance values.

	TRAIN RMSE				TPS RMSE			
	voltage		current		active power		reactive power	
0.2 nF/km	58,77	V	1,74	A	2,67	kW	82,57	kVAr
2 nF/km	59,85	V	1,77	A	2,52	kW	87,40	kVAr
5 nF/km	61,70	V	1,80	A	2,31	kW	95,95	kVAr
10 nF/km	64,83	V	1,87	A	2,10	kW	111,09	kVAr
12.5 nF/km	66,42	V	1,90	A	2,07	kW	118,78	kVAr
15 nF/km	68,03	V	1,93	A	2,11	kW	126,57	kVAr
17.5 nF/km	69,66	V	1,96	A	2,21	kW	134,52	kVAr
20 nF/km	71,31	V	2,00	A	2,36	kW	142,61	kVAr
22.5 nF/km	72,96	V	2,03	A	2,54	kW	150,79	kVAr
25 nF/km	74,62	V	2,06	A	2,76	kW	159,07	kVAr
30 nF/km	77,98	V	2,12	A	3,27	kW	175,87	kVAr
40 nF/km	84,83	V	2,25	A	4,47	kW	210,13	kVAr
60 nF/km	98,86	V	2,51	A	7,03	kW	276,71	kVAr

Table 3.10: RPE metrics for different line capacitance values.

	TRAIN RMSE		TPS RMSE	
	voltage	current	active power	reactive power
0.2 nF/km	0,25 %	0,56 %	0,04 %	2,04 %
2 nF/km	0,25 %	0,56 %	0,04 %	2,15 %
5 nF/km	0,26 %	0,58 %	0,03 %	2,37 %
10 nF/km	0,27 %	0,60 %	0,03 %	2,74 %
12.5 nF/km	0,28 %	0,61 %	0,03 %	2,93 %
15 nF/km	0,29 %	0,62 %	0,03 %	3,12 %
17.5 nF/km	0,29 %	0,63 %	0,03 %	3,32 %
20 nF/km	0,30 %	0,64 %	0,04 %	3,52 %
22.5 nF/km	0,31 %	0,65 %	0,04 %	3,72 %
25 nF/km	0,32 %	0,66 %	0,04 %	3,92 %
30 nF/km	0,33 %	0,68 %	0,05 %	4,34 %
40 nF/km	0,36 %	0,72 %	0,07 %	5,18 %
60 nF/km	0,42 %	0,80 %	0,10 %	6,82 %

This huge difference in reactive power is expected as an intrinsic characteristic of the catenary being inductive. Since the conventional π-type line model only considers lumped resistive and inductive parameters, the inclusion of the capacitance in the MTL line model affects the reactive power in the TPS.

The histogram errors for the $\boldsymbol{TS}_{lc}$ surface are presented in the appendix B, in Fig. B.3, where is visible the reduction of the error after the enhancement application of the π-type line model.

This enhancement is possible with the application of the function $f(\boldsymbol{P}_T, \boldsymbol{L}_d, \boldsymbol{LC})$, with the the coefficients of this function being presented in Table B.5 and Table B.6 (located at appendix B).

3.7 Application of Enhanced π-type Line Model into a Power Flow Analysis Tool

With the proposed enhanced π-type line model detailed, the following step is to illustrate the application of this enhanced model into a traditional power flow tool. This section will demonstrate the utilization of the obtained enhanced π-type line model in MatPower, when a multiple-branch line is considered.

From the Fig. 3.18, it is clear that the proposed enhanced model is valid for a simple 2-bus line. A three-step procedure is needed to apply this enhancement: i) generate the compensation curves; ii) calculate the power flow; and iii) apply the correction.

As the first step, this was extensively illustrated previously, which has resulted in the polynomial regression N-surface fitting functions in (3.32).

$$\boldsymbol{f}_{xn} = \begin{cases} \boldsymbol{f}_v & (\boldsymbol{L}_d, \boldsymbol{P}_t, \boldsymbol{PF}_t, \boldsymbol{EC}, \boldsymbol{RE}, \boldsymbol{LC}) \\ \boldsymbol{f}_i & (\boldsymbol{L}_d, \boldsymbol{P}_t, \boldsymbol{PF}_t, \boldsymbol{EC}, \boldsymbol{RE}, \boldsymbol{LC}) \\ \boldsymbol{f}_{P_{tps}} & (\boldsymbol{L}_d, \boldsymbol{P}_t, \boldsymbol{PF}_t, \boldsymbol{EC}, \boldsymbol{RE}, \boldsymbol{LC}) \\ \boldsymbol{f}_{Q_{tps}} & (\boldsymbol{L}_d, \boldsymbol{P}_t, \boldsymbol{PF}_t, \boldsymbol{EC}, \boldsymbol{RE}, \boldsymbol{LC}) \end{cases} \tag{3.32}$$

Then, the second step is to apply the power flow solver, illustrated in Fig. 3.24, in which is considered the MatPower tool.

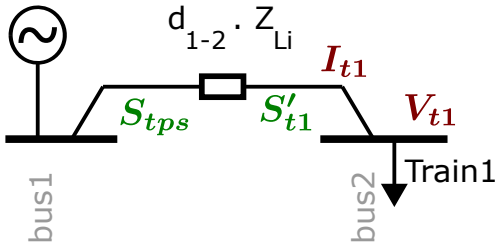

Figure 3.24: Application of power flow solver into a simple 2-bus line.

Finally, the following vectors are compensated to eliminate the error associated to the rail-earth and earth conductances, and line capacitance:

$$\begin{aligned} \boldsymbol{V_{t1}}_{\ comp} &= \boldsymbol{V_{t1}}_{\ init} + \boldsymbol{f}_v(\boldsymbol{L}_d, \boldsymbol{P}_t, \boldsymbol{PF}_t, \boldsymbol{EC}, \boldsymbol{RE}, \boldsymbol{LC}) \\ \boldsymbol{I_{t1}}_{\ comp} &= \boldsymbol{I_{t1}}_{\ init} + \boldsymbol{f}_i(\boldsymbol{L}_d, \boldsymbol{P}_t, \boldsymbol{PF}_t, \boldsymbol{EC}, \boldsymbol{RE}, \boldsymbol{LC}) \\ \boldsymbol{P_{tps}}_{\ comp} &= \boldsymbol{P_{tps}}_{\ init} + \boldsymbol{f}_{P_{tps}}(\boldsymbol{L}_d, \boldsymbol{P}_t, \boldsymbol{PF}_t, \boldsymbol{EC}, \boldsymbol{RE}, \boldsymbol{LC}) \\ \boldsymbol{Q_{tps}}_{\ comp} &= \boldsymbol{Q_{tps}}_{\ init} + \boldsymbol{f}_{Q_{tps}}(\boldsymbol{L}_d, \boldsymbol{P}_t, \boldsymbol{PF}_t, \boldsymbol{EC}, \boldsymbol{RE}, \boldsymbol{LC}) \end{aligned} \tag{3.33}$$

where the *init* and *comp* electric values are the before and after the application of the error compensation strategy. Noteworthy, the power factor and the decoupling ac-

tive/reactive issues must be taken into consideration when this procedure is applied, following:

$$\begin{aligned} \boldsymbol{S_t} &= \boldsymbol{P_t} + j\ \boldsymbol{Q_t} \\ &= \boldsymbol{P_t}\,(1 + j\ sign(\boldsymbol{PF_t})\ \tan(\cos^{-1}(\boldsymbol{PF_t}))) \end{aligned} \tag{3.34}$$

This procedure is better clarified when is considered the power compensation in the TPS, illustrated in Fig 3.25.

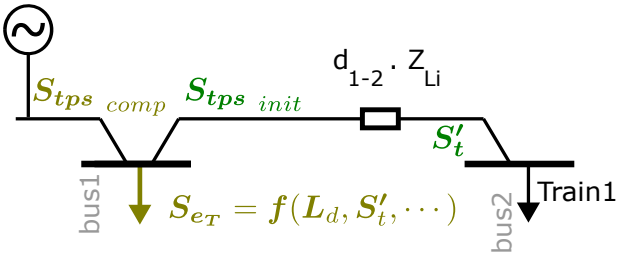

Figure 3.25: Final step of the application of the enhanced model into the simple 2-bus line.

The compensated TPS power will be:

$$\begin{aligned} \boldsymbol{S_{tps\ comp}} &= \boldsymbol{S_{tps\ init}} + \boldsymbol{f}_{P_{tps}}(\boldsymbol{L_d}, \boldsymbol{S_t}, \boldsymbol{EC}, \boldsymbol{RE}, \boldsymbol{LC}) + j\ \boldsymbol{f}_{Q_{tps}}(\boldsymbol{L_d}, \boldsymbol{S_t}, \boldsymbol{EC}, \boldsymbol{RE}, \boldsymbol{LC}) \\ &= \boldsymbol{S_{tps\ init}} + \boldsymbol{S_{e_T}} \end{aligned} \tag{3.35}$$

3.7.1 Demonstration for Multiple Trains

In this demonstration is considered the case study diagram of Fig. 3.26.

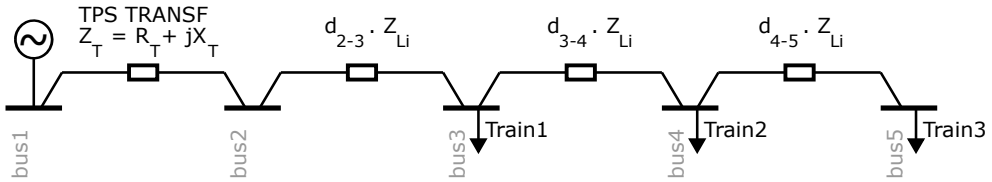

Figure 3.26: Case study of three trains to illustrate the application of enhanced model into PSSA-rail[4].

The first step is to solve the power flow obtaining the power vectors $\boldsymbol{S'_{t1}}$, $\boldsymbol{S'_{t2}}$, $\cdots$, $\boldsymbol{S'_{tn}}$, of Fig. 3.27, with $\boldsymbol{S_{e_{T1}}} = 0$, $\boldsymbol{S_{e_{T2}}} = 0$, $\cdots$, $\boldsymbol{S_{e_{Tn}}} = 0$.

Then, an iterative process is started:

1. All compensation power vectors, $\boldsymbol{S_{e_{T_1}}}$, $\boldsymbol{S_{e_{T_2}}}$, $\cdots$, $\boldsymbol{S_{e_{T_N}}}$, are updated based on the polynomial regression curves, simplified here to $\boldsymbol{S_{e_{T_b}}} = \boldsymbol{f}(\boldsymbol{L}_{d_{b_y - b_x}}, \boldsymbol{S'_{T_b}}, \boldsymbol{EC}, \boldsymbol{RE}, \boldsymbol{LC})$;

[4]The PSSA-rail is the developed tool described in chapter 5.

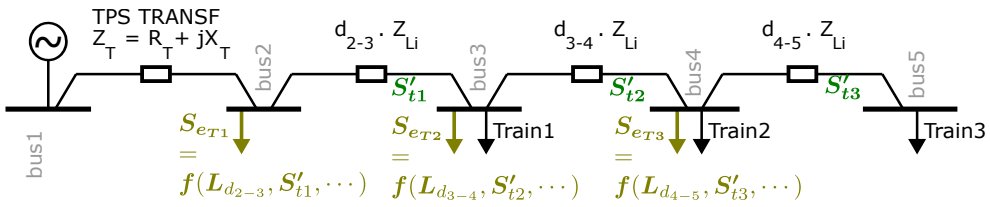

Figure 3.27: First step: running the MatPower for the initial configuration.

2. The MatPower solver is executed, and the difference vectors $\Delta \boldsymbol{S'_{T_1}}, \Delta \boldsymbol{S'_{T_2}}, \cdots, \Delta \boldsymbol{S'_{T_N}}$ are calculated as the difference of current branch power and previous one;

3. If the value $\sum \Delta \boldsymbol{S'_{T1}}$ is above a threshold tolerance, then the procedure is repeated.

The application of Enhanced π-type Line Model into MatPower is better explained in the Algorithm 1.

Algorithm 1: Application of Enhanced π-type Line Model into MatPower

```
1  INIT
2  PREPARE MatPower solver
3  Set S_eT1 = 0, S_eT2 = 0, ··· , S_eTN = 0
4  LAUNCH MatPower solver
5  LOOP
6  while NOT termination criteria do
7      for all buses b ∈ 1, 2, ··· , N do
8          SET S_eTb = f(L_{d_{b_y - b_x}}, S'_Tb, EC, RE, LC)
9      end
10     LAUNCH MatPower solver
11     for all buses b ∈ 1, 2, ··· , N do
12         SET ΔS'_Tb to be the difference between previous and current S'_Tb
13     end
14     if Σ_{b=1}^{N} ΔS'_Tb < threshold then
15         BREAK
16     end
17 end
18 END
```

3.8 Discussion and Conclusions

The energy information gathered by each train energy meter can be used to generate knowledge on the electrification system state. This knowledge generation procedure is partially made through power flow analysis algorithms. In this chapter were presented the approaches to obtain a railway line model capable of accurately generate the desired knowledge.

In the first part of this chapter, the procedures to obtain a simplified lumped-parameters π-type line model from a multi-conductor transmission line model were presented. In parallel, these two resultant models were compared, with the proposed comparison methodology, towards an evaluation on the resultant error on this simplification.

From the results of the comparison methodology, minimal errors are visible. Specifically, for the testing conditions of the testing surface ($\boldsymbol{TS}$) in (3.19), the errors in percentage are, respectively, 0.02 % and 0.15 % for the train voltage and current, and 0.09 % and 0.41 % for the TPS active and reactive power. The evaluation variables of result surface ($\boldsymbol{RS}$), in expression (3.20), are the relevant variables given by a power flow analysis algorithm. Other variables — i.e. TPS voltage, train active power and train reactive power — were not considered for the $\boldsymbol{RS}$ since the error is zero by definition (these variables were fixed).

Without the consideration of line capacitance and conductances for power flow analysis, it can be stated that the comparison of a complex MTL and a simplified lumped-parameter π-type line model will result in minimal errors. Also, part of these errors can be originated from the fact that the comparison procedure is associated with errors itself (the algorithm of the train model detailed in appendix A will stop its simulation once the input error of the power proportional-integral controllers is minimal, and if there is no convergence to this minimal error, the simulation is stopped after a certain time window (defined as 500 grid cycles)).

The second part of this chapter evaluates the parameters that are usually eliminated from the railway power flow simulation, specifically, the line conductance and capacitance. The methodology for this evaluation is to extend the $\boldsymbol{TS}$ in (3.19) to include discrete values for these parameters.

As outcomes of this methodology, the errors will increase, in comparison to the situation where these errors are not considered. For the train voltage and current, respectively, the percentage errors will grow from 0.02 % to 0.84 % and from 0.15 % to 1.59 %. In the TPS side, these errors will increase from 0.09 % to 0.77 % for the active power, and from 0.41 % to 4.53 % for the reactive power.

In the opinion of the author, these errors are more representative of a more accurate railway line, even if the included parameters are difficult to obtain (environmental conditions, ageing, etc. will affect the parameters).

Furthermore, from the generated result surfaces, that cover the discretization of these parameters, a multivariate polynomial fitting curve can be obtained to be used to enhance the lumped-parameters π-type model. The histograms of the comparison of the errors show a clear reduction on the errors after the application of the curve fitting tool.

However, these comparisons must be taken with caution. As example, in the $\boldsymbol{TS}_{ec}$

surface is considered 8 different values for the earth conductance. The enhancement is made with the information of the eight surfaces (for each earth conductance result surface). A more realistic situation will be with a generation of the fitting with less information, and the comparison of the elements that were not in the fitting information. In the Fig. 3.28 is illustrated a scenario for the histograms of the voltage errors that illustrate this situation.

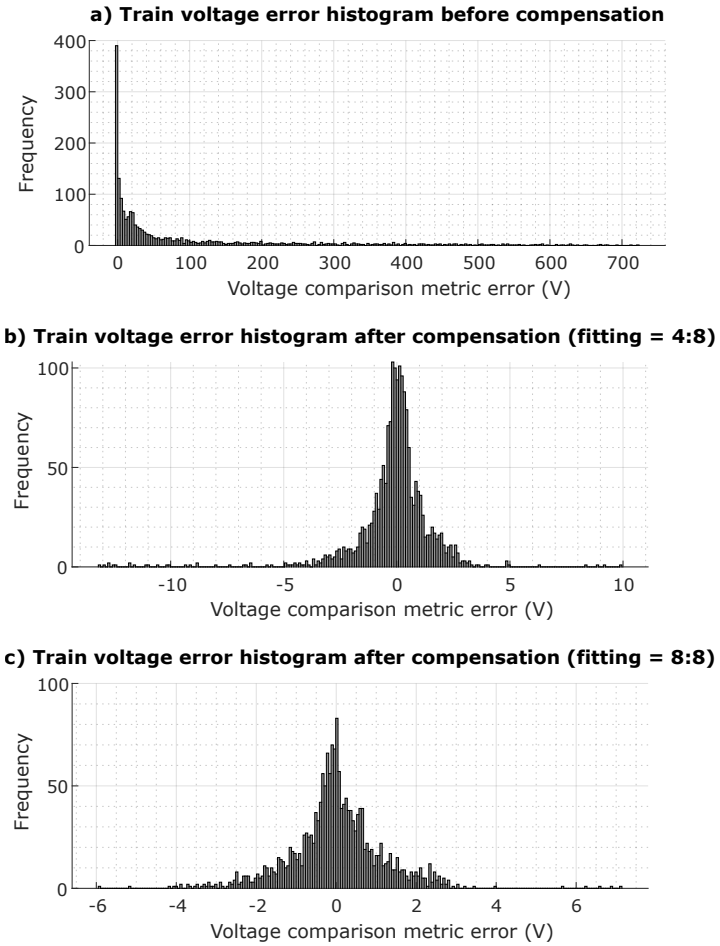

Figure 3.28: Histogram for different fittings, for the $\boldsymbol{TS}_{ec}$ surface.

Nevertheless, despite the usage of only half of the $\boldsymbol{RS}$ error surfaces for the fitting, the train voltage error is still minimal when compared to the usage of all the information for the fitting, as visible in the histogram graphs of Fig. 3.28.

In section 3.7 was clarified the integration of this enhanced model into MatPower, which is the solver used in the tool proposed in chapter 5.

3.9 Summary

It was raised in this chapter the evaluation of the railway electrical line model, resulting in an enhanced lumped-parameters line model. This model will be useful for the power flow analysis, as a way to extract the knowledge from the information generated by each train energy meter. Specifically, this enhanced lumped-parameters line model will be used in the PSSA-rail tool proposed in chapter 5.

In the following chapter is presented a methodology to simulate and generate the information of an entire railway line. This generation of information will be made through a multi-train simulator tool.

CHAPTER 4

Multi-train Simulator for Smart Railway Framework

In this chapter is addressed the topic **T2** — Multi-train tool to estimate the dynamics and energy consumption. This topic clearly presents the development steps of a tool to estimate any journey, which is the challenge for this thesis.

The Multi-train Simulator (MTS) tool is detailed in two parts. In the first part is detailed a train model, with the methodology to validate the model with real data from the energy meters on operation in a suburban line. Later, in this first part is presented the results as well as metrics that support this model. In the second part of this chapter is presented a heuristic approach to automatically generate the information of a train journey, based only in the train characteristics, the line geography and in the journey timetable. The results of this second part are also validated with the same real data.

The outcome of this chapter will be a tool to generate the information of an entire railway line, as illustrated in the graphical abstract in Fig. 4.1. The main outcome of this work will be a train simulation tool that considers all the physical constraints and limitations of the train model, as well as the timetable requirements. This train simulation tool will be capable of simulating the vehicle dynamics and energy consumption for an entire journey. By including the result for several train journeys, it is obtained a multi-train simulator with an accurate estimation of the dynamics of each train as well as the energy consumption by the global railway system.

The objectives of this chapter are:

- **Objective 2a**: Propose a methodology to obtain and validate a train model, in terms of its dynamic movement and in terms of the energy consumption;
- **Objective 2b**: Propose a multi-train simulation tool to automatically generate the train information for any journey, using the validated train model.

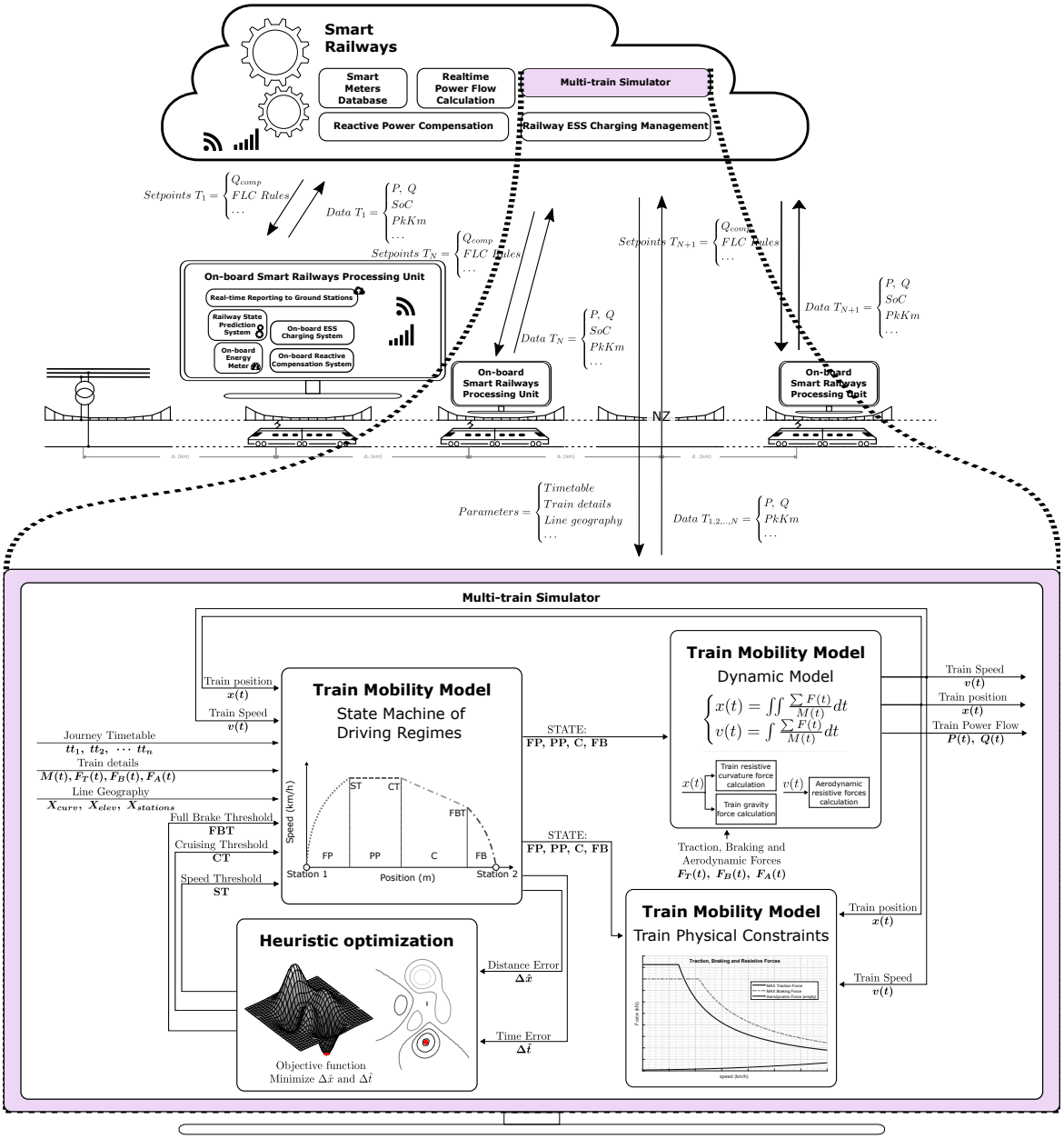

Figure 4.1: Graphical abstract of chapter 4 — Inclusion of multi-train simulator in a smart railway framework.

4.1 Introduction

The evaluation of a detailed energy monitoring in railway transportation system is a relevant topic. In particular, the availability of energy data is a grown topic in the railway industry, specifically for the evaluation of energy consumption and, as a final objective, the adaptation of railway operation towards the reduction of energy consumption.

The listed research opportunities associated to the topic **T2** presented in chapter 2, identifies the lack of availability of open-source simulation tools targeting the estimation of the dynamics and energy consumption of any train journey. It is addressed as one opportunity to develop a multi-train simulation and to present the implementation steps of the modules, as well as the comparison of the developed tool with real train data.

As presented in the graphical abstract of the Fig. 4.1, the input parameters for this multi-train simulation tool will be given by the expression in (4.1).

$$Parameters = \begin{cases} Journey\ Timetable \\ Train\ characteristics \\ Line\ geography \end{cases} \tag{4.1}$$

Thus, the output of this multi-train simulation tool will be the information of each train, being this formed from data given by the expression in (4.2).

$$Info\ T_{1,..,N} = \begin{cases} Dynamics\ Data = \begin{cases} x(t),\ v(t) \\ F_T(t),\ F_B(t) \end{cases} \\ Energy\ Data = \begin{cases} P(t),\ Q(t) \\ E(t) \end{cases} \end{cases} \tag{4.2}$$

4.2 Train Dynamic Model Formulation

The train dynamic model is divided into (i) Train Physical Movement, that describes the movement of the train, having in consideration all the forces that affect the movement; (ii) Train Physical Constraints, that limit the maximum forces of the train to comply with the characteristics of the vehicle; and (iii) Train State Machine as the part responsible for setting the train mode of operation.

4.2.1 Train Physical Movement

Considering the train as a single point of mass, the motion of the vehicle is based on basic physics formulations, mainly Newton second law, as given by the expression in (4.3) and in (4.4).

$$\frac{dv}{dt} = \frac{\sum F(t)}{M} \tag{4.3}$$

$$x(t) = \iint_0^T \frac{\sum F(t)}{M}\ dt \tag{4.4}$$

Furthermore, according to the references [82, 90], the train formulation can be described by the expression in (4.5).

$$\frac{dv}{dt} = \frac{\mu_f \ F_T(v) - \mu_b \ F_B(v) - F_a(v) - F_g(x) - F_c(x)}{M} \tag{4.5}$$

This formulation has the following notation:

$\boldsymbol{t}$	Time;
$\boldsymbol{v}$	Velocity of vehicle;
$\boldsymbol{x}$	Position/coordinate of the vehicle;
$\boldsymbol{\mu_f}$	Relative traction force;
$\boldsymbol{\mu_b}$	Relative braking force;
$\boldsymbol{M}$	Mass of the train;
$\boldsymbol{F_T(v)}$	Maximum traction force;
$\boldsymbol{F_B(v)}$	Maximum braking force;
$\boldsymbol{F_a(v)}$	Aerodynamic resistance to motion;
$\boldsymbol{F_g(x)}$	External force caused by track grade;
$\boldsymbol{F_c(x)}$	External force caused by track curve.

As listed in expression in (4.1), the restrictions on the journey timetable will affect the relative traction and braking force, μ_f and μ_b (which is imposed by the train driver, or in the case of this chapter, a heuristic algorithm).

The line geography, in expression (4.1), affects the train movement with the variation of the track gradient, as well as the curve resistance. These line geography track grade is a position-dependent force, presented in equation in 4.6, where g is the gravity acceleration, $\alpha(x)$ and $i(x)$ define the track grade as position dependent variables.

$$F_g(x) = -M \ g \ sin(\alpha(x)) \approx -M \ g \ i(x) \tag{4.6}$$

Similarly, the curve resistance is also a position dependent force, given by the equation in 4.7, where the track radius, $\boldsymbol{R(x)}$, in meters, decreases as long as a train reaches a curve.

$$F_c(x) = \frac{D_r}{R(x)}, \quad D_r = 6116 \tag{4.7}$$

The train characteristics of (4.1) are the constraints better described in the following subsection.

4.2.2 Train Physical Constraints

The train operation is limited by several constraints, associated mainly with the train speed, as illustrated in Fig. 4.2, for a train with the parameters given by Table 4.1.

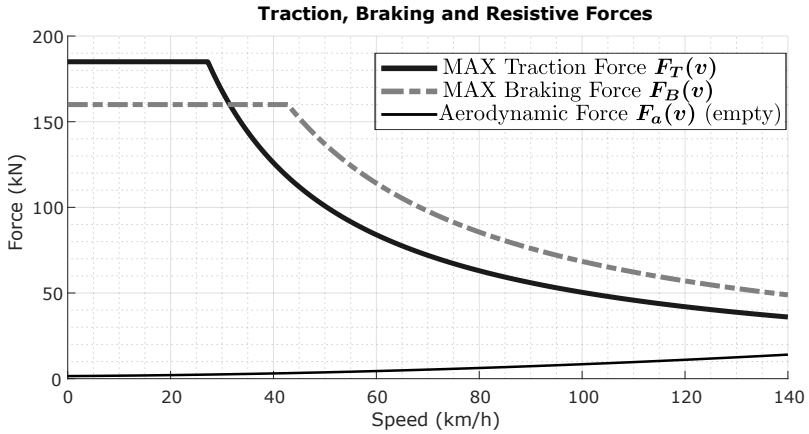

Figure 4.2: Traction, braking and resistive forces affecting the train movement.

Table 4.1: Train parameters.

	Symbol	**Value**
Maximum Traction Force	$max(F_T(v))$	185 kN
Train Maximum Power	P_{max}	1.4 MW
Maximum Braking Force	$max(F_B(v))$	160 kN
Train Maximum Speed	v_{max}	140 km/h
Braking Force at maximum speed	$T_{B,v_{max}}$	48.9 kN
Train mass (empty)	M_0	117.8 t
Davis coefficients	$A = 12.8$, $B = 0.56$ and $C = 0.0558$	
Train type	Electric Multiple Unit: Series 3400	

Regarding the traction force, the train has a limited traction force at lower speeds (185 kN). At higher speeds, the traction regime is limited by the maximum electrical power available in the train (1.4 MW) and follows the equation (4.8).

$$P_{max} = F\ v \tag{4.8}$$

The dash-dot line of Fig. 4.2 presents the maximum braking force. At a maximum speed of 140 km/h, the train has available the maximum braking force (48.9 kN), where the braking regime is constant braking power. At lower speeds, the braking force is limited by a constant braking force regime (160 kN).

The forces against the linear movement are also plotted in Fig. 4.2. Those forces combine the inertia of the train and the aerodynamic resistance. Those forces are given in Newton per tonne unit and follow the Davis equation in 4.9 with coefficients in Table 4.1.

$$F_a(v) = A + Bv + Cv^2 \tag{4.9}$$

4.2.2.1 Comparison of model with real measurements

The reference [73] identifies three alternatives for modelling the traction/braking forces in the train: (i) Look-up table approach using measured traction forces, (ii) Equation-based approach and (iii) Co-simulation approach.

The approach followed in this chapter is the equation-based approach for the modelling of longitudinal train dynamics. In Fig. 4.3 is presented traction and braking modelled forces in comparison with the forces measured in the traction converter for the presented case study.

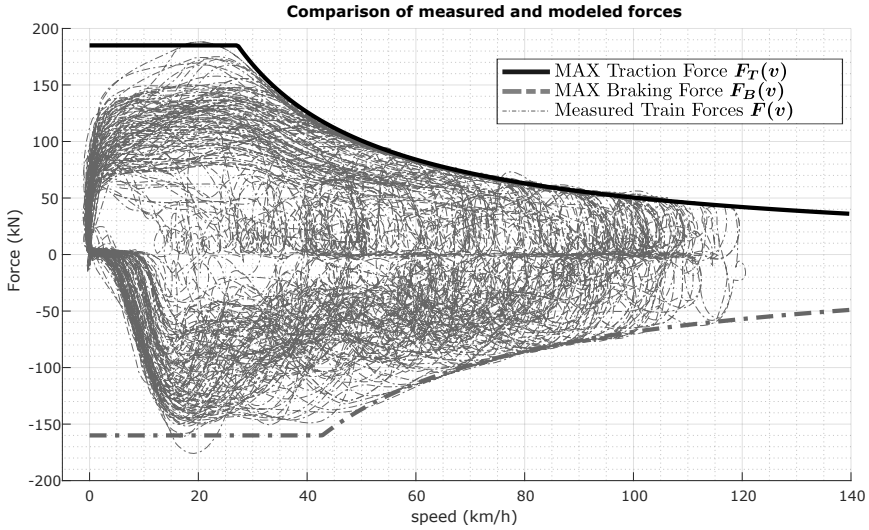

Figure 4.3: Comparison between measured forces in traction converter and the model of maximum forces.

The measured train forces presented in Fig. 4.3 were gathered from a dataset of 27 different journeys (each journey is around 1h) of a suburban electric multiple unit train. The dataset combines one time-series array of train speeds and two other arrays of traction and braking forces. By plotting the train $F_T(t) + F_B(t)$ as a function of the train speed, $v(t)$, this validated the equation-based modelled maximum traction and braking forces.

In the Fig. 4.3 is only presented the electric braking — or regenerative braking, where the traction converter changes its mode of operation. However, at lower speeds (and in emergency situations), the train braking is also supported by the pneumatic braking.

In Fig. 4.4a) is also illustrated the pneumatic braking based on a dataset of 27 train journeys, in which is combined the time-series array of speeds and the time-series array of percentage pneumatic braking force. Also, at lower speeds, the train driver avoids the usage of maximum available force, as visible in the Fig. 4.4b) where similar dataset plotting is presented for the percentage traction force. This driving mode is due to comfort restrictions, also defined as jerk, where there are limitations of abrupt changes in the train acceleration.

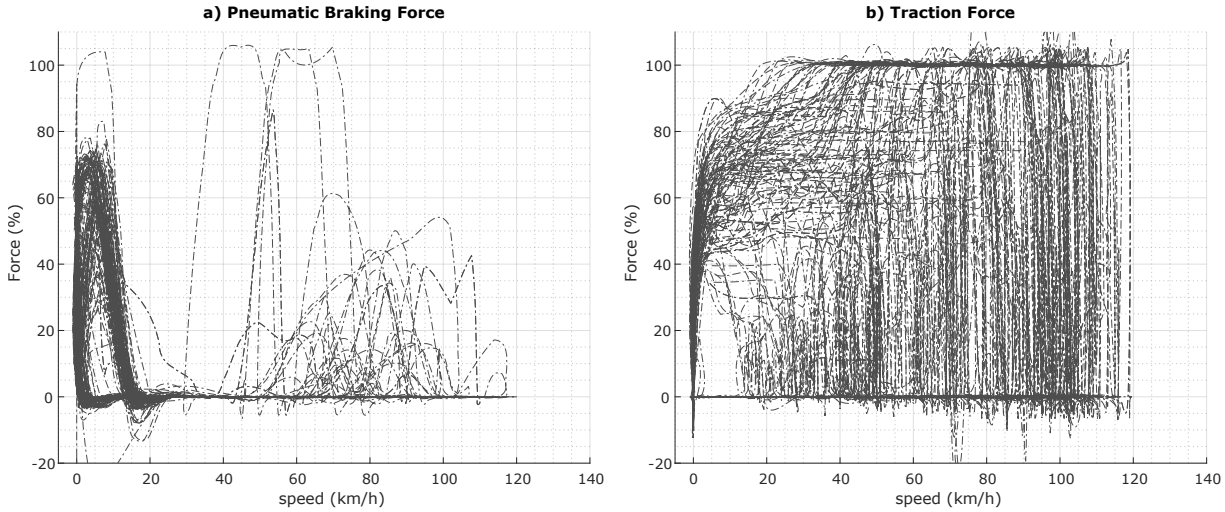

Figure 4.4: Percentage of actuating train forces, as function of the train speed: a) Pneumatic braking force; b) Train traction force.

4.2.3 Optimal Speed Profile

After the dynamics and the constraints of the train model, the final part of the train model concerns the driving profile. In Fig. 4.3 is illustrated that a train can be operated with any total force between the maximum traction and braking. Therefore, the train driver (or an automatic driving profile generator) needs to follow a driving profile to comply with the journey timetable.

From the optimal control theory [82, 90, 148], it can be identified the following train states under optimal control:

- **Full power/torque (FP)**: $\mu_f = 1$;
- **Partial power (PP) or cruising**: $\mu_f \in]0 - 1[$, where speed is constant;
- **Inertia motion or coasting (C)**: $\mu_f = 0, \mu_b = 0$;
- **Full braking (FB)**: $\mu_b = 1$.

In Fig. 4.5 is illustrated as an optimal speed profile based on the optimal control theory.

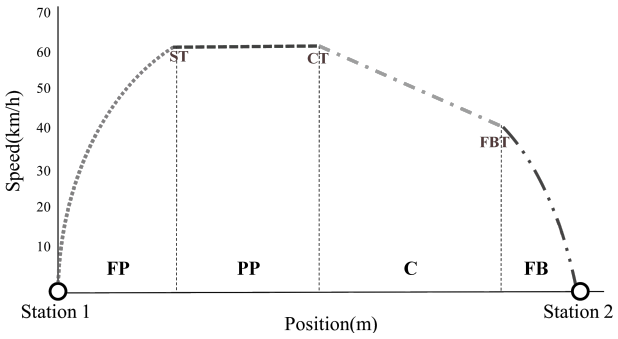

Figure 4.5: State machine: phase sequence for an optimal train operation.

From an optimal control theory-based speed profile, the following switching points will be taken into consideration.

- **Speed Threshold (ST)**: as the transition between FP and PP[1];
- **Cruising Threshold (CT)**: as the transition between PP and C, expressed as a percentage of the remaining distance. It is calculated in the transition FP→PP;
- **Full Brake Threshold (FBT)**: as a percentage of the absolute maximum distance needed to brake.[2]

Specifically, these points will be generated by the heuristic algorithm of this multi-train simulator tool. In Fig. 4.6 is presented the state machine for the train dynamic movement.

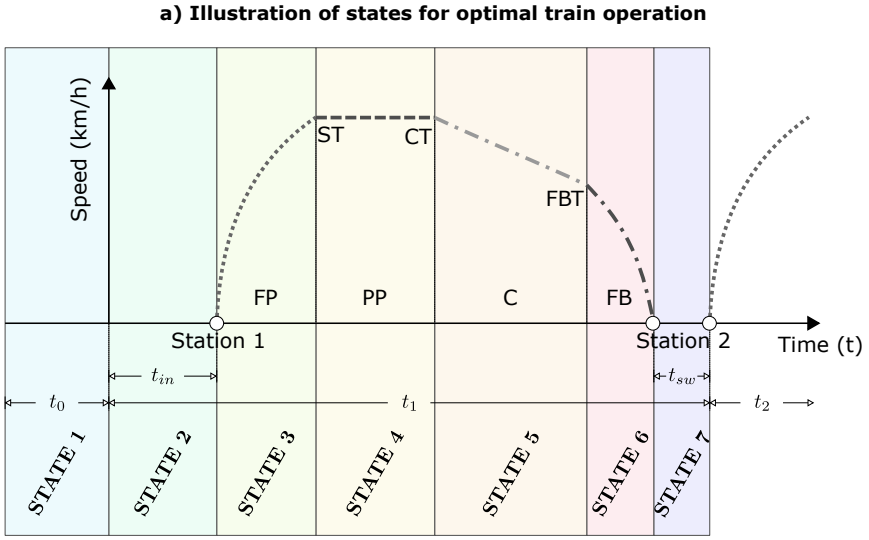

Figure 4.6: Implemented state machine. (Continues on next page).

[1]Expressed as a percentage of the maximum speed (140 km/h for the case study train).

[2]For the case study train, this distance is 1356 m. This absolute maximum distance needed was obtained with the simulation of the distance needed by the case study train to fully brake from the maximum speed, 140 km/h at maximum mass 167,9 t.

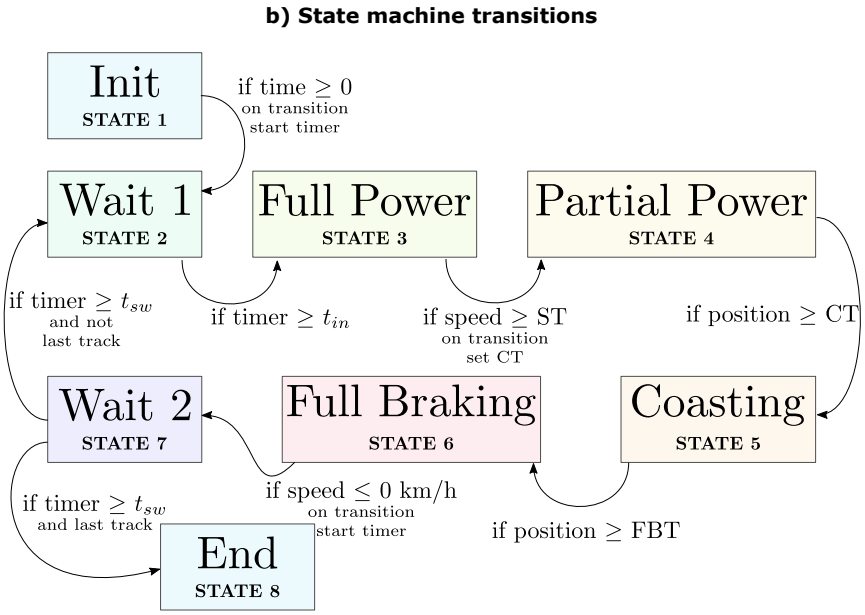

Figure 4.7: Implemented state machine. (Continued from previous page).

Besides the four states previously described, in this implementation, additional states were added to include the simulation of the train stopping in all the stations on an entire journey, between starting station and last station. The **Init** and **Wait1** states allow the simulation to schedule the initial departure time (t_{in}) from the first station. These states allow the train departure to be scheduled to match a specific hour of the day. In addition, the **Wait2** state ensures the fulfilment of the station waiting time (t_{sw}), according to the timetable.

4.3 Train Energy Model Formulation

The train energy model depends on the outputs of the dynamic model, specifically the traction force and the train speed, and depends on the characteristics of the electric train, whose architecture is illustrated in Fig. 4.7.

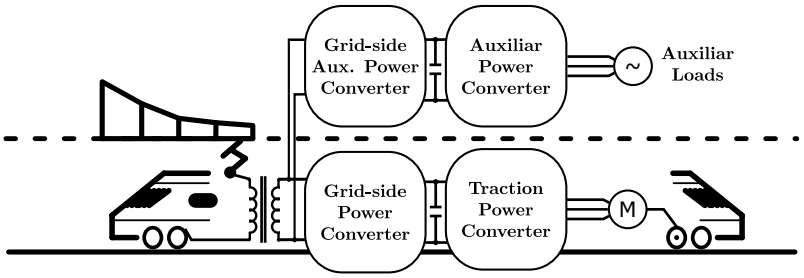

Figure 4.7: Train energy model.

Then, assuming that the catenary voltages and currents are almost sinusoidal waveforms, the train power at the pantograph is given by the equation in (4.10):

$$V_1 \; I_1 \; \cos(\phi_1) = (1+\xi) \; P_{cons} - (1-\xi) \; P_{gen} + (1+\xi) \; P_{aux} \tag{4.10}$$

where

$$P_{cons} = \begin{cases} F_t \; v & F_t > 0 \\ 0 & otherwise \end{cases} \tag{4.11}$$

$$P_{gen} = \begin{cases} -F_b \; v & F_b > 0 \\ 0 & otherwise \end{cases} \tag{4.12}$$

$$P_{aux} = \sum_{a=1}^{N} P_a \approx 100 \; kW \tag{4.13}$$

and ξ is a common losses factor associated with P_{cons}, P_{gen} and P_{aux}.

The auxiliary power comprises multiple loads P_a (such as heating, air-conditioning, illumination, doors, train control systems, passenger information systems, etc.) and was obtained using the methodology presented in appendix D.

For an unitary train power factor and considering a decoupled traction and braking force as the output of the dynamic model, the energy is given by (4.14):

$$\begin{aligned} E(t) &= \int_{t=0}^{t_{journey}} P(t) \;\; dt \\ &= \int_{t=0}^{t_{journey}} \Big[\Big(F_t(t) \;\; (1+\xi) + F_b(t) \;\; (\xi - 1) \Big) \; v(t) + (1+\xi) \;\; P_{aux} \Big] \;\; dt \end{aligned} \tag{4.14}$$

4.4 Train Models Validation

The validation of the train dynamic model is presented in appendix C, where three models are considered. Specifically, the first basic model does not consider nor the gravity force neither the curve resistant force. The second dynamic model evaluated only considers the gravity, following the profile in Fig. 4.8. Furthermore, the third dynamic model considers the gravity force and the track curvature resistance force, complemented by the Fig. 4.9.

Following the extensive comparison methodology presented in appendix C, this comparison results in the Root Mean Square Error (RMSE) metrics in Table 4.2.

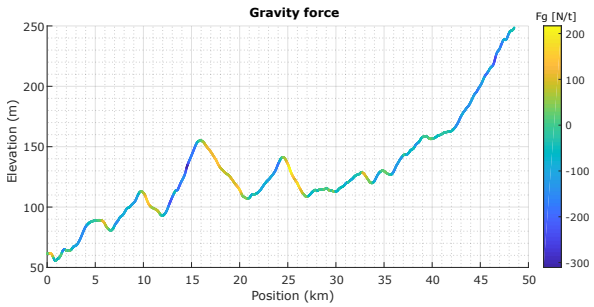

Figure 4.8: Elevation and gravity force as function of the line distance.

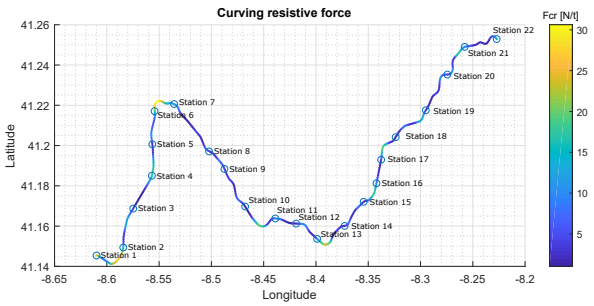

Figure 4.9: Absolute position and curvature resistive force.

Table 4.2: Comparison of dynamic train models

Dynamic model	**Speed difference** RMSE (km/h)	**Position difference** RMSE (m)	RSME (%)
Basic	**5.30**	**1694**	**3.48**
Gravity	**3.25**	**838**	**1.72**
Gravity + Curving	**3.04**	**500**	**1.03**

Then, the energy train model was also subject of a validation procedure, being presented in appendix D. In this analysis, three energy models were also evaluated. The first one considers no auxiliary power consumption and ideal unitary efficiency. The second model considers a fixed auxiliary power consumption of 100 kW (whose value was obtained following the methodology in appendix D). Then, the third model extends the second one, by including a non-unitary efficiency, of $\mu = 85$ %, combined on the onboard transformer and on the power conversion units (whose value was obtained following the methodology in appendix D).

The results of this energy model validation are presented in Table 4.3.

Table 4.3: Comparison of energy train models

Energy model	**Consumption difference** RMSE (kWh)	RMSE (%)
Basic Energy Model	**61.84**	**23.52**
Auxiliary Power + Unitary Efficiency	**12.23**	**4.78**
Auxiliary Power + Non-unitary Efficiency	**11.45**	**4.31**

4.5 Multi-Train Simulator

In previous sections was presented the train dynamic and energy consumption models. However, these models still need the definition of certain variables for each of the journey track segment, as visible in Fig. 4.10.

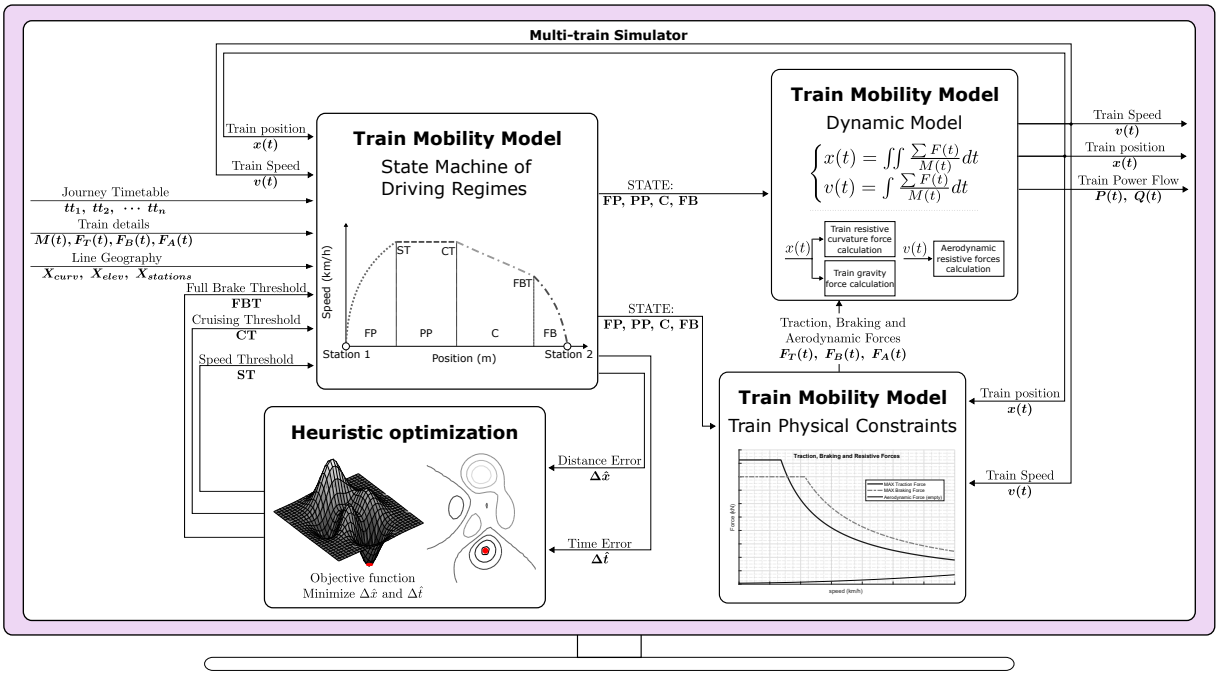

Figure 4.10: Global structure of Train Simulator.

A heuristic algorithm is responsible to replace the train driver in this simulator. This iterative process will test for each journey track segment those variables having as objective the compliance to the timetable constraints (identified as the distance and time errors).

4.5.1 Heuristic Algorithm

Usually, in normal real operation conditions, a train driver needs to follow a driving profile, having the requirement to comply with the timetable (among other requirements, not covered in this work). In broader terms, a train driver needs to move a train from one station to another, within a certain time window. In a practical operation, the train driver accelerates the train to the desired speed, then after a certain period of time (or distance), the train is in coasting until the driver starts the braking mode in order to stop.

As already presented, it was established in this work the definition of three transition states, that are defined by the heuristic algorithm, following the expression in (4.15).

$$\textbf{\textit{Heuristic Output}} = \begin{cases} ST: & Speed\ threshold \\ CT: & Cruising\ threshold \\ FBT: & Full\ brake\ threshold \end{cases} \tag{4.15}$$

Furthermore, after iterative testing, the heuristic algorithm uses the results in expression (4.16) to assess the tested elements.

$$\textbf{\textit{Heuristic Input}} = \begin{cases} \Delta\hat{x}: & Time\ error \\ \Delta\hat{t}: & Distance\ error \end{cases} \tag{4.16}$$

For a journey having N departure/stopping passenger stations, the heuristic algorithm will generate an array of $N-1$ ***Heuristic Output*** elements.

4.5.2 Rules and constraints

A valid result of the heuristic algorithm will be an array of ***Heuristic Output*** elements. To achieve such solutions, it was included the following rules:

- A minimum distance error (less than $\boldsymbol{X_{min}}$[3] around the train station);
- The time error higher than $\boldsymbol{T_{min} = 0}$ (the train is only allowed to departure after the time defined in timetable)
- The departure delay must be less than $\boldsymbol{T_{max}}$[4] after the time specified in the timetable.
- The distance and time errors should be not cumulative[5].

As illustrated in Fig. 4.10, the objective function is the minimization of the ***Heuristic Input*** results.

The implemented heuristic is described in the Algorithm 2.

[3] Arbitrarily defined 20 meters.

[4] Arbitrarily defined 10 seconds.

[5] Considering three stations as example, the distance and time errors when the train simulation reaches the third station will include the errors from the previous station.

Algorithm 2: Heuristics Main Loop

INIT
SET (Track under testing = 1); SET (iteration = 1);
SET (ST, CT and FBT) = rand(0,1)
LOOP
while *NOT termination criteria* **do**
  LOAD (ST, CT and FBT)
  LAUNCH (Simulation Model)
  GET *time error* and *position error*
  GET (OF) $\Longleftarrow f(time\_error,\ position\_error,\ iteration)$
  if ($\boldsymbol{T_{min}} \leq time\_error \leq \boldsymbol{T_{max}}$) ***and*** ($|position\ error| \leq \boldsymbol{X_{min}}$) **then**
    SET (ST, CT and FBT) $\Longleftarrow$ rand(0,1)
    GOTO: NEXT TRACK
    if *LAST TRACK REACHED* **then**
      BREAK
    else
      INCREASE (Track under testing); RESTART (iteration);
    end
  end
  INCREASE (ST, CT, FBT) $\Longleftarrow$ $rand(0,1) \times OF$
  if $iteration \geq MAX\ ITERATIONS$ **then**
    BREAK
  else
    INCREASE (iteration)
  end
end
END

A valid solution for the proposed heuristic algorithm is a solution where the timetable is guaranteed for all the journey track segments. In the following subsection are presented the results for one journey.

4.6 Single Journey Results

In this section is presented a comparison of the generated results by the multi-train simulation tool with a database of train journeys (provided by a partner company of a railway main operator). Illustrated in Fig. 4.11, this comparison is made on the train position, speed and energy consumption for each of the journey dataset of measurements.

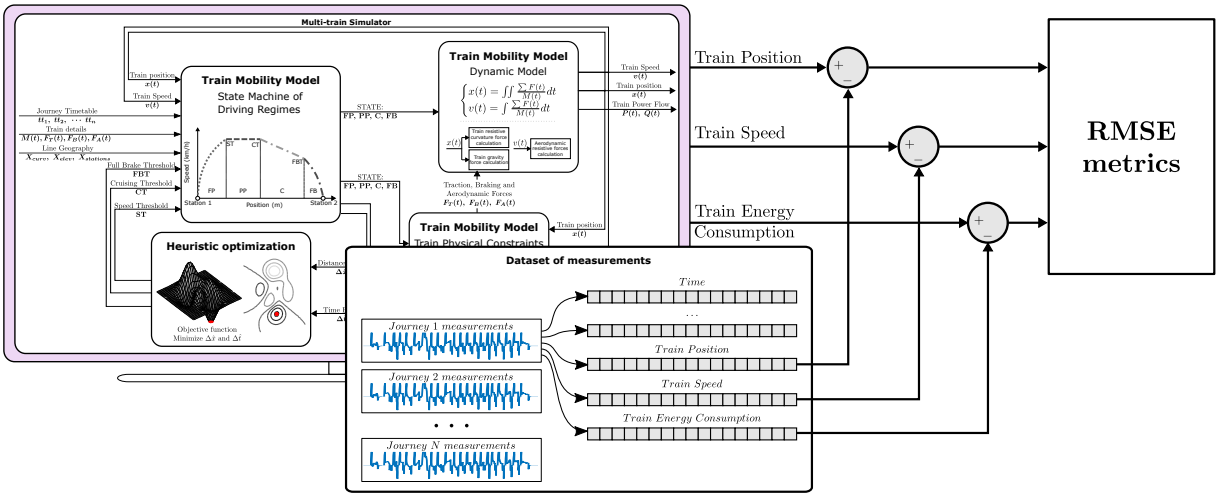

Figure 4.11: Validation methodology: each journey from a dataset of real measurements (gathered from a real train operation) is compared with the output of the train simulator.

The results for one train journey are presented in Fig. 4.12a) and Fig. 4.12b) for the speed error, and Fig. 4.12c) and Fig. 4.12d) for the position error.

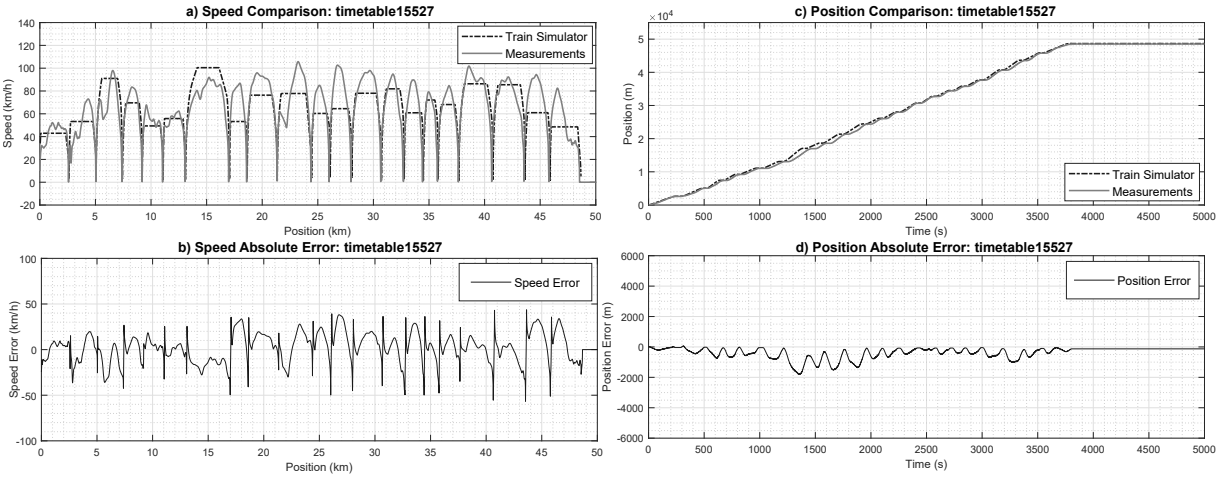

Figure 4.12: Comparison results for timetable journey with best RMSE position difference: a) Real measurements and train simulator speed results; b) Arithmetic speed difference; c) Real measurements and train simulator position results; d) Arithmetic position difference.

As illustrated by Fig. 4.11, all the available results were compared to a dataset of real measurements. The error between the train simulator and the measurements are presented in Table 4.4

For the eight journeys of the tested dataset, the speed difference value has an average RMSE of 17.6 km/h, while the position and consumption differences are 1.52 % and 13.51 % for the position and consumption RMSE metrics, respectively.

Table 4.4: Single-train simulation results

timetable number	Speed difference RMSE (km/h)	Position difference RMSE (m)	Position difference RMSE (%)	Consumption difference RMSE (kWh)	Consumption difference RMSE (%)
15513	16.40	456	0.9	31.33	10.95
15527	16.11	418	0.9	47.45	18.8
15529	15.23	699	1.4	50.75	22.3
15533	19.87	465	1.0	28.28	10.8
15535	18.65	576	1.2	29.41	11.1
15549	20.46	1785	3.7	23.78	8.7
15557	15.85	526	1.1	32.88	12.9
15559	18.44	1002	2.1	34.35	12.6
Average	**17.63**	**741**	**1.52**	**34.78**	**13.51**

However, these results must be taken with caution, since the operating conditions that lead to the measurements can be different. As example, in Fig. 4.13 and in Fig. 4.13 is illustrated the case with worst RMSE values.

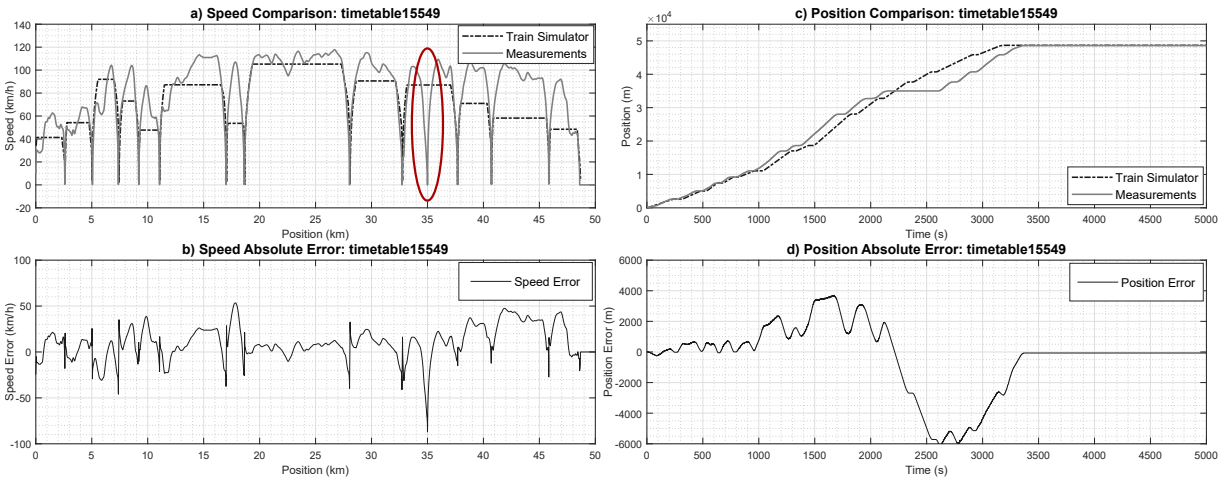

Figure 4.13: Comparison results for timetable journey with best RMSE position difference: a) Real measurements and train simulator speed results, highlighted with unexpected stop; b) Arithmetic speed difference; c) Real measurements and train simulator position results; d) Arithmetic position difference.

In this case, as highlighted in the Fig. 4.13, at $x_T = 35\ km$, the train has stopped for around 500 seconds for an unexpected event (as example: signalling, operation constraints, etc.). Thus, this is the worst result of the comparison ($position\ RMSE = 1785\ meters$).

With the previous results, it can be concluded that an accurate simulation of the dynamic train movement was reached. The RMSE values for energy consumption show an average of 13.5 %. However, there is no correlation between the errors of the estimated energy consumption and dynamic models. As the example in Fig. 4.14, for best and second worst position difference, the energy consumption RMSE is 18.9 % and 12.6 %, respectively.

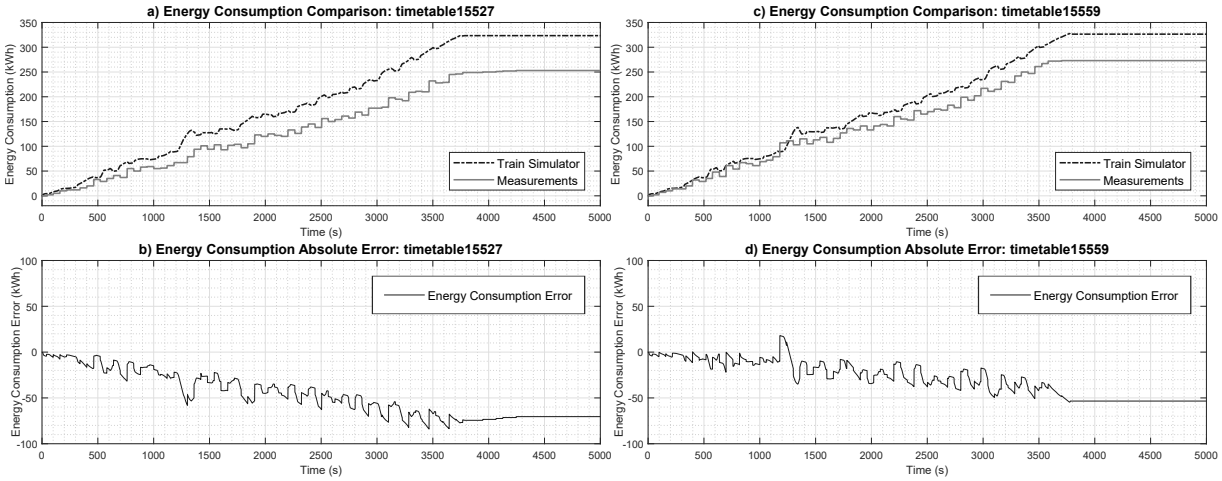

Figure 4.14: Energy comparison results for timetable journey with best and second worst RMSE position difference: a) Real measurements and train simulator energy results, for best RMSE position difference; b) Arithmetic energy difference (RMSE = 18.9 %); c) Real measurements and train simulator energy results, for second worst RMSE position difference; d) Arithmetic energy difference (RMSE = 12.6 %).

The simulation is not able to accurately estimate real operation conditions, due to the stochastic characteristic of the train operation. Essentially, the real operation is determined by countless uncertainties like the behaviour of train driver, or the effect of passenger boarding/leaving in the delays. Also, the speed profile heuristic generation previously presented does not consider any energy optimization strategy, which an experienced train driver or an automatic driving assistance system will certainly have. These two journey results in Fig. 4.14 clearly illustrates the simulation to be more energy demanding than the real measurements. Specifically, in average, each train simulation needs additional 34.8 kWh than the real operation (RMSE = 13.5 %).

The evaluation and comparison on the power consumption, in the Fig. 4.15, shows considerable differences on the results of the train simulator and on the real measurements. However, those differences are due to the listed stochastic uncertainties that were not able to be simulated. Essentially, in terms of power consumption these differences are caused by synchronism errors (delays in departure or arrival, as exemplified in the Fig. 4.15a)).

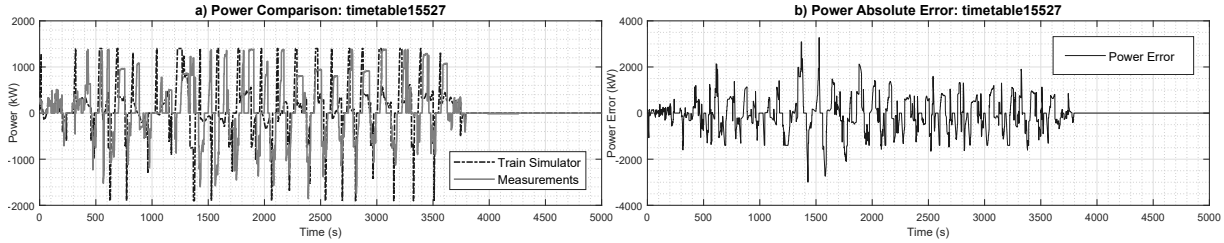

Figure 4.15: Power comparison results for timetable journey with best RMSE position difference: a) Real measurements and train simulator power results; b) Arithmetic power difference.

Nevertheless, from a purely simulation standpoint is achieved a good estimation of the train energy consumption. These results can be used in a multi-train simulation tool to evaluate strategies within the infrastructure.

4.7 Multi-Train Simulator Results

The results of the multi-train simulator will consider all the possible timetable journeys and estimate each of the train dynamics and energy consumption, using the methodology previously presented.

The first set of results is the presentation of the global train position for weekdays and the weekend, respectively, in Fig. 4.16 and Fig. 4.17.

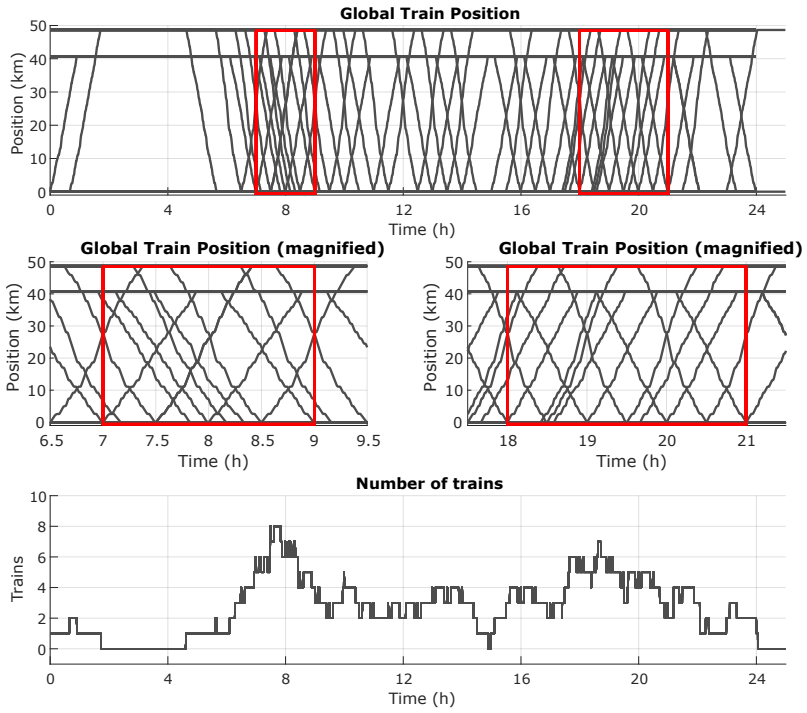

Figure 4.16: Global train position results for Train Simulator - Weekdays.

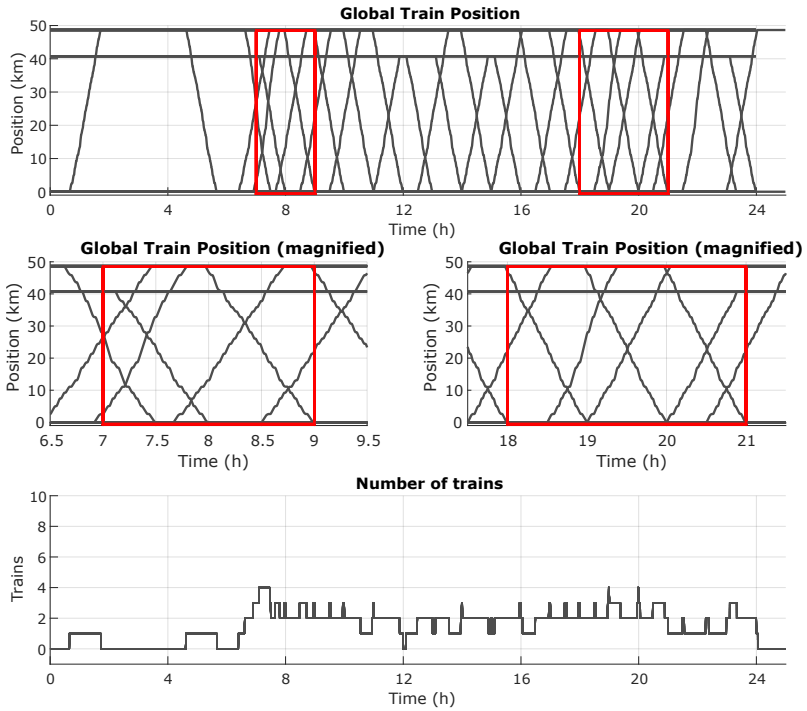

Figure 4.17: Global train position results for Train Simulator - Weekend.

The highlight on the train positions of Fig. 4.16 and Fig. 4.17 allows a better evaluation on each train movement during morning and evening rush hours.

From the results of all train power consumptions, considering only one traction power substation supplying the railway line, and considering an ideal catenary line ($R_l = 0$ and $X_l = 0$), it is possible to estimate the line total power consumption by adding the power of each train. This results in the graphs of Fig. 4.18, being the line power consumption coherent with the number of trains in the line (during the rush hour, the power consumption peak is around two times than during the regular hour).

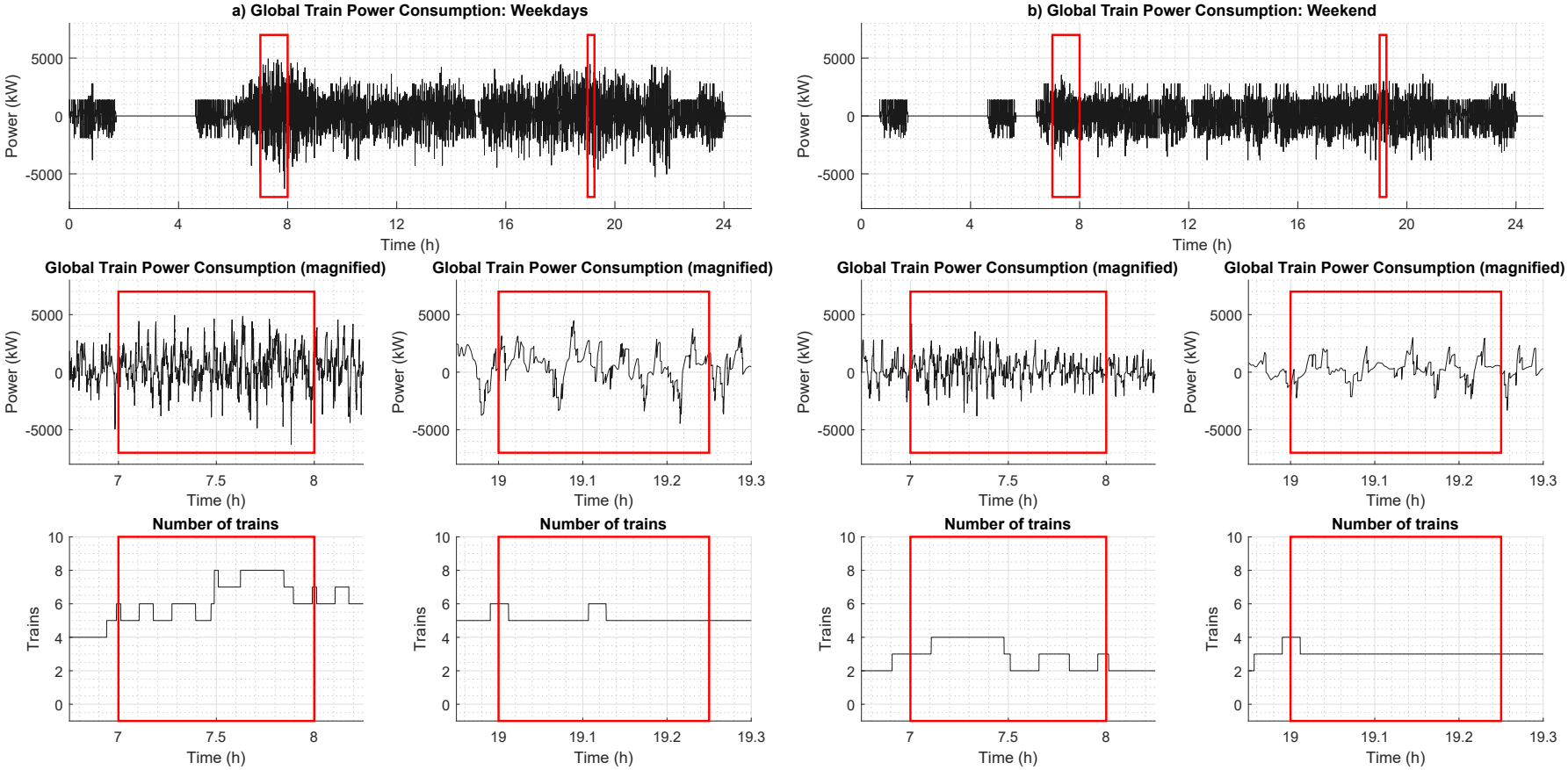

Figure 4.18: Global power consumption results for Train Simulator: a) Weekdays; b) Weekend.

In addition, the results of the multi-train simulator can display the global energy contribution of each of the two traction substations, as visible in Fig. 4.19 for the weekdays and weekends.

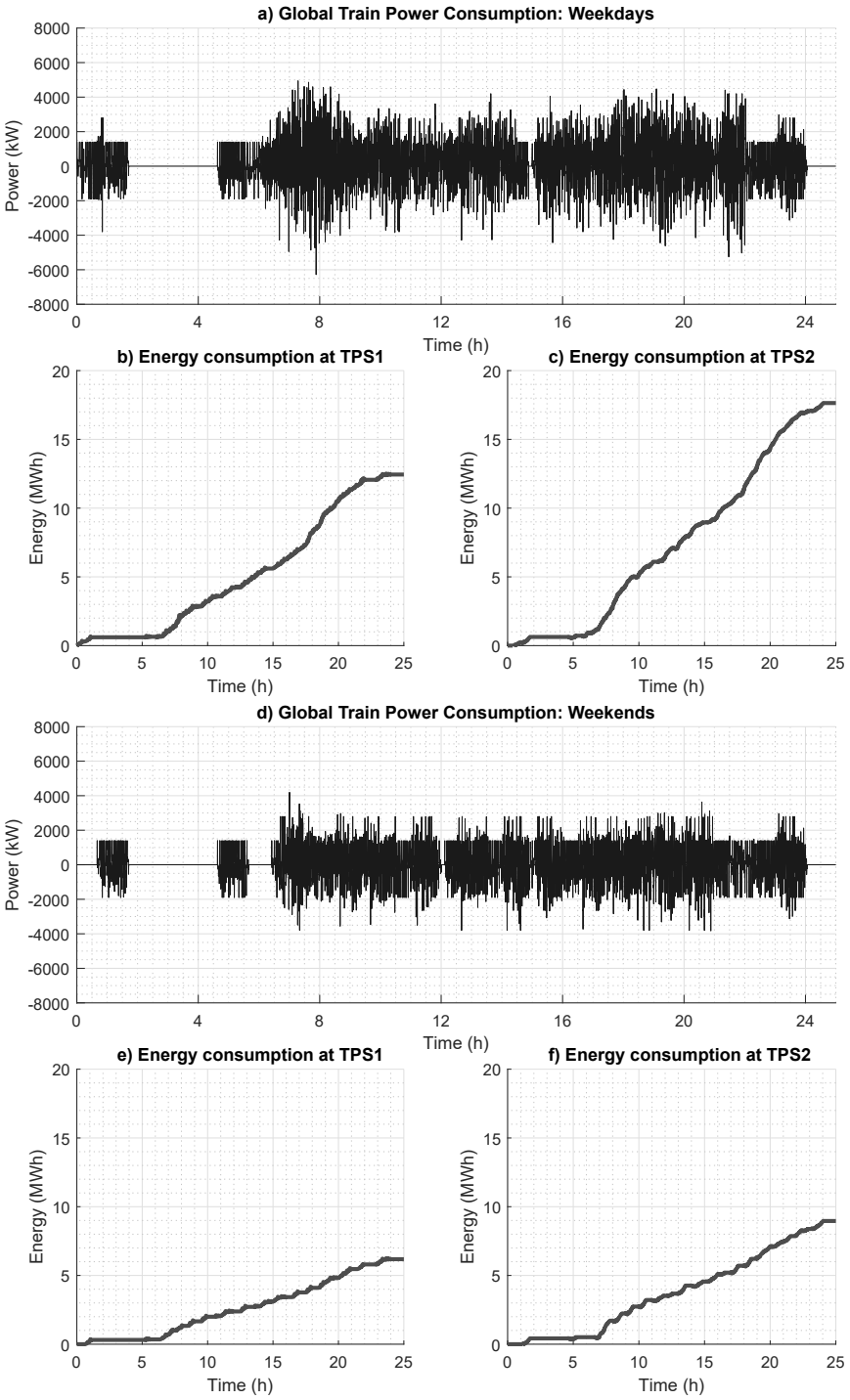

Figure 4.19: TPS energy consumption results: a-c) Weekdays; d-f) Weekends.

The results presented in Fig. 4.19 are obtained by combining the power consumption and the respective position of each train. Specifically, for each of the two Traction Power Substation (TPS) considered in the case study line of this chapter, the first step is to know the coverage of each substation which is given by the expression in (4.17).

$$\begin{cases} TPS_1 & \in [x_0 \ \cdots \ x_{nz}] \\ TPS_2 & \in [x_{nz} \ \cdots \ x_{end}] \end{cases} \tag{4.17}$$

As second step, the power of each traction substation can be obtained by the expression in (4.18)

$$\begin{cases} P_{TPS_1} & = \sum_{j=1}^{N} \left(P_j(t) \cdot w_j\right), \quad \begin{cases} w_j = 1 & if \ x_j(t) \in [x_0 \ \cdots \ x_{nz}] \\ w_j = 0 & otherwise. \end{cases} \\ P_{TPS_2} & = \sum_{j=1}^{N} \left(P_j(t) \cdot w_j\right), \quad \begin{cases} w_j = 1 & if \ x_j(t) \in [x_{nz} \ \cdots \ x_{end}] \\ w_j = 0 & otherwise. \end{cases} \end{cases} \tag{4.18}$$

Where for each journey j of the total N trains, the train power, $P_j(t)$ and train position, $x_j(t)$, are the results of the multi-train simulation tool. Finally, as visible in Fig. 4.19, the energy of each TPS can be obtained.

4.8 Discussion and Conclusions

This chapter presents a multi-vehicle train simulator tool. The objective of this chapter is to generate the relevant information for each train in a railway line, for a given time window. Furthermore, it was achieved a valid tool, using a validation methodology based on a comparison of the output of certain parts of the simulator with real measurements.

In the first part of this chapter was proposed the core of this tool: (i) a dynamic train model and (ii) an energy train model. This part was validated through real measurements, resulting in an RMSE of 3.04 km/h for the train speed, 1.03 % for the train position and 4.3 % for energy consumption.

Being this validation supported by extensive detail in appendix C and appendix D, it can be concluded that the inclusion of the detail on the track gradient and curvature, as well as in the auxiliary power and non-unitary efficiency, results in a detailed train model. Furthermore, the usage of this model for an accurate estimation of the relevant information is of advanced interest for a smart railway framework.

In the second part of this chapter is proposed a heuristic strategy to automatically generate the relevant information for any given timetable. The result of the train model having the movement profile generated by the heuristic algorithm was also compared to real measurements. As result of this comparison, the speed RMSE is 17.6 km/h, the position RMSE is 1.52 % and the energy consumption difference is 13.5 %.

As final results of the multi-vehicle train simulator, it is possible to evaluate the position of each train as a function of the time, for weekdays and weekends, where the Fig. 4.16 and Fig. 4.17 are illustrative of the possible evaluation. One example is the density of trains in each time instant.

Regarding the power flow evaluation, a simple analysis can be performed with the graphs of Fig. 4.18 and Fig. 4.19. However, these results must be carefully considered since those results do not take into account the voltage drop in the catenary as well as the losses in the system. Therefore, an extensive railway power flow analysis tool, like the one presented in chapter 5, must be taken into consideration for the analysis. Without a proper analysis of the power flow, this proposed tool is also capable of estimating the energy consumption in each TPS of the electrified line.

The proposed tool was designed to estimate feasible solutions for the train dynamic movement and energy consumption. However, certain design aspects were not taken into consideration for faster simulation. For example, by storing in a database the results of the heuristic for journeys with similar mobility requirements, it is possible to avoid repetitive calculations. Specifically, if two different journeys have the same partial track requirements (a train in station A has the same time window to go to station B), currently the heuristic algorithm will try to generate a new speed profile. By holding in database previous similar results and by bypassing the heuristic algorithm if the result was also obtained, the estimation process will be much faster than the current implementation.

One other improvement is in the braking of the train. Current implementation tries to estimate the braking process as an output of the heuristic algorithm. However, this braking process can be deterministic. For each passenger station, the braking distance is a function of the current train speed. This is better clarified in Fig. 4.20.

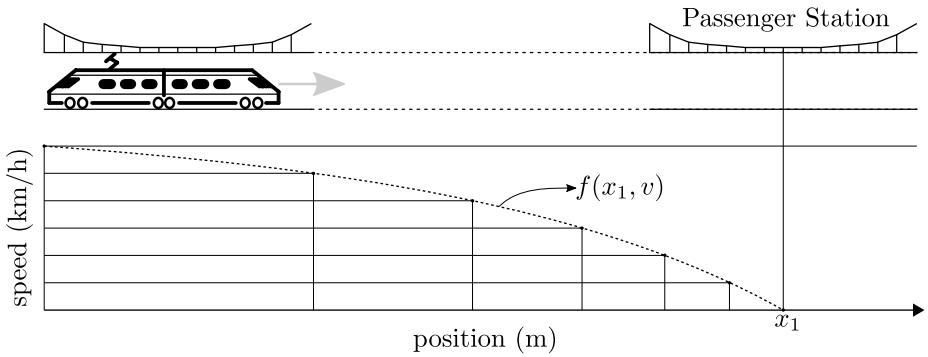

Figure 4.20: Illustration of procedure to have a deterministic train braking.

The braking curve, $f(x_1, v)$, can be obtained as a pre-processing step: for each passenger station, a simulation of the train is performed, considering a train moving from x_1 in the negative direction, where the traction force will be the maximum braking force (and considering the entire expression in (4.5)). Since the function $f(x_1, v)$ is a non-linear function, all the stations must be pre-simulated. With this adaptation, the heuristic algorithm only has to estimate the speed and cruising thresholds.

4.9 Summary

Despite the possible improvements discussed before in the proposed multi-train simulation tool, the main objective is achieved. For any given journey timetable, the proposed tool is capable of estimating the train dynamic movement and energy consumption, with low RMSE errors when compared with real train data. The estimated results can replace the information generated by the train energy meters (for simulation purposes).

As identified in chapter 2, the open research opportunities are in avoiding proprietary or commercially available simulation platforms. The objective proposed for this chapter was achieved and the proposed tool is a contribution to the scientific community.

The data generated by the tool presented in this chapter will be used in the following chapter 5, where the knowledge on the electrification system state will be extracted.

CHAPTER 5

PSSA-rail: Power System State Analyser Tool for Railways

In this chapter is addressed the topic **T3** – Development of PSSA-rail, a tool to extract the knowledge from the railway energy information. Furthermore, it is illustrated the usage of this tool to evaluate two strategies for energy optimization.

The essence in this tool is on the capability of estimating the knowledge of the power flow for an entire double-track railway line, for a long simulation time-window, where the electrical equivalent diagram is valid for the entire time window. In addition, the proposed tool enables studies on optimization scenarios.

This tool was implemented in a object-oriented language approach, which allows this tool to be tested for two different case studies. The first case study, comprising a 50 km railway line with two traction substations and 70 train journeys, uses the energy information produced in the tool of chapter 4. Furthermore, throughout this chapter, the detail and implementation steps of this tool will be illustrated with the first case study. The second case study uses real data from a 250 km railway line and having 7 traction substations and 252 train journeys. The demonstration of the validity of the tool for this second case study is presented in the appendix E.

The outcome of this chapter will be a tool to generate the knowledge of an entire railway line, capable of implementing strategies for energy optimization, as illustrated in the graphical abstract in Fig. 5.1.

The objectives of this chapter are:

- **Objective 3a**: Design and implementation of PSSA-rail tool, to extract knowledge of railway electrification using train energy information;
- **Objective 3b**: Evaluation and assessment of PSSA-rail features and limitations;
- **Objective 3c**: Demonstrate the flexibility and capability of the PSSA-rail tool to study and evaluate strategies, with illustration for two optimization scenarios.

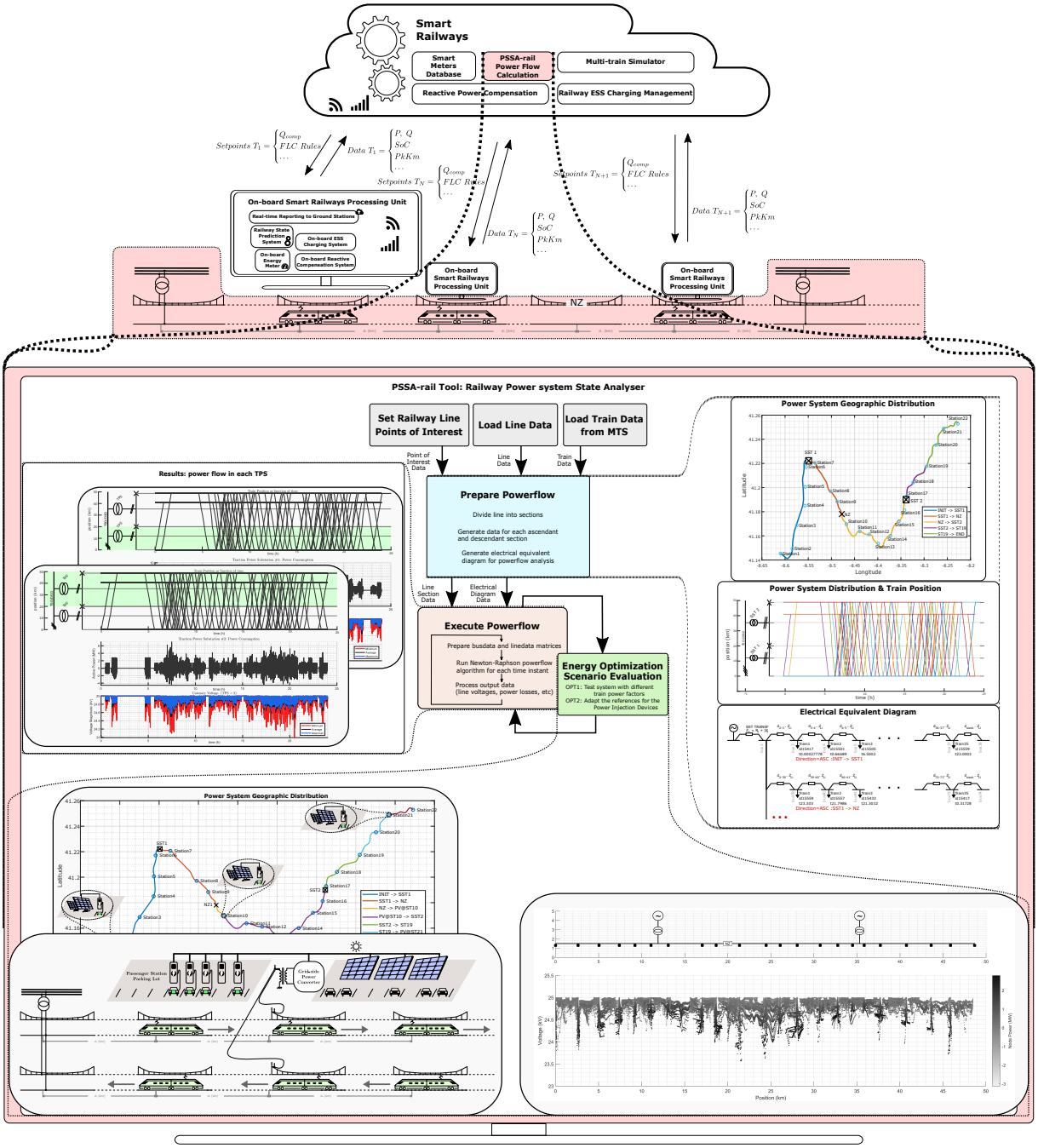

Figure 5.1: Graphical abstract of chapter 5 — Inclusion of railway power system state analyser tool in smart railway framework.

5.1 Introduction

As stated, the advantages of having the knowledge on the power flow of a railway line are clear, towards the achievement of the desirable improvements on the energy efficiency in this transportation domain. From Fig. 1.1, this knowledge is generated from the energy information, where this information can be generated by a multi-train simulation tool, like the one presented in chapter 4, or can be produced by onboard train energy meters. The standard EN50463 [149], is a good clarification and frame on the data that is part of this energy information.

The main objective of the tool proposed in this chapter is to generate the knowledge on the energy flow, using as input the energy related information in expression (5.1).

$$Info\ T_{1,..,N} = \begin{cases} Dynamics\ Data = \begin{cases} x(t),\ v(t) \\ F_T(t),\ F_B(t) \end{cases} \\ Energy\ Data = \begin{cases} P(t),\ Q(t) \\ E(t) \end{cases} \end{cases} \tag{5.1}$$

Then, the output of this tool, the knowledge on the power flow for the railway line, is given by the expression in (5.2).

$$PF\ Knowl\ TPS_{1,..,N} = \begin{cases} Energy\ Info = \begin{cases} P(t),\ Q(t) \\ E(t) \end{cases} \\ Train\ Info = \begin{cases} V_{T_1,...,T_n}(t) \\ I_{T_1,...,T_n}(t) \end{cases} \\ Optimization = \begin{cases} Metrics\ M_1, M2, \cdots, M_n \end{cases} \end{cases} \tag{5.2}$$

As raised in the research opportunities on the topic **T3** that has leaded to this chapter, the development of PSSA-rail, a tool that can extract knowledge on the energy of a railway line, for any time window, and for any railway line is a valuable contribution for the scientific community.

Therefore this tool has the following requirements:

- The tool must be flexible to simulate any railway line, with minor adjustments;
- The tool must be capable of performing an analysis on all the trains of a railway line, moving in both directions;
- The analysis must cover a broad time-window and the electrical equivalent model of the line must be valid for the entire simulation time-window;
- The tool should be capable of evaluating specific points-of-interest on the line.

5.1.1 Railway Electrification Model Formulation

The generation of knowledge related to the energy consumption is a power flow analysis problem. However, it is more complex than the conventional transmission/distribution power system. In the railway power system, due to the train movement, the line electrical parameters are not fixed and need to be calculated for each simulation time instance.

In Fig. 5.2 is presented the transversal and longitudinal sections of a 1×25 kV overhead catenary system railway electrification system considered in this chapter.

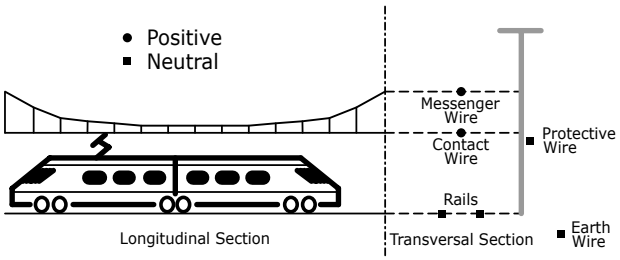

Figure 5.2: Conductor distribution of a 1×25 kV railway electrification system.

As highlighted in chapter 3, the proposed enhanced π-type line model is used in the PSSA-rail. Therefore, the power flow analysis tool used is MatPower [69], with the radial current summation method as the adopted solver[1]. Furthermore, the enhanced model was used with the default typical values for the earth conductances and line capacitance.

5.2 PSSA-rail System Architecture

This section presents the architecture and the implementation for the developed tool. A typical structure for this state analyser is illustrated in Fig. 5.3 where it has been used in [150, 151] work examples.

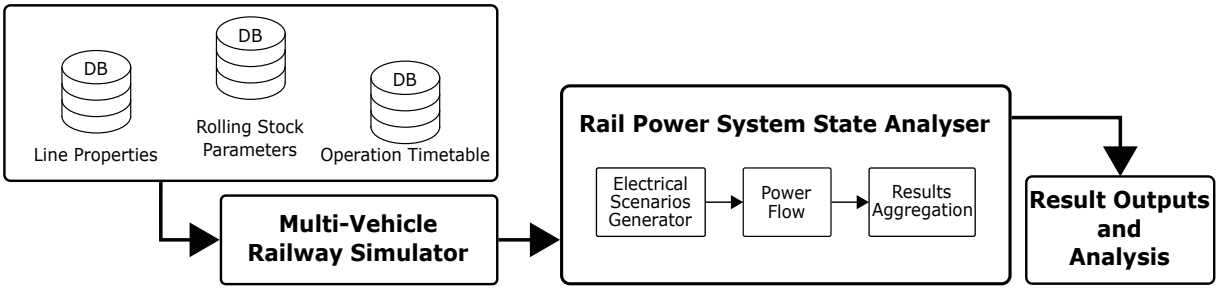

Figure 5.3: Typical structure of a railway power system state analyser.

[1]For specific analysis that requires not radial circuits there are available MatPower solvers like Newton-Raphson, Gauss-Seidel or Fast-Decoupled.

This structure is of advanced interest since it allows this power system state analyser to be fed with data generated by onboard energy meters, as illustrated in Fig. 5.4.

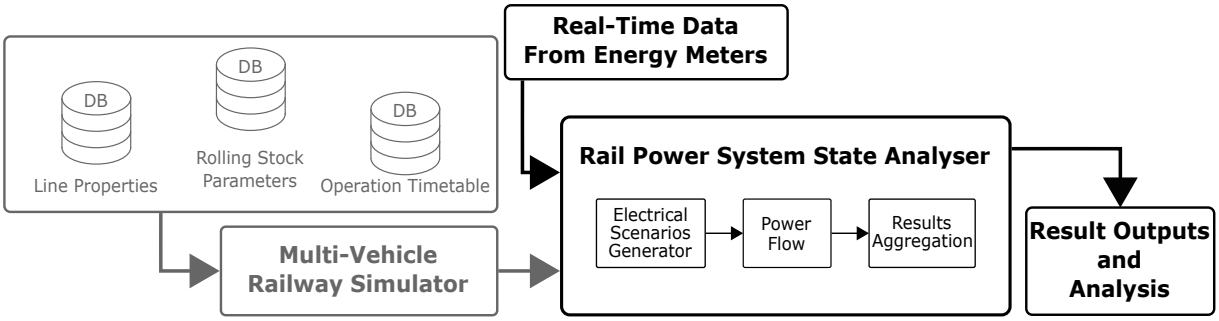

Figure 5.4: Typical structure of a railway power system state analyser with train energy information produced by the onboard energy meters.

5.2.1 Implementation of PSSA-rail

In Fig. 5.5 is illustrated the structure of the implemented tool.

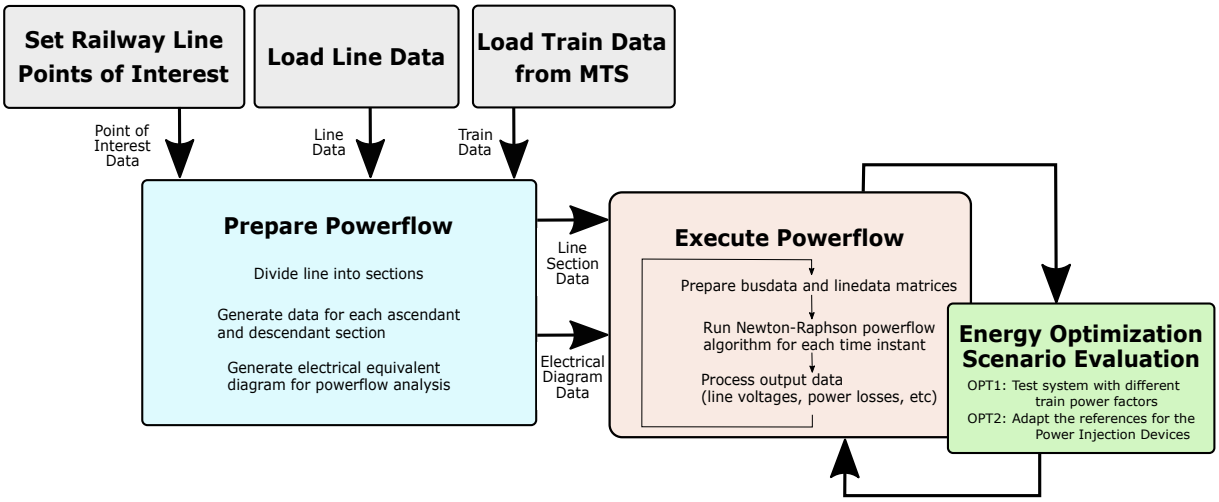

Figure 5.5: Implemented structure of PSSA-rail.

This tool was implemented in Matlab, with a object-oriented approach. This approach enables higher degree of flexibility for the analysis of any railway line.

Each developed module is a combination of methods and data. In Fig. 5.6 is presented the Unified Modeling Language (UML) diagram for the majority of the developed tool.

Figure 5.6: UML diagram of the railway power system state analyser.

The PSSA-rail is divided into four functional parts:

- Load Simulator Data Module;
- Prepare Simulation Module;
- Execute Simulation Module;
- Evaluation Scenario for the Energy Optimization Strategy.

As said, the ability to simulate any railway line is desirable. Therefore, the first *Load Simulator Data Module* must be compatible with the target railway line. As long as the relevant data is loaded with correct data structure, the remaining modules are flexible enough to perform the requirements of the tool.

5.2.2 Load Simulator Data Module

From the output databases of the *Load Simulator Data Module*, comprising the **train_data** database, **line_data** database and **PoI_line_data** database, it is possible to automatically generate the knowledge of the power system geographic distribution, in Fig. 5.7, and the power system distribution combined with the train position, in Fig. 5.8.

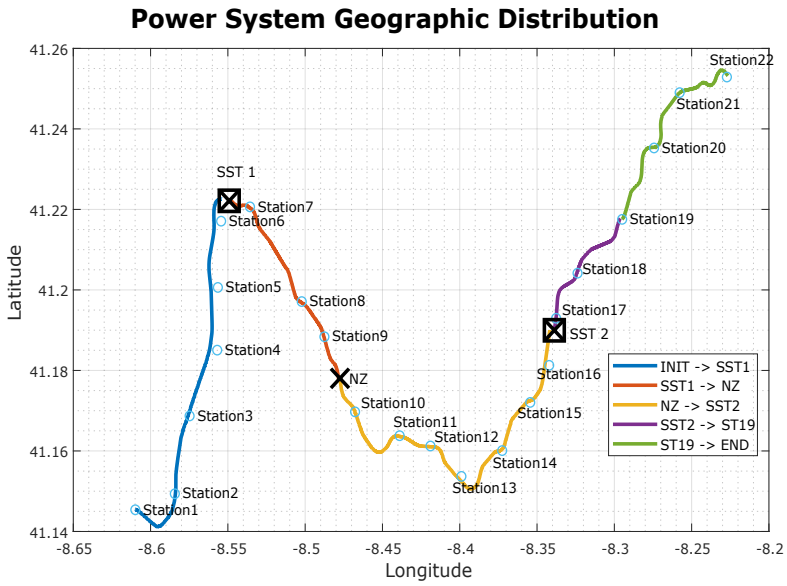

Figure 5.7: Output of the *Load Simulator Data Module*: Power system geographic distribution.

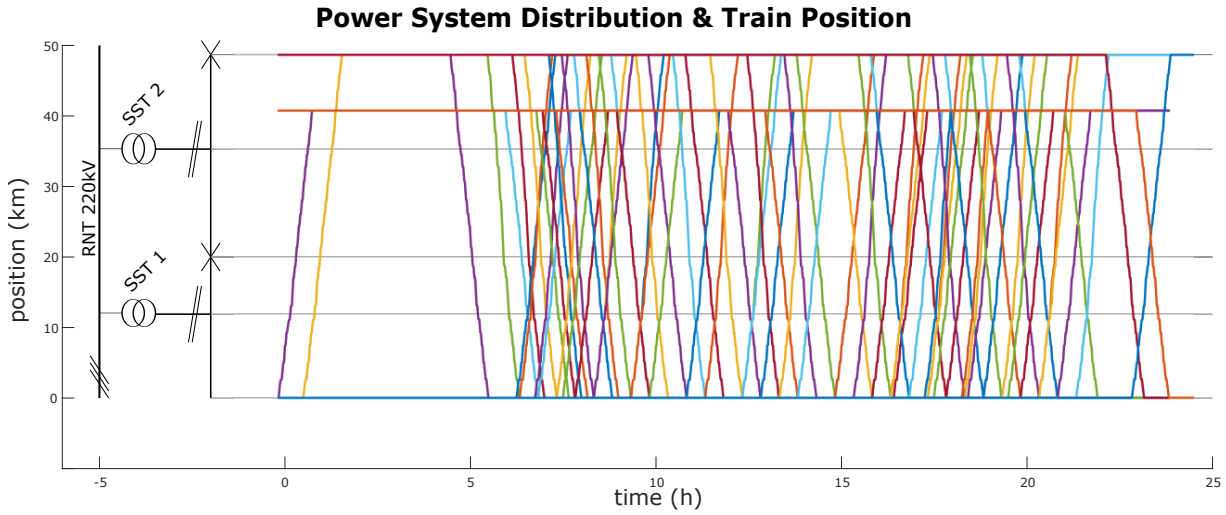

Figure 5.8: Output of the *Load Simulator Data Module*: Power system distribution and train positions as function of the time.

The first part of this knowledge extraction software is to gather the relevant data, in form of geographic line data and train data. In addition, the railway power system simulator needs to have the knowledge of the Point of Interest (PoI) to be studied.

The initial PoI are part of the line data parameters, such as the TPS position as well as the NZ position. Furthermore, the initial PoI are also automatically obtained part from the train data: each train arrival and departure must occur in a PoI, for the entire simulation time window[2].

Besides the initial PoI, other points of the line can be considered to evaluate, for instance, the inclusion of Power Injection Devices (PID) at specific points of the line, as listed as one of the optimization opportunities for this chapter.

A specific case study will be used, in this chapter, for demonstration purposes. Its main characteristics are:

i: 48 km of length with double-track rail;
ii: 22 passenger stations;
iii: Two TPS having one NZ;
iv: Specific journey train data generated by the tool in chapter 4;
v: Specific electrical line model of chapter 3.

[2]For each train journey, if the arrival or departure positions are not part of the PoI database, then a new PoI must be added to the **PoI_line_data** database. As example, in this case study, all trains departs/arrives in one of the following three passenger stations: **STA1**, **STA19** or **STA22**.

5.2.3 Prepare Simulation Module

Using the relevant input data, the first step to prepare the PSSA-rail analysis algorithm is to divide the line into sections. Considering the example of the power system geographic distribution presented in Fig. 5.7, where the six points of interest are *STA1, TPS1, NZ, TPS2, STA19, STA22*, this has resulted in:

- two sections associated to the **TPS1**: *STA1* $\longleftrightarrow$ *TPS1* and *TPS1* $\longleftrightarrow$ *NZ*;
- three sections associated to the **TPS2**[3]: *NZ* $\longleftrightarrow$ *TPS2*, *TPS2* $\longleftrightarrow$ *STA19* and *STA19* $\longleftrightarrow$ *STA22*.

Furthermore, the graph of Fig. 5.8 also helps in the division of the railway line into sections, where each train movement is evaluated in respect to the electrical infrastructure for the simulation time-window.

For each section the second step is to fill up the **line_section_data** database, which is consisted of two data structures for the ascendent and descendent tracks, like is illustrated in Fig. 5.6. This database is better presented in Fig. 5.9.

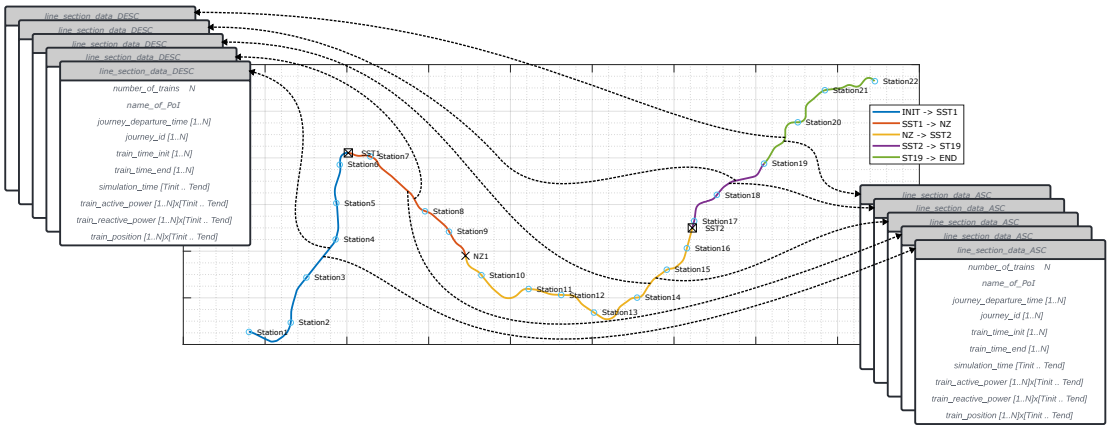

Figure 5.9: Illustration of the *Prepare Power Flow Module* for the **line_section_data** database generation.

This database essentially has two dimensions: the time, $[t_{init}, \cdots, t_{end}]$, and the trains, $[1, \cdots, N]$. It is also essential to ensure that the trains are ordered according to the departure time, for better calculation of the matrices associated with the line distances.

Then, the third step is to calculate the relative distances d_1, d_2, $\cdots$, d_N and the slack distance d_{slack}, for each time-step of the simulation time-window, for each of the line sections and based on the absolute train positions. This calculation is better described in Fig. 5.10.

[3]As example if a power injection device is placed in *STA10*, the corresponding TPS2 will now have four sections.

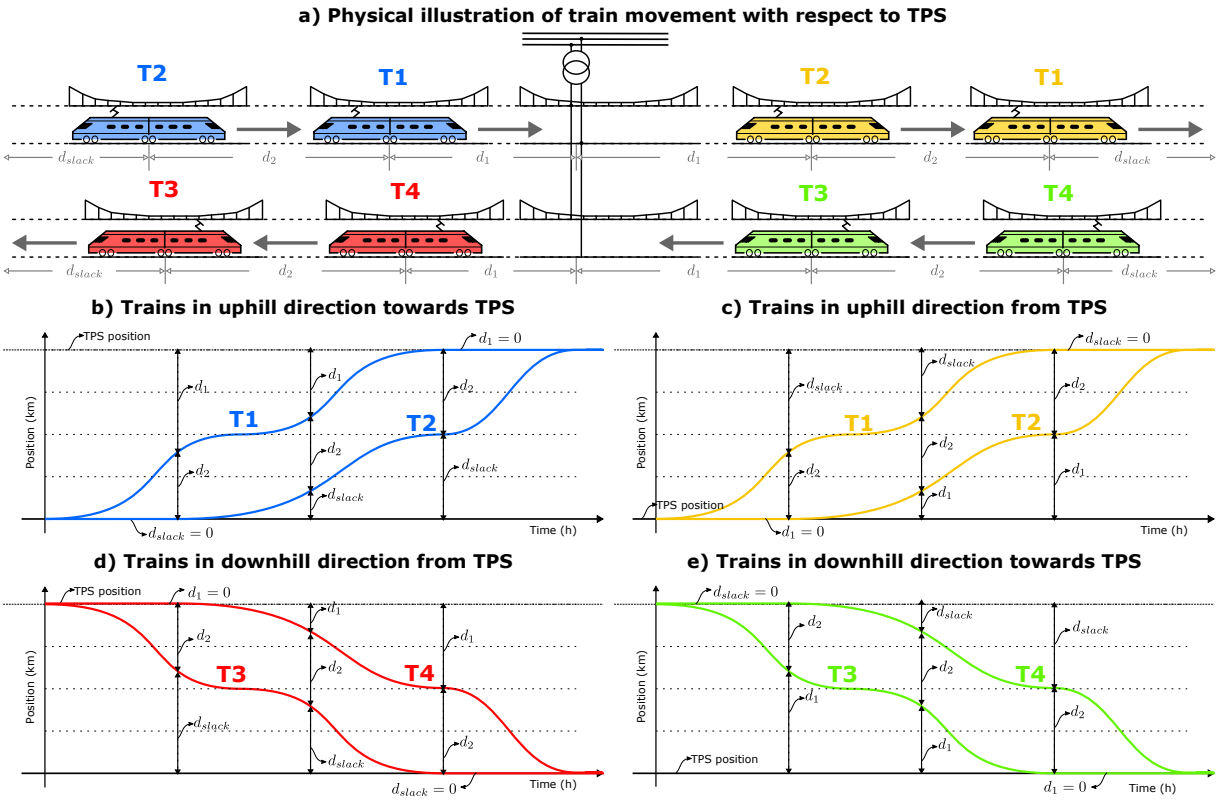

Figure 5.10: Illustration of train movement with respect to TPS for a simulation time-window.

Finally, for each instance of the simulation time-window and for each line section, the power of each train is "truncated", following the illustration of Fig. 5.11.

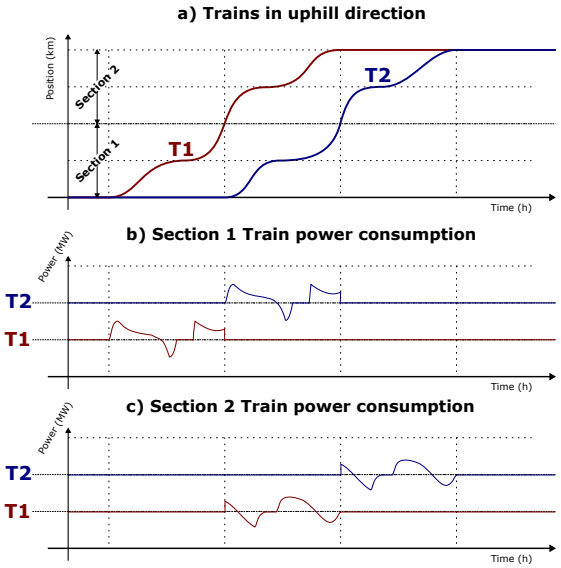

Figure 5.11: Illustration of train power consumption for each line section.

This module is also capable of automatically generate the electrical diagram for each TPS and for the entire simulation time-window. In Fig. 5.12 is presented the generated electrical diagram for the second TPS of the considered case study line, where are covered the three sections[4] which has resulted in six electrical branches.

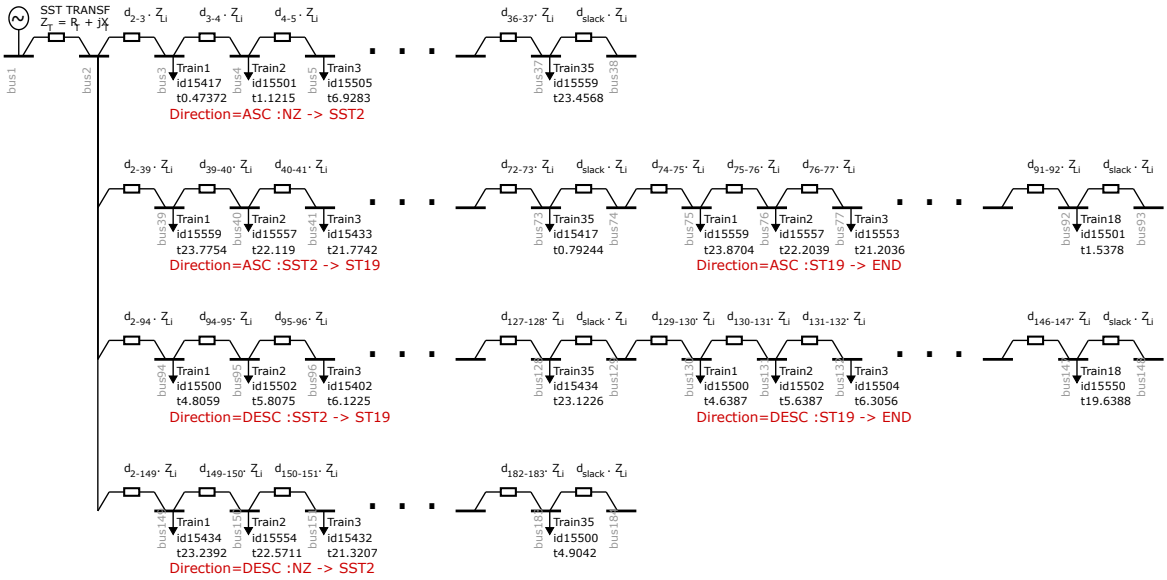

Figure 5.12: Automatic generated equivalent electrical diagram at TPS2 with all sections modelled.

It is assumed that the uphill and downhill line sections are only electrically connected in the TPS (which is a common practice in the normal operation of railway electrical systems, due to operation security issues [152]). In the presented electrical equivalent diagram, the "STA19" point of interest corresponds to an important passenger station where certain trains will depart/arrive in that station.

The resultant diagram will consider:

- 35 journeys in uphill/ASC section $NZ \rightarrow TPS2$ which corresponds to the bus 3 to 37 and the bus 38 representing the fixed position of NZ;
- 35 journeys in uphill/ASC section $TPS2 \rightarrow STA19$ which corresponds to the bus 39 to 73 and the bus 74 representing the fixed position of STA19;
- 18 journeys in uphill/ASC section $STA19 \rightarrow STA22$ which corresponds to the bus 75 to 92 and the bus 93 representing the fixed position of STA22 station;
- 18 journeys in downhill/DESC section $STA19 \rightarrow STA22$ which corresponds to the bus 130 to 147 and the bus 148 representing the fixed position of STA22 station;
- 35 journeys in downhill/DESC section $TPS2 \rightarrow STA19$ which corresponds to the bus 94 to 128 and the bus 129 representing the fixed position of STA19 station;

[4] $NZ \rightarrow TPS2$, $TPS2 \rightarrow STA19$ and $STA19 \rightarrow STA22$

- 35 journeys in downhill/DESC section *NZ* → *TPS2* which corresponds to the bus 149 to 183 and the bus 184 representing the fixed position of NZ;

5.2.4 Execute Simulation Module

The third module of PSSA-rail tool is responsible for solving the power flow for a given simulation time-window. Essentially, all the power flow input matrices are prepared, followed by running the power flow solver for each of the matrices and finally, the relevant energy knowledge data is extracted. This follows a three step procedure:

- Prepare the power flow solver data matrices for a given simulation time-window;
- Run the power flow solver matrices for all the time-steps of the simulation time-window;
- Retrieve the generated data as multiple databases, for further knowledge extraction.

This approach allows that each time-step can be simulated in a parallel processing approach, taking advantage on multi-core CPU computers to reduce the simulation time.

In the first step, for each time instance, the bus and branch matrices of MatPower solver are prepared. As the example in Fig. 5.13, all the train active power consumptions are loaded in each MatPower bus, according to the respective electrical equivalent diagram.

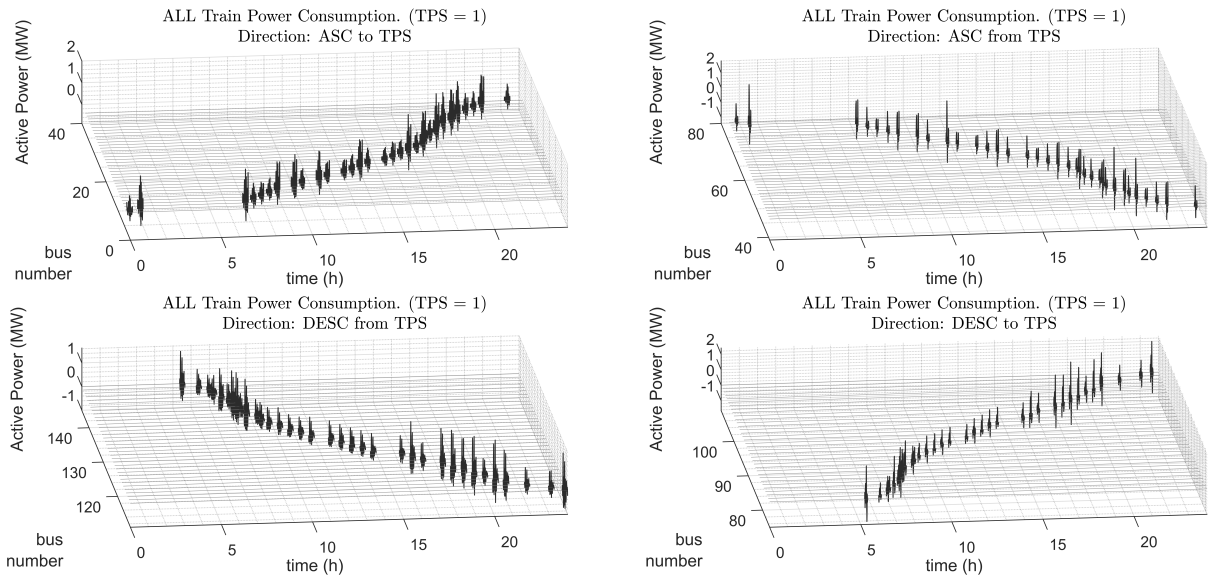

Figure 5.13: Active power in each bus node, in each section of the TPS1, for the simulation time-window of 24h.

After applying the second step and solving the power flow for all the matrices, one possible result is the evaluation of the voltage in each train, as visible in Fig. 5.14.

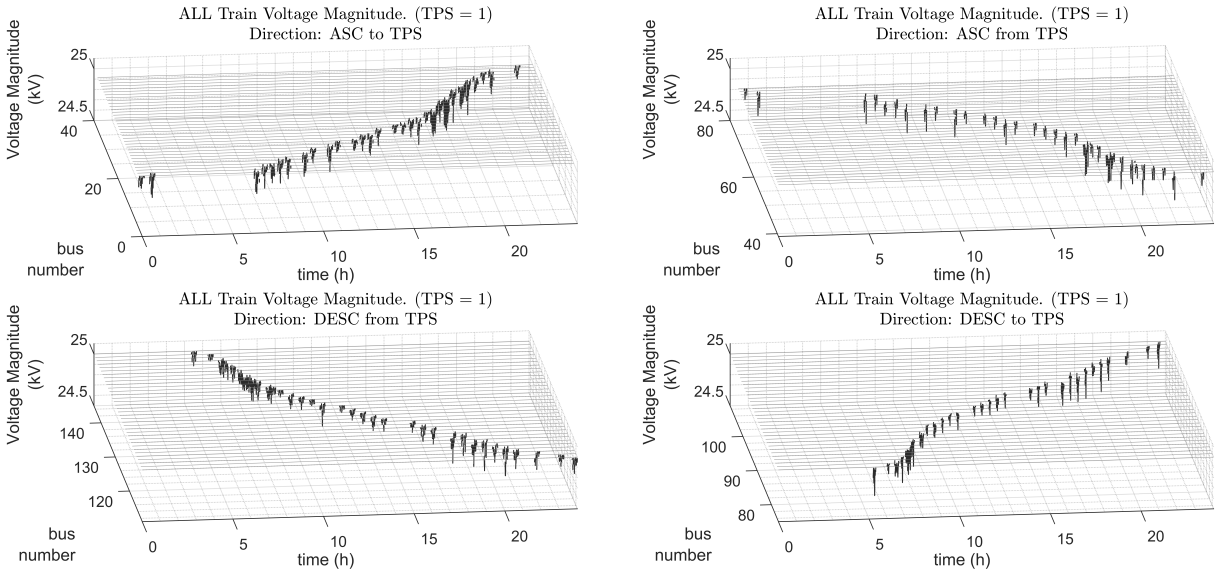

Figure 5.14: Resultant voltage magnitude in each bus node, in each section of the TPS1, for the simulation time-window of 24h. Note: for clarity reasons, for each bus node, it was only plotted the voltage during the train movement time-window. Therefore, this result must be taken with caution since it only illustrates the voltage in each train during its movement.

This second step requires the power flow solving methodology proposed in chapter 3, specifically with the application of the Algorithm 1.

From the output results of the MatPower execution, the final step of this *Execute Simulation Module* is to produce multiple databases of results. Those databases are essentially tables where each row is a time-step of the simulation time-window, the first column is the timestamp and the following columns are related to the database variable.

Those databases are stored in the class property *RUNTIME_DATA* of Fig. 5.6 specifically in multiple *process_output_data* instances, following the knowledge in expression (5.3).

$$
TPS_{1,..,N} = \begin{cases}
TPS\ Power & = \begin{cases} time & : [T_{init} \ \cdots \ T_{end}] \\ P(t) & : [T_{init} \ \cdots \ T_{end}] \\ Q(t) & : [T_{init} \ \cdots \ T_{end}] \end{cases} \\
TPS\ Energy & = \begin{cases} time & : [T_{init} \ \cdots \ T_{end}] \\ E(t) & : [T_{init} \ \cdots \ T_{end}] \end{cases} \\
Train\ Info & = \begin{cases} time & : [T_{init} \ \cdots \ T_{end}] \\ V_{T_1,...,T_n}(t) & : [T_{init} \ \cdots \ T_{end}] \times [1 \ bus_N] \\ I_{T_1,...,T_n}(t) & : [T_{init} \ \cdots \ T_{end}] \times [1 \ bus_N] \end{cases} \\
Branch\ Info & = \begin{cases} time & : [T_{init} \ \cdots \ T_{end}] \\ V_{1,...,n}(t) & : [T_{init} \ \cdots \ T_{end}] \times [1 \ branch_N] \\ I_{1,...,n}(t) & : [T_{init} \ \cdots \ T_{end}] \times [1 \ branch_N] \end{cases} \\
\cdots & = \begin{cases} time & : [T_{init} \ \cdots \ T_{end}] \\ \cdots \end{cases}
\end{cases} \tag{5.3}
$$

5.2.5 Optimization Strategy Module

The last relevant module of the PSSA-rail is integrated within the *Execute Simulation Module*, for further implementation of optimization strategies. For each analysis, specific routines are executed. In this chapter are evaluated two different optimization strategies:

- Adaptation of each train internal control loop, with decoupled adaptation of the reactive power, for specific power factor values. This strategy will be explained and extended in section 5.4.
- Inclusion of power injection devices in new points of interest, for the injection of active power with specific objectives. This strategy will be explained and extended in section 5.5.

In the following section are presented some relevant results generated by PSSA-rail.

5.3 PSSA-rail Simulation Results

In Fig. 5.15 and Fig. 5.16 are illustrated the output results for the case study railway line, regarding the power flow and line voltage, respectively.

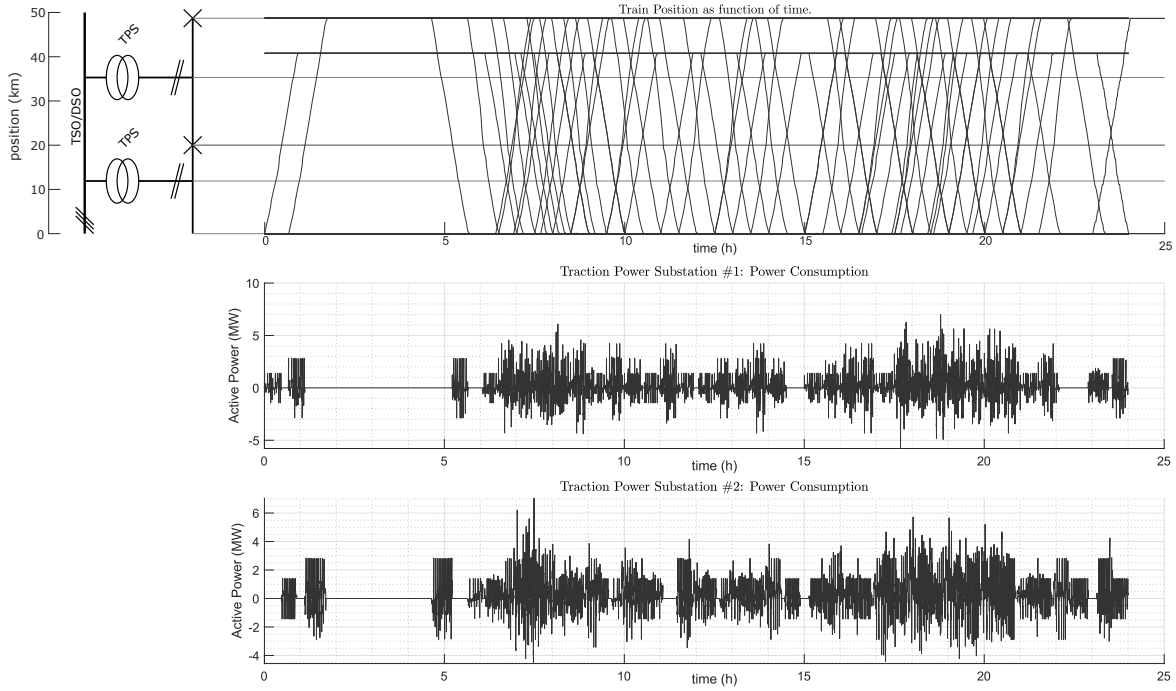

Figure 5.15: Power flow results for the case study railway line: (top) illustration of the journey's timetable and TPS coverage; (middle) active power flow in TPS1; (bottom) active power flow in TPS2.

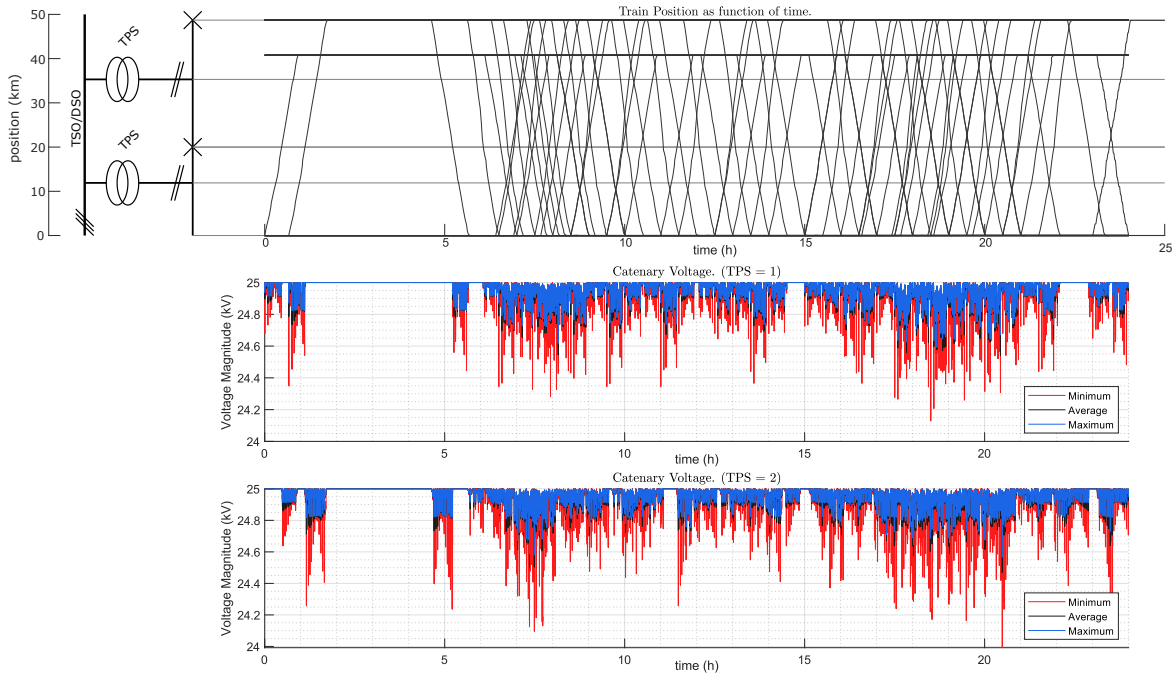

Figure 5.16: Results on catenary voltage for the case study railway line: (top) illustration of the journey's timetable and TPS coverage; (middle) maximum, average and minimum voltage in TPS1; (bottom) maximum, average and minimum voltage in TPS2.

In addition to the power flow result in Fig. 5.15, the PSSA-rail tool is able to estimate the reactive power, as well as the relevant information of expression (5.3). The voltage results in Fig. 5.16 are generated using the matrix $V_{T_1,\ldots,T_n}(t) : [T_{init} \ \cdots \ T_{end}] \times [1 \ bus_N]$, from the maximum, average and minimum voltages of all the buses in each time-step of the simulation time-window. Furthermore and regarding the energy, it is possible to estimate this value, for each of the branches of the TPS, as illustrated in Fig. 5.17.

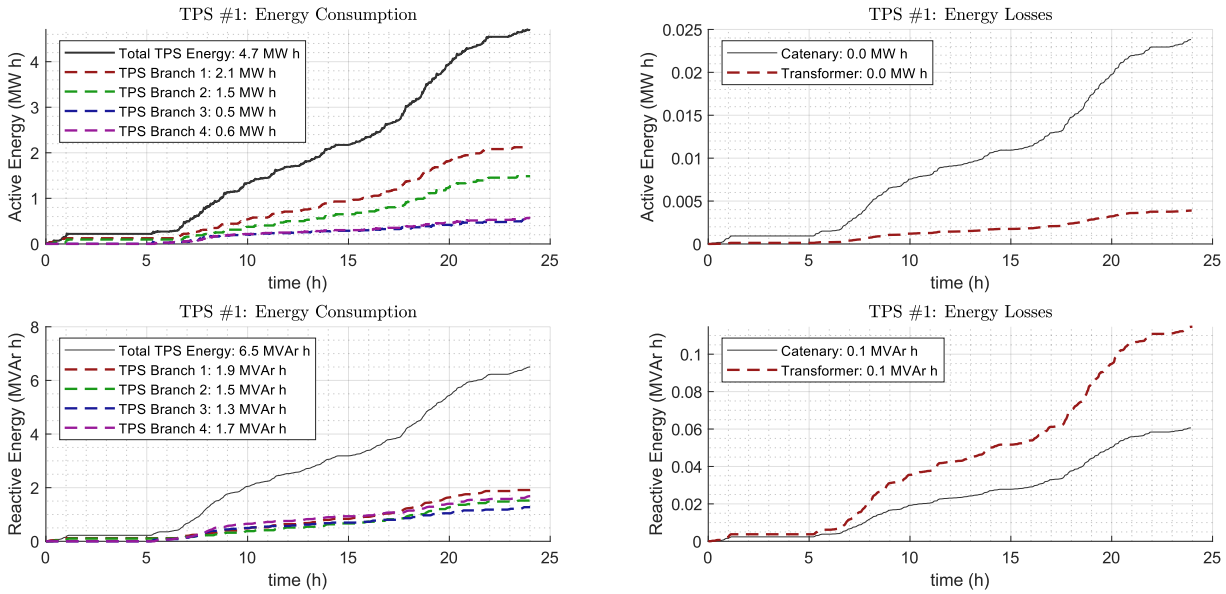

Figure 5.17: Energy flow (active and reactive) for the case study railway line: net total and branch energy consumption in TPS1; Catenary and transformer energy losses in TPS1.

The results on Fig. 5.17 were obtained having all trains with PF = 0.9 ind. Regarding the transformer model used in PSSA-rail, both TPS have a 20 MVA single-phase power transformer with $^{X}/_{R_T}$ ratio is near 30, where the nominal conduction losses are 0.3 % of nominal power and the empty losses are neglected. Also, the reactive energy associated to losses shown in Fig. 5.17 is a mathematical representation obtained by the integral of the reactive power difference in the branch.

These energy results must be taken with caution, in particular for the high reactive power value in the TPS (which is consequence of the the adopted power factor) and the existence of important intervals of regeneration. In Fig. 5.18 is illustrated the adopted internal control loop of each train. Then, the train power factor is only inductive, even when trains are in regenerative mode (In fact, even with important intervals of regeneration, the train voltage is mostly below 25 kV, as visible in Fig. 5.16).

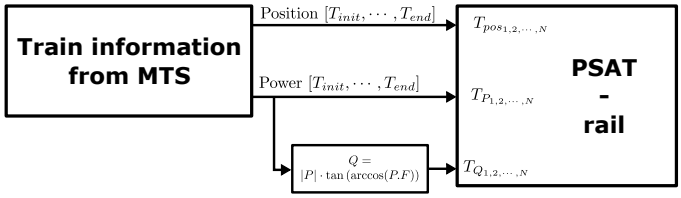

Figure 5.18: Schematic of the internal structure of the train active/reactive power control loop, adopted in the PSSA-rail.

The results of Fig. 5.17 also show different values at the branches. It should be noted two aspects: first, each branch has different lengths, covers different line profiles (in terms of positive/negative track gradients) and has different train journeys; then, the effect of having the neutral zone and the TPS also affects the results, where a train crosses the NZ or the TPS with inertia, resulting in the branch before the crossing to have more demand for power than the branch after the crossing.

This effect is visible in Fig. 5.19, where the branches 3 and 4, corresponding to the ones with lower net energy consumption, are the branches of higher energy regeneration. Furthermore, having the schematic of Fig. 5.10 as example, considering the neutral zone in the right side, the branch number four (trains in downhill direction from TPS) is the one where the all trains arrive at with kinetic energy and those trains complete the journey in this section[5].

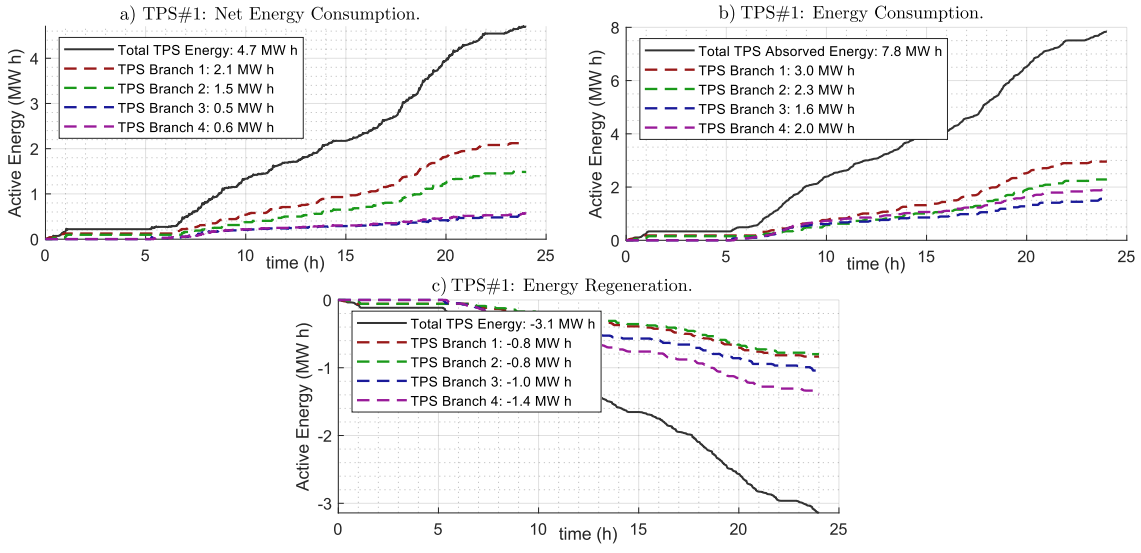

Figure 5.19: Energy flow for the case study railway line: a) net total and branch in TPS1; b) consumption-only in TPS1; c) regeneration-only in TPS1.

[5]From the results in Fig. 5.19, in branch 4 is regenerated more 40 % energy than average. However, this particular result can also be consequence of the line gradient, where the final station of branch 4 is placed in a lower elevation, as visible in the Fig. C.6

In this section was presented some generic results automatically generated by PSSA-rail tool for any TPS. This tool was also validated applying it to a second railway line, in appendix E, where other results are also presented.

The following two sections will present the methodology and results for two of the optimization strategies considered in this chapter.

5.4 Optimization Scenario 1: Adapting Train Power Factor

In the first part of this chapter was presented the PSSA-rail basic operation. The second part of this chapter is to illustrate the usage of the proposed tool for the study of specific optimization scenarios.

The first testing scenario enabled by this tool is in the adaptation of each train power factor, with respective improvement of the line voltage profile. As stated in chapter 3, specifically in Fig. 3.3, an increase on the reactive power in the TPS (mainly a consequence of low Power Factor (PF) in the trains) results in a lower train voltage.

The following graphs of Fig. 5.20 presents the evaluation of catenary voltage as function of the position and the train power.

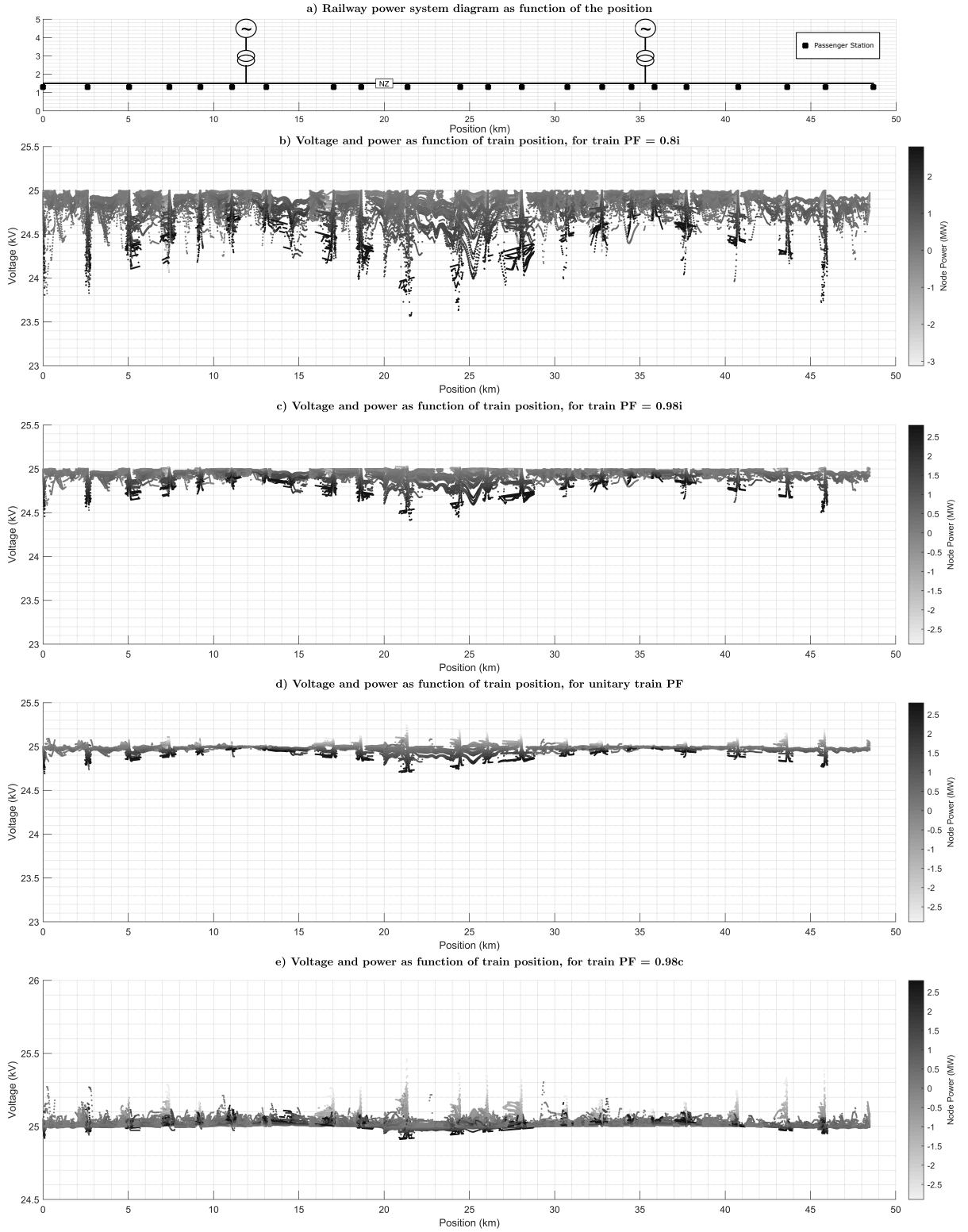

Figure 5.20: Voltage and power of each train as function of the position on the catenary, for different train PF values. Note: the black squares in the electrical diagram represent the position of the passenger stations.

The first conclusion is on the concentration of power demand of trains near the passenger stations. It is visible that the positions where the voltage is lower[6] is when the train power consumption is higher and is coincident with the position of each passenger station (represented by the black squares). This is expected due to the intrinsic behavior of the trains, where a high demand for power, either in consumption and in regeneration, is necessary for the train departure and arrival at the passenger stations.

As expected, the lower the inductive power factor, the higher the voltage drop. As examples of Fig. 5.20b) and the Fig. 5.20c), if all the trains adapt the power factor from 0.8i to 0.98i, the minimum voltage in the catenary for an entire day will increase from a minimum value around 23.6 kV to a value near 24.5 kV.

5.5 Optimization Scenario 2: Inclusion of Power Injection Devices

From the previous results and conclusions, it is clear that the most interesting position to install Power Injection Devices (PID) is in the neighbourhood of certain passenger stations. Furthermore, it is also identified that the further away from the TPS, the higher the voltage drop, as expected.

The results of Fig. 5.20b) illustrate the passenger stations 1, 2, 10, 11 and 21 as the ones having higher voltage drop and in Fig. 5.21 is considered the installation of PID arbitrarily distributed from the points of higher voltage drop.

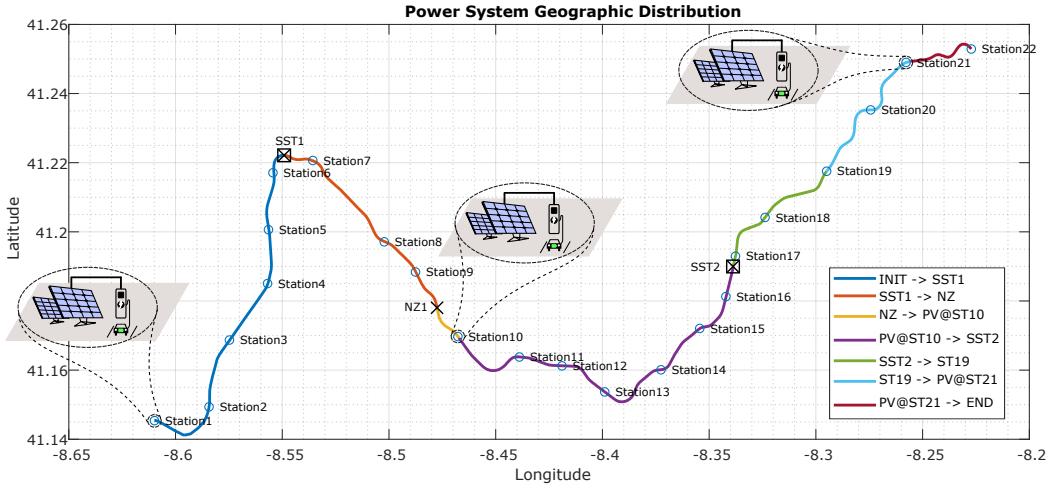

Figure 5.21: Geographical distribution of the case study railway line having PID in stations 1, 10 and 21, from left to right in Fig. 5.20.

[6]Or higher, for trains operating in capacitive power factor

A PID is an electrical equipment that is connected to the catenary line and is able to exchange active and reactive power. It is illustrated in this example as an ideal electronic power converter, as visible in Fig. 5.22.

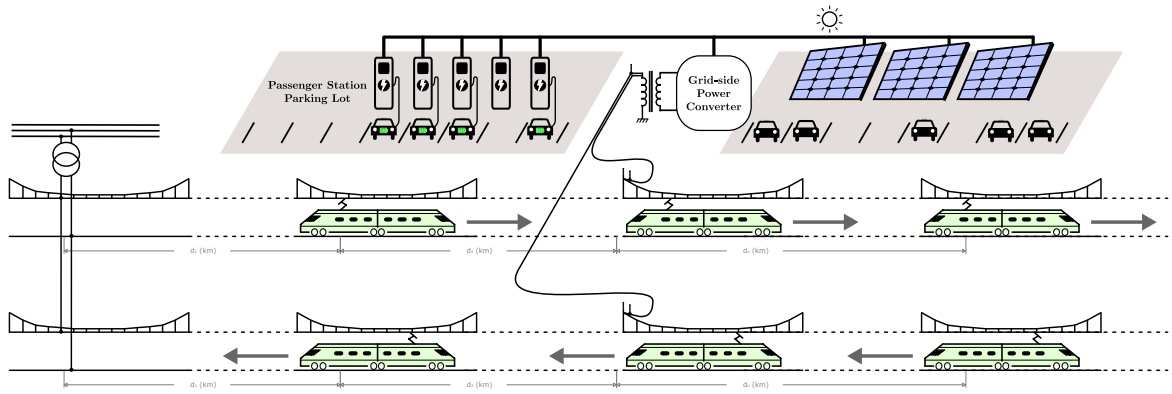

Figure 5.22: Illustration of a Power Injection Device.

The management of the active power can be addressed with PSSA-rail. For preliminary demonstration purposes it was chosen a simple strategy where all the available power generated from the PV panels is either injected into the catenary or in a generic ESS. The optimization algorithm follows the droop curves as illustrated in Fig. 5.23.

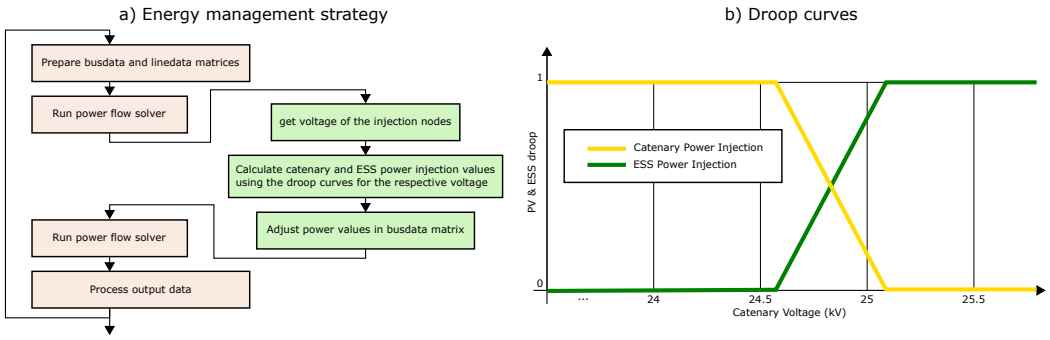

Figure 5.23: Energy management strategy for PID.

As example, if the voltage in the catenary is bellow 24.5 kV, all the available PV power is injected into the catenary; if the catenary voltage is above 25.5 kV, all the generated power is stored in the generic ESS.

In this section are arbitrary considered two demonstration scenarios, based on Fig. 5.21, where two levels of installed PV power are considered: 2×100 kW and 2×250 kW. The peak power in both TPS is near 7MW, as visible in Fig. 5.15. Furthermore, from the findings of the PSSA-rail, the daily energy consumption is 4.7 MWh and 6.1 MWh, respectively for TPS #1 and TPS #2.

In Fig. 5.24 and Fig. 5.25 are presented the results for the two levels of power in study.

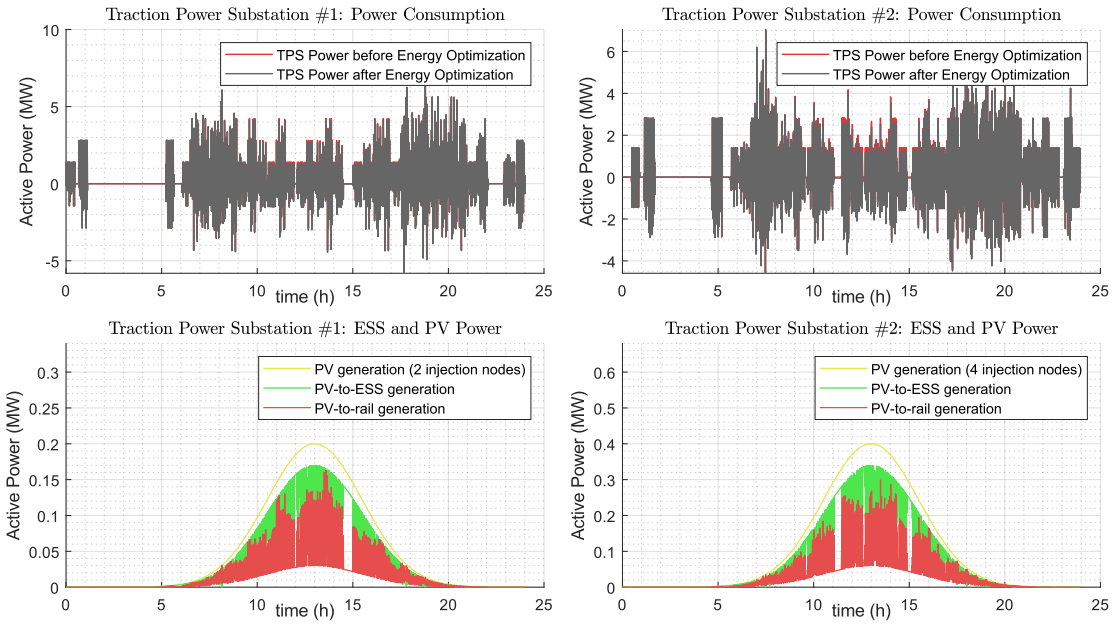

Figure 5.24: Active power evaluation before and after the inclusion of 2×100 kW PID. In the TPS #1, two injection points are associated to STA1, where is injected in both sides of the catenary; in TPS #2 are considered four injection nodes in STA10 and STA21.

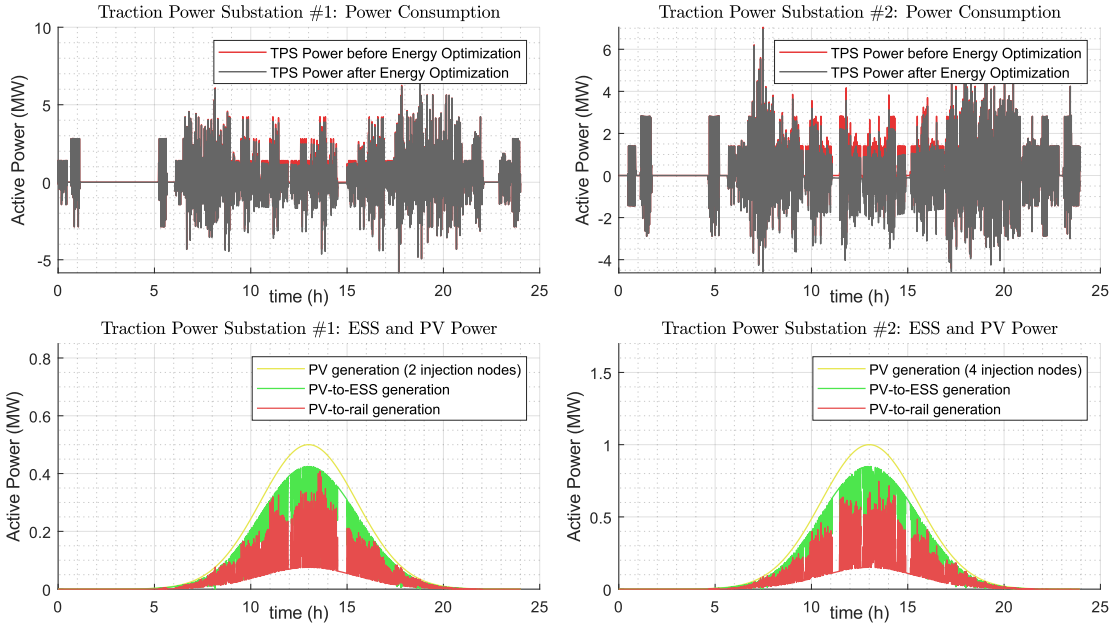

Figure 5.25: Active power evaluation before and after the inclusion of 2×250 kW PID. In the TPS #1, two injection points are associated to STA1, where is injected in both sides of the catenary; in TPS #2 are considered four injection nodes in STA10 and STA21.

Fig. 5.24 and Fig. 5.25 shows the peak-shaving effect of this strategy. As expected, the increase of PV power generation results in higher reduction of power in the TPS.

This reduction is reflected in the TPS energy consumption, where around one third of the generated energy is injected into the catenary, as visible in Fig. 5.26 and Fig. 5.27.

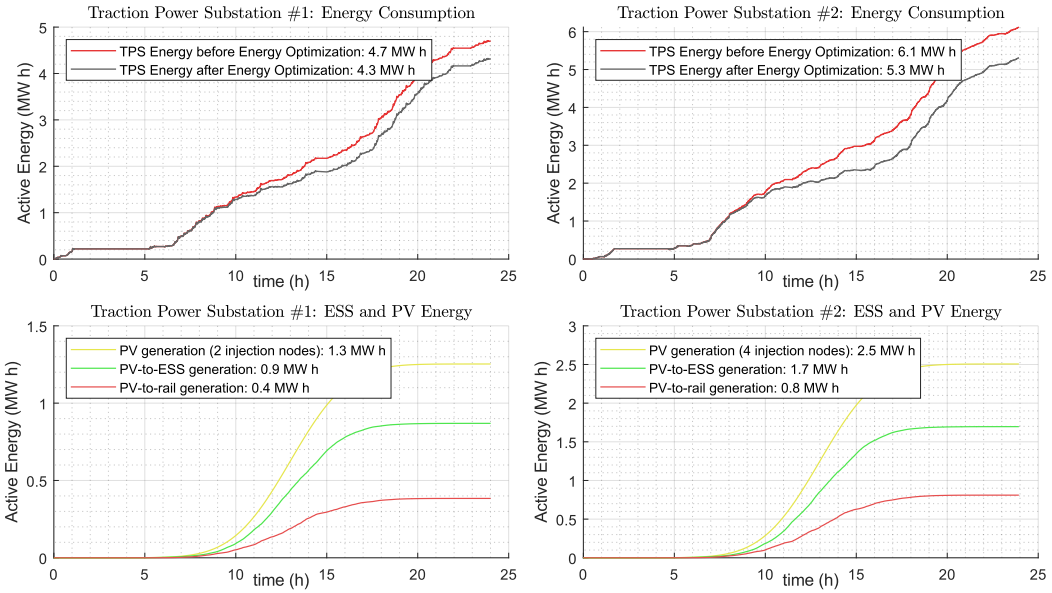

Figure 5.26: Energy (active) evaluation before and after the inclusion of 2×100 kW PID.

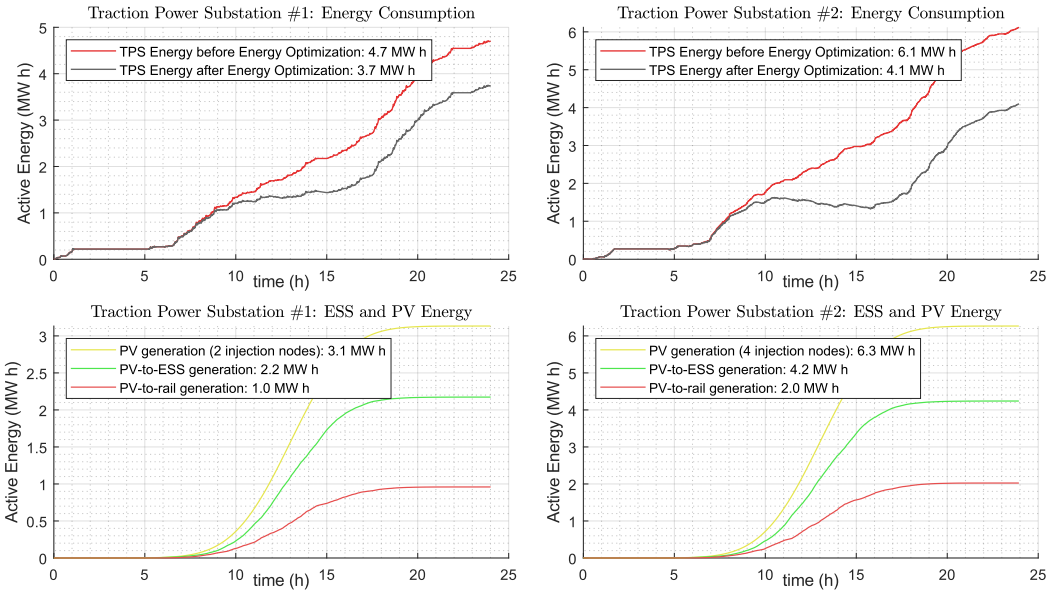

Figure 5.27: Energy (active) evaluation before and after the inclusion of 2×250 kW PID.

From the presented results, the inclusion of 2×100 kW PID in the passenger stations 1, 10 and 21 reduces the TPS net energy consumption in 8.5 % and 13.1 %, for each respective TPS. For the 2×250 kW PID, for the same passenger stations and for the same droop curve, the reduction is 21.3 % and 32.8 %, respectively, for TPS#1 and TPS#2.

As expected, this optimization scenario also contributes to the reduction of the minimum voltage levels, where the graphs of Fig. 5.28 and Fig. 5.29 are illustrative of this improvement.

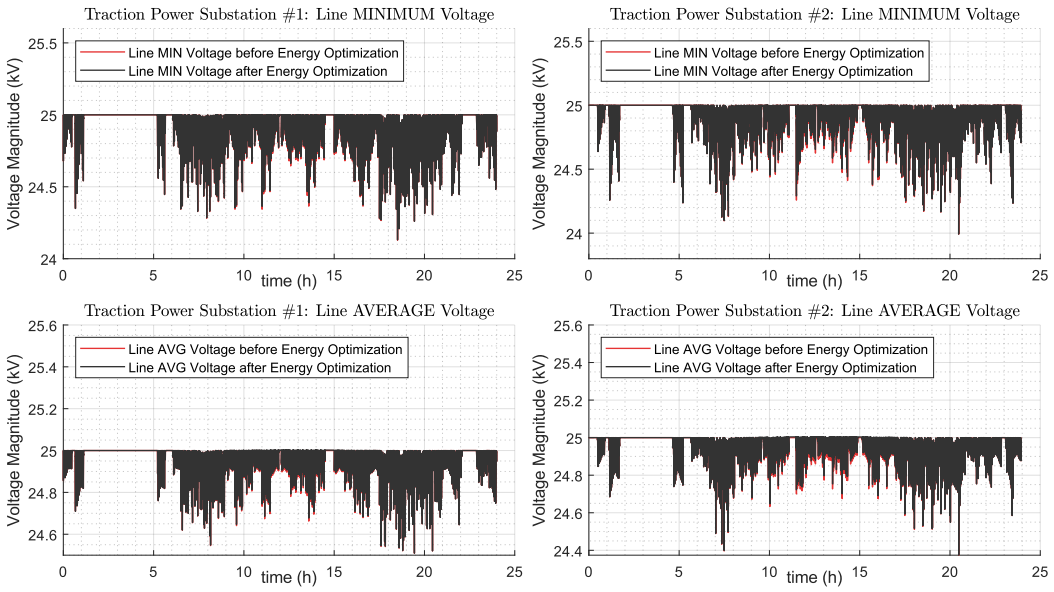

Figure 5.28: Voltage (magnitude) evaluation before and after the inclusion of 2×100 kW PID.

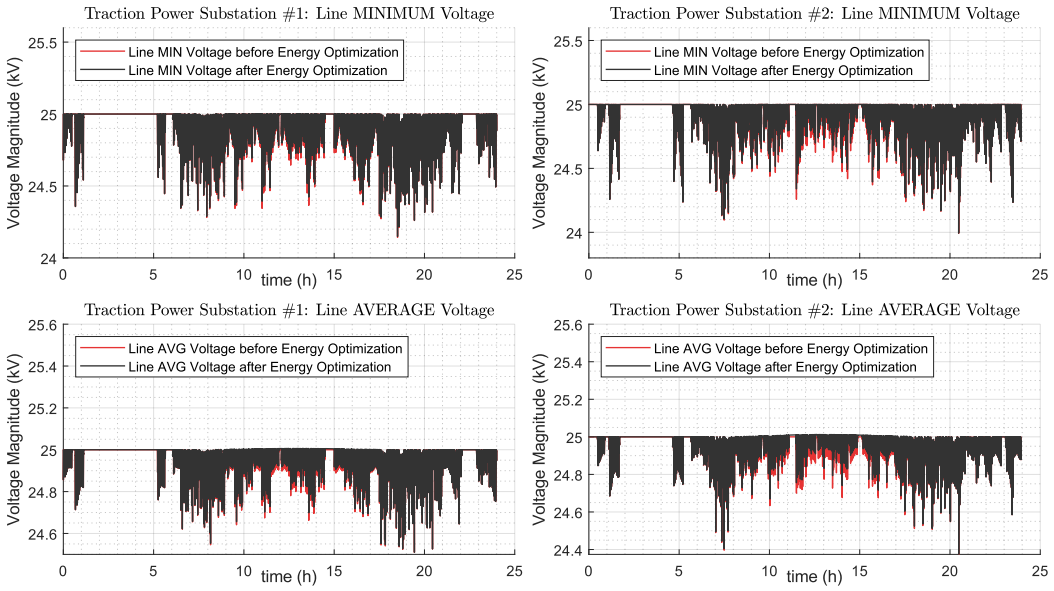

Figure 5.29: Voltage (magnitude) evaluation before and after the inclusion of 2×250 kW PID.

When applying the 2×250 kW PID, the voltage drop is higher (comparing to 2×100 kW PID), as can be seen in the Fig. 5.29, where the red traces (before installing the PID) are more visible, as expected.

Finally, these improvements are achieved with a decrease of the catenary power losses, as visible in Fig. 5.30 and Fig. 5.31.

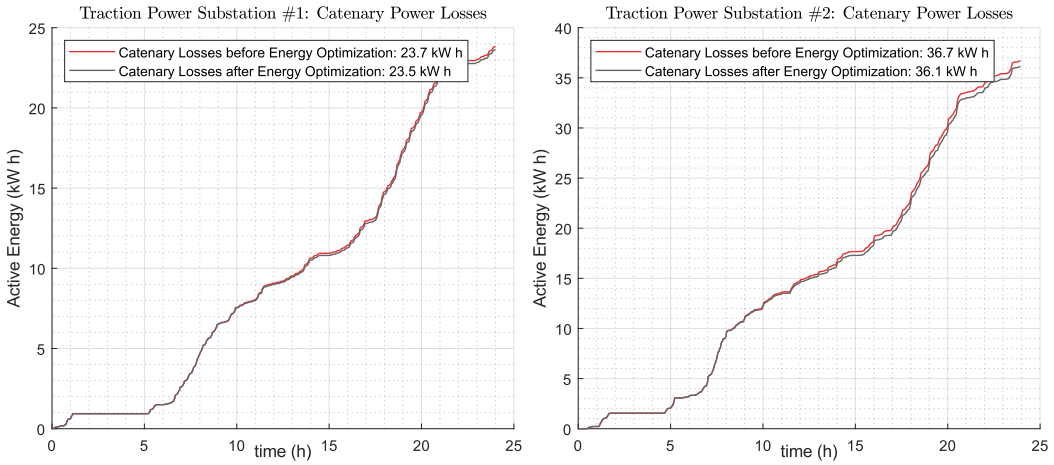

Figure 5.30: Catenary energy losses evaluation before and after the inclusion of 2×100 kW PID.

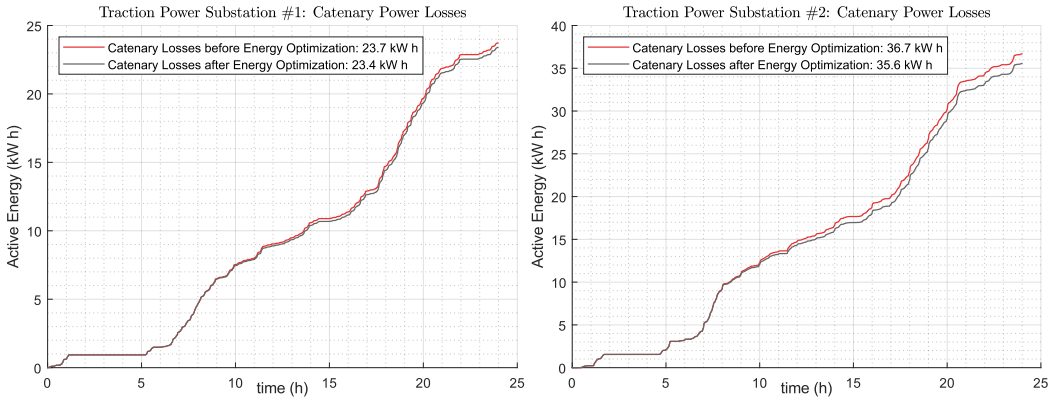

Figure 5.31: Catenary energy losses evaluation before and after the inclusion of 2×250 kW PID.

Specifically, with 2×100 kW PID the power losses in the catenary are reduced in 0.8 % and 1.6 %, for each respective TPS; with 2×250 kW PID, the reduction is 1.3 % and 3.0 %.

It should be highlighted that a part of the generated power could be injected into the catenary even when the catenary voltage is in the interval $[25 \cdots 25.5]\ kV$, and as a consequence, injected into the grid. Even thought, in this situation, the catenary losses are still below the losses without the installation of PID, which will not be the case if the droop curve has a different profile for voltages above 25 kV.

The increase of the PID power value from 2×100 kW to 2×250 kW is linear with the percentage reduction of TPS net energy consumption (−21.3 % is equal to 2.5 times −8.5 %, and the same applies to the TPS#2). One reason for this linearity is on the droop characteristic curve. However, a more deterministic analysis is necessary to evaluate all the

different degrees of freedom, like the droop curve characteristic, the PID power capabilities or the number of PID installations per TPS. Also, the energy storage subsystem of PID must be deeply analysed. In this section is only considered that the ESS is uni-directional load that handles the excess of energy from PV; an alternative improved management strategy must consider the energy regeneration as an alternative method to charge the PID ESS; also the ESS can contribute with active power to the catenary, to support the grid.

In this section is illustrated another capability of PSSA-rail with the inclusion of PID in the catenary line. It was demonstrated that the PSSA-rail tool is capable of easily analyse energy management strategies, with the inclusion of new scripts, such as the green scripts in Fig. 5.23a).

5.6 Discussion and Conclusions

This chapter proposes a tool to evaluate the electrical operation of a railway line infrastructure. This tool should be capable of extracting knowledge on the power flow, using the energy information.

This chapter was divided in two parts, where the first part is focused on the presentation of the tool. The approach used in this part was to provide enough detail on the implementation of this software package.

5.6.1 Requirement Compliance of PSSA-rail

The proposed implementation complies with the four requirements raised in the introduction section, each of them being addressed as following.

5.6.1.1 PSSA-rail Implemented in a Object-Oriented Programming Approach

First, the usage of an object-oriented programming approach enables the required flexibility to simulate any railway line. The results presented in this chapter have demonstrated the operation for a case study of a 50 km double-track line, having two traction substations and 70 daily journeys. Furthermore, this tool was also tested for a second railway line, of 250 km double-track line, having 7 traction substations and 252 train journeys, having the results presented in appendix E.

The reasoning for having this requirement is also in the desired future directions of this tool. As an ideal objective, it is desired that this tool can operate as a digital twin of a given railway line. This means that the input data can be either from simulation of

from a real train. An object-oriented programming approach for the PSSA-rail eases the implementation of this challenging mode of operation.

5.6.1.2 Simulation of All Train Journeys Moving in Both Directions

The second requirement is associated with the capability of the simulation of all train journeys moving in both directions. In this, the tool targets double-track lines, where each track is independently evaluated.

It is a common practice in the railway infrastructure to have the catenary electrically isolated between track sides, for security reasons [152]. In the situation of occurrence of a short-circuit or other defect in any point in the catenary, an automatic system placed in the traction substation measures the behaviour of the short circuit and estimates the point of occurrence of the phenomena. Therefore, in practical normal operation, a double-track 1×25 kV railway line have at least four different branches exiting the traction substation. Abnormal situations require specific analysis, which are not the objective of PSSA-rail.

Furthermore, for single-track lines, this architecture was not considered for the capabilities of PSSA-rail. This specific case study should consider the idea of PSSA-rail of dividing the railway line into sections, where some of the sections are double-track ones for the train crossing occurrence. The *Prepare Simulation Module* needs to be adapted in the single-track sections, as illustrated in Fig. 5.32, whereas in double-track sections (where the train overtaking occurs) is considered the presented implementation solution of this chapter.

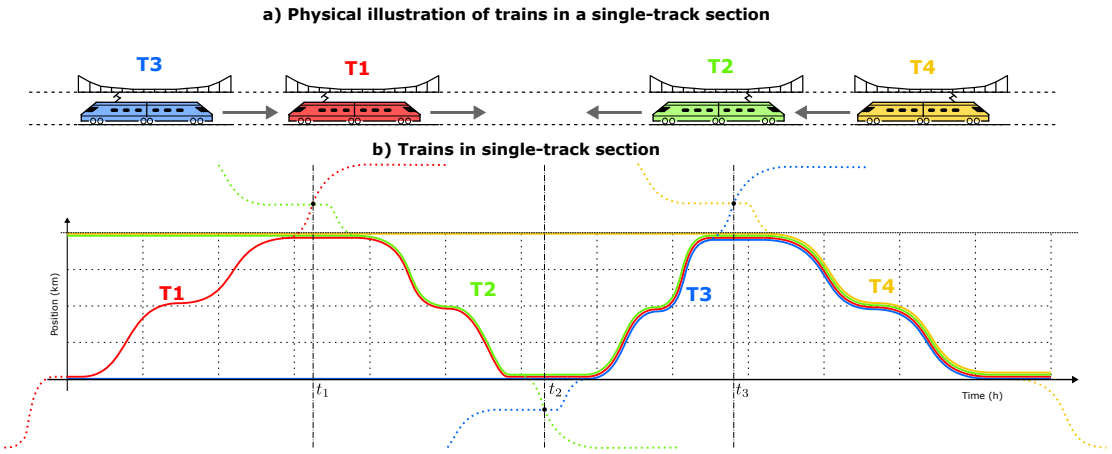

Figure 5.32: Adaptation of the Prepare Simulation Module for single-track sections. The times t_1, t_2 and t_3 are the time instants where the trains intersect each other, in double-track sections

5.6.1.3 Simulation of a Broad Time-Window

Then, the third requirement is related to the need of simulating a broad time-window. In the two demonstrations of PSSA-rail, it was considered a simulation time-window of one day. This ensures that, during that simulation time-window, the electrical equivalent diagram is static, where all train daily journeys are contemplated. By static, it means that the number of nodes and branches are the same throughout the entire simulation. The tool automatically adapts the branch impedances and node power consumption according to the system state at a simulation time-step, using the absolute train positions and power consumptions.

Despite the advantages of this approach, with the compliance of this third requirement, the computational requirements for the PSSA-rail should be taken into consideration, in particular in the system memory. As example, the usage of parallel processing taking advantage of all available Central Processing Unit (CPU) cores requires a pre-allocation in Random-Access Memory (RAM) of the needed dataset. Furthermore, if the simulation time-window is reduced, the issues associated to the needed memory are alleviated.

Finally, with the compliance of this requirement, if during the simulation time-window there is an occurrence of a train overtaking, the PSSA-rail is not capable of simulating this occurrence. The solution is easy to be implemented: if the simulation time-window is divided in periods, where the splitting of the time-window corresponds to the instant of the train overtaking occurrence, then this issue is solved. As illustrated in the example of Fig. 5.33, if the faster train T2 needs to overtake one slower train, T3, then this event is only possible in certain parts of the railway line (certain passenger stations are one example, as well as dedicated line sections).

By dividing the simulation time in time-windows (Δt_1 and Δt_2), split in the time instance of the occurrence of the overtaking situation ($t_\times$), and by considering the position of the overtaking as a line point of interest, it is enabled the possibility to simulate any railway line for a broad simulation time-window.

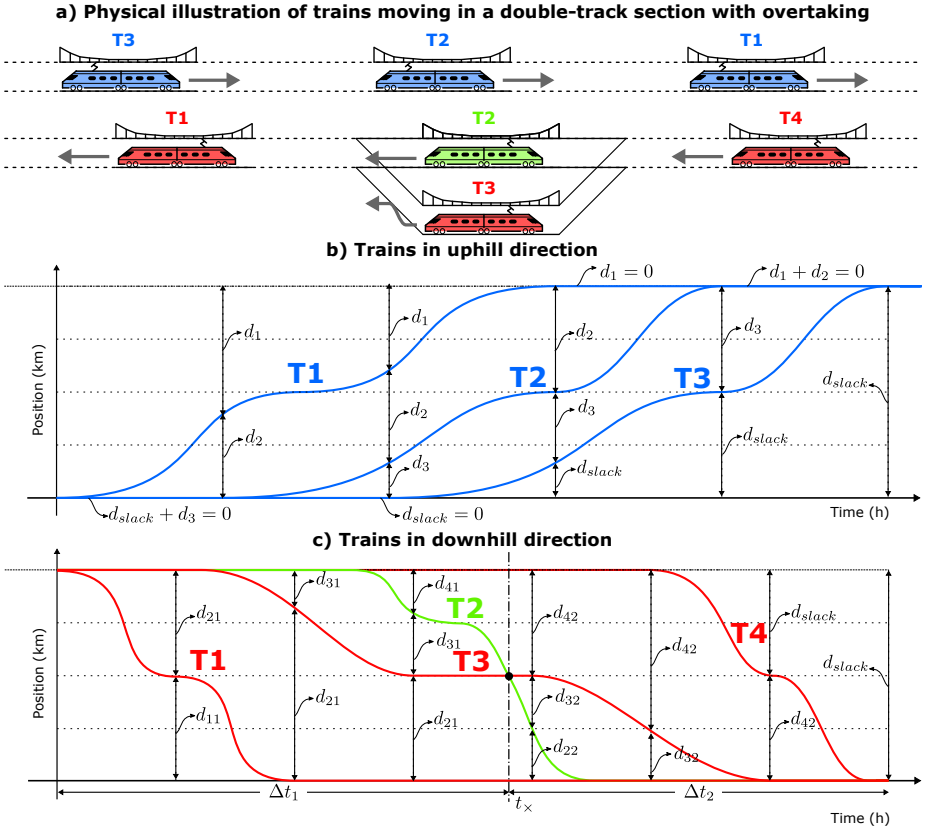

Figure 5.33: Adaptation of the PSSA-rail to contemplate train overtaking situations. Two simulation time-windows Δt_1 and Δt_2 were considered to contemplate the overtaking occurring at $t_\times$ when a fast train, T2 overtakes a slower train, T3.

5.6.1.4 Simulation of Specific Line Points of Interest

The fourth requirement is in the capability of the PSSA-rail tool to automatically divide the line into PoIs based on the electrical line characteristics. Furthermore, for specific analysis, is possible to include new PoIs.

This is needed with the optimization strategy 2, where the passenger stations are evaluated to consider the injection/consumption of energy, through the PID.

This is also needed if the PSSA-rail tool is adapted for the analysis of 2×25 kV electrification schemes, where the new points of interest will be the absolute position of the auto-transformer apparatus, following the illustration of Fig. 5.34.

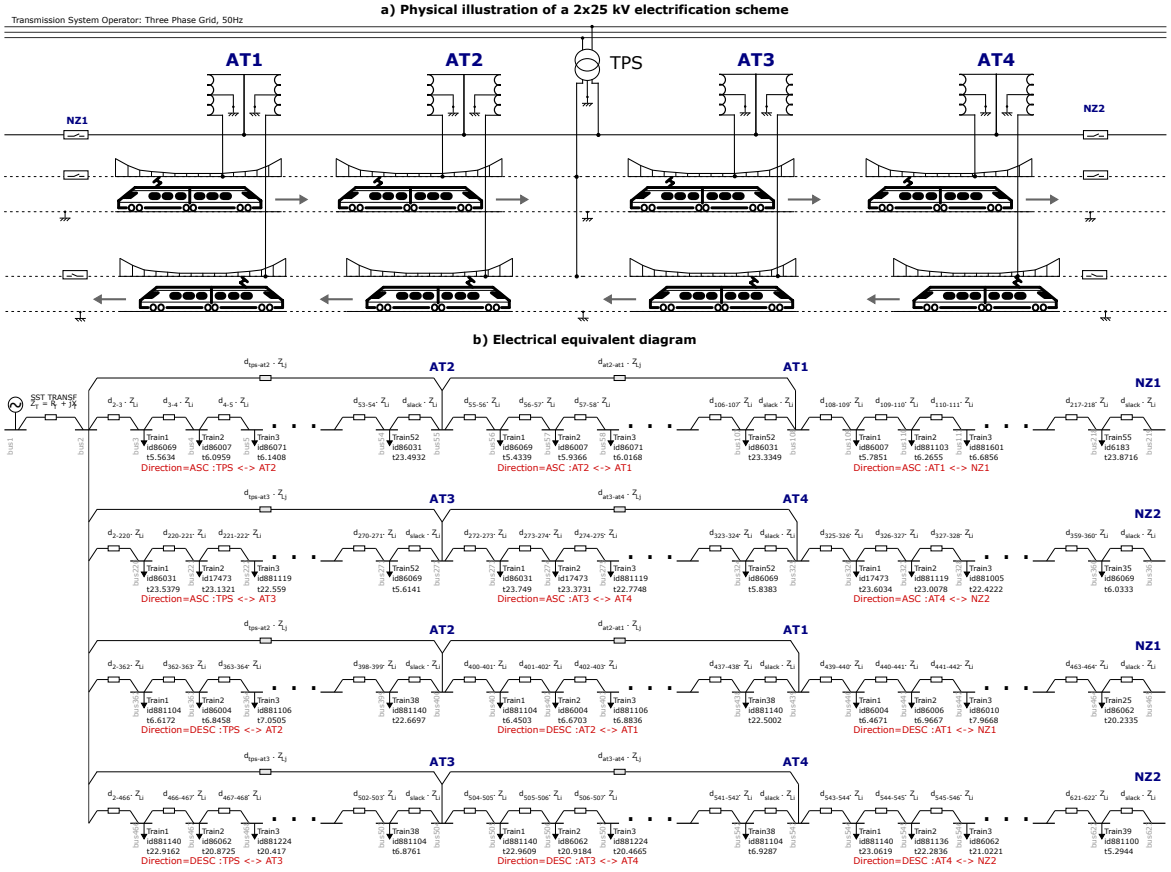

Figure 5.34: Adaptation of the PSSA-rail to contemplate 2x25kV electrification scheme.

However, the evaluation of a 2×25 kV needs to be carefully evaluated since the impedances Z_{Li} and Z_{Lj} of Fig. 5.34 are not decoupled. Then, a further simplification methodology similar to the proposed in chapter 3 can be considered for the analysis of this electrification scheme.

This approach of dividing the railway line into sections divided by the PoI also allows the simulation of secondary side lines, if those lines are supplied by the same traction substation. The electrical equivalent diagram generated by PSSA-rail will be adapted to consider new branches placed at the PoI.

Furthermore, the approach presented in this chapter is also compatible with the inclusion of power transfer devices at the neutral section, where some energy exchange can occur in this PoI common to both subsequent traction substations. This needs the simultaneous simulation of both substations, as illustrated in the proposal of Fig. 5.35 with the power transfer device actively adapting the value of active power injection (based on the voltage difference between both sides of the neutral zone or other relevant strategy).

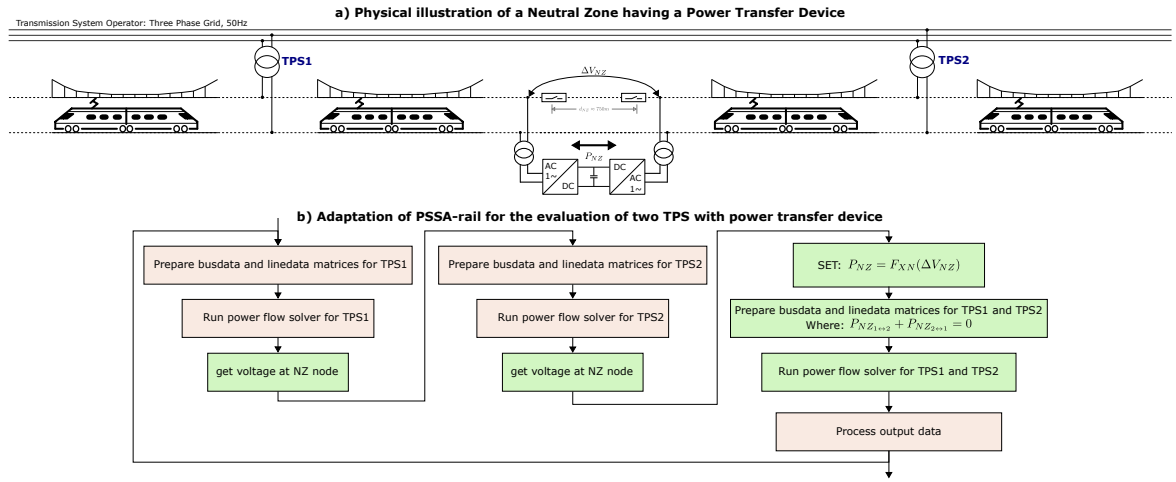

Figure 5.35: Adaptation of the PSSA-rail to contemplate the usage of power transfer devices in the neutral zone.

The usage of power transfer devices on the neutral zone must be taken with extensive analysis (which was not the focus of this chapter). First, the value of active power must be calculated to minimize the losses in both lines. One active learning approach might be an interesting solution to define this value of active power (specifically, to define the function $P_{NZ} = F_{XN}(\Delta V_{NZ})$). Second, the value of reactive power can also be independently controlled. In chapter 6, this reactive power compensation is further analysed, with the injection of reactive power at neutral zones to increase the catenary voltage.

The discussion on the requirements compliance of PSSA-rail is useful, not only to illustrate the decisions taken on the design of PSSA-rail, but also to evaluate the future improvements for this tool towards multiple analysis scenarios. The preliminary discussion of the actions to be made in the PSSA-rail demonstrates the flexibility for any scenario, capability for the simulation of all trains of any scenario, for a broad simulation time-window and for any electrification scheme. An extensive demonstration of PSSA-rail for two optimization strategies was covered in the second part of this chapter and will be discussed as following.

5.6.2 Capabilities of PSSA-rail

One of the major highlights of PSSA-rail is the flexibility and versatility of the tool. In the previous section was discussed the necessary changes of PSSA-rail towards specific simulation scenarios (like single-line railways, 2×25 kV electrification, neutral-zone power transfer devices, as an example). This discussion emphasises the relevance of the defined requirements.

In addition to all pointed capabilities of the tool, this final discussion section presents a validation of the tool to evaluate specific optimization scenarios, which were addressed in the second part of this chapter.

The first optimization scenario, presented in the second part of this chapter, proposes the adaptation of the train power factor fixed values and the evaluation of the voltage improvement on the catenary line. As expected, it was seen optimization improvements on the catenary voltage. This support the research opportunity for the chapter 6.

It is known that the adaptation of the train reactive power to a less inductive one will lead to an increase in the catenary voltage, which enables to have a more controlled reactive power in the traction substation and an increase of the railway infrastructure capacity. However, this increase requires a specific analysis, with a more deterministic simulation (where the PSSA-rail is more appropriate for the simulation of stochastic scenarios). This deterministic analysis will be addressed in this thesis, specifically in chapter 6.

The second optimization strategy illustrates one capability of the PSSA-rail, where an analysis of the injection of active power can be performed, having specific optimization criteria. The energy management strategy considered in this chapter was a simple droop characteristic strategy, where the decision is made based on the catenary voltage. The obtained results show the expected reductions in the TPS energy consumption and a small reduction of the catenary losses.

However, the analysis presented in this second optimization scenario is dependent on fixing several degrees of freedom. The stochastic evaluation made in this chapter justifies the advantages of the railway infrastructure on installing power injection devices. This supports the research opportunity for the chapter 7, where is presented a deterministic situation, having one train journey as a case study. A deterministic analysis can be useful to design a control strategy that takes into consideration all degrees of freedom in this second optimization strategy: from and to the catenary power flow; from and to ESS; and even a limitation of the PV power generation.

5.7 Summary

This chapter proposes the developed PSSA-rail tool, which is capable to generate the knowledge on the railway system state using train energy information. As discussed, two lines of research have emerged, leading to the following two chapters.

In chapter 6 is studied in a deterministic situation the impact on the railway infrastructure if the reactive power is compensated. Furthermore, in chapter 7, the management of the active power in energy storage systems can be analysed in a deterministic situation.

CHAPTER 6

Railway Reactive Power Compensation Strategy

The purpose of a generalized and interconnected framework for smart railways, supported by tools and strategies for power flow management at its core, is to improve the operation of the railway transportation system. In previous chapter 5 was presented the PSSA-rail tool, which can implement optimization scenarios in a stochastic manner.

One specific improvement to the railway transportation system, addressed in this chapter to cover the topic **T4**, is the increase of the railway infrastructure capacity — essentially to have more trains in the line, without any physical reinforcement of the electric apparatus while keeping the timetable. The knowledge of the power system state will be used to automatically adapt each train operation, by adjusting the train reactive power to a less inductive one.

Divided in two parts, in the first part of this chapter is presented and validated the reactive power compensation strategy, achieving a 50 % infrastructure capacity increase, either for compensation at Neutral Zone (NZ) and for mobile compensation in each of the trains. In the second part is discussed a solution, based on a droop strategy, that targets the issues associated with the impossibility to have real-time knowledge of the railway system state.

The outcome of this chapter will be a strategy for reactive power flow management towards infrastructure capacity increase. In the graphical abstract of Fig. 6.1 are illustrated the contents of this strategy.

The objectives of this chapter are:

- **Objective 4a**: Propose a methodology to increase the railway infrastructure capacity with the management of the reactive power flow;
- **Objective 4b**: Demonstrate the increase of the infrastructure capacity for deterministic scenarios;
- **Objective 4c**: Discuss the implementation steps of this strategy, from a practical viewpoint and within the smart railways framework.

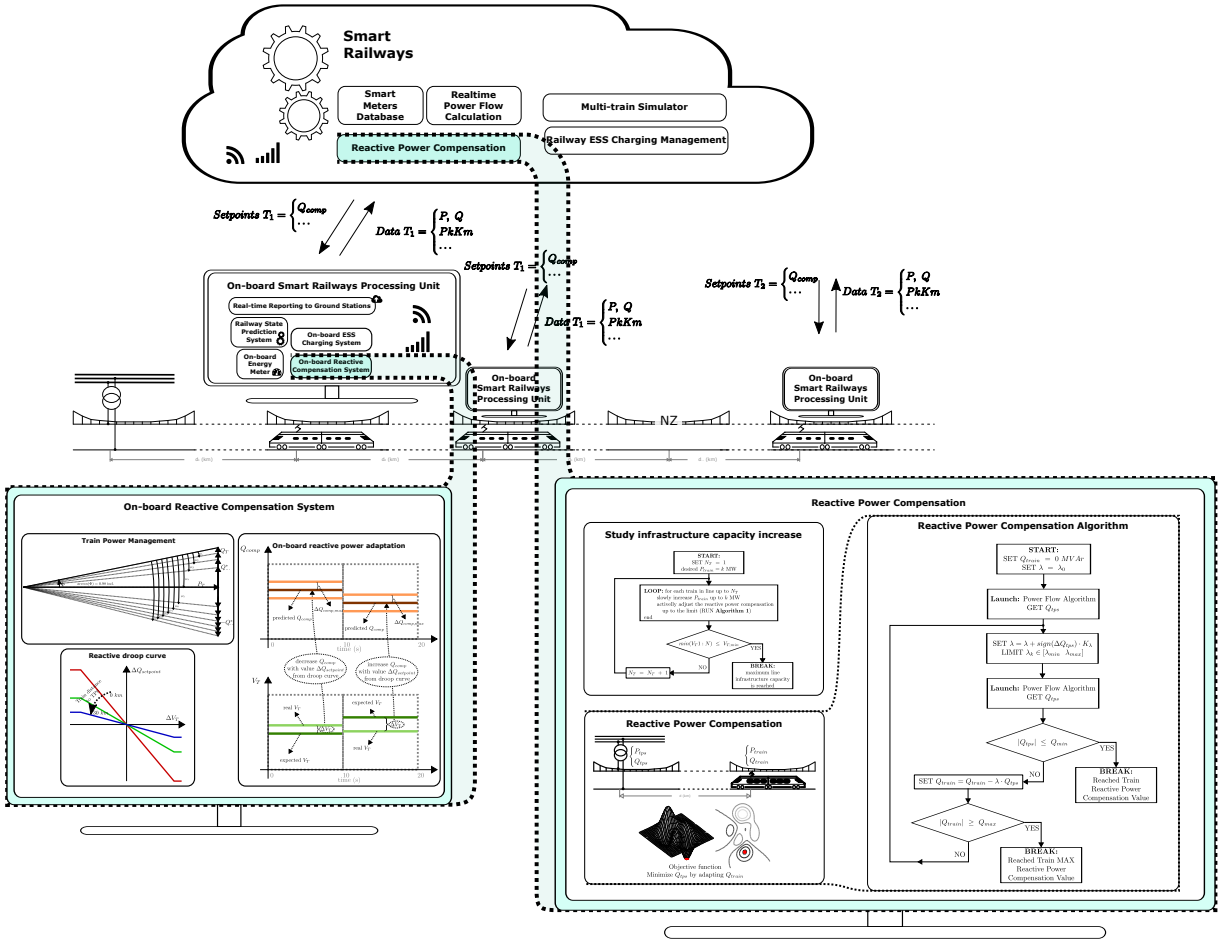

Figure 6.1: Graphical abstract of chapter 6 — Inclusion of reactive power compensation in smart railway framework.

6.1 Introduction

Fuelled by the mission "Moving European Railway Forward", the Shift2Rail European program have the objectives of cost reduction, increase of the reliability and punctuality [3, 103]. Furthermore, doubling the railway infrastructure capacity another goal of this program. This chapter addresses this challenge raided by the Shift2Rail – the increase of the railway infrastructure capacity – with the management of the reactive power.

The increase of railway infrastructure capacity is an extensive research area where the evaluation is made with the application of definitions, metrics, methodologies and tools [153]. Despite there is no standard definition of railway infrastructure capacity, it can be defined as the number of trains that can safely pass over a segment of the line, within a selected time-window.

In the literature review associated with this topic **T4**, presented in chapter 2, this capacity is mostly associated with infrastructure constraints, traffic parameters and operation parameters. Regarding the electrification perspective, generally, the railway infrastructure capacity is directly affected by the current collection quality of the electric train, which is normally determined by both the mechanical and electrical aspects. The mechanical aspects concern the train–infrastructure interactions, like pantograph-catenary [154, 155], and the wheel-rail [156], which determines the stability of electric transmission and is a source of electrical issues. Due to the inductive characteristic of the railway transmission line, as highlighted in chapter 3, this electrical aspect will directly affect the quality of supply of electric trains.

In chapter 5 was shown that, for the same catenary line, the adoption of different train power factors will affect the minimum voltage level. However, the infrastructure capacity will also affect the voltage drop: the higher the number of trains in the railway line, the higher the voltage drop. According to the IEC60850 [113], in AC 1 $\times$ 25 kV electrification scheme, the lowest non-permanent voltage is 0.7 p.u. (17.5 kV), whereas the lowest permanent voltage is 0.76 p.u. (19 kV). Specifically, if the voltage is higher than the lowest permanent voltage, the train can consume all its demand power; if the lowest non-permanent voltage is reached, a limit of operation is achieved and the train power must be clipped to zero.

This is the limit of the infrastructure capacity that will be considered in this chapter: if the infrastructure has any of the trains with a voltage level that does not allow the operation with the maximum power, then is reached the maximum limit.

From the listed research opportunities associated with the topic **T4** presented in chapter 2, one alternative to the inclusion of railway power quality compensators is with the adaptation of each train internal control loop. As highlighted, this train internal compensation is not a new topic, being proposed in the 2003 Ph.D thesis of Kulworawanichpong a centralized compensation strategy [101], where several limitations have not justified a clear implementation of such strategy. Not only the technological advantages of the last years on communications and on computational processing power can support this real-time reactive power compensation, but also a smart railways framework is the most likely solution to achieve this goal.

This chapter is structured into six sections. In the following Section 6.2 is presented the materials and models, starting with a basic model and covering the used simulation framework. Section 6.3 presents the methodology for the reactive power compensation strategy, with an illustration for a particular scenario. Section 6.4 presents the rest of the methodology and the results for the increase in the railway infrastructure capacity with the adaptation of the reactive power in the catenary. Section 6.5 discusses a conceptual

architecture to implement this reactive power compensation strategy, with the usage of a smart metering framework. A final discussion and the conclusions of this chapter are presented in Section 6.6.

6.2 Materials and Methods

This section covers the models and simulation framework required for power flow analysis and for reactive power control. The combination of these models, the simulation framework and the compensation strategy will be the scientific contribution for a new strategy to reactive power control in the railway system.

6.2.1 Basic Model

The basic model considers the Traction Power Substation (TPS), the catenary line and the electric train. The electric train is simplified from the dynamic model as follows:

$$\frac{dv}{dt} = \frac{F_T(v) - w(v) - g(x)}{M(t)} \tag{6.1}$$

where $F_T(v)$ is the traction force, $w(v)$ is the aerodynamic resistive force and $g_(x)$ represents the track gradient and curvature forces. The electric active power is directly related to the train dynamic movement and the reactive power is the one to control. At higher speeds, the maximum traction force is limited by the maximum available power [12]. Therefore, the train can be simplified to a decoupled active and reactive power load.

Regarding the catenary line, in this chapter is used a simplified π-type line model. As highlighted in chapter 3, the power flow problem is a non-linear problem that needs an iterative-based solver. Similarly to chapter 3, in this chapter is used the MatPower tool [69], using the Newton-Raphson power flow calculation method.

Through the sensibility analysis presented in the introduction section of chapter 3, the control of train power factor affects the active and reactive power flow in the TPS, as illustrated in Fig. 3.4. Furthermore, the adaptation of the TPS reactive power will affect the train voltage magnitude and phase, as visible in Fig. 3.3.

Thus, the adaptation of the train power factor will result in the adaptation of the catenary voltage drop, where the less inductive the power factor is, the lower the value of the voltage drop.

6.2.2 Simulation Framework

The simulation framework of this work is now presented in Fig. 6.2, where the TPS, a railway line and a single train are illustrated.

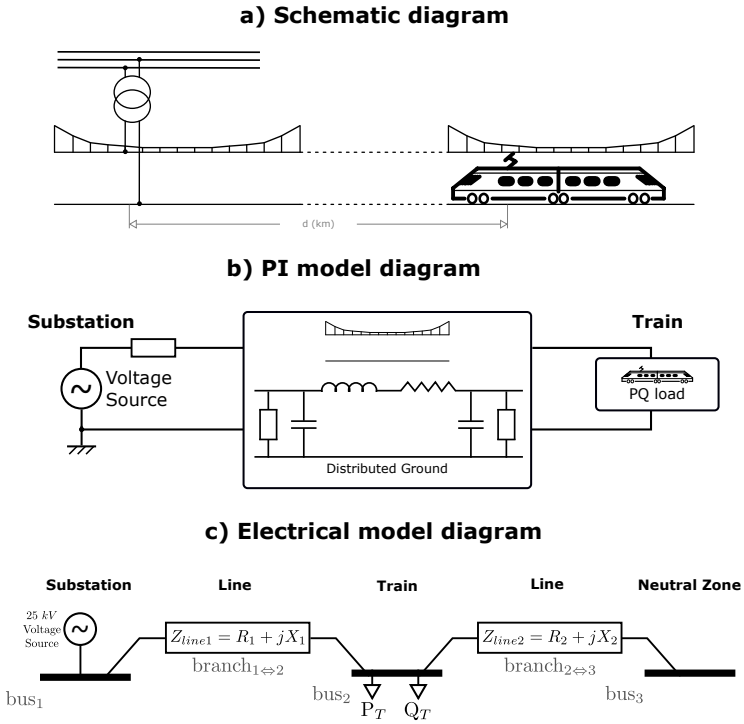

Figure 6.2: Framework of the 1 × 25 kV models: a) Illustration of physical representation; b) π-type model diagram; c) Considered bus-branch model for MatPower (Note: the traction transformer is not considered in this work).

The power flow problem considered in this simple model is non-linear, as previously discussed. The usage of MatPower and, in particular, the Newton–Raphson solver, allows this problem to be solved. Therefore, for a fixed supply voltage and specific branch parameters, the train power consumption can be fixed regardless of the voltage drop in the line. With this, the voltages in the nodes can be calculated, as well as the consumed supply power in the TPS.

Considering the simple model in Fig. 6.2c, this has four variable parameters: (i) a variable line distance, $\boldsymbol{d}_L$; (ii) a variable train power, $\boldsymbol{P}_T$; (iii) a variable train power factor, $\boldsymbol{PF}_T$; and (iv) a variable line $^X/_R$ ratio, $^{\boldsymbol{X}}/_{\boldsymbol{R}_L}$.

Similarly to the analysis made in chapter 3, to better evaluate the model, these parameters can be spawned across a surface of possible parameters $\boldsymbol{S}(\boldsymbol{L}_d, {}^{\boldsymbol{X}}/_{\boldsymbol{R}_L}, \boldsymbol{P}_T, \boldsymbol{PF}_T) \in \mathbb{R}^4$, where $\boldsymbol{d}_L \in]0 \quad d_{max}]$, ${}^{\boldsymbol{X}}/_{\boldsymbol{R}_L} \in [{}^{\boldsymbol{X}}/_{\boldsymbol{R}_{min}} \quad {}^{\boldsymbol{X}}/_{\boldsymbol{R}_{max}}]$, $\boldsymbol{P}_T \in [P_{min} \quad P_{max}]$ and $\boldsymbol{PF}_T \in [0 \quad 1]$. The surface of possible parameters has infinite possible solutions.

One element of the surface of parameters can be parametrized as set of parameters $\boldsymbol{SP}(\boldsymbol{L}_d, {}^{\boldsymbol{X}}/_{\boldsymbol{R}_L}, \boldsymbol{P}_T, \boldsymbol{PF}_T) \in \boldsymbol{S}$, where

$$\text{Set of parameters: } \boldsymbol{SP} = \begin{cases} \boldsymbol{L}_d & \\ {}^{\boldsymbol{X}}/_{\boldsymbol{R}_L} & \\ \boldsymbol{P}_T & \\ \boldsymbol{PF}_T & \\ Voltage\ @\ bus_k & k = \{1,\ 2\} \\ Power\ bus_k & k = \{1,\ 2\} \\ Line\ losses & P\ and\ Q \end{cases} \tag{6.2}$$

To study the behaviour of this model, it is possible to generate several $\boldsymbol{SP}$ elements, using probability distribution function for each of the four parameters, inside the defined interval of values. Assuming that, for each parameter, N random possibilities are generated. Then, the surface of solutions depends on testing N^4 different elements, resulting in a huge computational power required for this model and a hard task to evaluate the model. A more direct analysis, in particular, a sensibility analysis, will better illustrate and validate the behaviour of the model.

6.2.3 Sensibility Analysis

A sensibility analysis is an adequate tool to evaluate the variation of certain input variables, in particular, the variation of the parameters. In this analysis, three parameters can be defined as variable and the fourth can be fixed, as better explained in the following results.

Considering a testing surface, given by the expression:

$$\boldsymbol{S} = \begin{cases} \boldsymbol{L}_d & [0.1\ :\ 2\ :\ 30.1] \quad (in\ \text{km}) \\ {}^{\boldsymbol{X}}/_{\boldsymbol{R}_L} & \{2\ :\ 1\ :\ 5\} \\ \boldsymbol{P}_T & [-20\ :\ 2\ :\ 20] \quad (in\ \text{MW}) \\ \boldsymbol{PF}_T & \{0.8\ 0.9\ 0.95\ 1\} \quad \text{ind.} \end{cases} \tag{6.3}$$

By fixing the ${}^{\boldsymbol{X}}/_{\boldsymbol{R}_L}$ ratio, then this leaves room to vary the other three variables. Thus, the sensibility analysis can be seen within the train voltage value, as visible in Fig. 6.3.

Complementarily, the second sensibility analysis is made by fixing the $\boldsymbol{PF}_T$ value. The remaining parameters will be varied towards an evaluation of the resultant voltage value, as visible in Fig. 6.4.

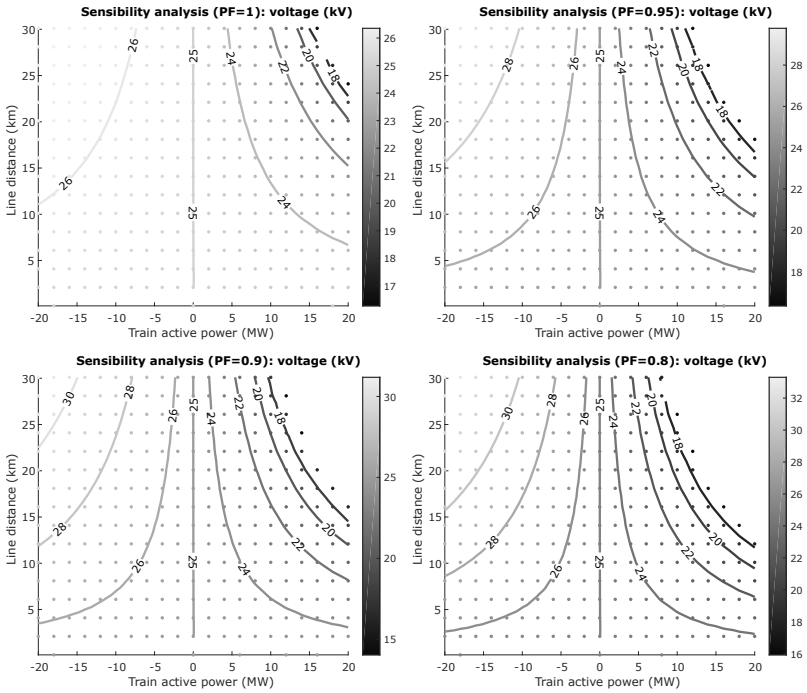

Figure 6.3: Sensibility analysis for $X/R_L = 3$: voltage levels for different train power factor values, spawned across different train active power values and line distances.

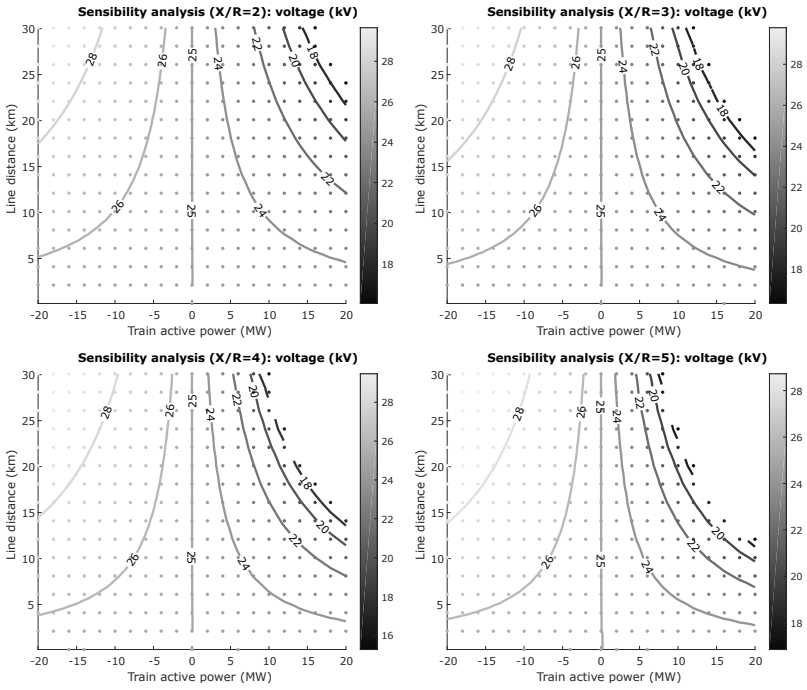

Figure 6.4: Sensibility analysis for $PF_T = 0.95$: voltage levels for different X/R_L ratios.

From the evaluation of the parameters of the model, it is clear that the X/R_L ratio will affect the train voltage. Specifically, a higher X/R_L ratio results in higher longitudinal voltage drops in the line, which is a characteristic of high inductive lines. Nevertheless, the characteristics of the line depend on several aspects related to the design of the electrification and, therefore, in this work, a fixed value for the X/R_L ratio (specifically, $R_L = 0.15$ Ω/km and $X_L = 0.45$ Ω/km) is considered.

The only aspect that can be manipulated is the train power factor. By having higher power factor values, this reduces the voltage drop. Therefore, in the following section, the reactive power compensation is detailed.

6.3 Reactive Power Compensation

As previously illustrated, it is clear the advantage of controlling the reactive power in the railway electrification. This section covers the used methodology to improve the traction power supply with the adaptation of the train power factor, using references coming from measurements from TPS. A simple reactive power compensation algorithm is firstly presented and then, is demonstrated in the performance of the proposed algorithm.

6.3.1 Algorithm for Reactive Power Compensation

The adopted optimization strategy was based on the compensation strategy from [101], where the train reactive power is iteratively adapted, based on solving the power flow problem, to achieve a minimum reactive power in the TPS. This simple algorithm is presented in the Algorithm 3, based on the fixed steepest descent method, where Q_{MIN} is a tolerance value for the reactive power and the λ is the step size for the iterative process.

Algorithm 3: Reactive Power Compensation using fixed steepest descent method

```
1  begin
2      SET Q_k = 0 Mvar;
3      SET λ = λ_0
4      while NOT termination criteria do
5          LAUNCH (Power Flow Algorithm)
6          GET Q_TPS
7          if |Q_TPS| ≥ Q_min then
8              SET Q_{k+1} = Q_k − λ Q_TPS
9          else
10             BREAK
11         end
12     end
13 end
```

Considering the following set of parameters $\boldsymbol{SP}$, where

$$\boldsymbol{SP} = \begin{cases} \boldsymbol{L_d} \;=\; 30 \text{ km} & \\ \boldsymbol{X}/\boldsymbol{R_L} \;\approx\; 3 & R = 0.155\ \Omega/\text{km} \\ \boldsymbol{P_T} \;=\; 10 \text{ MW} & \\ \boldsymbol{PF_T} \;=\; 0.90 \text{ ind.} & \text{(initial value)} \end{cases} \tag{6.4}$$

Fig. 6.5 presents the results for the proposed algorithm (with fixed $\lambda_0 = 0.25$), for the optimization of $\boldsymbol{SP}$.

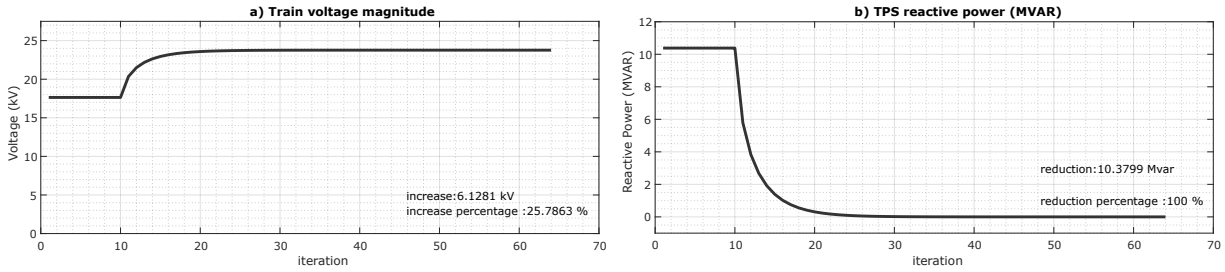

Figure 6.5: Illustration of algorithm evolution for reactive power compensation: a) Evolution of train voltage; b) Evolution of TPS reactive power. Note that, for illustration purposes, the reactive compensation procedure is only enabled at iteration $it = 10$.

This result clearly illustrates the major advantages of this reactive power compensation. The train voltage increases 25.8% and the resultant reactive power in the traction substation is zero. Regarding the train operation, as illustrated in Fig. 6.6, the train active power consumption is unaffected, as expected; the reactive power is considerably changed, from an inductive power factor to a capacitive one; the big advantage is on the reduction of the apparent power consumption which is directly related to a reduction in train power losses (in train transformer and power converters).

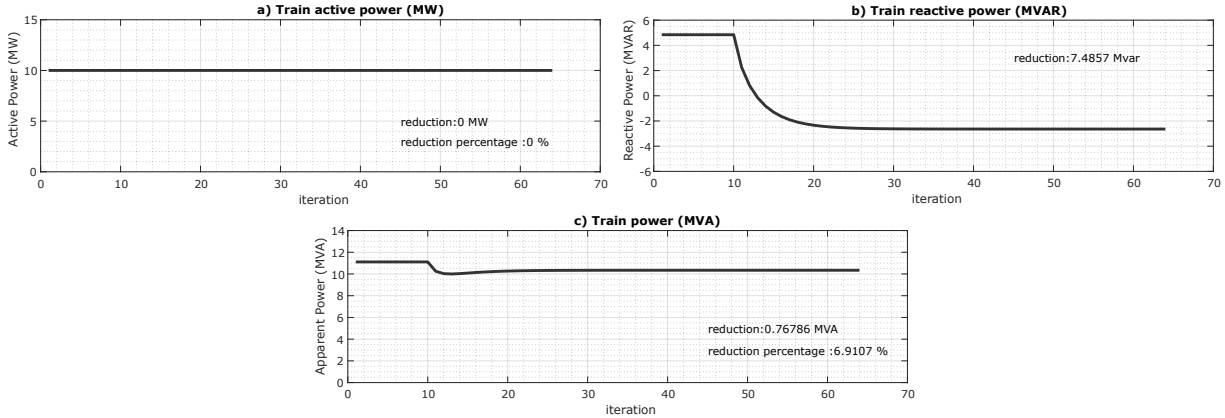

Figure 6.6: Illustration of algorithm evolution for reactive power compensation: a) Evolution of train active power; b) Evolution of train reactive power; c) Evolution of train apparent power.

Finally, the major advantage of this strategy is visible in Fig. 6.7, where the power losses in catenary can be reduced by half.

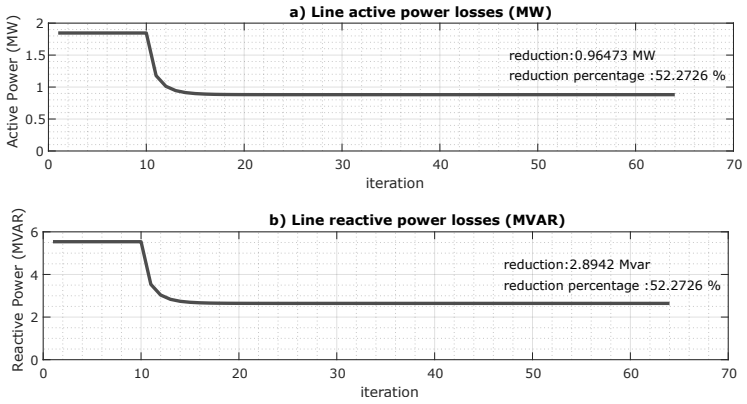

Figure 6.7: Illustration of algorithm evolution for reactive power compensation: a) Evolution of active power losses in catenary; b) Evolution of reactive power losses in catenary.

These results used an initial inductive train power factor of 0.9. In the following subsection, a sensibility analysis will be made to better evaluate the potential improvement from initial different power factors.

6.3.2 Sensibility Analysis

Fig. 6.7 presents the visible power losses in the catenary, for $\boldsymbol{SP}$ in (6.4). A sensibility analysis will be performed for a fixed $^{\boldsymbol{X}}/_{\boldsymbol{R}_L} \approx 3$, with the results in Fig. 6.8.

As expected, for lower values for $\boldsymbol{PF}_T$, this results in a higher reduction in the line losses. This value is expected since trains will have more margin to adapt the power factor value to a capacitive one.

In the following section, this algorithm will be included to compensate the reactive power in two situations:

- Compensation in NZ through a Pulse-Width Modulation (PWM) controlled SVC, using real-time remote measurements of power flow at TPS;
- Compensation made by each train through internal adaptation of the control loop, using real-time knowledge on power flow of railway electrification line.

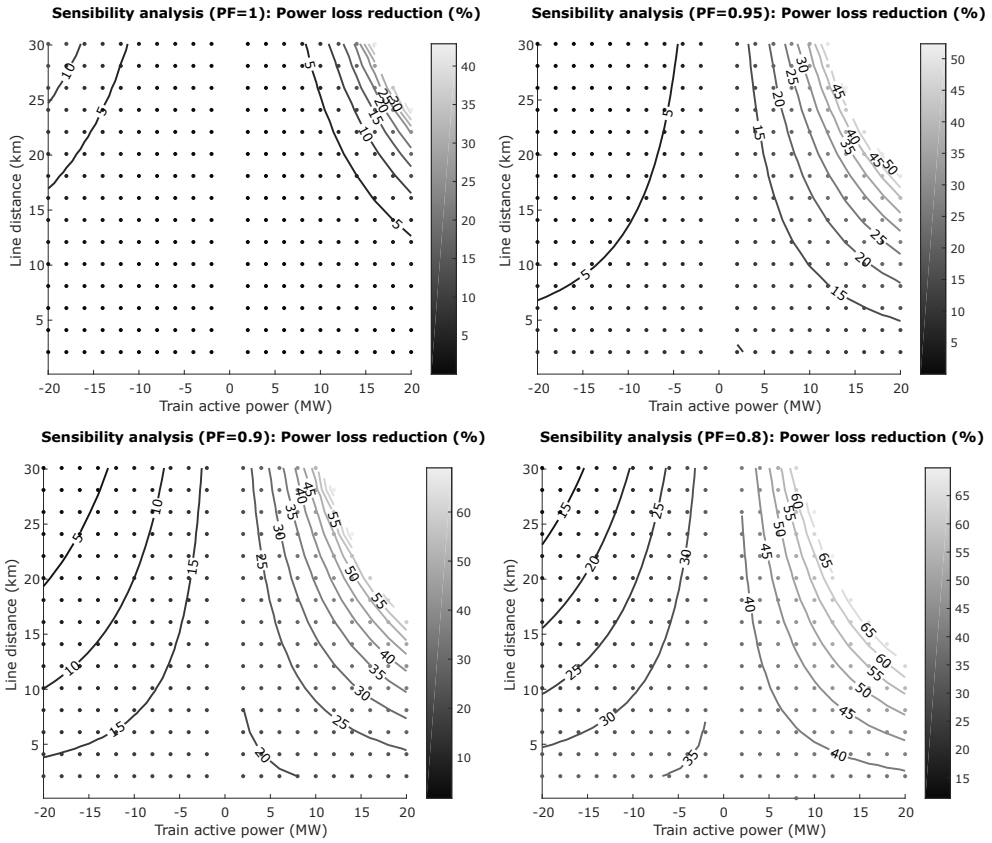

Figure 6.8: Sensibility analysis for reactive power compensation: line power loss reduction, in percentage, for different power factors. Note that the values near 0 MW or near 0 km are not relevant for this demonstration.

6.4 Increase of the Railway Infrastructure Capacity

This section proposes to increase the infrastructure capacity of a railway line (increase of the number of trains), with the adoption of a reactive power compensation strategy.

The railway infrastructure capacity will be considered, in this section, as the maximum number of trains that can exist in a railway line, all of them separated with the same distance among each other and that the voltage levels on the line are according to IEC60850 [113]. The safety issues such as the minimum distance that a train must be apart from each other will not be considered (the impact will be discussed later).

Consider a railway line branch, with a fixed length separating the TPS and a neutral zone and having N trains. To better evaluate the infrastructure capacity, in the implemented model illustrated in Fig. 6.9, the distances $d_1, d_2, \cdots, d_{n+1}$ are all the same, as well as all the train powers, P_T and Q_T.

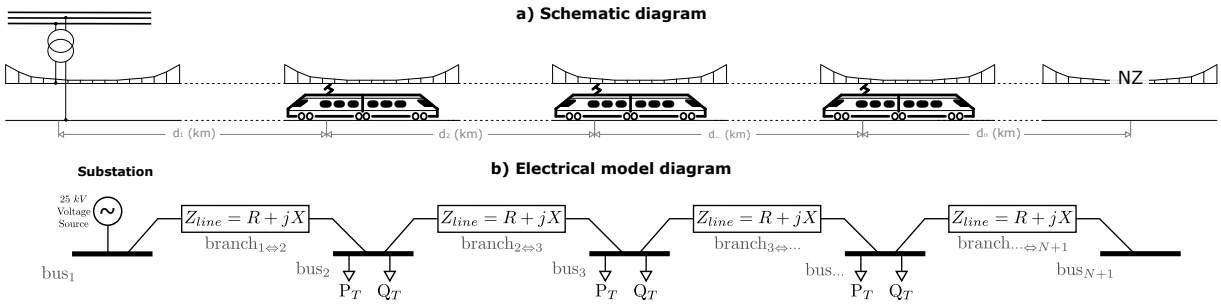

Figure 6.9: Framework for the increase of railway capacity: a) Illustration of physical representation; b) Considered bus-branch model for MatPower.

With this consideration, three different case studies can be listed:

- Study of railway capacity without compensation (Baseline);
- Installation of a Static VAr Compensator located at neutral zone;
- Onboard compensation in all trains;

6.4.1 Baseline: Railway Capacity without Compensation

This section takes into account a railway line having a fixed length $D_{TPS\Leftrightarrow NZ} = 29.2$ km (corresponding to the maximum distance of a track section of a real 250 km railway line, the same as considered in the appendix E).

The procedure to evaluate the railway capacity is illustrated in Fig. 6.10, where the addition of trains to the railway line is iteratively tested.

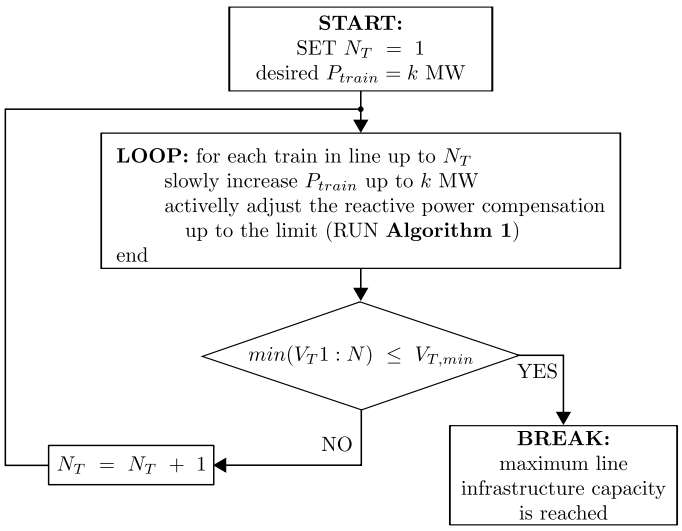

Figure 6.10: Flowchart to test the increasing of capacity procedure.

Specifically, considering that the line has N trains, each train will be separated among them by a fixed distance:

$$d_T = \frac{D_{TPS \Leftrightarrow NZ}}{N+1} \tag{6.5}$$

It is noteworthy that the usage of variable train distances will result in opening a degree of freedom that, only with an extensive probabilistic analysis (for different distances), it is possible to obtain reasonable results. Nevertheless, similar results are expected.

In this baseline case study, the procedure in Fig. 6.10 will not consider the active adjustment of reactive power. The maximum infrastructure capacity is then achieved when the voltage in the line is lower than the IEC60850 minimum non-permanent voltage (17.5 kV [113]). The decision for choosing the non-permanent voltage was arbitrary between the two minimum IEC60850 voltage limits (both voltage level values are valid for the following analysis, expecting similar results; the window between these two levels must not be considered as a steady-state train operation).

Fig. 6.11 illustrates the results, where a relation of the number of trains and the minimum voltage level is illustrated for different cases.

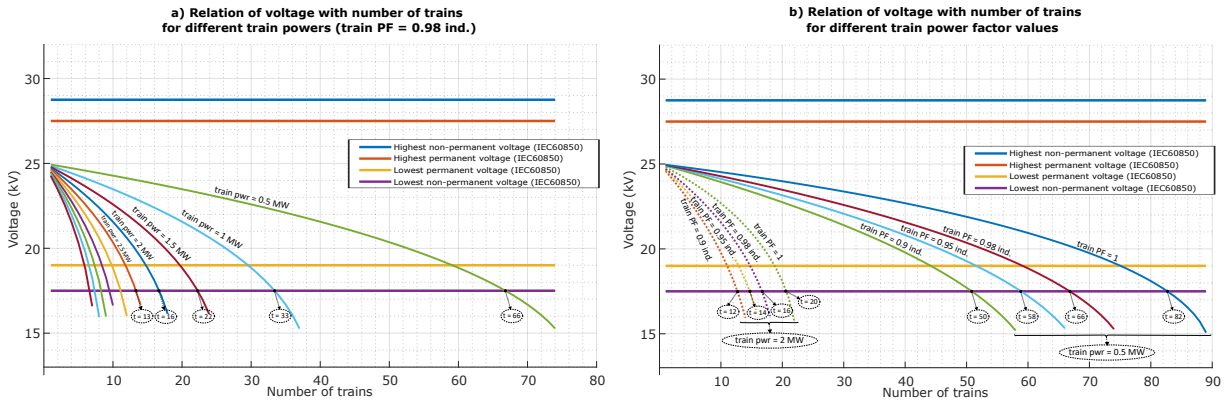

Figure 6.11: Relation of number of trains with voltage in neutral zone: a) Variation of active power in each train, for fixed $PF = 0.98$ ind.; b) Variation of power factor in each train, for fixed active power of 0.5 MW and 2 MW.

Fig. 6.11a shows the dependence of minimum voltage level and the number of trains, for different power values in each train. In theory, it is possible to have 16 trains in the line, all consuming 2 MW with $PF = 0.98$ ind., without achieving the lower value of non-permanent voltage (17.5 kV according to IEC60850).

Fig. 6.11b shows the voltage for different train power factors, where the increase to unitary power factor from $PF = 0.9$ ind. results in an increase of the railway capacity around 67% (for $P_t = 2$ MW, increase from 12 to 20 trains).

Table 6.1 extends the evaluation of railway capacity for different train power consumptions and for different train power factors.

Table 6.1: Maximum number of trains, for different train power consumptions and for different train power factors. Note: the percentage reduction from unitary power factor is presented in parentheses. As an example, the baseline for $P_T = 2$ MW and $PF = 1$ is 20 trains; then, for $PF = 0.9$ ind., it is only possible to have 12 trains (8 less than the unitary power factor, corresponding -40% less than baseline).

	Train Power Factor			
Train Active Power	0.9 ind.	0.95 ind.	0.98 ind.	1
0.5 MW	50 (-39.0%)	58 (-29.3%)	66 (-19.5%)	82 (0%)
1 MW	25 (-39.0%)	29 (-29.3%)	33 (-19.5%)	41 (0%)
2 MW	12 (-40.0%)	14 (-30.0%)	16 (-20.0%)	20 (0%)
3 MW	8 (-38.5%)	9 (-30.8%)	11 (-15.4%)	13 (0%)
4 MW	6 (-40.0%)	7 (-30.0%)	8 (-20.0%)	10 0%)
5 MW	5 (-37.5%)	5 (-37.5%)	6 (-25.0%)	8 (0%)

From this baseline, two possible strategies for the railway reactive compensation will be covered, considering each train starting with $PF = 0.98$ ind.

6.4.2 Reactive Power Compensation in the Neutral Zone

In the second case study, the reactive power compensation will be made with an SVC in the neutral zone, having the objective of minimizing the TPS reactive power. Fig. 6.12 presents the lower voltage in line, as a function of the number of trains in the line.

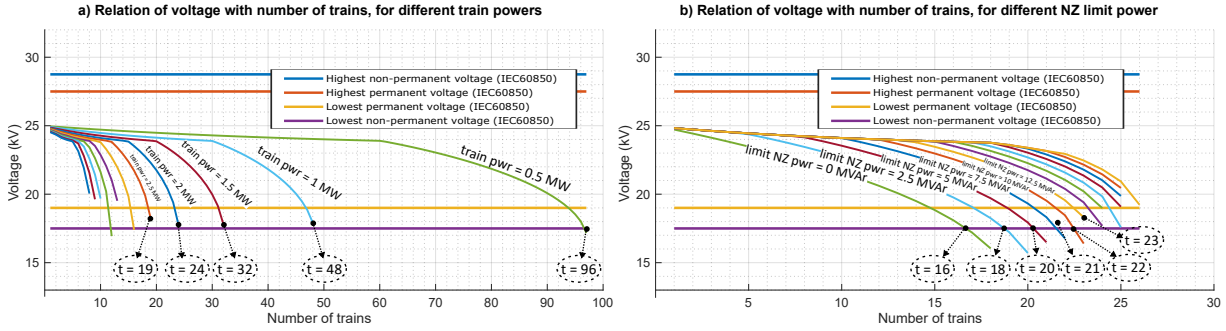

Figure 6.12: Relation of number of trains ($PF = 0.98$ ind.) with lower voltage in line: a) Variation of active power in each train, for fixed NZ limit power (15 MVA maximum power, as example, visible after 30 trains for 1 MW train power); b) Variation of NZ limit power, for fixed train active power of 2MW.

Table 6.2 extends the evaluation of railway capacity for different power consumptions and for different compensation limits at the neutral zone.

Table 6.2: Maximum number of trains, for different train power consumptions and for different Neutral Zone power limits. Note: the percentage improvement from baseline is presented in parentheses (where 0 MVAr means no compensation). As an example, the baseline for $P_T = 2$ MW is 16 trains; then, for $Q_{NZ} = 20$ MVAr, it is possible to have nine more trains (+56% more than baseline).

	Neutral Zone Power Limit (for Compensation)				
Train Active Power	0 MVAr	5 MVAr	10 MVAr	20 MVAr	30 MVAr
0.5 MW	66 (0%)	81 (+22.73%)	90 (+36.36%)	100 (+51.52%)	105 (+59.09%)
1 MW	33 (0%)	40 (+21.21%)	45 (+36.36%)	50 (+51.52%)	52 (+57.58%)
2 MW	16 (0%)	20 (+25%)	22 (+37.50%)	25 (+56.25%)	26 (+62.50%)
3 MW	11 (0%)	13 (+18.18%)	15 (+36.36%)	16 (+45.45%)	17 (+54.55%)
4 MW	8 (0%)	10 (+25%)	11 (+37.50%)	12 (+50%)	12 (+50%)
5 MW	6 (0%)	8 (+33.33%)	8 (+33.33%)	9 (+50%)	10 (+66.67%)

From the results of Table 6.2, it is possible to identify a relation between the maximum number of trains, $N_{trains,max}$, in the line and the power of each train, $P_{train}[MW]$, following (6.6):

$$N_{trains,max} = K_{NZ,lim} \frac{1}{P_{train}} \tag{6.6}$$

Also, it is possible to estimate the $K_{NZ,lim}$ parameter, since it follows a polynomial function and is dependent on the power limit of the SVC of NZ, P_{NZ}. For the obtained results, this can be extrapolated to the expression[1] in (6.7):

$$N_{trains,max}(P_{NZ}, P_{train}) = \frac{K_2(P_{NZ})^2 + K_1 P_{NZ} + K_0}{P_{train}} \tag{6.7}$$

The evaluation of the percentage improvement of the railway infrastructure capacity, in Table 6.2, shows that this improvement is mostly dependent on the NZ reactive power. Specifically, it follows a polynomial trendline, as illustrated in Fig. 6.13.

The analysis of the trendline shows that, for the considered railway line, the maximum train capacity improvement is around 50% to 60%. However, for higher NZ installed power (above 25 MVAr), it is expected that the capacity improvement will flatten, mostly due to the voltage limitation in the NZ (according to the railway standards, the SVC can not impose a voltage higher than 1.1 p.u).

[1] where $K_0 = 33.4$, $K_1 = 1.35$ and $K_2 = -0.0252$, for this case study.

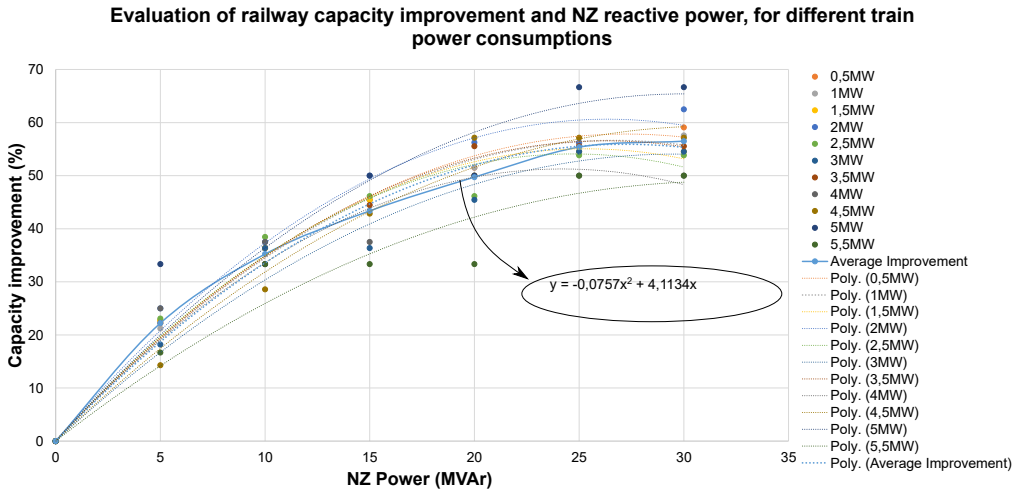

Figure 6.13: Relation of capacity improvement with the increase of the NZ reactive power. The dots display the Table 6.2 percentage improvement values; the smaller dot lines present polynomial regression curves from each of those points. The blue dash-dot line (Average improvement) presents a polynomial regression curve from the average of all the improvement values.

6.4.3 Mobile Reactive Power Compensation

Previously, it was considered that the reactive power compensation is performed in NZ. It was visible that the capacity improvement is mostly dependent on the NZ power capability and not on the train power demand.

In this section, the reactive power compensation is performed in each train, where it will be limited by the maximum compensation, which means minimum capacitive power factor. By considering a train operating in any power factor, then the apparent power is given by the following expression:

$$|S| = \frac{P}{PF}, \qquad P \in]0\ P_N], \quad PF \in]0\ 1] \tag{6.8}$$

The variation of the apparent power in relation with an unitary power factor is:

$$|\Delta S| = \frac{P}{PF} - P \tag{6.9}$$

If expressed in percentage of P, this variation is only dependent on the power factor:

$$\Delta S[\%] = \left(\frac{1 - PF}{PF}\right) * 100 \tag{6.10}$$

Fig. 6.14 illustrates the variation of power, $\Delta S[\%]$, for different train power factors.

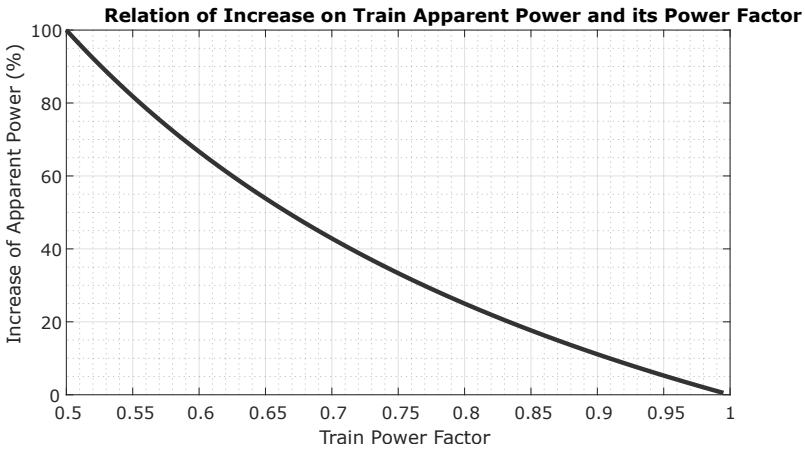

Figure 6.14: Relation of changing power factor, from unitary one, with an increase of train apparent power.

Similarly to the NZ reactive power compensation algorithm, the mobile reactive power compensation algorithm will adapt the reactive power in one bus (e.g.,bus k), to minimize the reactive power in another bus (specifically, bus $k-1$). However, the difference here is that the same algorithm is replicated to all of the trains in the line.

To better illustrate the expected behaviour of the compensation scheme, if the train in bus_3 in Fig. 6.9 is considered, this train compensation objective is to have a zero value of reactive power feeding the $branch_{2\Leftrightarrow 3}$, at bus_2. This is achieved with the adjustment of power factor, as exemplified in Fig. 6.15, where, from the baseline train reactive power Q_T, this is reduced to Q^*.

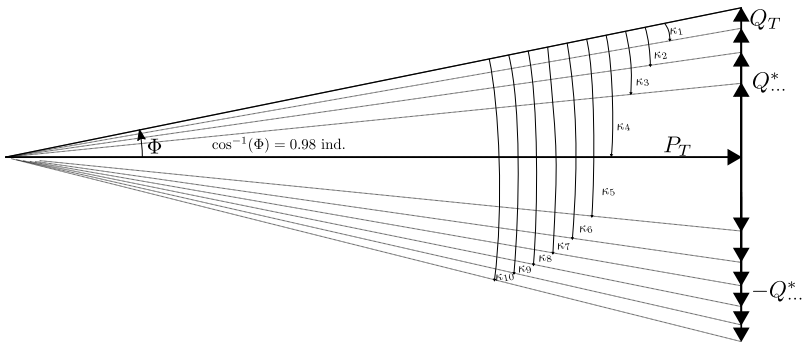

Figure 6.15: Illustration of the adjustment of power factor for mobile reactive power compensation.

In Fig. 6.15 and the following results, the train will start with an inductive power factor (0.98) as a baseline. Then, fixed increments of κ_x will be considered, where $\arccos(\kappa_1) = 0.005$.

Fig. 6.16 presents the results for mobile reactive power compensation, where maximum train limit PF is 0.98 cap. (in Fig. 6.16a) and follows the different κ_x, in Fig. 6.16b.

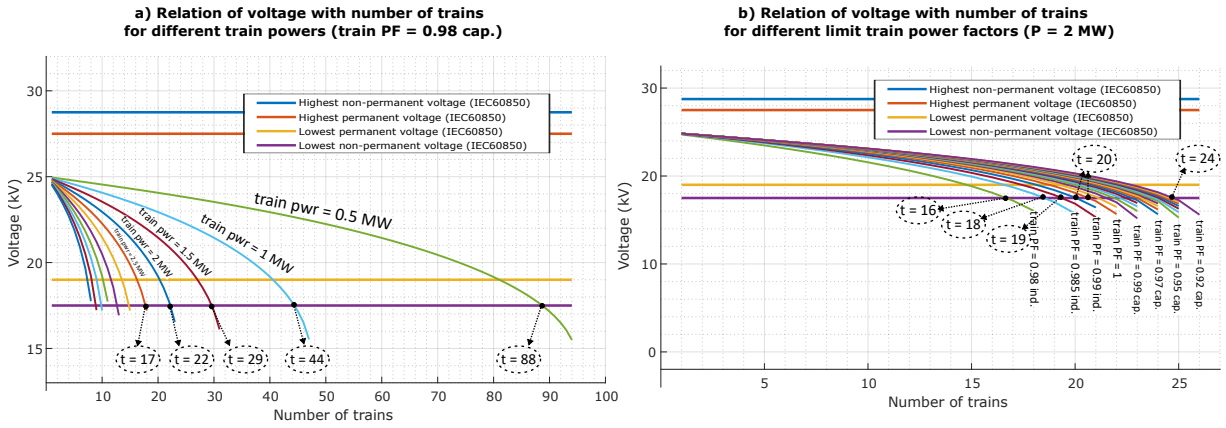

Figure 6.16: Relation of number of trains (PF = 0.98 ind.) with lower voltage in line: a) Variation of active power in each train, for fixed train PF limit (0.98 cap.); b) Variation of compensation, for fixed train active power of 2 MW.

In Fig. 6.16b, it is clear that simple adaptation of reactive power in each train will increase the number of trains. Specifically, changing the PF from 0.98 ind. to 0.94 cap. will result in an increase in 50% in the number of trains. This result is obtained with the increase of the train apparent power in 6.4% (by using Equation (6.10) for PF 0.94 cap.). All the results are presented in Table 6.3.

Table 6.3: Maximum number of trains, for different train power consumptions and for different power factor limit. Note: the percentage improvement from baseline (train PF = 0.98 ind.) is presented in parentheses. As an example, the baseline for $P_T = 2$ MW is 16 trains; then for PF = 0.92 cap., it is possible to have eight more trains (+50% more than baseline).

	Train Active Power					
Train Power Factor	**0.5 MW**	**1 MW**	**2 MW**	**3 MW**	**4 MW**	**5 MW**
0.98 ind.	66 (+0%)	33 (+0%)	16 (+0%)	11 (+0%)	8 (+0%)	6 (+0%)
0.985 ind.	74 (+12%)	37 (+12%)	18 (+13%)	12 (+9%)	9 (+13%)	7 (+17%)
0.99 ind.	77 (+17%)	38 (+15%)	19 (+19%)	12 (+9%)	9 (+13%)	7 (+17%)
0.995 ind.	80 (+21%)	40 (+21%)	20 (+25%)	13 (+18%)	10 (+25%)	7 (+17%)
1.00	82 (+24%)	41 (+24%)	20 (+25%)	13 (+18%)	10 (+25%)	8 (+33%)
0.99 cap.	86 (+30%)	43 (+30%)	21 (+31%)	14 (+27%)	10 (+25%)	8 (+33%)
0.98 cap.	88 (+33%)	44 (+33%)	22 (+38%)	14 (+27%)	11 (+38%)	8 (+33%)
0.96 cap.	92 (+39%)	46 (+39%)	23 (+44%)	15 (+36%)	11 (+38%)	9 (+50%)
0.94 cap.	95 (+44%)	47 (+42%)	24 (+50%)	16 (+45%)	12 (+50%)	9 (+50%)
0.92 cap.	98 (+48%)	49 (+48%)	24 (+50%)	16 (+45%)	12 (+50%)	10 (+67%)

It is possible to identify a correlation between the capacity improvement (in percentage) and the limit for train power factor. These results are presented in Table 6.4.

Table 6.4: Comparison of power factor with apparent power increase and average improvement of railway infrastructure capacity.

Train Power Factor	Power Increase	Capacity Improvement
0.98 ind.	−2.0%	0.0%
0.985 ind.	−1.5%	10.7%
0.99 ind.	−1.0%	15.5%
0.995 ind.	−0.5%	20.2%
1.00	0.0%	23.9%
0.99 cap.	1.0%	28.6%
0.98 cap.	2.0%	32.7%
0.97 cap.	3.1%	39.1%
0.96 cap.	4.2%	40.2%
0.95 cap.	5.3%	41.1%
0.94 cap.	6.4%	44.9%
0.93 cap.	7.5%	46.5%
0.92 cap.	8.7%	51.2%

It can be easily concluded that, if the trains operate with capacitive power factors, the number of trains in the line can be increased. However, the implementation of this strategy should be in compliance with the standard EN 50388-1 [157], by ensuring that the capacitive reactive power compensation made by each train is clipped to zero, once the catenary nominal voltage is reached. Besides, in the regenerative mode as stated in the same standard, the voltage is likely to increase and, then, capacitive reactive power compensation must be avoided.

6.5 Smart Railway Framework

In Fig. 1.1 is illustrated the levels of information in the smart railways framework. After the analysis of the energy information, whose procedure was presented in chapter 5, it is generated the knowledge on the power flow.

A smart power flow management of the railway electrification is addressed in this section, taking into consideration the findings of previous sections.

6.5.1 The Problem of Mobile Reactive Power Compensation

One limitation of the railway infrastructure is the impossibility of each train to measure the power flowing along the catenary (it is impossible to have current sensors measuring the downstream and upstream currents). The onboard energy measurement and data

transmission to ground stations [149] have been implemented in the past few years by railway operators and the details on this measurement have been actively researched [158].

A reactive power compensation strategy must have accurate measurements of the power flow in the catenary. Specifically, as illustrated in Fig. 6.17, the train T_N must have the knowledge of the power flow at upstream, in the train T_{N-1} node.

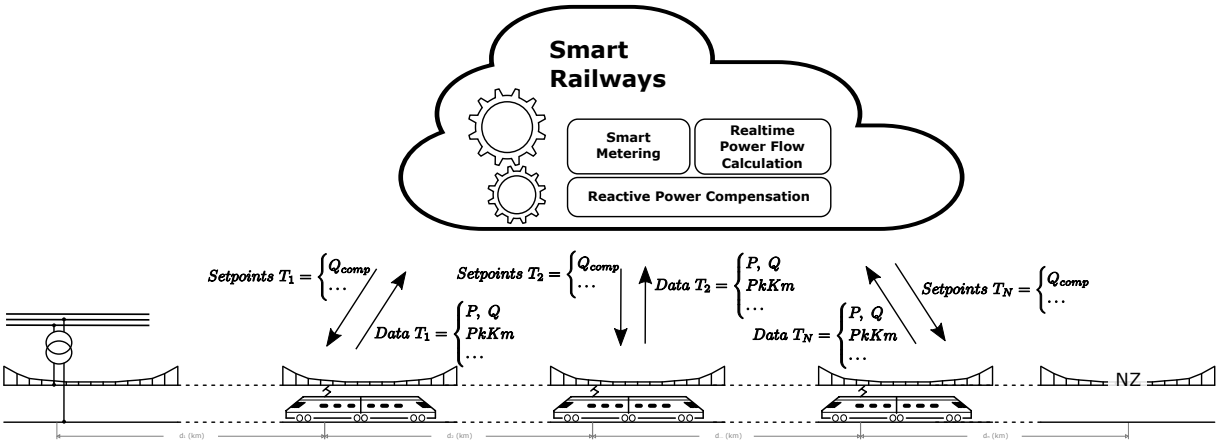

Figure 6.17: Integration of reactive power compensation in a smart railway framework.

This knowledge of the catenary power flow is not an easy task due to several issues:

- It requires the implementation of onboard energy meters in all trains (or in the majority) and in the TPS;
- Requires data reporting to a central station (data gathering);
- It is needed to calculate the power flow in each node and dynamically adapt this calculation mechanism to consider all trains in the traction section (power flow calculation);
- In the case of reactive power compensation strategy, the generated setpoints must be sent to each train (setpoints updating)
- All of these procedures must be made within real-time constraints.

The optimal operation for reactive power compensation will be achieved without delay in the *Data Gathering* $\longrightarrow$ *Power flow calculation* $\longrightarrow$ *Generation of reactive power references* $\longrightarrow$ *Setpoints updating* procedure flow.

In chapter 5 was illustrated one of the elements of the presented procedure. Specifically, the power flow knowledge generation is a complex task, which depends on four complex modules of PSSA-rail. This difficult task will have a non-negligible execution time. Considering the Fig. 6.18 for the illustration of the execution times of these tasks.

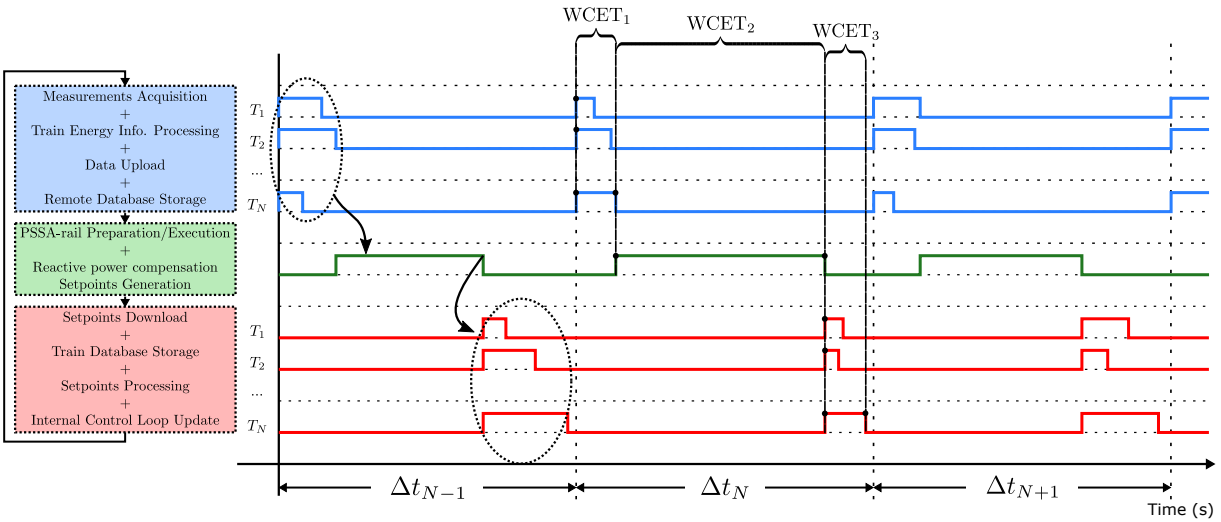

Figure 6.18: Evaluation of execution timings for a reactive power compensation strategy without smart railway framework.

In the left of Fig. 6.18 is presented the steps for the execution of the proposed strategy from a more practical implementation viewpoint. The centralized process, illustrated in green, can only generate new reactive power setpoints to each of the trains after all of the trains complete the first task, illustrated in blue. The Worst-Case Execution Time (WCET) will be the sum of the individual WCET values, as illustrated, and then, the Δt_N must be stipulated following:

$$\Delta t_N \gg \sum_{Task=1}^{N} WCET_{Task} \tag{6.11}$$

Considering the best-case execution time of PSSA-rail of 20 ms and considering that the reactive power compensation takes 25 iterations to generate all the setpoints of reactive power compensation of all trains, then, it could be estimated at around 500 ms to generate new reactive power setpoints. Furthermore, considering also a maximum communication latency of 100 ms, it would be an acceptable value of $\Delta t_N = 1\ s.$ (with considerable challenges for a practical implementation)[2].

The estimation of Δt_N is important for the analysis of the proposed reactive power

[2]The results of the simulation of the 86 400 points of the day, in the best execution scenario, have taken near 30 min in a 16-core CPU server. Then, ignoring the parallelism aspects, each simulation time-step can be estimated to be 20 ms.
The 25 iterations were estimated taking into account the results present in Fig. 6.5, where the algorithm needs around 55 iterations to achieve a result within an arbitrary optimization tolerance, for one train. Then, for a variable λ and for a more aggressive λ_0 for the optimization, and because the same optimization is run in parallel for all trains, this 25 number of iterations was arbitrated.
The latency value of 100 ms is a requirement metric by the International Telecommunication Union (ITU), for the maximum Long-Term Evolution (LTE) latency, according to [159].

compensation strategy, specifically to estimate what is the expected update rate of new setpoint values. Complementarily, since the train active power is a very dynamic variable (in order of the time, where the accelerations and decelerations occur within short time-windows), a high value for the Δt_N will not be compatible with the desired optimal operation. Then, in a practical implementation of a reactive power compensation strategy, the avoidance of non-optimal operation and the dependence of real-time requirements should be adopted.

6.5.2 A Solution for Mobile Reactive Power Compensation

First, the majority of the tasks to achieve this smart power flow management must not have real-time execution requirements. As illustrated in Fig. 6.19, only the update of the reactive power compensation setpoint in the internal control loop must be executed in real-time. Furthermore, prediction algorithms (that estimate future consumptions and train positions) are necessary. Assuming that this train prediction algorithm can predict a future time window (for example, 10 s) with a specific accuracy (for example, 20 % in error) then, in the worst case, the predictor algorithm generates a train reactive power setpoint with a 20% error.

A solution is then proposed to include real-time and non-real-time tasks, as well as the inclusion of prediction algorithms in the loop, as illustrated in Fig. 6.19.

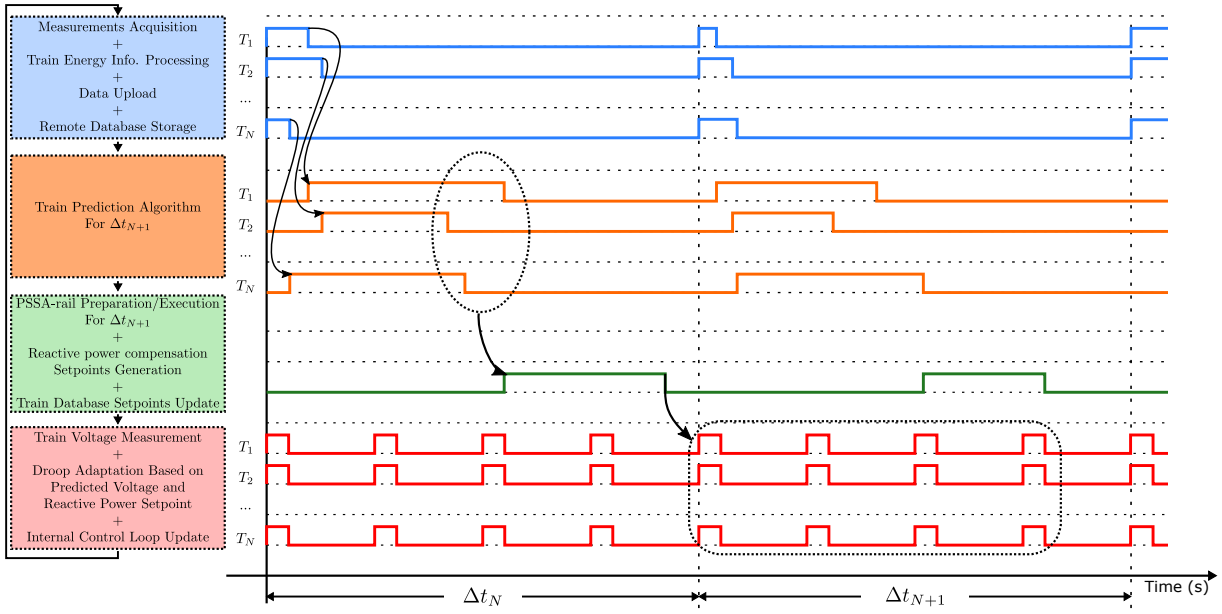

Figure 6.19: Evaluation of execution timings for a reactive power compensation strategy with smart railway framework.

After the acquisition of the measurements, processing into train energy information, upload and storage in a centralized database, illustrated in blue in Fig. 6.19, the onboard processing unit will start a prediction task for the train. This prediction task, illustrated in orange in Fig. 6.19, uses the information of the measurements for the time-window Δt_{N-1}, to predict the power consumption and the train movement for the next time-window, Δt_{N+1}. Furthermore, after the completion of the prediction task by each train, the generated prediction for the time-window Δt_{N+1} is sent to a remote processing unit, illustrated in green in Fig. 6.19, where the power flow knowledge will be extracted, together with the reactive power compensation strategy.

This PSSA-rail preparation/execution task configured with a reactive power compensation strategy will be executed to Δt_{N+1} time-window. Contrary to the green task of Fig. 6.18, where a single time-step is analysed, this new task of Fig. 6.19 will be executed to all the time-steps of Δt_{N+1} time-window. Despite the expected increase of the worst case execution time (WCET_2 in this case), it should be highlighted that this time-window analysis is now compatible with parallel processing, being more in line with the architecture of the PSSA-rail (and then, the new WCET_2 will not be the previous value multiplied by the number of time-steps of the Δt_{N+1} time-window).

Finally, the red task illustrated in Fig. 6.19 is now adapted to properly use the knowledge generated by the estimated reactive power compensation references. This task is independent: it does not require real-time constraints since it is capable of operating in degraded mode, where no references are received from the remote processing unit.

Besides the reactive power setpoints generated by the green task of Fig. 6.19, naturally, this module also estimates the respective train voltages after the application of the reactive power compensation. This predicted voltage value can be used to improve the algorithm in the following way:

- If the train voltage is above the expected voltage value, then it means that the amount of reactive power injected is above the optimal value;
    - Then, the onboard reactive power compensation system (viewed as an algorithm that adapts the power factor depending on the desired reactive power value) will reduce the value of reactive power.
- If the train voltage is below the expected, then the onboard reactive power compensation system will increase the injection of reactive power.

A droop-like approach can be used to help stabilize the reactive power control.

This onboard adaptation will follow a droop characteristic curve, as illustrated in Fig. 6.20: the higher the deviation of the voltage and the closer the train is to the NZ, the higher the correction to Q_{comp}.

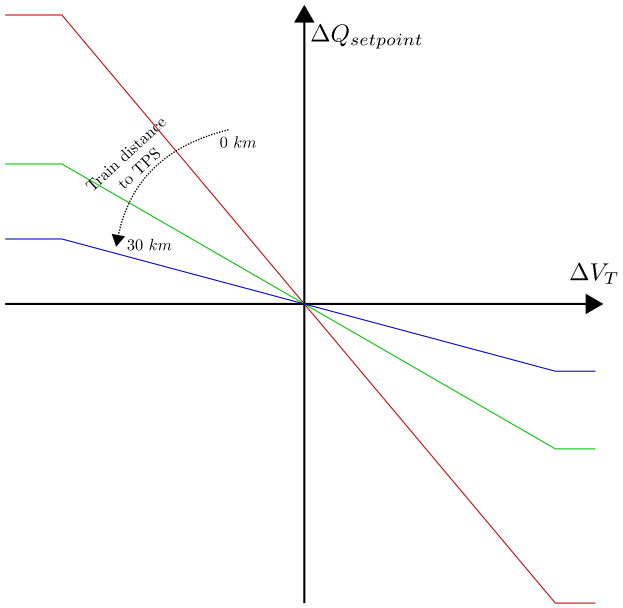

Figure 6.20: Droop strategy for onboard adjustment. The ΔV_T is the difference between the real train voltage and the expected train voltage. The $\Delta Q_{setpoint}$ is the output of the droop curve, where this value is added to the predicted Q_{comp}.

The slope of the droop characteristic curve might be difficult to obtain. As an example, if all trains have the same droop characteristic curve, it is possible to have a resonance behaviour. This train–network interactions and resonance is a well-known issue [56], where the converter control loops must be immune to low-frequency oscillation, harmonic resonance and harmonic instability phenomena (specifically with the tuning of current and voltage control loops, as well as the estimation of the phase angle of the incoming voltage). Therefore, the proposed droop approach most likely reduces a possible low-frequency oscillation in the reactive power.

In this conceptual implementation, the droop characteristic must be dependent on the distance between the train and the TPS, as well as the number of trains separating a compensation one and the TPS. For example, considering two scenarios of one train in the line, where one train is positioned closer to the NZ and the other scenario considers the train near the TPS, with the same variation of reactive power in both trains, the effect on the train voltage is less visible in the train closer to TPS. Then, the droop curve might be adjusted accordingly.

Considering the example in Fig. 6.21, the usage of the real measured voltage for onboard adaptation of the reactive power will contribute to having an operation closer to the optimal (in comparison with only following the Q_{comp} setpoints).

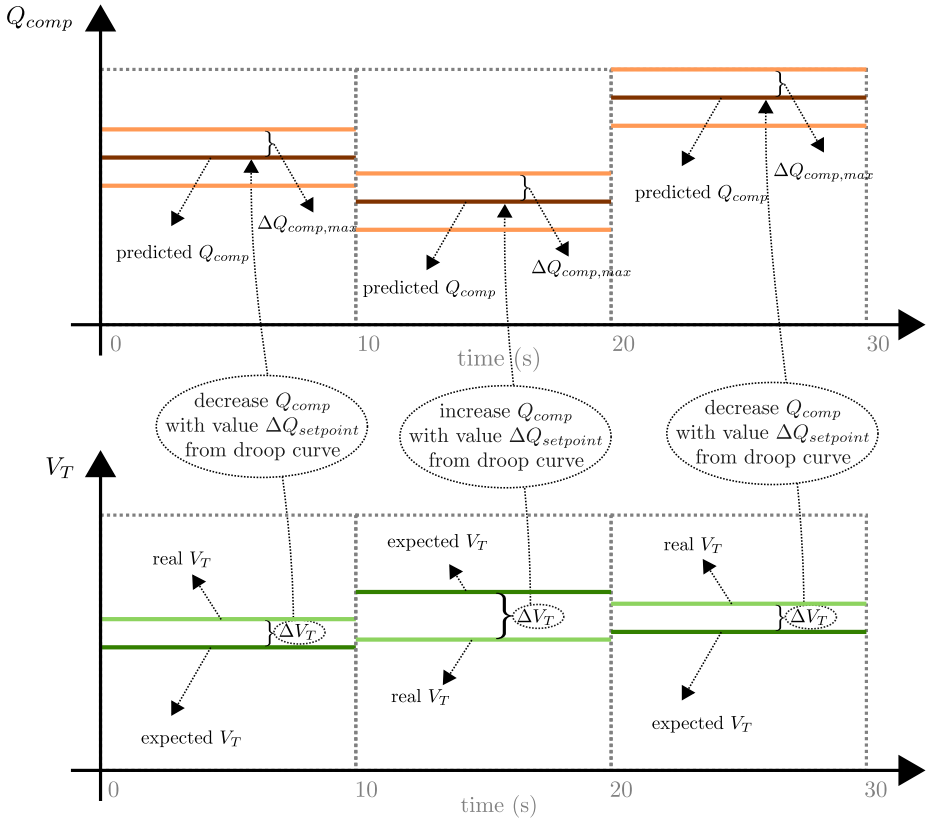

Figure 6.21: Illustration of the onboard adaptation, supported by the predicted Q_{comp} and $V_{T,estim.}$ from the smart railways framework.

6.6 Discussion and Conclusions

The work in this chapter results from the recent lack of coverage of railway reactive power control in the scientific literature. In fact, the reactive power control towards the increase of railway infrastructure capacity is not an active research topic, as addressed in chapter 2 on the research opportunities for topic **T4**.

With a smart power flow management strategy, the increase of railway energy efficiency is clear, not only with the reduction of the reactive power consumption from the transmission/distribution system operator but also with the reduction of line power losses. The example of Fig. 6.7 illustrates the potential of reduction of catenary power losses up to 50%, with this reactive power management.

The approach to study the infrastructure capacity improvement is the new hypothesis covered with this work. Specifically, two reactive power compensation strategies are compared, regarding the railway infrastructure capacity.

The integration of a Static VAR Compensator in the neutral zone can increase the

railway capacity up to 50% in the studied use case. One of the findings is that this value almost does not depend on the power of the trains: the 50% infrastructure capacity increase is achieved regardless of each train nominal power consumption.

The second (proposed) compensation strategy considers the integration of the reactive power compensation within each train. With this strategy, it is possible to increase the railway capacity up to 50%, only with an increase of train apparent power below 10%.

These findings led to one other question regarding the practical real-time implementation of these compensation schemes. The discussion of this issue was started in the previous section 6.5, which has led to the proposal of a solution considering a two-level control, with the inclusion of prediction algorithms and separation of real-time tasks from non-real-time ones.

In following are addressed more general discussion aspects.

6.6.1 The Path to Reactive Power Compensation

The SVC compensation strategy is based on the inclusion of power electronic devices within the proximity of NZ. Usually, the compensation strategy performed by SVC devices is local and does not take into consideration the measurements of the reactive power in the TPS. In this work, a communication channel is considered, where the reactive power is measured in the TPS and used in the NZ to inject reactive power.

The proposed mobile reactive power compensation scheme requires that each train can adapt its power factor. This requirement is not compatible with some of the currently used trains, since the technology used does not allow this level of adaptation. The infrastructure managers can promote modernization of train fleet, with a cost reduction of operation for trains able to adapt the reactive power.

As highlighted in chapter 1, the onboard energy metering and the data exchange with ground stations is a reality nowadays, which eases the implementation of this strategy.

Finally, as a preliminary incentive, the billing should accommodate the injection of the reactive power, similarly to the situation happening in certain countries, where the regenerated energy is billed in favour of the railway operator. The clear advantages for the infrastructure managers should allow, in theory, the elimination of the reactive (capacitive) power billing. Further billing strategies should accommodate this effort that the railway operators might take, to improve the power quality. The injection of reactive power can be seen as a service that the railway operators can provide.

6.6.2 Degrees of Freedom & Limitations

The findings in this work were obtained with certain open degrees of freedom, such as each train power consumption, the NZ SVC power limitations and the maximum capacitive power factor for each train.

One limitation of the study concerns to the safety aspects. For example, considering the results for 1 MW trains in Table 6.3 where this resulted in a maximum of 33 trains with $PF = 0.98$ *ind.*, this means that each train is around 900 m apart from each other. As referred in chapter 4 regarding the full brake threshold, the case study train requires at least 1.36 km to fully brake from the maximum speed. Naturally, for lower speeds, this distance is reduced. Nevertheless, the results obtained in the section 6.4 might be impossible to obtain with train dynamic movement requirements of the case study.

Certain degrees of freedom were closed with justifications made throughout the chapter. As an example, the $^{X}/_{R_L}$ ratio was fixed since it depends on the characteristics of the electrification. The line distance was also fixed. It is expected that these two parameters do not affect the railway capacity (in percentage).

The other fixed parameter is the distance between each train. This corresponds to an ideal situation: in a realistic situation, the train dynamic constraints, journey timetables, signalling, among others, will affect each train position and the distance between trains will not be all the same. However, only with an extensive statistical analysis is it possible to evaluate if variable train distances result in different results. It is expected, as an example, that, if the majority of trains are more concentrated near the TPS, the resultant minimum voltage will be higher than the fixed distance presented in this work.

This stochastic analysis can be simulated with PSSA-rail, in which the integration of this strategy is preliminarily evaluated as follows.

6.6.3 Integration of reactive power compensation in PSSA-rail

In this chapter was addressed a deterministic analysis of reactive power compensation. The strategies that were validated through deterministic analysis can be further evaluated in PSSA-rail, which can evaluate the effectiveness of such strategies in a stochastic scenario. The adaptation of PSSA-rail to contemplate the strategy proposed in this chapter has a preliminary proposal illustrated in Fig. 6.22.

This adaptation of PSSA-rail is visible in the scripts in green on Fig. 6.22c) where after the simulation without compensation (*run power flow solver*), an iterative process is started to test the reactive power compensation algorithm while the variation of the power in the branches is above a tolerance. The references of reactive power compensation can be calculated using the proposed methodology in section 6.3, or can be obtained in offline: a lookup-table is generated as function $F_{XN}(S_{N_{-1}\leftrightarrow N}, P_{train_N}, L_{N_{-1}\leftrightarrow N})$ as illustrated in

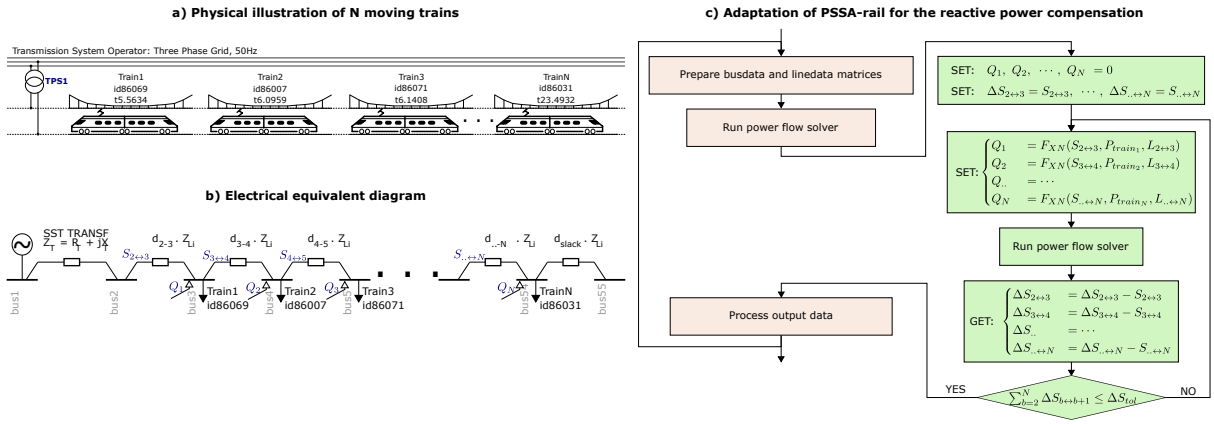

Figure 6.22: Adaptation of the PSSA-rail to contemplate the reactive power compensation strategy.

Fig. 6.22. After the execution of the iterative process, then the output data is processed and the PSSA-rail execution continues to the next time-step.

This reactive power compensation proposal may be subject to further stochastic validation, where the proposed methodology in Fig. 6.22 can be considered.

6.7 Summary

A hypothesis was established and demonstrated in this chapter, with the proposal of a reactive power compensation strategy that results in an increase of infrastructure capacity up to 50 %, only with an increase of train energy consumption of less than 10 % in the analysed use case. This strategy follows the findings presented in chapter 5, where was presented the PSSA-rail tool.

In the first part of this chapter is explored in a deterministic way the topic of reactive power compensation, followed by an analysis of compensation in NZ and in each train. The results show the possibility to achieve infrastructure capacity increase up to 50%.

Later, in this work, a smart railway framework is proposed, focused on solving the issues regarding this reactive power compensation strategy. A solution is then presented based on a droop controller and a smart metering strategy, which enables the trains to be closer to an optimal point of operation.

The gap between current railways and future smarter railways can be reduced with smart management of the power flow in railway electrification, particularly with the strategy proposed in this chapter. In the following chapter is presented another strategy, with the management of railway energy storage systems.

CHAPTER 7

Charging Strategy for Railway Energy Storage Systems

As long as there is available energy-related information with enough quality and quantity, the extracted knowledge can be used to enhance the railway operation.

This chapter targets the topic **T5**: a strategy to enhance the energy efficiency with power flow management of railway energy storage systems.

This strategy comprehends a two-level architecture where the low-level control in real-time the charging of the storage system; the upper-level adapts the parameters of the lower-level control with an automatic optimization algorithm. The low-level is controlled with a Fuzzy Logic Controller and the upper-level uses a Genetic Algorithm (GA) optimizer.

This chapter is divided into two parts. In the first part is presented the methodology and simulation framework of the FLC and the GA meta-heuristic, followed to the presentation of the results for a case study train journey. As global results, the reduction of regenerated energy flowing into the catenary is 22.3 % with the fuzzy logic controller. With the optimization strategy, this reduction can be further extended to 28.7 %.

Similarly to chapter 6, in the second part is discussed the integration of the smart railway framework in this strategy to answer the implementation aspects of this solution. Then is presented a general discussion and conclusions.

The outcome of this chapter will be a two-level charging controller for the onboard and wayside railway energy storage systems, as illustrated in the graphical abstract in Fig. 7.1.

The objectives of this chapter are:

- **Objective 5a**: Propose a methodology to increase the energy efficiency of railway energy storage systems;
- **Objective 5b**: Demonstrate the increase of energy efficiency for a train journey case study estimated in chapter 4;
- **Objective 5c**: Discuss the implementation steps of this strategy, from a practical viewpoint and within the smart railways framework.

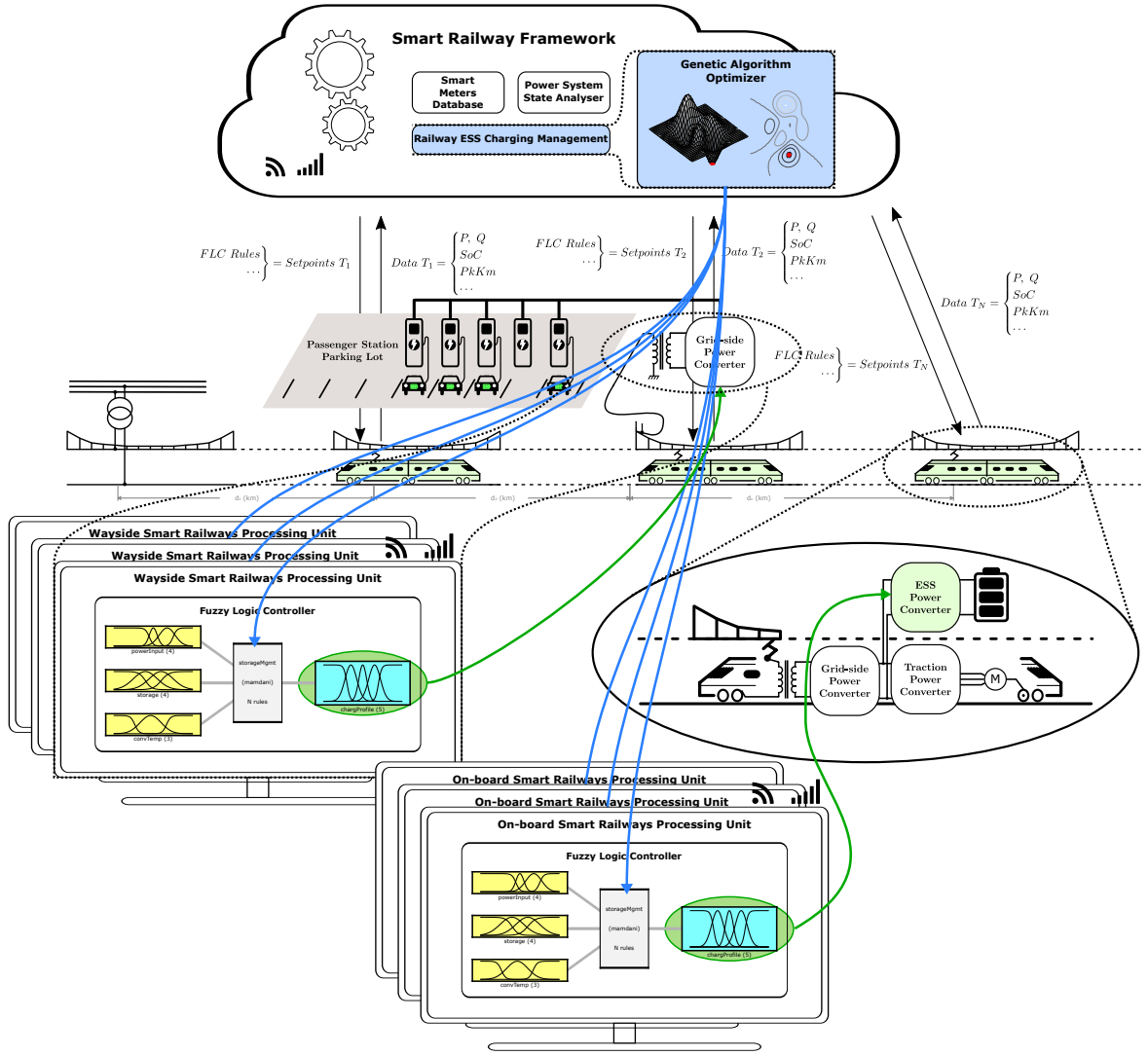

Figure 7.1: Graphical abstract of chapter 7 — Inclusion of power flow management in railway energy storage systems.

7.1 Introduction

The huge power requirements of future railways require the usage of energy-efficient strategies towards a more intelligent railway system.

From an arbitrary train journey produced by the tool in chapter 4, a modern train with regenerative capabilities power consumption has the profile presented in Fig. 7.2a). In Fig. 7.2b), is visible a huge dispersion of the power consumption/regeneration, which is caused mostly by the need to guarantee a given journey timetable, and in this case, stop in every passenger station.

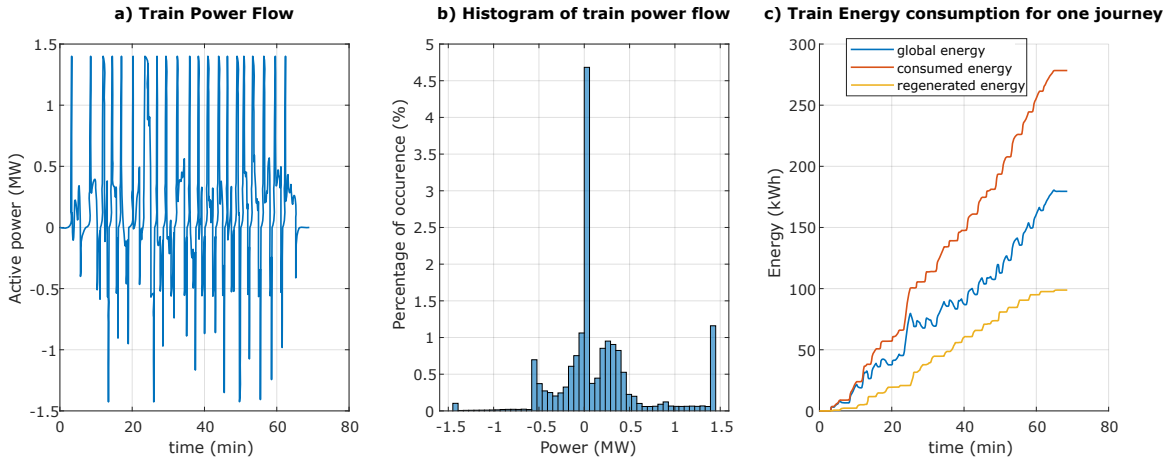

Figure 7.2: Details on a train journey power flow: a) Power consumption/regeneration for a sub-urban train journey; b) Histogram of train power flow; c) Train energy consumption.

According to EN 50388-1 [157], the train can inject the regenerative energy in the railway electrification system, as long as the limit voltage levels are not achieved. However, in certain situations, the regenerated energy cannot be returned to the Transmission/Distribution System Operator (TSO/DSO). Therefore, in these cases, most of the regenerated energy must be dissipated in the train rheostatic system and the billed energy will not be the blue graph of Fig. 7.2c), being instead the red graph.

According to [160], in the worst case where the headway between trains is big, almost all of the regenerated energy will not be absorbed by another train and it will result in around 60% of energy losses.

Therefore, in similar conditions, there is a need to minimize the regenerated energy without affecting the train dynamic characteristics. One way to achieve this is with the use of railway Energy Storage Systems (ESS).

One of the strategies evaluated in chapter 5 was the power flow management of wayside systems, within stochastic scenarios. The findings in chapter 5 led to the analysis of the management of energy storage systems in a more deterministic manner.

Besides, from the research opportunities of topic **T5** highlighted in chapter 2, it was concluded that the integration of diversified energy storage systems into the future railways will be expected. Also, the management of these railway ESS will need to address non-scheduling strategies, which will be considered in the work presented in this chapter. In addition, a two-level management strategy will be studied and analysed, following other works for generic storage systems, where the real-time level is ensured by a multi-input Fuzzy Logic Controller (FLC), and the upper-level genetic algorithm improves the parameters of the FLC, with an automatic searching procedure.

The main objective of this chapter is to present a charging strategy for railway ESS, by proposing a two-level hierarchical EMS strategy using a FLC with a Genetic Algorithm (GA) optimizer. The objective of this approach is to have a distributed processing architecture with two levels: a local processing unit for real-time update of the storage charging profile, based on real-time measurements; and a remote central processing unit, common to all trains, that optimizes the operation of the local units. The proposed strategy is presented in Fig. 7.3.

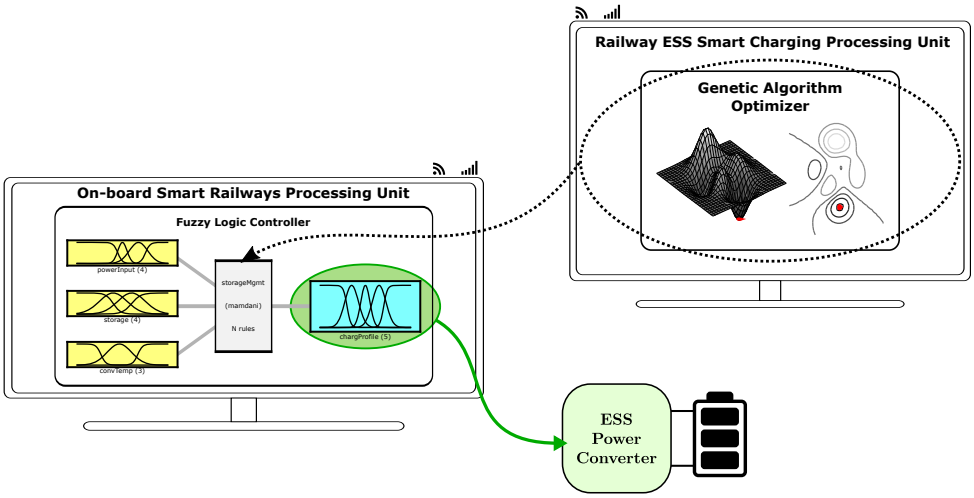

Figure 7.3: Proposed two-level hierarchical architecture tor the railway EMS.

This chapter will contribute to a new railway EMS strategy based on a two-level hierarchical architecture. This strategy is a generic one:

1. It is demonstrated for a case study of a single train journey, but is compatible to have multiple input variables for the local-processing unit;
2. It includes the usage of a GA for multiple optimization criteria;
3. It comprehends an automatic learning algorithm, based on a database of results produced by the GA.

This decoupled operation allows the desired automatic learning, based on the real-time operation of each train, and sharing with all other trains the results of the GA optimization.

This chapter is divided into five sections. In section 7.2 is presented the materials and methods used in this work (the FLC and the GA). In section 7.3 is covered the results, without and with the optimization enabled, and later are discussed the results. In section 7.4 is presented and discussed a conceptual implementation of such railway smart charging strategy. Finally, in section 7.5 is presented a general discussion and the conclusions of this chapter.

7.2 Materials and Simulation Frameworks

In chapter 5 was highlighted the need for a deterministic analysis of the power flow management of railway energy storage systems. Then, in this section is considered a deterministic scenario of one train journey and a onboard energy storage system.

This section presents the methodology and simulation frameworks used to support the proposed onboard railway charging strategy.

This strategy requires that trains will have a disposal of an energy storage unit, as illustrated in Fig. 7.4.

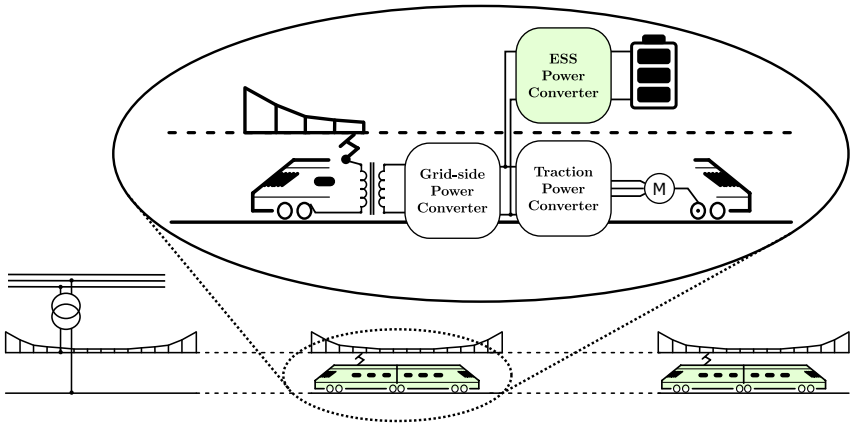

Figure 7.4: Illustration of the onboard train ESS.

In Fig. 7.4 is presented an AC 1x25 kV electrification scheme, which is the system under study in chapter 4, having the sub-urban trains with a nominal power consumption of 1.4 MW. However, this work targets any type of train, as long as it has capabilities for regenerative braking operation. Furthermore, the technology and power electronics topology and control solution to implement such an ESS is not the focus of this work. It was considered that the traction converter has the DC bus accessible and it is considered that train has enough physical space to include the bi-directional power converter, batteries of some sort of technology and all the auxiliary elements to ensure proper operation (battery management systems, safety apparatus, among others).

Having these elements into consideration, the results of this chapter were obtained with an arbitrarily chosen hypothetical and generic ESS hardware. Specifically, the power capabilities of the ESS was set to have 350 kW of charging/discharging maximum power (25% of the train power consumption) and 35 kWh of stored energy (6 minutes to fully charge the ESS when the charging profile is constant and with an absolute per-unit (p.u.) value). Regarding the efficiency of the ESS, recent research on railway ESS has established the efficiency for battery ESS to be 80-90% and the efficiency of the super-capacitor ESS is 95-98% [50, 161]. It is reasonable to consider in this study a unitary efficiency for the

ESS if recent technological advancements on super-capacitors and in Silicon Carbide (SiC) transistors are taken into consideration. Then, the focus of this study is on the capabilities of the FLC and the GA optimization algorithms.

Regarding the charging strategy, this comprises two levels of processing: a real-time FLC which generates references for the ESS power converter; and an optimization GA, running offline, which increases the energy efficiency of the global ESS.

The architecture for such a charging strategy is visible in Fig. 7.5.

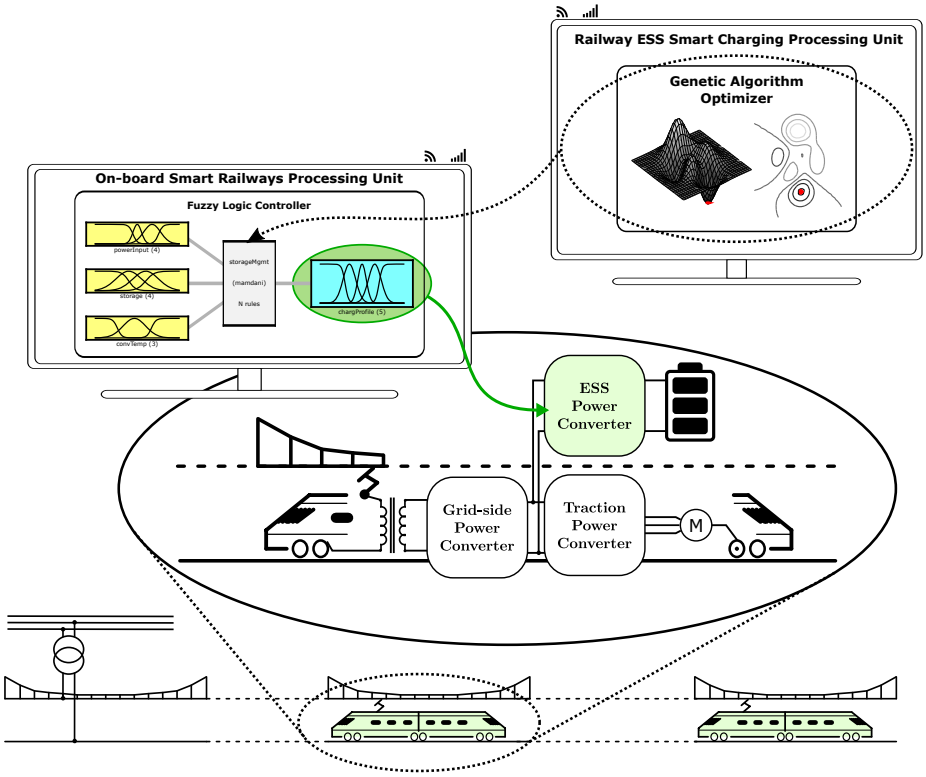

Figure 7.5: Integration of FLC + GA charging strategy with the train onboard ESS hardware.

Specifically, the GA optimizer generates a fuzzy rule-set corresponding to the optimal operation of a specific train consumption profile. Then and in real-time, the FLC adapts the power of the train ESS power converter, resulting in the charging or discharging of onboard batteries.

7.2.1 Proposed Fuzzy-Based ESS Charging

In this subsection, the proposed fuzzy-based charging strategy is detailed. The main core of the energy storage control system is a Mamdani FLC, proposed in [162], having the structure illustrated in the Fig. 7.6a.

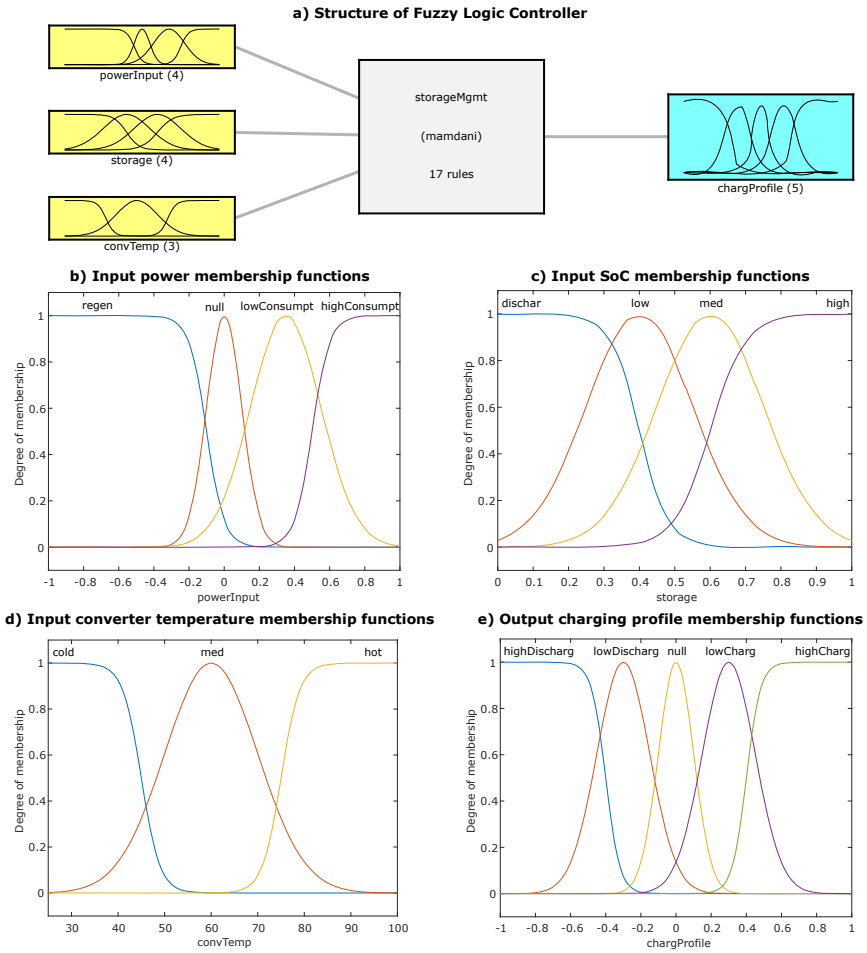

Figure 7.6: Implemented fuzzy logic controller: a) Structure of controller; b) MF of train power consumption input variable; c) MF of ESS state of charge input variable; d) MF of converter temperature input variable; e) MF of charging percentage of the ESS output variable.

The Fuzzy Logic Controller has multiple inputs (the train power flow value, the ESS State of Charge (SoC) and a variable representing the temperature of the ESS) and one output (the set point for the ESS power flow). From Fig. 7.6b to Fig. 7.6e is illustrated the FLC Membership Functions (MF) for the input and output variables.

The first input is the power consumption of the train and it can be categorized as: i) consumption (if the train is in the traction mode and the energy flows from the catenary to the wheels); or ii) regeneration (if the train is in braking mode and the regenerated energy from the motors flows back to the catenary).

The second input is the onboard ESS SoC and corresponds to 100% ($storage = 1$) if the system is fully charged or 0% ($storage = 0$) if the system is fully discharged (considering those values the absolute maximum/minimum voltage values and considering that reaching SoC values above 80% and below 20% should be avoided by the controller).

To promote a reasonable usage of the ESS, a third variable is proposed. This variable mimics the semi-conductors heating and the battery state of health and is a quadratic function of the charging power. As example, the temperature is cold if is below 50° C.

On the FLC output, a variable is proposed to define the ESS charging profile, in an absolute p.u. value. As example, if the output is $chargProfile = 1$, then the power flow in power converter is 350 kW from the DC-bus to the storage system.

In this work, the FLC is tested with a randomly selected train journey power consumption produced by the tool in chapter 4. This testbed corresponds to a near 70-minute train journey. The train power consumption presented in Fig. 7.2 is the independent input of the testbed. The objective of the proposed testbed is better clarified in Fig. 7.7.

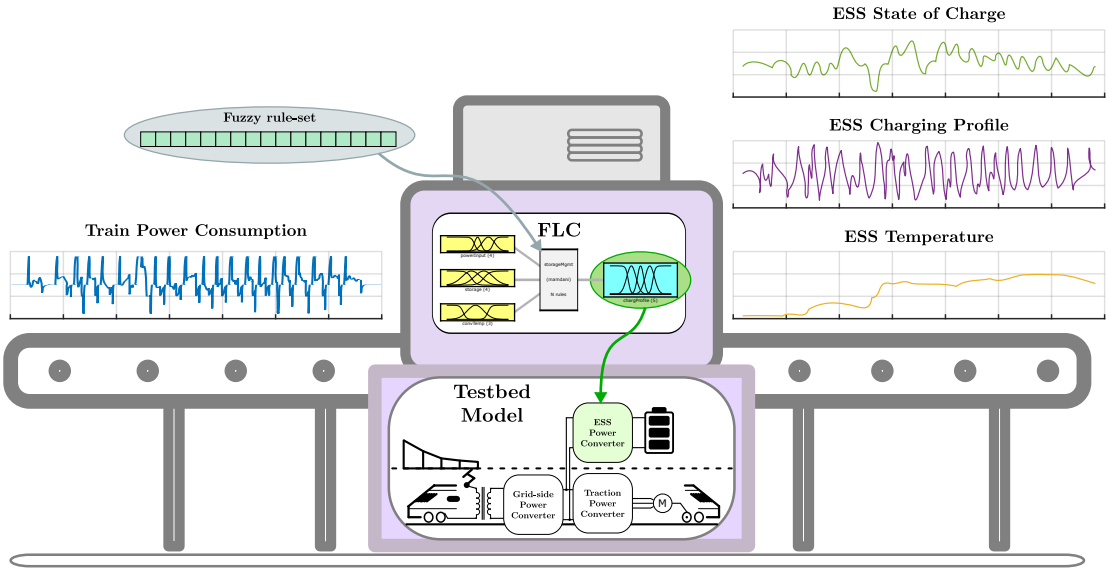

Figure 7.7: Illustration of the testbed: at each time instant, the train power consumption is used together with state of charge and temperature to generate a charging profile; then from the generated charging profile, the SoC and the ESS temperature are updated.

The SoC and the converter temperature depend on the previous result of the FLC output variable. Iteratively for each time instant, the stored energy and the ESS temperature variables are calculated from previous values, following the Fig. 7.8

The K_{ESS} constant defines the storage capacity and the charger design limitations. The K_{temp} and the K_{dissip} represent the temperature increase of the ESS, as a quadratic function of the power, and a dissipation factor to promote the temperature reduction, respectively. In this work, no effort was made to use a specific ESS system and these values were arbitrarily chosen. To ensure the physical limits, the dependent input variables are limited by its admissible maximum and minimum values and, in the case of the occurrence of over-temperature, over-charge or over-discharge events, the charging profile value is changed to avoid those events.

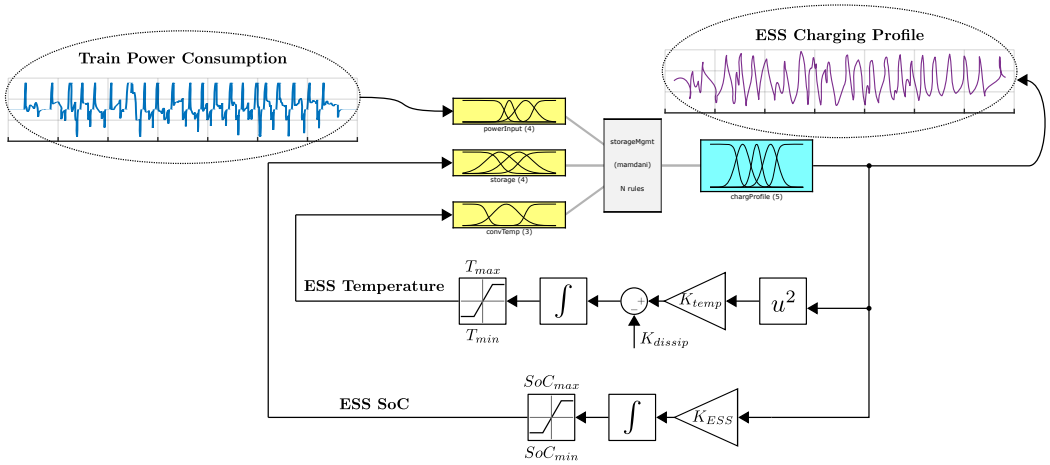

Figure 7.8: Detail on the calculation of the ESS Temperature and ESS SoC.

Regarding the FLC rule-set, in this work, these rules were manually defined from the expected behaviour of the system. Specifically, 17 different rules were defined based on the relevant combinations of input MF and output MF, being presented in Table 7.1 (please refer to MF from Fig. 7.6b to Fig. 7.6e for the physical meaning of each rule-set). The weights of the FLC rule-set used in this work, are an array starting with a value of 0.5 and this array can be adjusted by an optimization algorithm, as explained as follows.

Table 7.1: List of fuzzy rules with the initial weights.

	RULE		Weight
1	**If** ((powerInput is regen))	**then** (chargProfile is highCharg)	0.5
2	**If** ((powerInput is highConsumpt))	**then** (chargProfile is highDischarg)	0.5
3	**If** ((storage is high))	**then** (chargProfile is highDischarg)	0.5
4	**If** ((storage is dischar))	**then** (chargProfile is highCharg)	0.5
5	**If** ((powerInput is null)) **and** (storage is high)	**then** (chargProfile is lowDischarg)	0.5
6	**If** ((powerInput is null) **and** (storage is med))	**then** (chargProfile is null)	0.5
7	**If** ((powerInput is null) **and** (storage is low))	**then** (chargProfile is lowCharg)	0.5
8	**If** ((powerInput is lowConsumpt) **and** (storage is high))	**then** (chargProfile is null)	0.5
9	**If** ((powerInput is lowConsumpt) **and** (storage is med))	**then** (chargProfile is null)	0.5
10	**If** ((powerInput is lowConsumpt) **and** (storage is low))	**then** (chargProfile is lowCharg)	0.5
11	**If** ((convTemp is hot))	**then** (chargProfile is null)	0.5
12	**If** ((powerInput is regen) **and** (convTemp is cold))	**then** (chargProfile is highCharg)	0.5
13	**If** ((powerInput is highConsumpt) **and** (convTemp is cold))	**then** (chargProfile is highDischarg)	0.5
14	**If** ((storage is high) **and** (convTemp is cold))	**then** (chargProfile is highDischarg)	0.5
15	**If** ((storage is dischar) **and** (convTemp is cold))	**then** (chargProfile is lowCharg)	0.5
16	**If** ((convTemp is med))	**then** (chargProfile is lowDischarg)	0.5
17	**If** ((convTemp is med))	**then** (chargProfile is lowCharg)	0.5

7.2.2 Proposed Meta-Heuristic Rule Weight Adjustment

As a way to define the fuzzy rules, human knowledge is a good starting point to obtain a charging strategy for the FLC. In this section is proposed a GA as a meta-heuristic to define the weights of the fuzzy rules, having an objective function as the optimization criteria.

An ordinary GA algorithm is presented in Algorithm 4. For the implemented GA each individual of the GA population will have an array of 17 weights (genes) and a value for its objective function that will be obtained in the FLC for a given testbed.

Algorithm 4: Fundamentals on GA meta-heuristics.

```
1 Generate the initial population
2 Compute fitness
3 while creiteria not satisfied OR max generations do
4 |   Selection
5 |   Crossover
6 |   Mutation
7 |   Compute fitness
8 end
```

Therefore, each individual of the GA population will have an array of 17 weights (genes) and a value for its objective function that will be obtained in the FLC for a given testbed.

The crossover process considers the best individuals and a new individual is generated having part of the genetic material from the parent individuals. The mutation considers the random increase/decrease of certain genes. Besides, if the genetic material form previous generation has changed, within a mutation process, and if the new individual is within the top individuals, then changing again this portion of genetic material will have a higher probability to increase the value of the objective function for a future generation.

The initial population is generated from five individuals having the weights defined from human knowledge in the previous section (0.5). Furthermore, 35 new individuals were generated as mutations from those individuals to complete the initial population. The integration of this GA in the FLC rule-set weight adjustment can be better explained in the Fig. 7.9.

After each FLC rule-set weight is tested, for a time-series array of train power consumption, this results in three time-series arrays of ESS: SoC, Temperature and the Charging Profile. Also, the energy at pantograph (consumed and regenerated) is calculated using the train power consumption and ESS charging profile time-series arrays. From these arrays, four partial metrics are extracted:

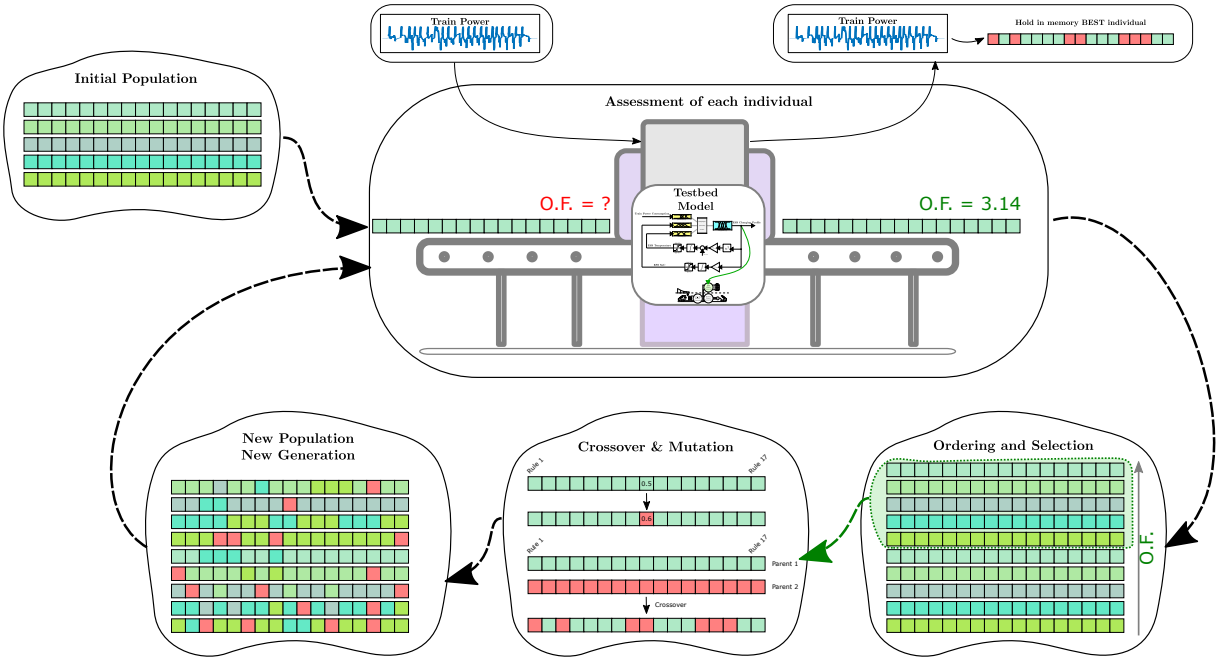

Figure 7.9: Illustration of the integration of GA in this work.

- The rms value of the graph of converter temperature;
- The rms value of the resultant charging profile;
- The difference between the initial and the final value of the ESS SoC;
- The final value of the regenerated energy.

As optimization criteria, it is considered the objective to avoid peak values in the first two metrics (avoiding high stress on the ESS, by having a high square value of the charging profile). In the remaining metrics, the optimization objective is to minimize the difference between the final and initial values of SoC and to minimize the difference between the regenerated energy without and with the ESS.

In the design of the global objective function metric, all four metrics are considered, having arbitrarily defined weights to better fulfil the expected behaviour of the system (in terms of convergence speed, the stability of the GA, intuition, etc.). Therefore, to obtain the results presented in section 7.3, the converter temperature and charging profile metrics, have received small weights, and the SoC variation and global energy reduction have received a higher weight (with the global energy reduction tuned to rapidly reduce this metric).

7.3 Results and Preliminary Discussion

In this section are presented the results of the proposed methodology. In particular, the section is illustrated with the results from the application of the GA on the proposed evaluation testbed. This testbed corresponds to the power of a train journey through 22 passenger stations, as illustrated in Fig. 7.10. Later, this methodology is evaluated and discussed.

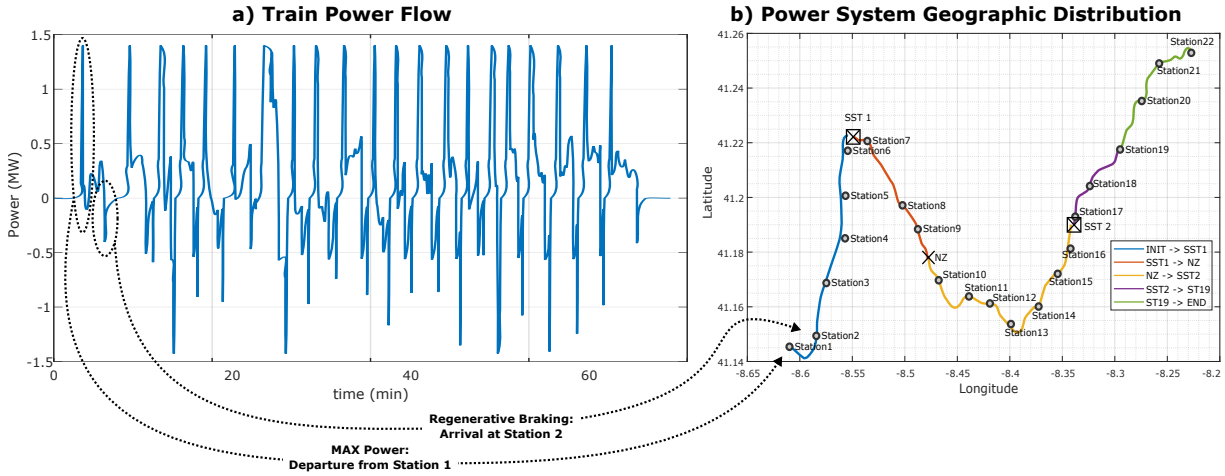

Figure 7.10: Geographic detail on the train power consumption profile: a) Power consumption for one journey; b) Geographic distribution of all 22 passenger stations. Note: the 21 peaks in the train power flow correspond to each departure from stations 1 to 21, as illustrated.

7.3.1 Preliminary Knowledge of System Behavior

The following results present the testbed evaluated with the 17 known rules. For different generations (throughout the evolution of the GA), and the same independent power consumption input (Fig. 7.11a), in Fig. 7.11b is illustrated the evolution of the stored energy; in Fig. 7.11c is presented the evolution of the charging profile, and in Fig. 7.11d is visible the evolution of the converter temperature. (Note: these illustrations are visible with different coloured plots).

At each generation, 40 new individuals are generated from the previous population, where 25 of the individuals result from crossing the genetic material (the weight of FLC rules) from the previous generation and the other 15 as result from mutations on the population. Between generations, only the five best individuals are eligible to pass to the next generation. The evolution of the objective function is presented in Fig. 7.12.

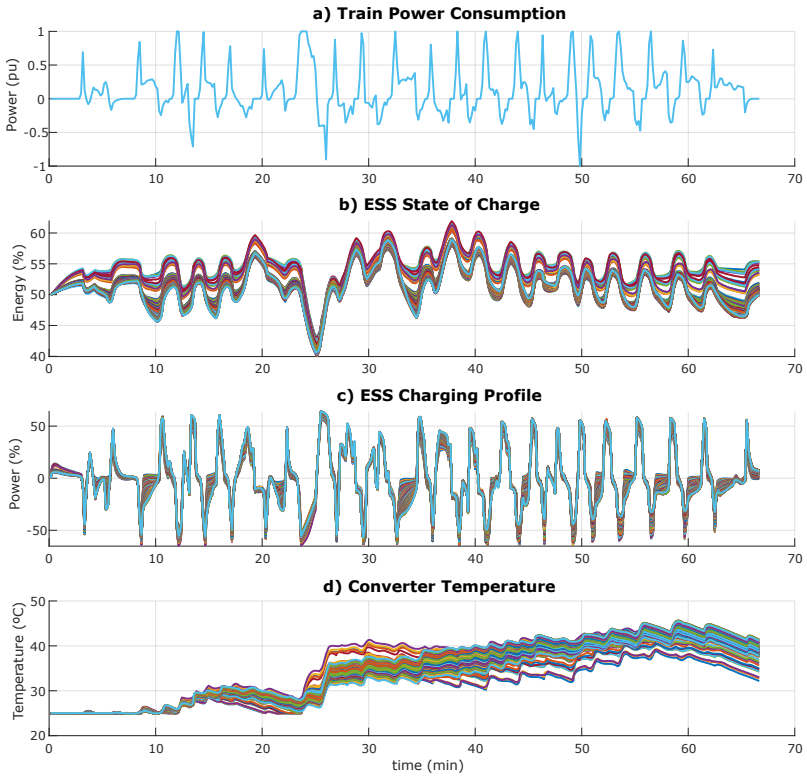

Figure 7.11: Evolution of testbed variables, in order of time, for different meta-heuristic generations of fuzzy rule weights: a) Power consumption for one journey; b) Stored energy; c) Charging profile; and d) Converter temperature.

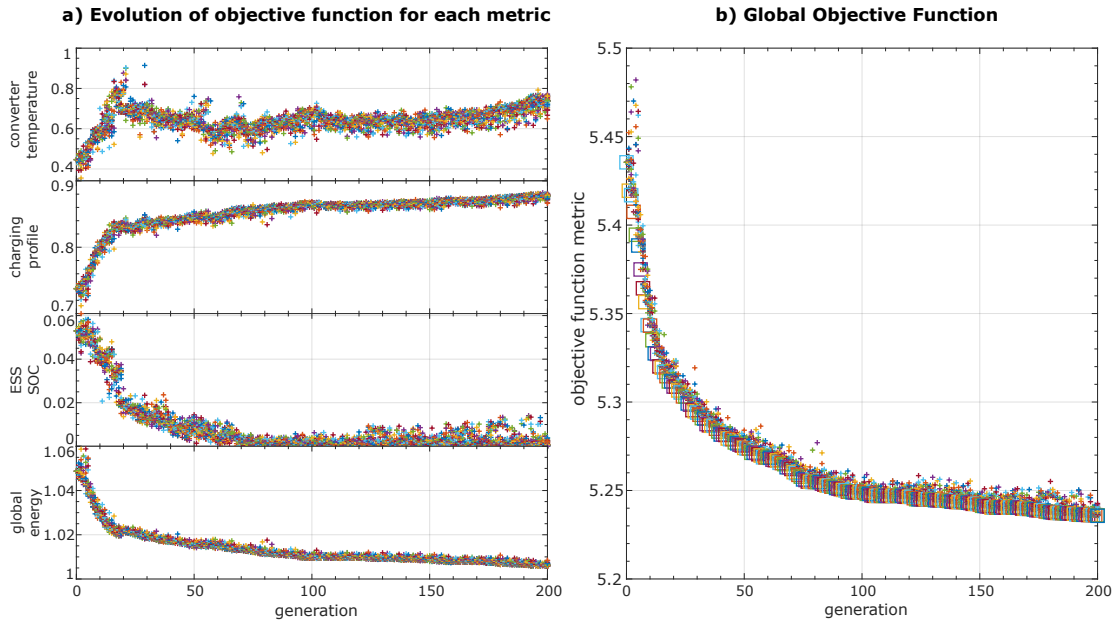

Figure 7.12: Evaluation of objective function: (a) Individual evaluation of each metric for all generations; (b) Global objective function as dependent of the generation.

Figure 7.12a shows the evolution of individual objective functions. By providing different weights for each of the metrics, following the expression in (7.1), a global objective function is presented in Fig. 7.12b.

$$\begin{aligned} globalOF = \; & \lambda_1 \, \mathbf{n_1} \, \sqrt{mean(T_{ESS} - T_{ambient})^2} \\ & + \lambda_2 \, \mathbf{n_2} \, \sqrt{mean(ChargProfile)^2} \\ & + \lambda_3 \, \mathbf{n_3} \, |SoC[end] - SoC[init]| \\ & + \lambda_4 \, \mathbf{n_4} \, (ratio \; with/without \; ESS) \end{aligned} \tag{7.1}$$

Each of the individual objective functions was normalized to result in a near-unitary value, with the gains, $n_1 \cdots n_4$, in expression (7.1). The weighting factors $\lambda_1 \cdots \lambda_4$ were defined taking into consideration the relative importance of each one in the optimization procedure.

Figure 7.12 illustrates the weights of all individuals of the same generation, plotted with "+" in the graphs, having the best individual of a generation highlighted with a square (in Fig. 7.12b). For each rule, the FLC rule weights evolution for 200 generations are presented in the heat map graph of Fig. 7.13.

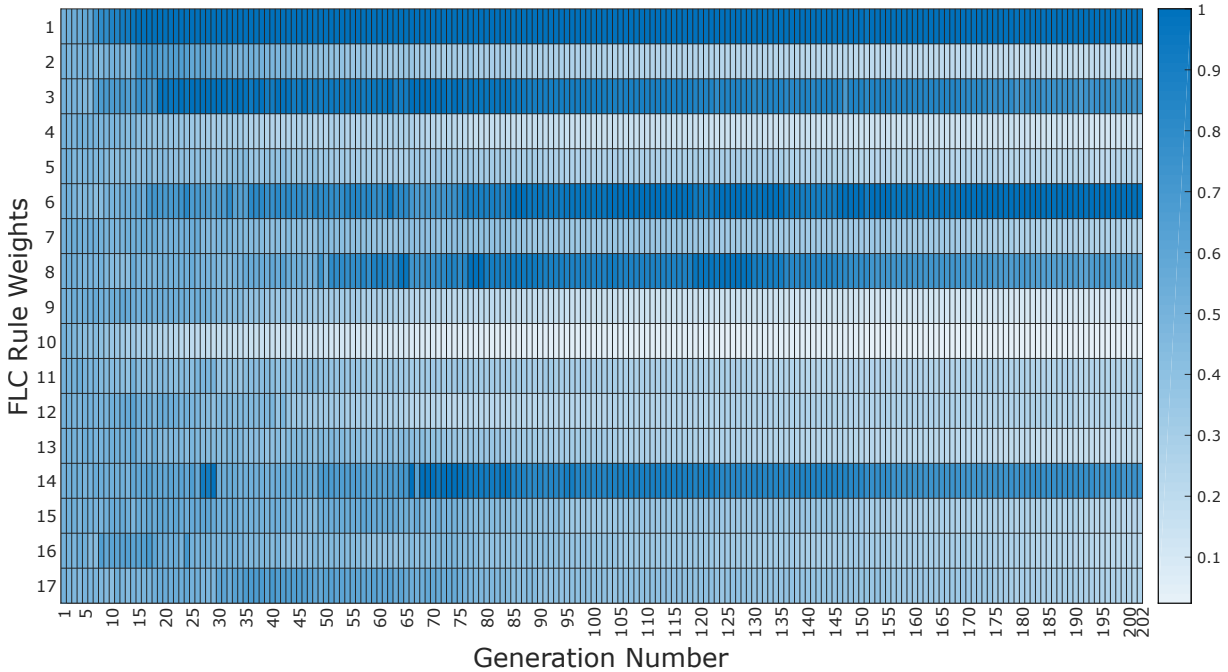

Figure 7.13: Heat map of the best individual for all FLC rule weights for each generation.

From the previous heat map result, certain rules will contribute more to the expected optimality. As an example, the heuristic algorithm will increase the weight of rules 1, 3, 6,

8 and 14, and reduce the weight of remaining rules, to achieve the desired lower value of the objective function.

In Fig. 7.14 are presented the output FLC surface as function of the ESS SoC and the input power, having the third input fixed (ESS Temperature), before and after the optimization. It is visible the modification of the FLC rule surface, where for example, higher values for charging profile are achieved for higher values of regenerative power and for a more discharged battery.

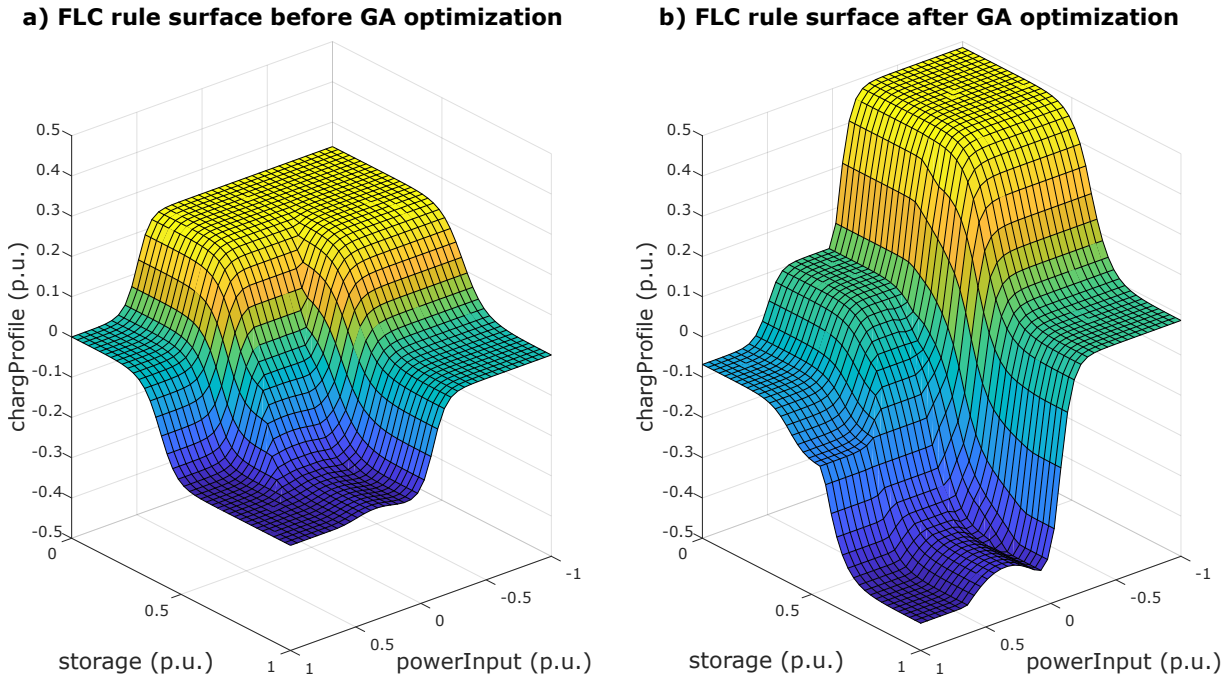

Figure 7.14: Evolution of FLC rule surface: a) Before optimization; b) After optimization

7.3.2 Evaluation of Energy Optimization

In Fig. 7.15 is presented the comparison of the train journey energy consumption/regeneration for the three possible cases in the study:

- A train without onboard ESS, in Fig. 7.15a;
- A train with ESS, with a FLC charging controller but without fuzzy weights optimization (only with the 17 known rules having the same weights), in Fig. 7.15b;
- A train with onboard ESS, with the charging controller based on FLC, using the GA optimization criteria over the 17 known rules, in Fig. 7.15c;

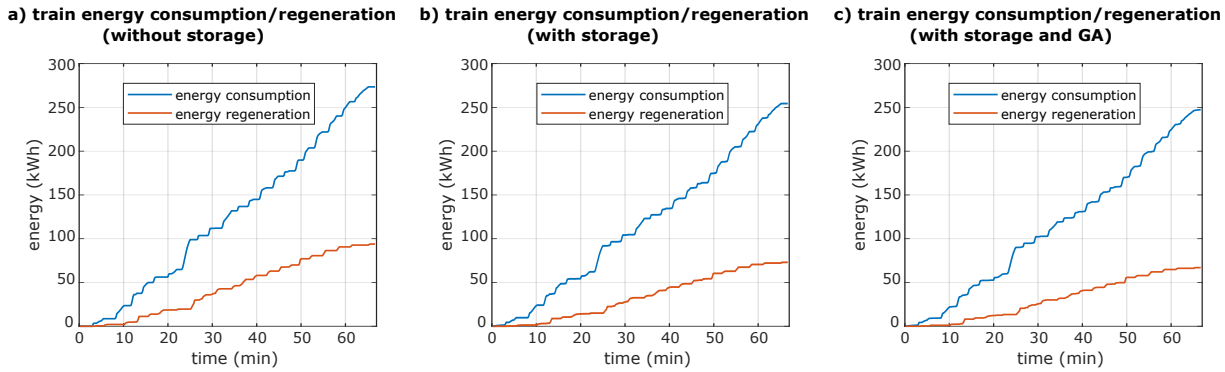

Figure 7.15: Comparison of train energy consumption/regeneration graphs: a) without onboard ESS; b) with onboard ESS; c) with onboard ESS and GA optimization.

In Table 7.2 is summarized the comparison of the train energy for the three cases in the study: the inclusion or not of the onboard ESS and the inclusion or not of the optimization procedure.

Table 7.2: Energy optimization results.

	Train energy			
	Consumption		Regeneration	
	kWh	%	kWh	%
Without onboard ESS	273.5	100	93.9	100
With ESS, with known rules, without GA optimization	254.4	93.0	73.0	77.7
With ESS, with known rules, with GA optimization	247.4	90.5	67.0	71.3

The train energy consumption value is calculated from the energy flowing from the catenary to the train; the value for regenerative energy corresponds to the energy flowing from train to the catenary. From the results in Table 7.2, globally, a maximum near 28.7% of reduction on the regenerated energy is achieved, as well as a reduction of 9.5% of energy consumption.

As a baseline, the simple usage of FLC without any optimization results in 22.3% in the reduction of regenerated energy. The utilization of GA requires only computational processing and it ultimately can achieve 6.4% in the reduction of regenerated energy. This is of advanced interest since without adding more ESS elements or increasing the power capabilities of the converter, it is possible to achieve a more optimal operation.

7.3.3 Discussion on Presented Results

The proposal in this chapter is very flexible, either in considering more input variables for the FLC and in considering other optimization strategies (e.g. other meta-heuristics, neural networks based, etc).

As an example, the catenary voltage level, measured in train pantograph, could be an important input variable for the FLC. The catenary voltage provides a good image of the state of the system. Clearly, the rules should be easy to be defined: "if the catenary voltage is low, then the ESS should discharge; otherwise, it should charge". Another variable can be the train speed. This variable provides information for near-future energy needs: "if the train is stopped, then it most likely requires high demand for power in near future, for the departure; if the speed is high, then it might be needed to store a high amount of energy in the ESS".

However, this is strongly dependent on the train position and on the operation conditions of other trains. Such analysis will need the adaptation of a tool like the one presented in chapter 5, as will be discussed later.

The obtained results also depend on the ESS technology. The chosen unitary efficiency has led to the presented results and it should be considered different and smaller improvements in energy efficiency depending on the ESS technology. However, with the consideration of super-capacitors and SiC transistors that can lead to an efficiency of 98% [50, 161], the expected results must be closer to the obtained ones. Future research directions are possible with the study of the case study for different parameters (different capacities for ESS, different ratings, different efficiency values, etc.).

In the following section is discussed a practical implementation of the proposed methodology framed in a smart railway framework.

7.4 Smart Railway Framework

As previously discussed, the presented charging strategy considers a specific train journey. However, for a practical implementation, a smart railway framework must be considered, as illustrated in Fig. 7.16.

The hardware for onboard ESS is connected to each train DC bus. The references for the charging profile come from the "Onboard Smart Railways Processing Unit", which is a computational platform that reports data from each train to a remote processing unit (represented in Fig. 7.16 by the cloud) and receives setpoints to improve the energy efficiency.

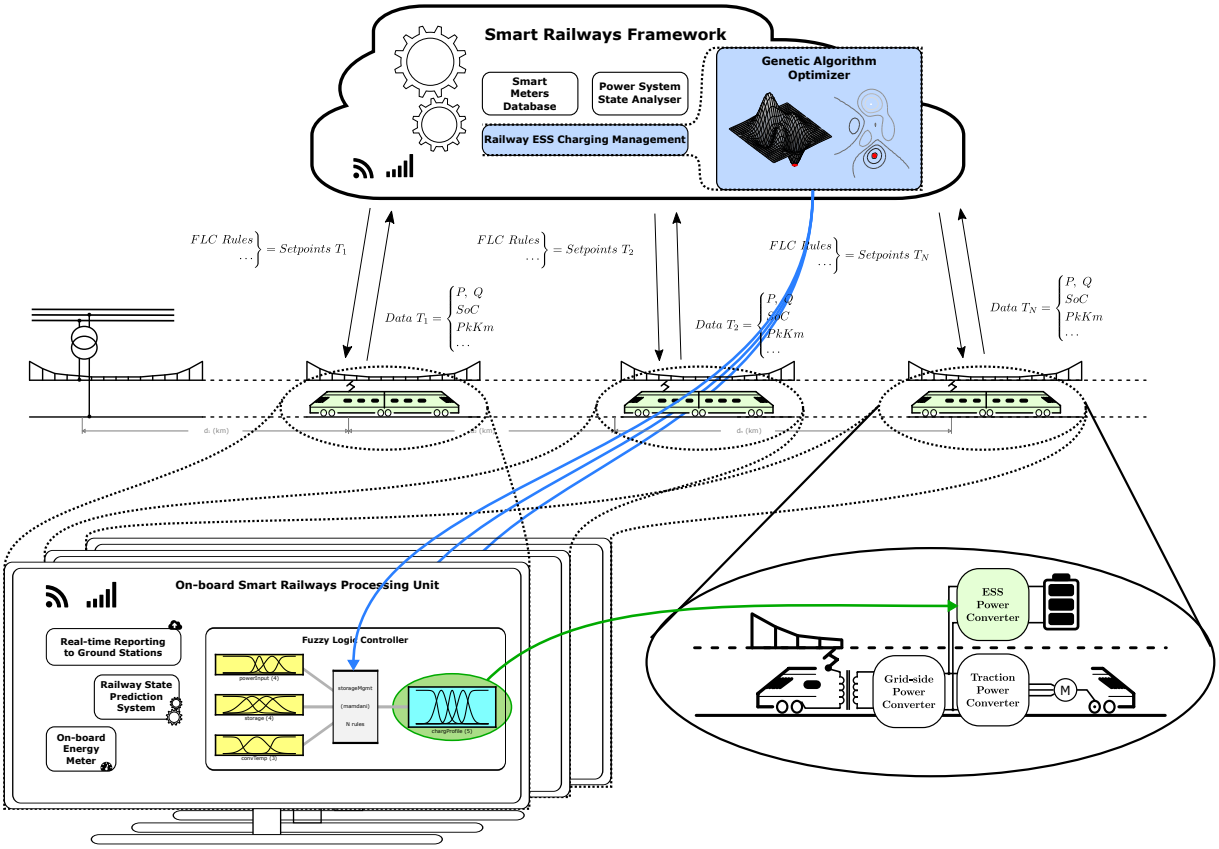

Figure 7.16: Smart railways framework to support the railway onboard charging strategy for multiple trains.

This generation of FLC rules is performed remotely by the GA, and it must be based on the result of onboard train prediction algorithm: each train generates a prediction, then it compares this prediction with a database of predictions and finally, it updates the FLC rule-set. This strategy is better explained in Fig. 7.17.

As an example, if the prediction algorithm is capable of generating a one-minute prediction of the train power consumption, then this array of predictions is compared to a database of previously generated FLC rule-sets. The comparison is performed through the Root Mean Square Error (RMSE): the prediction is compared with all arrays in the database, in a 1×N approach (where N is the size of the database); then the arrays are ordered and the one having the lower RMSE is selected (specifically, the previously processed FLC rule-set is selected, correspondent to the lower RMSE). It should be noted that this comparison procedure can be fast (as an example, the RMSE comparison of a 1000 points prediction array with a database of 10 000 elements takes around 0.2 s in a modern computer).

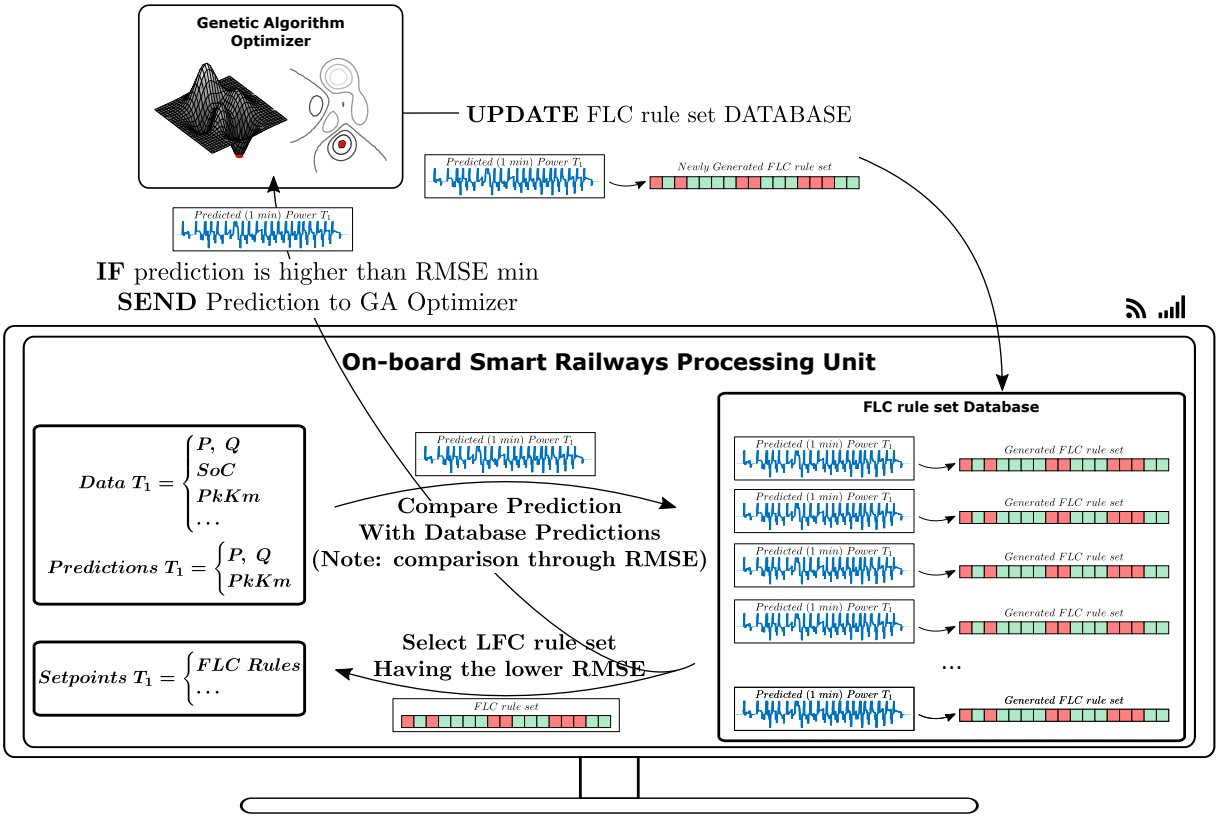

Figure 7.17: Strategy for real-time operation of onboard smart railways processing unit.

Besides, if the predicted power consumption is quite different from any of the elements in the database — the lower value of the comparison RMSE is higher than a minimum RMSE — then the train sends the predicted value to the cloud, and the GA will generate a new fuzzy rule-set for the corresponding array. Finally, this is sent back to all trains (considering that all trains have similar ESS device).

In Fig. 7.18 is illustrated exactly how the information should flow between the two sides.

7.5 Discussion and Conclusions

The initial approach of a storage charging controller, focused on multiple optimization criteria, and applied to railway transportation systems, is presented here. The proposed strategy is a two-level hierarchical EMS, where the real-time processing level is ensured by a fuzzy logic controller and the higher level is responsible for the optimization through a genetic algorithm. This optimization strategy combines the knowledge of the expected behaviour of the system, by manually defining the rules of a fuzzy logic controller and,

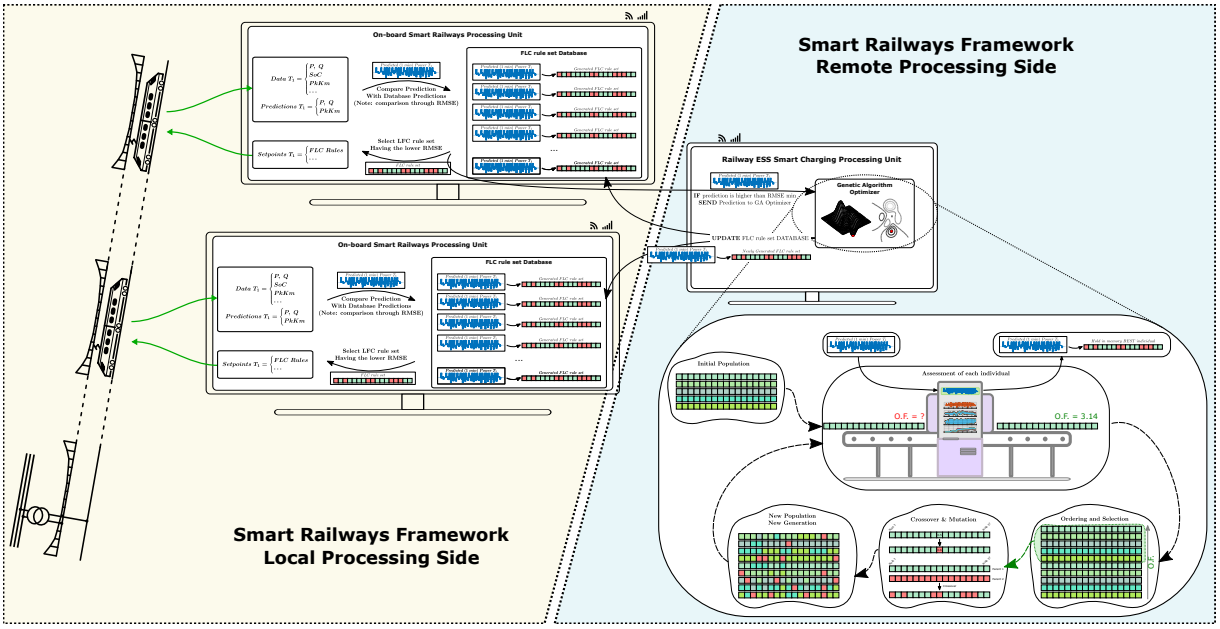

Figure 7.18: Illustration on the information flow between local and remote processing units.

later, a meta-heuristic is used to adjust the weight of the fuzzy rules.

In previous section was presented a discussion on the need for the integration of the proposed strategy within a smart railway framework, similarly to the strategy proposed in chapter 6. This section targets a general discussion.

7.5.1 Flexibility of the Strategy for Wayside

This proposed charging strategy can also be included in wayside ESS. In this, it is needed a real-time evaluation of the system state. Therefore, it is required that every train has onboard energy meters and these measurements must be transmitted in real-time to a remote database where with such information, is possible to calculate the power flow in the railway electrification.

With this remote power flow analysis and measurements, the wayside can take advantage of the excess of energy injected by each train when they are operating in regenerative braking. Also, the opposite is viable, where the wayside railway ESS can support the departure of trains when their demand is nearly the maximum available torque and power.

In Fig. 7.19 is illustrated a particular case of wayside ESS, specifically the electric vehicles parked in passengers station parking lot.

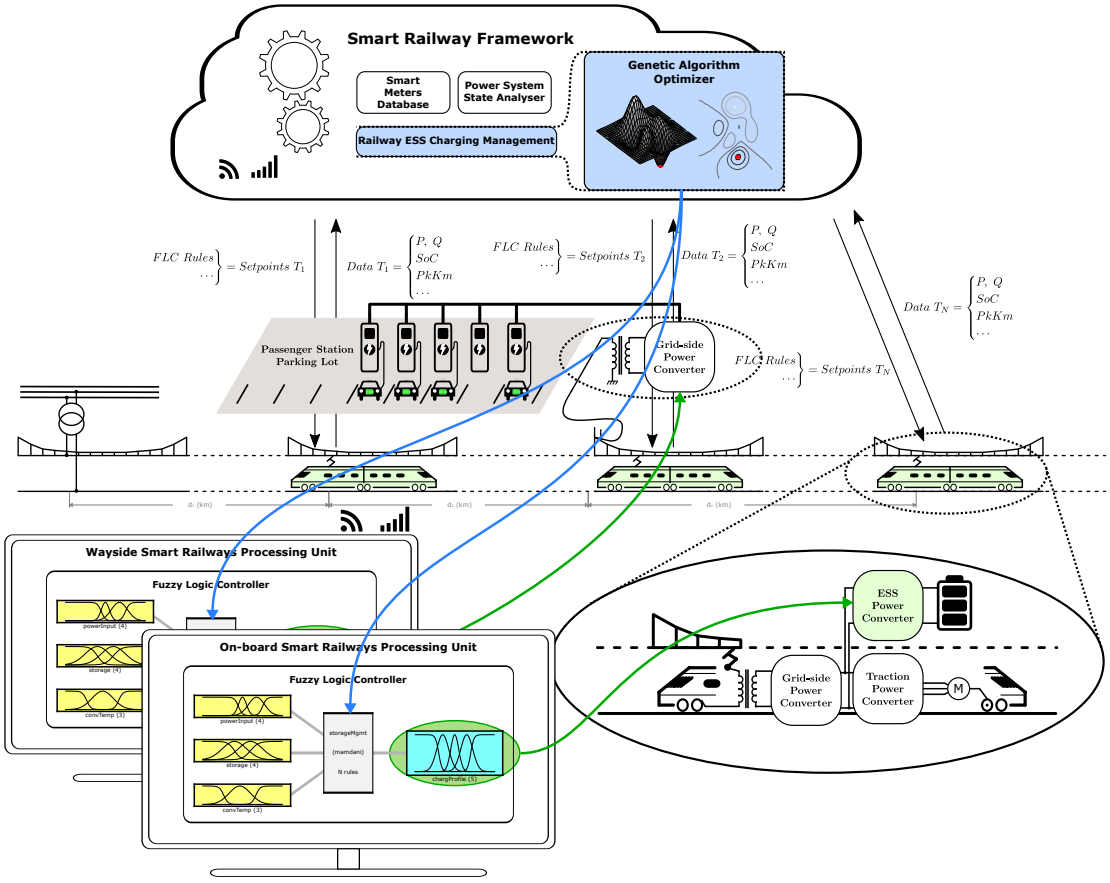

Figure 7.19: Smart railways framework to support the wayside and onboard railway charging strategy.

In the example of the Fig. 7.19, the wayside ESS comprises a passenger parking lot, having electric vehicle chargers where the energy for this chargers comes from the catenary. The passenger stations are the points on the line where, naturally, the train mostly needs to brake and accelerate. Therefore, this place is a point of interest to have the power injection. The flexibility of the proposed two-level hierarchical energy management strategy is now demonstrated.

7.5.2 Integration of the Strategy into PSSA-rail

In this chapter was addressed a deterministic analysis of power flow management of railway ESS. Similarly to the adaptation proposal of PSSA-rail in chapter 6, the strategy presented in this chapter can be adapted for a stochastic scenario, with a preliminary proposal illustrated in Fig. 7.20.

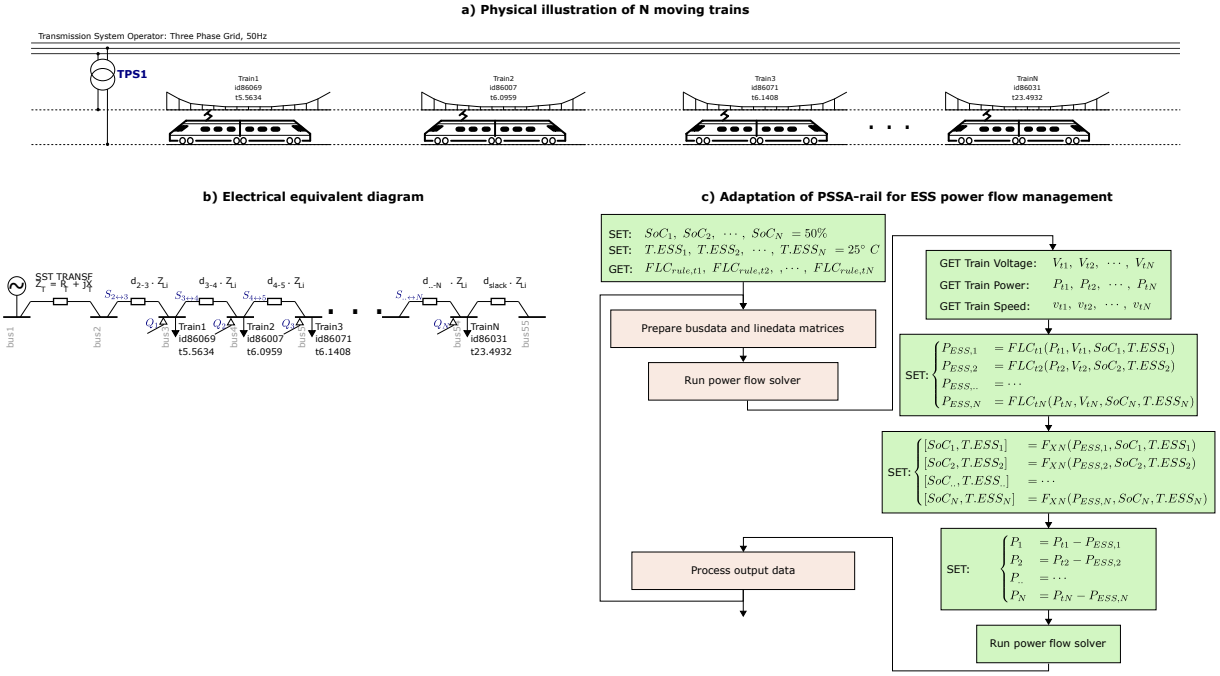

Figure 7.20: Adaptation of the PSSA-rail to contemplate the active power compensation strategy.

It should be carefully considered the effect of multiple nodes for the same train in the implementation steps: the train power consumption P_{tN} must be associated to the correct bus P_N. Also, as an initial step, all the FLC rules for every journey, $FLC_{rule,tN}$, must be generated with a new testbed and genetic algorithm (this new testbed is only to consider the new variables: train voltage and speed). Finally, it should be highlighted that this analysis can not be performed in parallel processing: each simulation time is dependent on previous state (specifically in the SoC and ESS temperature variables).

7.5.3 Final Remarks

The contribution of this chapter was partially demonstrated in the first part of this chapter, with a case study of a single train journey. The focus of this work was to validate that a feasible charging solution having multiple input variables can be easily implemented with an FLC. This charging solution can result in the high reduction of the regenerated energy (near 22.3% in the presented case study). Later, as an optimization strategy, a meta-heuristic can achieve an additional 6.4% of regenerated energy reduction, on top of baseline.

With the demonstration of the feasibility of the solution for a single train journey case study, the second part of this chapter tries to clarify, with a conceptual discussion, the integration of the proposed algorithms into a smart railway framework for energy

management. In here are addressed questions regarding the need to have prediction models in train onboard processing units, and the need to hold a database with the results of the GA outcomes. The big advantage of the proposed algorithm is the ability for automatic learning.

With the discussion on the solution, further research directions have emerged. First, the prediction of the train state is needed to better adapt the real-time operation of the FLC. Then is required a power system state analyser, like PSSA-rail, that is capable to generate the knowledge on the global railway electrification state. This task is computationally demanding since not only it requires the collection of all power consumptions of all trains, as well as their geographical positions, but also, it needs to automatically calculate the power flow in the catenary. Not only this task performs the calculation for the instantaneous time-stamp, but also for the prediction time window, similarly to the strategy in chapter 6.

A reliable communication link is also required for the operation of the proposed strategy. With a well-designed software solution combined with faster computational resources and with a faster communication link, it is enabled the operation of this energy management system with good performance. The lower the latency between the data acquisition and the decision, the better the operation of this strategy.

The valid demonstration of the proposal together with the relevant scientific contributions leads to the conclusion that with a smart railway framework it is possible to increase the railway energy efficiency, with a high degree of flexibility.

7.6 Summary

This chapter targets a power flow management strategy to increase the energy efficiency of a railway line with trains using onboard ESS. It was presented a charging strategy with a two-level hierarchical EMS, using a fuzzy logic controller for the real-time ESS management and a genetic algorithm for the optimization with an automatic searching procedure. The results show a reduction of 22.3 % in the regenerated energy and an additional 6.4 % reduction after the optimization. The proposed strategy was then framed with the smart railway framework, towards an extended discussion of the practical implementation steps of the strategy.

This chapter ends the presentation and discussion of strategies for power flow management in smart railways.

CHAPTER 8

Conclusions

In this chapter, a compilation of the main achievements and conclusions is presented. Some guidelines for future work starting on the established and assumed limits are also described which hopefully will enrich the work developed so far.

8.1 Research Findings

In this thesis, it was made a study on tools and strategies to support the power flow management in smart railways. In its essence, the demonstration for improvements either in the infrastructure capacity and on energy efficiency are the clear advantages that were answered in this interesting topic of smart railways. By taking advantage on the lack of clear frameworks for railway smart grid, that can support the challenging universe of railway power systems, this led to the proposal of the tools and the strategies. During the course of this thesis, several issues were identified, treated and accomplished.

As described in section 1.1, the main challenges are the proposal of an interconnected and generalized framework for power flow management in smart railways. This framework require: i) the measurement and data acquisition; ii) the processing of the data transforming it into information; iii) the extraction of knowledge using specific algorithms; and iv) the decision and actuation upon the generated knowledge.

The findings of this thesis are focused in the five main fields of study:

Railway line simplification methodology, that proposed a comparison methodology and an enhancement of a line model, being presented in chapter 3.
The findings on topic **T1** (Railway electrification line model analysis) can be listed as following:

- The comparison of a 6×6 multi-conductor transmission line model and a lumped-parameter π-type line model shows relative percentage errors below 0.5 %, supporting the conclusion of the similarity of the models for power flow analysis.

- The inclusion of parameters like rail-earth and earth conductances and line capacitance will contribute to a considerable increase in the errors (4.5 % for the reactive power, for typical parameter values).
- With the offline calculation of the errors, the lumped-parameter π-type line model can be enhanced resulting in a drastic reduction of the errors.

Multi-vehicle railway simulation tool, where the information of the dynamics and energy consumption of any train journey is generated, with the demonstration and validation in chapter 4, leading to publications [12] and [13].
The findings on topic **T2** (Multi-train tool) can be listed as following:

- The inclusion of gravity and resistive curvature forces in the train dynamic movement model led to the reduction of the RMSE errors of the train speed and position. Specifically, the train speed RMSE has reduced from 5.3 km/h to 3.0 km/h; the train position relative RMSE reduced from 3.5 % to 1.0 %.
- Furthermore, the inclusion of auxiliary power and non-unitary efficiency in the train energy model drastically reduces the train energy consumption RMSE from 23.5 % to 4.3 %.
- The proposed heuristic algorithm can estimate the dynamic movement and energy consumption of any train journey, with an average train speed RMSE of 17.6 km/h, a relative position RMSE of 1.52 %, and an energy consumption RMSE of 13.5 %, when compared with real measurements.

Railway power system state analyser – PSSA-rail tool, where this proposed tool is able to generate the knowledge of the railway power flow state. In chapter 5 (and appendix E) was demonstrated this tool for two case studies.
The findings on topic **T3** (PSSA-rail tool) can be listed as following:

- The four raised requirements for the PSSA-rail tool allow the development of a highly versatile and flexible tool for the simulation of the majority of railway scenarios.
- The developed tool allows the analysis of the power flow of, at least, two different railway lines, in which the output results of PSSA-rail are very similar to the results produced by a proprietary tool, as shown in appendix E.
- The PSSA-rail tool allows the adaptation to include optimization scenarios. It was demonstrated the operation of the tool in the analysis of two optimization scenarios — different train PF and inclusion of power injection devices — which shows the modularity of the tool.

- The analysis of different train power factor values shows the expected improvements in the catenary voltage stabilization with the management of the train reactive power flow; furthermore, the inclusion of power injection devices shows improvements in the reduction of the TPS energy consumption (8.5 % reduction per 2×100 kW of installed PID photovoltaic power, for the TPS#1) and the catenary losses (up to 3% reduction).

Infrastructure Capacity Increase, where the adaptation of the train power factor leads to a potential increase of the number of trains supplied by the same TPS. This reactive power compensation was proposed and demonstrated in chapter 6, which has led to the publication in [14].
The findings on topic **T4** (Strategy to increase infrastructure capacity), when using the adopted use case, can be listed as following:

- A train located 30 km away from the TPS, with $PF = 0.9$ ind. and $P_t = 10$ MW, in a line with $^{X}/_{R_L} = 3$, if the train adapts the power factor to remotely reduce the TPS reactive power to zero, then the voltage improvement is 25.8 %, the reduction of train apparent power is 6.9 % and the losses in the catenary are reduced by 52.3 %.
- Considering the infrastructure capacity as the maximum number of trains that can run in a railway line without achieving the minimum standardized voltage levels, the railway infrastructure capacity can be increased by 50 % with a wayside compensator placed in the NZ, or can be increased with the same value of 50 % if each train actively manages the reactive power flow with the injection of reactive power.
- If a train (with $PF = 0.98$ ind.) starts to inject reactive power and if the value of the train apparent power increases by 8.7 %, then the railway infrastructure capacity increases by 51.2 %.
- It is essential to adopt a two-level power flow management strategy, with a smart railway framework, for this strategy to operate properly within the raised constraints.

Charging strategy for railway energy storage systems, where the generated knowledge on the power system electrification state is used to increase the energy efficiency. In chapter 7 was presented the strategy, in which the onboard processing unit uses the real-time knowledge of several input variables, and feeds a FLC to generate the charging reference for the ESS. Furthermore, a learning algorithm based on GA meta-heuristics automatically tunes the FLC rules to enhance the system

global operation. This topic led to the publications [15] and [16].
The findings on topic **T5** (Strategy to increase energy efficiency) can be listed as following:

- The combination of the expertise of a railway engineer and an automatic machine learning algorithm can be achieved with a two-level management strategy, where the real-time is supported by a fuzzy logic controller and the automatic artificial learning is supported by the genetic algorithm meta-heuristic;
- For the case study considered in chapter 7, it was demonstrated a maximum reduction of regenerated energy of 28.7 %, where 6.4% of this reduction is promoted by the genetic algorithm. Furthermore, is also achieved a reduction of 9.7 % in energy consumption.
- The implementation steps of this strategy require a two-level power flow management architecture, as in topic **T4**, with a smart railway framework, for this strategy to operate correctly within the raised constraints.

With the proposed methodologies and research findings it was possible to answer the questions raised in section 1.2 and confirm the initial statement.

RQ1: How to reliably estimate the train information regarding dynamic movement and energy consumption for any journey?

The railway system is very complex and the simulation of the railway system depends on several software blocks and algorithms. By analysing the works in the literature, it is clear that several of the tools are proprietary and of limited access by the scientific community. The multi-train simulation tool proposed in chapter 4 can estimate the information of any train journey of a railway line, with high degree of similarity when compared with real train data. This tool uses a train model where variable gravity and resistive curvature forces were considered, as well as the auxiliary power consumption and non-unitary efficiency, thus contributing to the reduction of RMSE errors when compared with a basic train model.

RQ2: How to extract the relevant knowledge from train energy information with high level of flexibility, targeting successfulness evaluation of optimization strategies?

The scientific community shows that the majority of railway tools to evaluate the power flow are proprietary or of difficult implementation. Then, the proposal of a tool to extract the knowledge from the energy information is of advanced interest to evaluate the success of new strategies for the railway transportation systems. In chapter 5 is presented the designed and implemented PSSA-rail tool. The developed tool allows the simulation

of any railway line, considering all trains moving in both directions, with the simulation valid for a broad time-window, where the electrical equivalent of the line is valid for the considered time-window, and is capable of simulating specific points of interest. It was demonstrated that the PSSA-rail can extract the knowledge of any railway line (as demonstrated in chapter 5 and in the appendix E). The comparison of the results produced by the PSSA-rail tool and by a proprietary tool shows, in appendix E, very similar results. Then, the tool allows the evaluation of optimization scenarios, as demonstrated for the different train power factor values and for the inclusion of power injection devices connected to the catenary, where the results show improvements respectively, in the increase of the catenary voltage level and the reduction of TPS energy consumption and catenary power losses.

RQ3: What are the gains in infrastructure capacity and energy efficiency with the adoption of a two-level railway power flow management strategy?

The success of the framework for smart railways depends on the ability to use the knowledge generated to act in the railway power system. In the topic **T4** was proposed a two-level reactive power management strategy designed to contribute to increase the railway infrastructure capacity. The results reveal increased values up to 50 % with management of reactive power of each train, only with an increase of train power value of 8.7 %. Moreover, the topic **T5** has demonstrated that for a specific case study, the adoption of a two-level Railway Energy Storage Systems management strategy can achieve a reduction of 28.7 % in energy regeneration and 9.7 % in energy consumption, with a multi-variable and highly-flexible fuzzy logic controller. More importantly, 6.4 % of the reduction is due to the genetic algorithm optimization strategy, so this reduction is only achieved with additional computing. A proper operation within the raised constraints in chapter 6 and chapter 7 drives this two-level management strategy to be in line with the Smart Railway Framework.

As stated in section 1.2, *the extracted knowledge can be used to enhance the railway operation*. This enhancement targets an increase of people and goods mobility, with costs reduction, bringing environmental gains to the society and opens the way to potential economic benefits with increased competitiveness. Additionally, and as also stated in section 1.2, the knowledge extraction requires the availability of *energy information with enough quality and quantity*. The information quality can be assumed as a reality nowadays with the availability of data collection systems like onboard energy meters. The technological advancements in communication systems and in the railway digitalization brings this energy information to a higher-level in terms of quality and quantity.

8.2 Framework for Smart Railways

This thesis is conceived based on the nuclear concept of the Smart Railway Framework for power flow management. This concept has the ultimate goal of achieving improvements in the railway operation, where the the objectives of Shift2Rail are the finest example of this goal.

Several works have been proposed, from power flow management hierarchical architectures, like REM-S [31], to complete systems with digital/virtual twin of an entire railway [100].

The tools and strategies proposed in this thesis have this ultimate goal to contribute to improve the railway system. Fig. 8.1 synthesises the integration of the proposed tools and strategies of this thesis on the Smart Railway Framework.

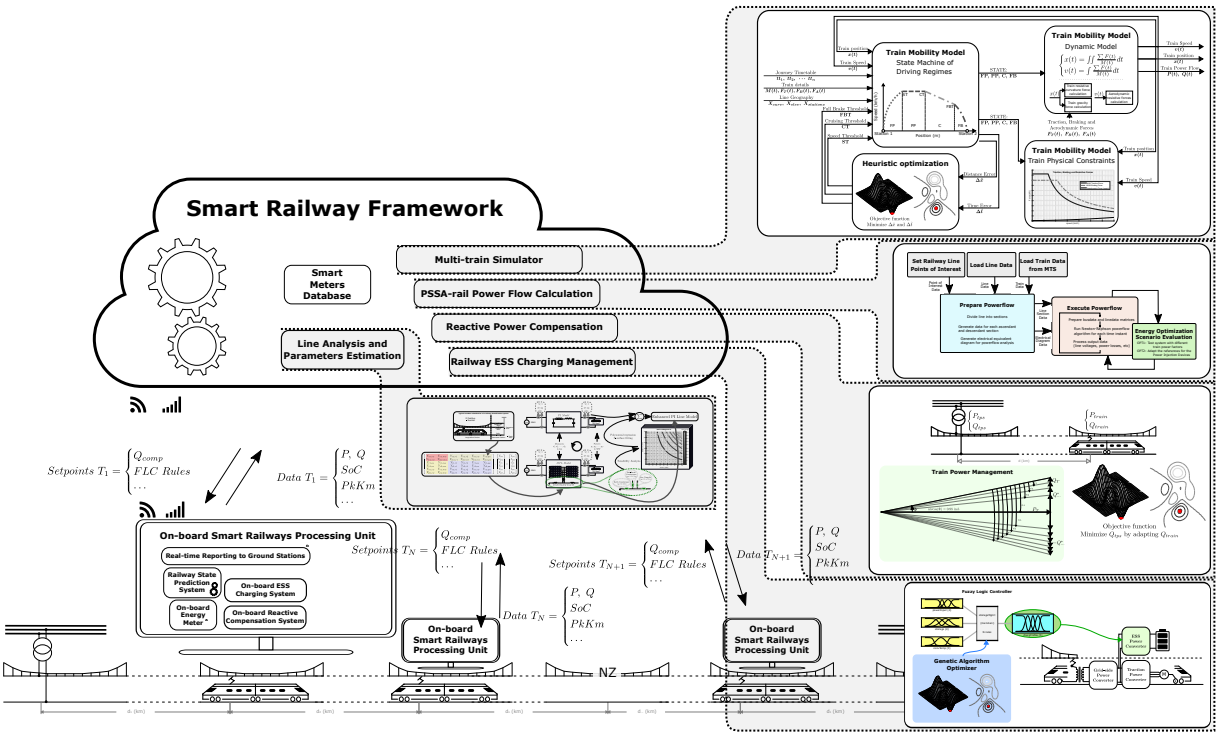

Figure 8.1: Smart Railway Framework.

Some of the algorithms of these tools and strategies are offline-type, like the railway line simplification of chapter 3. Also, in the tool presented in chapter 4 where is considered an offline-type objective. This tool can also be an online-type one if it has a prediction objective, or if this train simulation tool is part of a digital/virtual twin train. Similarly, the tool of chapter 5 was demonstrated in this thesis with offline-type input data. A Smart Railway Framework for power flow management depends on a power flow knowledge

extraction tool to operate with online/real-time data.

The technological and regulatory advancements are the motto for the implementation of new strategies and tools to support those strategies.

The drivers for a more sustainable transportation sector are well known and a smart railway sector will have a central role in this challenge.

8.3 Guidelines for Future Work

Notwithstanding to the results achieved that validated the proposed statement and answered the research questions, there is margin to improve. In addition to all the discussed future directions made in each topical chapters, three main future research directions were identified.

The first topic is on the communication within the layers of the smart railway framework pyramid. During the development of this thesis, it was explored a communication strategy for railways, specifically with the usage of Wi-Fi access points in the passenger stations, to reduce the data transmission costs between trains and ground stations. This strategy is addressed in the appendix F and led to publication [163]. However, new communication technologies like LTE-R, 5G [164, 165] or very low earth orbit satellite communications, like Starlink system, [166], appears to be interesting solutions for railway communication. A study on the communication requirements for the smart railways framework might be worth to look at.

The second topic is on the prediction of railway system state. Despite the current advances in communication technologies, the bottleneck for a real-time operation can be in the processing tasks of the knowledge extraction algorithms. Then, a prediction module where the future system state is estimated is a good future research direction to reduce the dependence on real-time communication and simple knowledge extraction algorithms. The usage of energy consumption prediction strategies like the one proposed by Tang et al. [167], where the daily traction energy consumption was estimated with an error of 2.17 %, or the work of [168], for hourly forecasting, might be worth to look at.

Finally, the PSSA-rail tool was implemented with a vision for integration to a digital twin. Essentially, the input data of this tool can be either the output data of the multi-train simulator of chapter 4, or data from a commercial simulator tool, like the data used in the demonstration in appendix E. Like it was illustrated in Fig. 5.4, where the input data of PSSA-rail can be from real-time data from energy meters, the future directions on this tool that be worth to look at is in the digital twin approach [100], where the simulation

is interconnected with a real train operation. The PSSA-rail can be adapted either in the prepare and execute simulation modules, where small simulation time-windows might be compatible to the real-time operation. This capability of the PSSA-tool might be a good future research direction.

8.4 Final Remarks

It is the author's belief that the proposed tools and strategies for power flow management in smart railways will be valuable contributions to the scientific community, and will answer to the challenge of the reduction of the gap between current railways and future smarter railways.

Appendices

APPENDIX A

PQ Electric Train Model

In chapter 3 was considered an electric train model to support the evaluation of the railway line parameters. This model is better described in this appendix.

A.1 Introduction

An electric train model was built in MatLab/Simulink as a controlled voltage source, in series with an impedance. These way, in normal operation mode, the value of the voltage source can be controlled towards desired PQ power values, regardless of the catenary voltage. In other degraded modes, this electric model can be more close to normative restrictions.

In this appendix, the PQ Electric Model is detailed, having its integration illustrated in Fig. A.1.

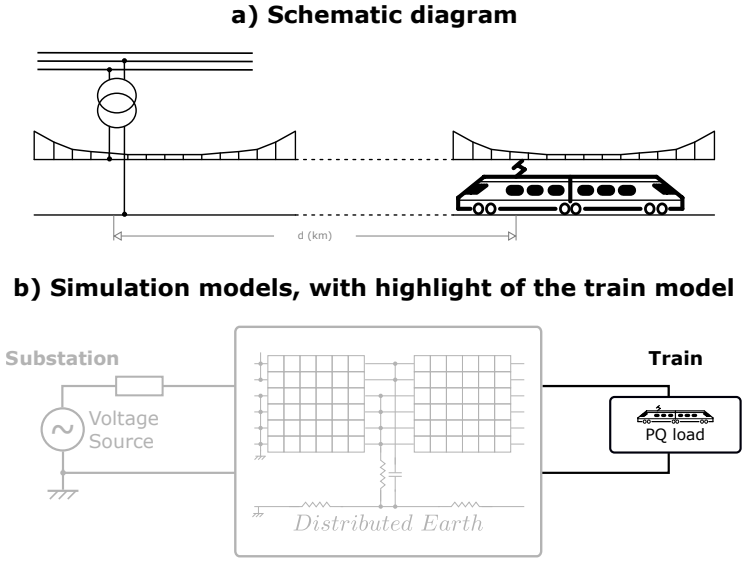

Figure A.1: Integration of the train model in the simulation environment.

A.2 Model Requirements

The train is modelled as a load in which the power is invariant to the catenary voltage level. However, a power limitation must occur to comply with interoperability requirements, in the situation that the train reaches an under-voltage level. According to the IEC60850 [113], the lowest non-permanent voltage is 0.7 p.u. (17.5 kV) whereas the lowest permanent voltage is 0.76 p.u. (19 kV). Specifically, if the voltage is higher than the lowest permanent voltage, the train can consume all its demand power; if is reached the lowest non-permanent voltage, the demand power is clipped to zero. In this train load model, the second situation will not occur since is dependent on the existence of other trains imposing a higher demand for power. Therefore, a 18 kV voltage level for this power limitation was chosen, where, in this situation, the limit protection is activated. This imposes a reduction in the train available traction force.

Matlab/Simulink was the chosen simulation platform [169], due to its capabilities for time-based simulation required for the train model. To consider the train electrical requirements, a Voltage Source Converter (VSC) was used and implemented in Simulink. The used VSC model is an average simulation model based on [58].

This VSC has active and reactive power control loops, a current control loop and a synchronisation part, as illustrated in Fig. A.2, where the DC-bus voltage is considered constant.

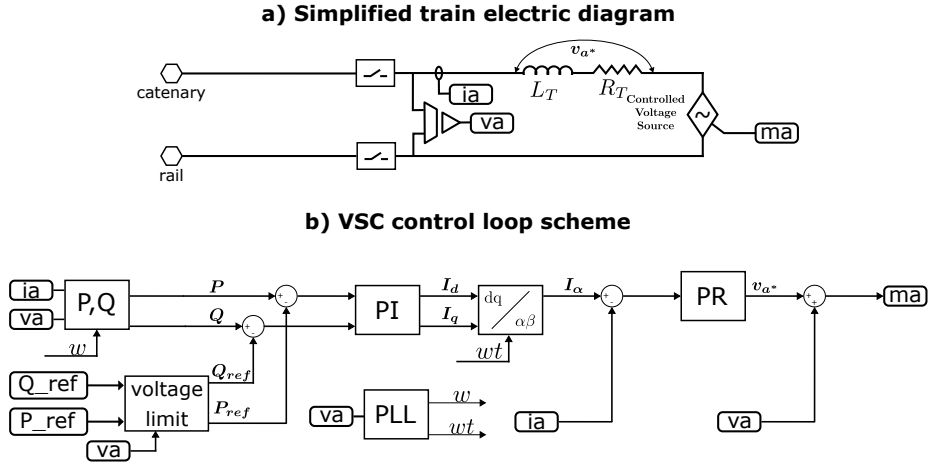

Figure A.2: Implemented train model: VSC as a PQ load.

For a defined power reference and power factor, the control loop will adapt the VSC operation to the desired setpoint. The synchronization part was based on the Synchronous Reference Frame Phase-Locked Loop (SRF-PLL) with amplitude normalization scheme, as revised in [170]. The ωt reference will be later used for the rotating-to-stationary frame transformation (Park's inverse transformation).

The current control loop was implemented with a non-ideal Proportional-Resonant (PR) controller, as revised in [171], with a transfer function defined by (A.1).

$$G_{PR}(s) = K_p + \frac{K_i^2 s}{s^2 + 2\omega_c s + \omega_0^2} \tag{A.1}$$

In this train electrical model, the non-ideal PR controller was used since it allows non-infinite gain at resonant frequency. The reference generated by the PR controller can be seen as the voltage drop in the train inductor, $\boldsymbol{v_{a^*}}$. As illustrated in Fig. A.2b), the input of the PR controller is the error between the reference current and the inductor train current, $I_\alpha - I_a$.

Two proportional-integral controllers, in the synchronous reference frame domain generate the active and reactive current references. Later, the two references are transformed to the stationary frame and the I_α value is the current reference used by the PR controller.

Finally, from the measurements of the active and reactive power consumption and with the comparison with the train power reference (resulting in active and reactive power error), this error value is then used by a proportional-integral controller to generate, respectively, the active and reactive current references. To ensure the fulfilment of the under-voltage protection, a pseudo-saturation state machine structure was implemented, limiting the voltage level in the minimum defined value.

A.3 Validation of Implemented Simulation Models

The behaviour of the train load model is better supported with the simulation of two cases: the train consuming the maximum power at small distance (10 MW at 10 km, PF = 0.9 ind.); and the train with voltage limit reach (40 km, unable to reach 10 MW, PF = 0.9 ind.). In both cases, is used the multi-conductor line model, from Fig. A.1b).

A.3.1 Train at 10 km, 10 MW active power reference, PF = 0.9 ind.

In Fig. A.3 is presented the case of a train simulation, located 10 km away from the traction substation and supplied by a catenary line.

In the first 100 ms of operation, the train establishes synchronism to the catenary voltage, then it closes the switch and controls the current to zero (resulting in a small overshoot in the current, as gradually tends to zero). After 100 ms, the π-type controllers receive the desired power reference resulting in the increase of the active and reactive power towards the power references, as visible in the graph of Fig. A.3c).

A.3.2 Train at 40 km, 10 MW active power reference, PF = 0.9 ind.

In the second case where train is located at 40 km, presented in Fig. A.4, after the same initial 100 ms behavior of the first situation, the train is unable to reach the desired 10 MW reference due to under-voltage limitations.

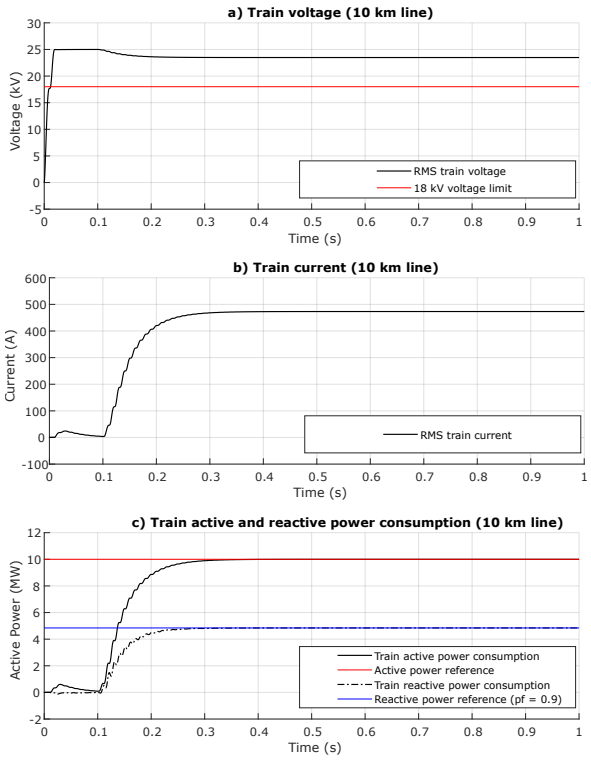

Figure A.3: Train results for a train, consuming the maximum power (10 MW) and having PF = 0.9 ind., at a small distance (10 km): a) Voltage at pantograph (black) and limit voltage (red); b) Current in train; c) Active and reactive power consumption (black) and respective power references (red and blue).

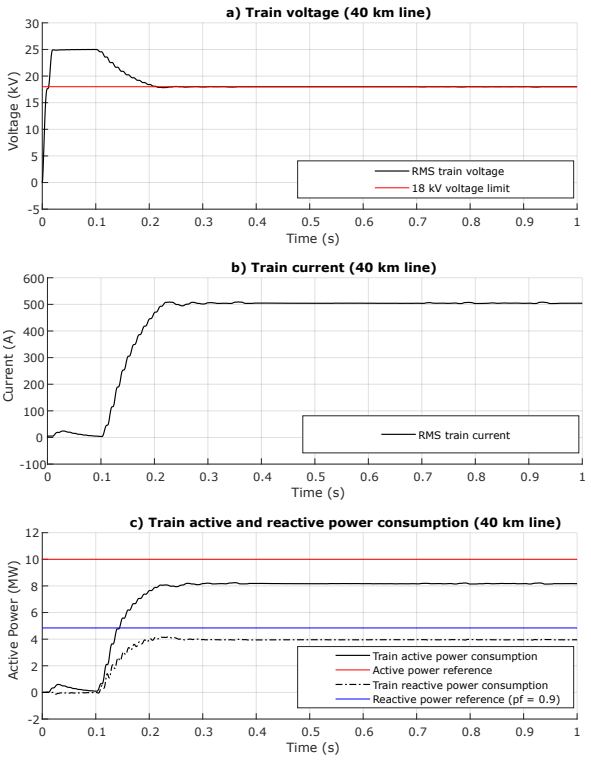

Figure A.4: Train results for a train, consuming the maximum available power and having PF = 0.9 ind., at a long distance (40 km): a) Voltage at pantograph (black) and limit voltage (red); b) Current in train; c) Active and reactive power consumption (black) and respective power references (red and blue).

As soon as the minimum 18 kV voltage level is reached (at around 210 ms), the train active and reactive powers are locked. The behavior of the adaptation of the active power (while maintaining PF = 0.9 ind.) towards having the 18 kV voltage level is visible in Fig. A.4: first the under-voltage is detected at around 210 ms, and then the active power is halted (with a slowly oscillation, controlling towards 18 kV voltage level) until is reached the maximum available power. The reactive power is also limited, being this reference dependent of the active power and on the desired PF, following:

$$Q_{ref} = P_{ref} \cdot \tan(\cos^{-1}(PF)) \tag{A.2}$$

APPENDIX B

π-type Line Model Enhancement Results

In chapter 3 was presented the results for the baseline comparison and the enhancement validation.

The validation of the baseline is visible through histogram graphs in Fig. 3.20, illustrating the errors before and after the application of the enhancement procedure.

This enhancement procedure depends on generated coefficients, where the baseline coefficients are in Table 3.4.

Due to the extension of these results, in this appendix are presented the correspondent results for the railway π-type line model enhancement.

B.1 Enhancement Comparison

This first section covers the presentation of the enhancement comparison of the line model. This comparison is supported with histogram graphs that illustrates the before and after of the application of the enhancement.

B.1.1 Earth conductance

Regarding the earth conductance, the enhancement is visible in the histogram graphs of Fig. B.1.

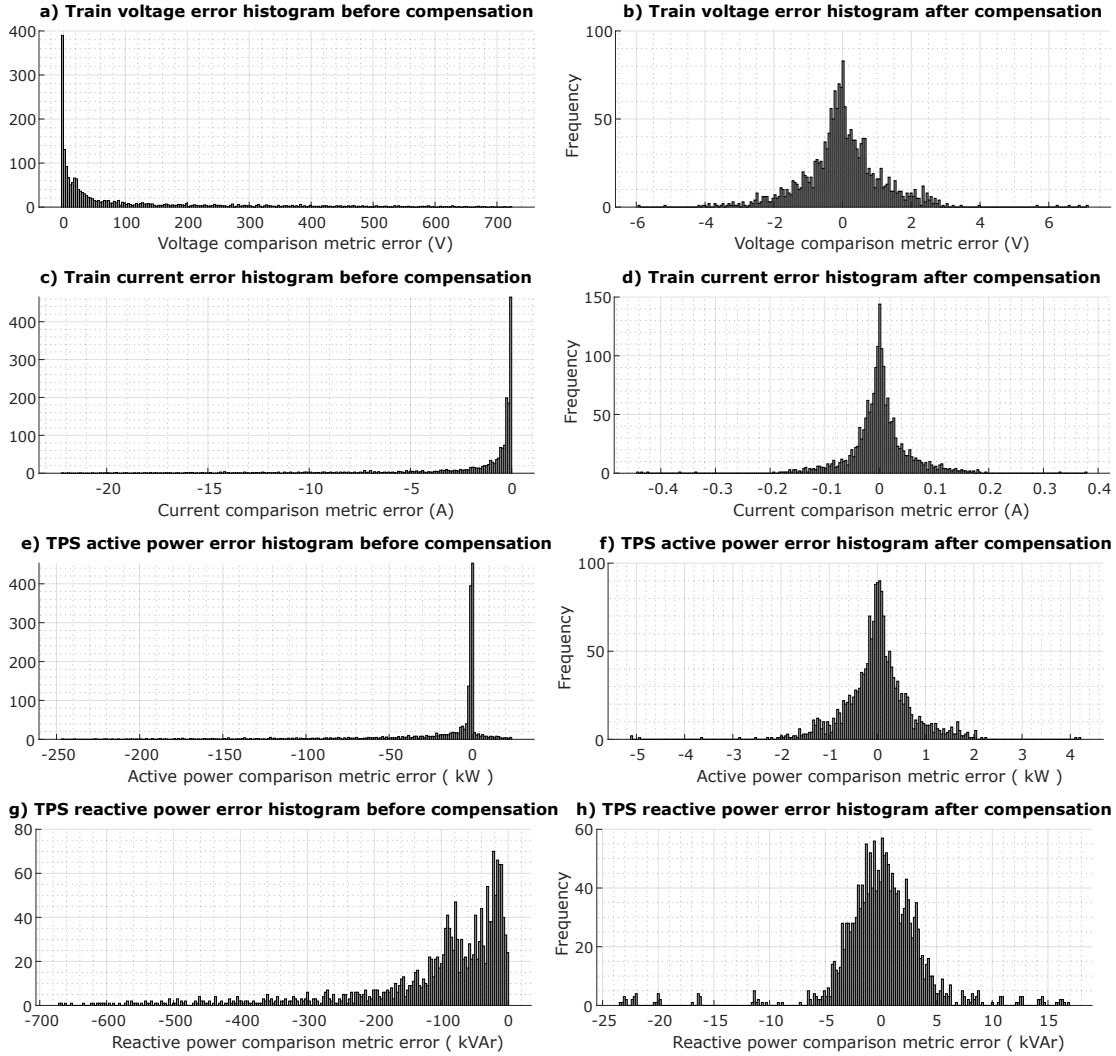

Figure B.1: Histogram of the errors before and after the application of the methodology for the $\boldsymbol{TS}_{ec}$ surface.

To obtain the histograms, the $\boldsymbol{TS}_{ec}$ surface covers a universe of $15 \times 15 \times 8 = 1800$ points. All of these points of the surface were used to generate the left-side histograms of Fig. B.1.

After the application of the enhancement, the train voltage error is reduced from a large value to a value between -6 V to 7 V (for all the 1800 points). The remaining results are within minimal errors.

B.1.2 Rail-Earth conductance

In Fig. B.2 is presented the histogram graphs before (left) and after (right) the application of the enhancement, for a sensibility analysis on rail-earth conductance.

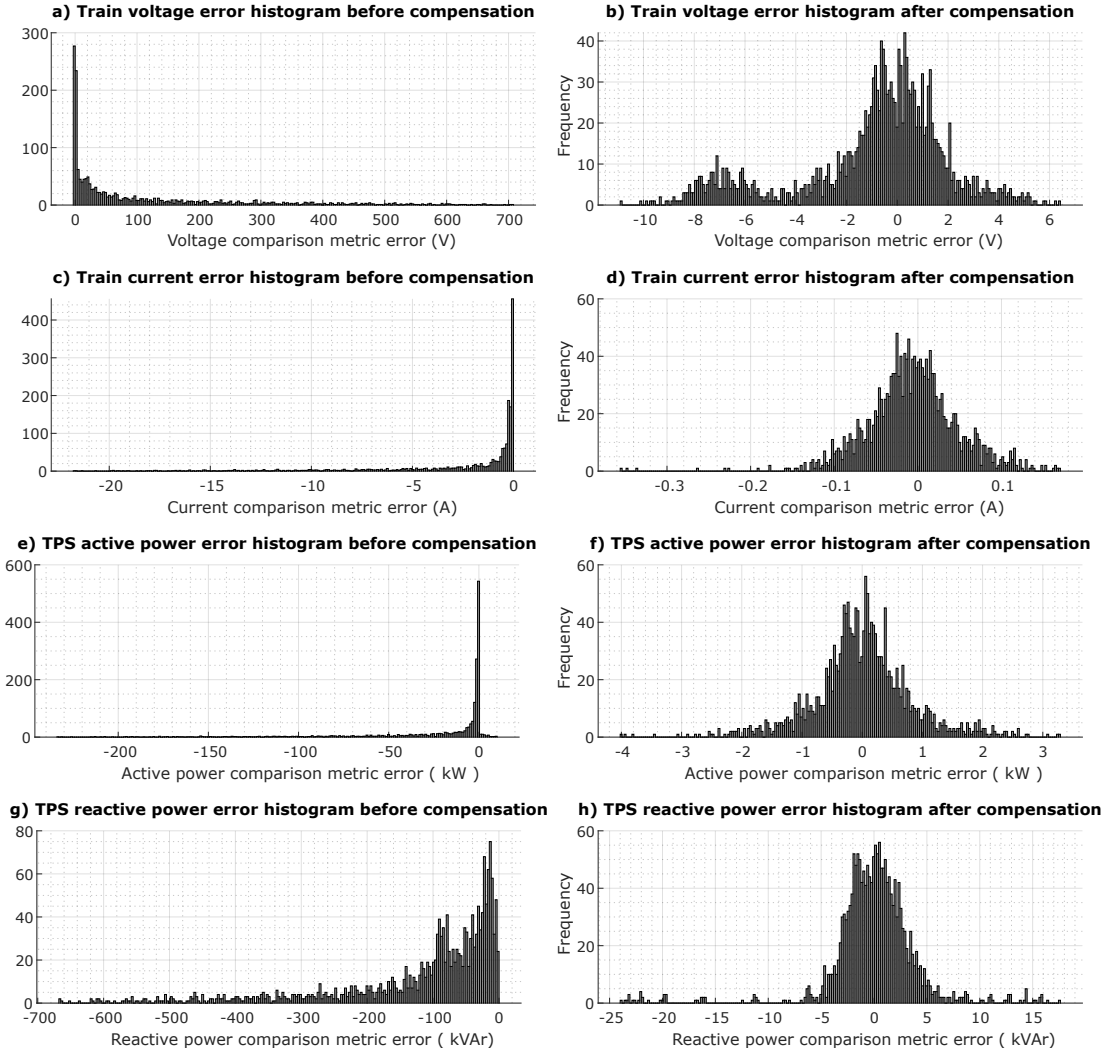

Figure B.2: Histogram of the errors before and after the application of the methodology for the $\boldsymbol{TS}_{re}$ surface.

Similarly, all the results after applying the enhancement procedure are minimal.

B.1.3 Line Capacity

Furthermore, the line capacity was also target of a sensibility analysis, being also the results used for an enhancement of the lumped-parameters π-type line model. In Fig. B.3 is presented the histogram graphs to validate this enhancement, where the errors on the right side of the Fig. B.3 are minimal.

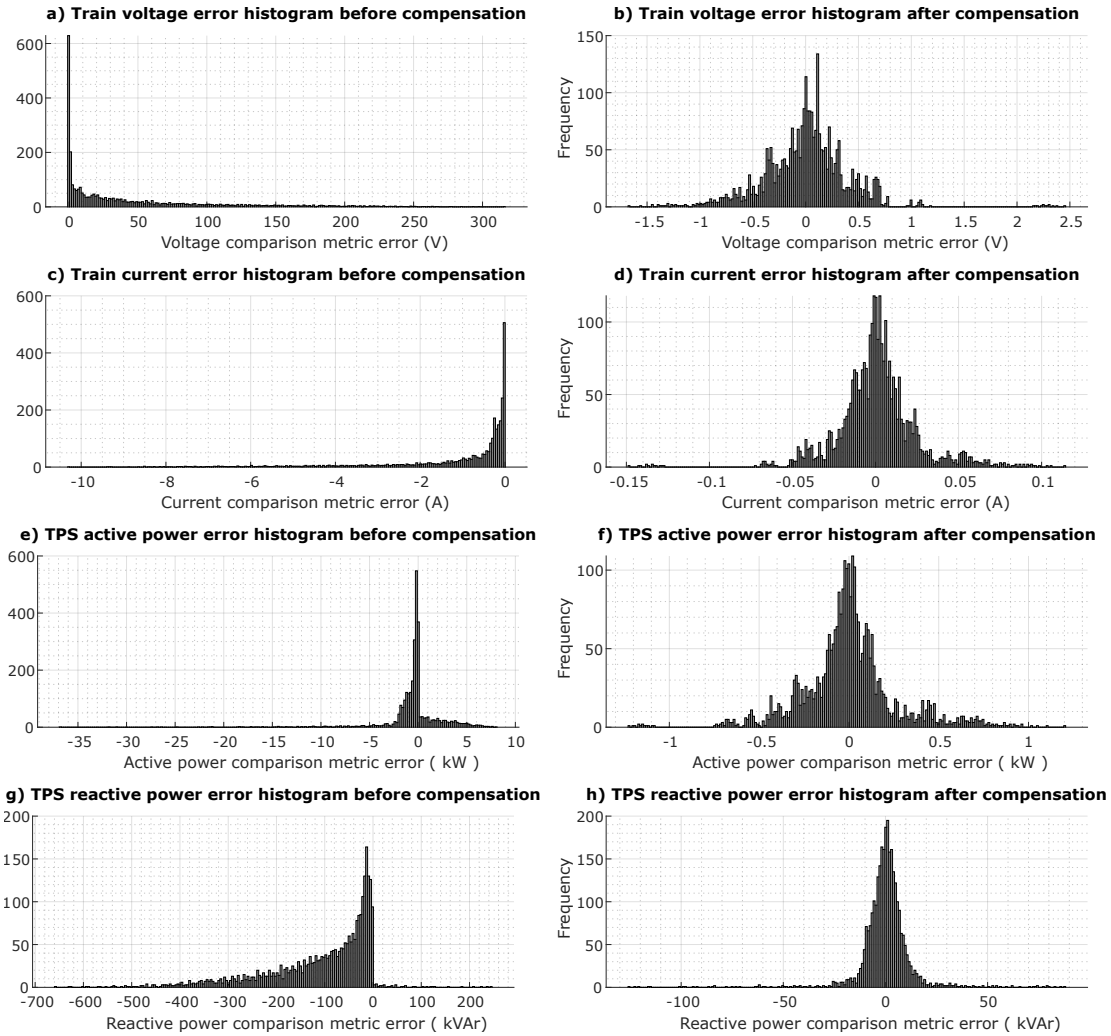

Figure B.3: Histogram of the errors before and after the application of the methodology for the $\boldsymbol{TS}_{lc}$ surface.

B.2 Enhancement Coefficients

To obtain the results on the histogram graphs on Fig. B.1, Fig. B.2 and Fig. B.3, showing a drastic reduction on the errors, it was used a enhancement procedure based on the application of a polynomial multivariate function, whose coefficients were generated based differences between models.

Therefore, in this section are listed the coefficients for each of the enhancements.

B.2.1 Earth conductance

The coefficients for the enhancement based on the sensibility analysis on the earth conductance are presented in Table B.1 and Table B.2.

Table B.1: List of generated coefficients from $\boldsymbol{TS}_{ec}$ (1 of 2).

	TRAIN		TPS	
	voltage	current	active power	reactive power
$(\boldsymbol{EC})$	4,06277E+00	-9,80083E-01	-7,85819E+03	-3,44283E+04
$(\boldsymbol{EC})^2$	1,34575E+02	1,01480E+00	-7,43265E+04	1,43929E+05
$(\boldsymbol{EC})^3$	-1,18141E+03	2,08167E+01	5,39595E+05	1,37078E+05
$(\boldsymbol{EC})^4$	1,20040E+03	-2,42324E+01	-5,25177E+05	-2,94567E+05
$(\boldsymbol{EC})^5$	0,00000E+00	0,00000E+00	0,00000E+00	0,00000E+00
$(\boldsymbol{L}_d)$	-1,65155E+00	5,37886E-02	5,68445E+01	-9,22296E+02
$(\boldsymbol{L}_d) * (\boldsymbol{EC})$	2,39320E+00	1,01952E-01	7,98588E+02	4,28934E+03
$(\boldsymbol{L}_d) * (\boldsymbol{EC})^2$	1,19911E+01	-6,83403E-01	-2,96199E+03	-2,50800E+04
$(\boldsymbol{L}_d) * (\boldsymbol{EC})^3$	4,81917E+01	-3,79244E-01	-2,15239E+04	1,15466E+04
$(\boldsymbol{L}_d) * (\boldsymbol{EC})^4$	-9,23352E+01	1,54044E+00	3,52244E+04	1,77706E+04
$(\boldsymbol{L}_d) * (\boldsymbol{EC})^5$	3,24154E+01	-5,89981E-01	-1,18318E+04	-8,76239E+03
$(\boldsymbol{L}_d)^2$	3,21617E-01	-1,24905E-02	2,11167E+01	-5,68181E+02
$(\boldsymbol{L}_d)^2 * (\boldsymbol{EC})$	-9,14454E-01	6,40203E-03	1,64485E+02	-6,85044E+00
$(\boldsymbol{L}_d)^2 * (\boldsymbol{EC})^2$	-4,27557E-01	1,83524E-02	1,09895E+02	7,19472E+02
$(\boldsymbol{L}_d)^2 * (\boldsymbol{EC})^3$	1,28292E+00	-3,39782E-02	-3,54109E+02	-9,19991E+02
$(\boldsymbol{L}_d)^2 * (\boldsymbol{EC})^4$	-4,23672E-01	1,02699E-02	1,11400E+02	2,56024E+02
$(\boldsymbol{L}_d)^3$	-1,87122E-02	1,25238E-03	-7,04436E+00	6,82429E+01
$(\boldsymbol{L}_d)^3 * (\boldsymbol{EC})$	5,80799E-02	-5,28699E-04	-1,02023E+01	-1,02255E+01
$(\boldsymbol{L}_d)^3 * (\boldsymbol{EC})^2$	-2,74077E-02	4,87270E-04	1,00177E+01	3,55984E+00
$(\boldsymbol{L}_d)^3 * (\boldsymbol{EC})^3$	2,08596E-03	-8,51602E-07	-7,99595E-01	2,03075E+00
$(\boldsymbol{L}_d)^4$	3,98969E-04	-6,54096E-05	5,67773E-01	-3,96873E+00
$(\boldsymbol{L}_d)^4 * (\boldsymbol{EC})$	-1,25154E-03	7,15344E-06	1,00778E-01	3,13722E-01
$(\boldsymbol{L}_d)^4 * (\boldsymbol{EC})^2$	3,23314E-04	-7,01043E-06	-1,16018E-01	-1,31647E-01
$(\boldsymbol{L}_d)^5$	1,55499E-06	1,72535E-06	-1,81634E-02	1,19419E-01
$(\boldsymbol{L}_d)^5 * (\boldsymbol{EC})$	9,30899E-06	1,57507E-08	7,73532E-04	-2,42717E-03
$(\boldsymbol{P}_T)$	-2,78721E+00	1,39067E-01	7,33976E+02	-9,66642E+03
$(\boldsymbol{P}_T) * (\boldsymbol{EC})$	-7,08783E+00	6,90299E-01	1,20096E+04	1,60926E+04
$(\boldsymbol{P}_T) * (\boldsymbol{EC})^2$	2,29675E+01	-2,53084E+00	-1,23745E+04	-9,32829E+04
$(\boldsymbol{P}_T) * (\boldsymbol{EC})^3$	1,36912E+02	-9,65694E-01	-7,26769E+04	5,74628E+04
$(\boldsymbol{P}_T) * (\boldsymbol{EC})^4$	-2,32215E+02	4,64594E+00	1,08186E+05	4,89836E+04
$(\boldsymbol{P}_T) * (\boldsymbol{EC})^5$	7,90816E+01	-1,78332E+00	-3,48331E+04	-2,75896E+04
$(\boldsymbol{P}_T) * (\boldsymbol{L}_d)$	8,67223E-01	-6,74952E-02	-4,78006E+02	-1,88588E+03
$(\boldsymbol{P}_T) * (\boldsymbol{L}_d) * (\boldsymbol{EC})$	-2,89254E-01	-6,31626E-02	-1,56092E+03	-8,15048E+02
$(\boldsymbol{P}_T) * (\boldsymbol{L}_d) * (\boldsymbol{EC})^2$	-3,36140E+00	1,64234E-01	2,44965E+03	4,35810E+03
$(\boldsymbol{P}_T) * (\boldsymbol{L}_d) * (\boldsymbol{EC})^3$	6,37412E+00	-2,01869E-01	-1,67895E+03	-6,66618E+03
$(\boldsymbol{P}_T) * (\boldsymbol{L}_d) * (\boldsymbol{EC})^4$	-2,08224E+00	5,49853E-02	2,72374E+02	2,03257E+03
$(\boldsymbol{P}_T) * (\boldsymbol{L}_d)^2$	4,33237E-02	6,73797E-03	5,37656E+01	9,85015E+01
$(\boldsymbol{P}_T) * (\boldsymbol{L}_d)^2 * (\boldsymbol{EC})$	-1,87001E-01	4,19901E-03	7,94096E+01	6,50568E+01
$(\boldsymbol{P}_T) * (\boldsymbol{L}_d)^2 * (\boldsymbol{EC})^2$	5,69231E-03	7,11814E-04	-2,91889E+01	6,01038E+01
$(\boldsymbol{P}_T) * (\boldsymbol{L}_d)^2 * (\boldsymbol{EC})^3$	-8,54192E-03	4,84095E-04	1,72285E+01	-2,70599E-01
$(\boldsymbol{P}_T) * (\boldsymbol{L}_d)^3$	-2,88179E-03	-2,55216E-04	-2,28550E+00	-5,02574E+00
$(\boldsymbol{P}_T) * (\boldsymbol{L}_d)^3 * (\boldsymbol{EC})$	6,77700E-03	-1,86389E-04	-2,55685E+00	-4,11202E+00

Table B.2: List of generated coefficients from $\boldsymbol{TS}_{ec}$ (2 of 2).

	TRAIN		TPS	
	voltage	current	active power	reactive power
$(\boldsymbol{P}_T) * (\boldsymbol{L}_d)^3 * (\boldsymbol{EC})^2$	1,28892E-04	-2,15036E-05	-1,42060E-01	-7,02223E-01
$(\boldsymbol{P}_T) * (\boldsymbol{L}_d)^4$	9,39444E-05	3,54537E-06	4,14229E-02	-8,93409E-02
$(\boldsymbol{P}_T) * (\boldsymbol{L}_d)^4 * (\boldsymbol{EC})$	-8,28634E-05	2,53487E-06	3,32788E-02	5,96389E-02
$(\boldsymbol{P}_T) * (\boldsymbol{L}_d)^5$	-1,13586E-06	-7,78502E-09	-2,73476E-04	2,76898E-03
$(\boldsymbol{P}_T)^2$	1,96739E+00	-1,29824E-01	-1,08749E+03	1,15541E+04
$(\boldsymbol{P}_T)^2 * (\boldsymbol{EC})$	1,03313E+00	-8,86779E-02	-2,02614E+03	-1,54598E+03
$(\boldsymbol{P}_T)^2 * (\boldsymbol{EC})^2$	-4,66989E+00	2,88789E-01	3,88898E+03	7,79017E+03
$(\boldsymbol{P}_T)^2 * (\boldsymbol{EC})^3$	6,15201E+00	-3,46082E-01	-2,73995E+03	-1,09503E+04
$(\boldsymbol{P}_T)^2 * (\boldsymbol{EC})^4$	-1,75997E+00	9,20905E-02	4,27499E+02	3,22796E+03
$(\boldsymbol{P}_T)^2 * (\boldsymbol{L}_d)$	-5,37137E-01	3,21234E-02	2,91018E+02	1,29159E+03
$(\boldsymbol{P}_T)^2 * (\boldsymbol{L}_d) * (\boldsymbol{EC})$	-1,13275E-01	1,14400E-02	2,14154E+02	1,74388E+02
$(\boldsymbol{P}_T)^2 * (\boldsymbol{L}_d) * (\boldsymbol{EC})^2$	-6,43967E-02	-5,82475E-04	-1,77291E+02	1,90362E+02
$(\boldsymbol{P}_T)^2 * (\boldsymbol{L}_d) * (\boldsymbol{EC})^3$	-2,91092E-02	3,22886E-03	9,85970E+01	7,86921E+00
$(\boldsymbol{P}_T)^2 * (\boldsymbol{L}_d)^2$	4,52740E-02	-2,65563E-03	-2,60976E+01	-3,49846E+01
$(\boldsymbol{P}_T)^2 * (\boldsymbol{L}_d)^2 * (\boldsymbol{EC})$	7,45763E-03	-4,42973E-04	-2,70717E+00	-1,31833E+01
$(\boldsymbol{P}_T)^2 * (\boldsymbol{L}_d)^2 * (\boldsymbol{EC})^2$	3,99939E-03	-2,12543E-04	-3,08414E+00	-4,63515E+00
$(\boldsymbol{P}_T)^2 * (\boldsymbol{L}_d)^3$	-1,32869E-03	7,65496E-05	7,57852E-01	2,44011E+00
$(\boldsymbol{P}_T)^2 * (\boldsymbol{L}_d)^3 * (\boldsymbol{EC})$	-2,24821E-04	1,01928E-05	9,98077E-02	2,67733E-01
$(\boldsymbol{P}_T)^2 * (\boldsymbol{L}_d)^4$	1,39215E-05	-7,49870E-07	-7,47466E-03	-2,20342E-02
$(\boldsymbol{P}_T)^3$	-5,52698E-01	3,89704E-02	3,57186E+02	-5,77810E+03
$(\boldsymbol{P}_T)^3 * (\boldsymbol{EC})$	-1,04481E-01	8,76263E-03	1,28814E+02	2,02792E+02
$(\boldsymbol{P}_T)^3 * (\boldsymbol{EC})^2$	-8,88855E-02	4,53891E-03	-3,94195E+01	1,73940E+02
$(\boldsymbol{P}_T)^3 * (\boldsymbol{EC})^3$	-2,23214E-02	2,43078E-03	6,30397E+01	3,46011E+01
$(\boldsymbol{P}_T)^3 * (\boldsymbol{L}_d)$	7,98515E-02	-5,34111E-03	-4,78555E+01	-3,49918E+02
$(\boldsymbol{P}_T)^3 * (\boldsymbol{L}_d) * (\boldsymbol{EC})$	1,85641E-02	-1,21377E-03	-1,10659E+01	-3,18619E+01
$(\boldsymbol{P}_T)^3 * (\boldsymbol{L}_d) * (\boldsymbol{EC})^2$	6,13988E-03	-4,52951E-04	-6,10446E+00	-1,04926E+01
$(\boldsymbol{P}_T)^3 * (\boldsymbol{L}_d)^2$	-3,93636E-03	2,42683E-04	2,27299E+00	6,45452E-01
$(\boldsymbol{P}_T)^3 * (\boldsymbol{L}_d)^2 * (\boldsymbol{EC})$	-6,70420E-04	4,31169E-05	4,81216E-01	1,07230E+00
$(\boldsymbol{P}_T)^3 * (\boldsymbol{L}_d)^3$	6,02715E-05	-3,41217E-06	-3,26226E-02	-1,06614E-01
$(\boldsymbol{P}_T)^4$	8,01660E-02	-5,81093E-03	-5,53094E+01	1,25020E+03
$(\boldsymbol{P}_T)^4 * (\boldsymbol{EC})$	1,79430E-02	-1,33980E-03	-1,29931E+01	-3,50052E+01
$(\boldsymbol{P}_T)^4 * (\boldsymbol{EC})^2$	5,71508E-03	-4,44702E-04	-5,52672E+00	-1,04577E+01
$(\boldsymbol{P}_T)^4 * (\boldsymbol{L}_d)$	-5,38682E-03	3,86600E-04	3,48500E+00	4,02519E+01
$(\boldsymbol{P}_T)^4 * (\boldsymbol{L}_d) * (\boldsymbol{EC})$	-8,90214E-04	6,62116E-05	7,17743E-01	1,65361E+00
$(\boldsymbol{P}_T)^4 * (\boldsymbol{L}_d)^2$	1,22041E-04	-8,36689E-06	-7,93061E-02	6,55252E-02
$(\boldsymbol{P}_T)^5$	-5,93049E-03	4,34143E-04	4,23371E+00	-1,21012E+02
$(\boldsymbol{P}_T)^5 * (\boldsymbol{EC})$	-8,97940E-04	6,87222E-05	7,36975E-01	1,72365E+00
$(\boldsymbol{P}_T)^5 * (\boldsymbol{L}_d)$	1,34718E-04	-1,02432E-05	-9,22622E-02	-1,64864E+00
$\boldsymbol{X}0$	1,59477E+00	-3,42457E-02	2,43315E+02	1,16187E+03
$(\boldsymbol{P}_T)^6$	1,76110E-04	-1,29107E-05	-1,28642E-01	4,30744E+00
$(\boldsymbol{L}_d)^6$	-1,08098E-07	-1,79675E-08	2,07301E-04	-1,39455E-03
$(\boldsymbol{EC})^6$	-1,60855E+02	3,41513E+00	6,86378E+04	4,83917E+04

B.2.2 Rail-Earth conductance

For rail-earth conductance, the coefficients are presented in Table B.3 and Table B.4.

Table B.3: List of generated coefficients from $\boldsymbol{TS}_{re}$ (1 of 2).

	TRAIN		TPS	
	voltage	current	active power	reactive power
$(\boldsymbol{RE})$	-5,43595E-01	3,29044E-03	7,87030E+01	3,57863E+01
$(\boldsymbol{RE})^2$	3,29410E-01	-3,52313E-03	-8,16832E+01	-3,48260E+01
$(\boldsymbol{RE})^3$	-3,65787E-02	4,31148E-04	1,10942E+01	2,40731E+00
$(\boldsymbol{RE})^4$	1,54607E-03	-1,92344E-05	-5,26844E-01	-5,61684E-02
$(\boldsymbol{RE})^5$	-2,55803E-05	3,27295E-07	9,24706E-03	5,12151E-04
$(\boldsymbol{L}_d)$	-2,01717E+00	1,00215E-01	8,81953E+02	-3,10932E+02
$(\boldsymbol{L}_d) * (\boldsymbol{RE})$	-2,53513E-01	3,26243E-03	5,81785E+01	6,19044E+01
$(\boldsymbol{L}_d) * (\boldsymbol{RE})^2$	9,10070E-03	-1,20014E-04	-3,52211E+00	2,70612E-01
$(\boldsymbol{L}_d) * (\boldsymbol{RE})^3$	2,01960E-04	-2,49212E-06	7,33672E-03	-1,39336E-01
$(\boldsymbol{L}_d) * (\boldsymbol{RE})^4$	-7,45278E-06	9,72807E-08	1,04357E-03	2,99762E-03
$(\boldsymbol{L}_d) * (\boldsymbol{RE})^5$	4,75926E-08	-6,26900E-10	-8,04854E-06	-1,68217E-05
$(\boldsymbol{L}_d)^2$	5,86676E-01	-2,24352E-02	-2,13030E+02	-5,93113E+02
$(\boldsymbol{L}_d)^2 * (\boldsymbol{RE})$	9,48095E-03	-1,41689E-04	-8,30317E-01	-5,92512E+00
$(\boldsymbol{L}_d)^2 * (\boldsymbol{RE})^2$	-9,56977E-04	1,26266E-05	2,41182E-01	2,15161E-01
$(\boldsymbol{L}_d)^2 * (\boldsymbol{RE})^3$	1,21062E-05	-1,71074E-07	-3,93961E-03	-1,51150E-03
$(\boldsymbol{L}_d)^2 * (\boldsymbol{RE})^4$	-3,47321E-08	4,86851E-10	1,35244E-05	-4,22743E-07
$(\boldsymbol{L}_d)^3$	-5,71646E-02	2,26247E-03	2,17124E+01	6,20556E+01
$(\boldsymbol{L}_d)^3 * (\boldsymbol{RE})$	6,41500E-04	-6,48668E-06	-2,12985E-01	4,79480E-02
$(\boldsymbol{L}_d)^3 * (\boldsymbol{RE})^2$	8,74591E-06	-9,80771E-08	-2,49966E-04	-5,05971E-03
$(\boldsymbol{L}_d)^3 * (\boldsymbol{RE})^3$	-1,37430E-07	2,03809E-09	3,90748E-05	3,43968E-05
$(\boldsymbol{L}_d)^4$	2,71138E-03	-1,16830E-04	-1,12392E+00	-3,24870E+00
$(\boldsymbol{L}_d)^4 * (\boldsymbol{RE})$	-2,56579E-05	2,56271E-07	4,73089E-03	5,47975E-03
$(\boldsymbol{L}_d)^4 * (\boldsymbol{RE})^2$	1,79679E-07	-3,05732E-09	-8,80588E-05	8,87284E-06
$(\boldsymbol{L}_d)^5$	-6,37068E-05	3,02547E-06	2,97977E-02	9,18936E-02
$(\boldsymbol{L}_d)^5 * (\boldsymbol{RE})$	1,13881E-07	-1,52077E-10	4,08246E-05	-9,98572E-05
$(\boldsymbol{P}_T)$	-4,66451E+00	2,80338E-01	2,52517E+03	-6,31139E+03
$(\boldsymbol{P}_T) * (\boldsymbol{RE})$	-3,75357E-01	3,35729E-03	4,54043E+01	7,87467E+01
$(\boldsymbol{P}_T) * (\boldsymbol{RE})^2$	4,36729E-02	-4,66128E-04	-1,08729E+01	-4,70397E+00
$(\boldsymbol{P}_T) * (\boldsymbol{RE})^3$	-1,84011E-03	2,92141E-05	7,36839E-01	2,13989E-01
$(\boldsymbol{P}_T) * (\boldsymbol{RE})^4$	3,01707E-05	-5,73085E-07	-1,47885E-02	-3,74708E-03
$(\boldsymbol{P}_T) * (\boldsymbol{RE})^5$	-1,58071E-07	3,26948E-09	8,49510E-05	2,06792E-05
$(\boldsymbol{P}_T) * (\boldsymbol{L}_d)$	2,44157E+00	-1,18038E-01	-1,02806E+03	-3,19788E+03
$(\boldsymbol{P}_T) * (\boldsymbol{L}_d) * (\boldsymbol{RE})$	-5,59072E-02	-4,49144E-05	2,83107E+00	-4,93035E+00
$(\boldsymbol{P}_T) * (\boldsymbol{L}_d) * (\boldsymbol{RE})^2$	9,51292E-04	-1,26463E-05	-4,00938E-01	5,71044E-02
$(\boldsymbol{P}_T) * (\boldsymbol{L}_d) * (\boldsymbol{RE})^3$	1,27652E-08	5,01323E-08	3,77331E-03	-3,85418E-03
$(\boldsymbol{P}_T) * (\boldsymbol{L}_d) * (\boldsymbol{RE})^4$	-2,79660E-08	1,14747E-10	-8,96456E-06	2,01363E-05
$(\boldsymbol{P}_T) * (\boldsymbol{L}_d)^2$	-1,46229E-01	1,20223E-02	1,02405E+02	2,53432E+02
$(\boldsymbol{P}_T) * (\boldsymbol{L}_d)^2 * (\boldsymbol{RE})$	6,71187E-04	1,97840E-05	4,02570E-01	1,19779E-01
$(\boldsymbol{P}_T) * (\boldsymbol{L}_d)^2 * (\boldsymbol{RE})^2$	-4,84926E-05	6,71564E-07	1,19051E-02	1,29773E-02
$(\boldsymbol{P}_T) * (\boldsymbol{L}_d)^2 * (\boldsymbol{RE})^3$	1,65366E-07	-2,86107E-09	-8,42719E-05	3,70111E-06
$(\boldsymbol{P}_T) * (\boldsymbol{L}_d)^3$	6,64924E-03	-4,97824E-04	-4,07660E+00	-1,31862E+01
$(\boldsymbol{P}_T) * (\boldsymbol{L}_d)^3 * (\boldsymbol{RE})$	7,48254E-05	-1,62939E-06	-2,99184E-02	-2,42821E-02

Table B.4: List of generated coefficients from $\boldsymbol{TS}_{re}$ (2 of 2).

	TRAIN		TPS	
	voltage	current	active power	reactive power
$(\boldsymbol{P}_T) * (\boldsymbol{L}_d)^3 * (\boldsymbol{RE})^2$	3,47258E-07	-5,75451E-09	3,68732E-06	-2,99955E-04
$(\boldsymbol{P}_T) * (\boldsymbol{L}_d)^4$	-1,38934E-04	8,97079E-06	6,88772E-02	1,23523E-01
$(\boldsymbol{P}_T) * (\boldsymbol{L}_d)^4 * (\boldsymbol{RE})$	-1,45425E-06	3,12047E-08	4,28808E-04	7,63550E-04
$(\boldsymbol{P}_T) * (\boldsymbol{L}_d)^5$	1,08922E-06	-5,93732E-08	-4,08375E-04	4,44940E-04
$(\boldsymbol{P}_T)^2$	2,79846E+00	-1,88786E-01	-1,72321E+03	1,01068E+04
$(\boldsymbol{P}_T)^2 * (\boldsymbol{RE})$	1,12955E-02	-4,72397E-04	-1,09598E+00	-1,64146E+01
$(\boldsymbol{P}_T)^2 * (\boldsymbol{RE})^2$	2,08843E-04	-3,84751E-05	-8,69675E-01	-4,77801E-01
$(\boldsymbol{P}_T)^2 * (\boldsymbol{RE})^3$	-5,51224E-06	8,34416E-07	1,90750E-02	1,00864E-02
$(\boldsymbol{P}_T)^2 * (\boldsymbol{RE})^4$	3,93881E-08	-5,23505E-09	-1,17295E-04	-6,65953E-05
$(\boldsymbol{P}_T)^2 * (\boldsymbol{L}_d)$	-7,43160E-01	4,46936E-02	4,11326E+02	1,61605E+03
$(\boldsymbol{P}_T)^2 * (\boldsymbol{L}_d) * (\boldsymbol{RE})$	-2,55761E-03	2,11209E-04	3,05945E+00	4,74547E+00
$(\boldsymbol{P}_T)^2 * (\boldsymbol{L}_d) * (\boldsymbol{RE})^2$	8,51718E-06	-8,21088E-07	-1,98503E-02	-6,75971E-03
$(\boldsymbol{P}_T)^2 * (\boldsymbol{L}_d) * (\boldsymbol{RE})^3$	-6,38325E-08	3,22693E-09	7,29501E-05	3,26546E-05
$(\boldsymbol{P}_T)^2 * (\boldsymbol{L}_d)^2$	5,98397E-02	-3,44243E-03	-3,33273E+01	-5,59544E+01
$(\boldsymbol{P}_T)^2 * (\boldsymbol{L}_d)^2 * (\boldsymbol{RE})$	7,18197E-05	-5,58046E-06	-5,77204E-02	-1,64433E-01
$(\boldsymbol{P}_T)^2 * (\boldsymbol{L}_d)^2 * (\boldsymbol{RE})^2$	-3,32286E-08	1,71929E-08	3,48920E-04	2,66828E-04
$(\boldsymbol{P}_T)^2 * (\boldsymbol{L}_d)^3$	-1,70789E-03	9,39001E-05	9,10257E-01	2,91470E+00
$(\boldsymbol{P}_T)^2 * (\boldsymbol{L}_d)^3 * (\boldsymbol{RE})$	-5,21565E-07	6,73617E-09	-4,35794E-04	9,83758E-04
$(\boldsymbol{P}_T)^2 * (\boldsymbol{L}_d)^4$	1,68477E-05	-8,36852E-07	-7,91076E-03	-2,47250E-02
$(\boldsymbol{P}_T)^3$	-7,31774E-01	5,19840E-02	4,85562E+02	-5,45384E+03
$(\boldsymbol{P}_T)^3 * (\boldsymbol{RE})$	-2,42815E-03	1,87856E-04	2,19708E+00	4,66765E+00
$(\boldsymbol{P}_T)^3 * (\boldsymbol{RE})^2$	1,29566E-06	-2,27047E-07	-4,65786E-03	-5,18315E-03
$(\boldsymbol{P}_T)^3 * (\boldsymbol{RE})^3$	-6,94245E-08	6,52122E-09	1,06582E-04	1,43331E-04
$(\boldsymbol{P}_T)^3 * (\boldsymbol{L}_d)$	1,05319E-01	-7,06367E-03	-6,51435E+01	-3,93184E+02
$(\boldsymbol{P}_T)^3 * (\boldsymbol{L}_d) * (\boldsymbol{RE})$	2,05664E-04	-1,38273E-05	-1,64066E-01	-3,36772E-01
$(\boldsymbol{P}_T)^3 * (\boldsymbol{L}_d) * (\boldsymbol{RE})^2$	3,55088E-07	-2,83721E-08	-4,73316E-04	-6,01989E-04
$(\boldsymbol{P}_T)^3 * (\boldsymbol{L}_d)^2$	-4,99213E-03	3,11101E-04	2,99244E+00	2,35983E+00
$(\boldsymbol{P}_T)^3 * (\boldsymbol{L}_d)^2 * (\boldsymbol{RE})$	-5,13646E-06	3,22861E-07	4,35758E-03	7,49536E-03
$(\boldsymbol{P}_T)^3 * (\boldsymbol{L}_d)^3$	7,36998E-05	-4,24214E-06	-4,17972E-02	-1,27464E-01
$(\boldsymbol{P}_T)^4$	1,00773E-01	-7,36883E-03	-7,05554E+01	1,21132E+03
$(\boldsymbol{P}_T)^4 * (\boldsymbol{RE})$	2,09313E-04	-1,62759E-05	-1,86234E-01	-4,00664E-01
$(\boldsymbol{P}_T)^4 * (\boldsymbol{RE})^2$	3,46901E-07	-3,08794E-08	-4,51038E-04	-6,81742E-04
$(\boldsymbol{P}_T)^4 * (\boldsymbol{L}_d)$	-6,74401E-03	4,82416E-04	4,44203E+00	4,26420E+01
$(\boldsymbol{P}_T)^4 * (\boldsymbol{L}_d) * (\boldsymbol{RE})$	-7,79421E-06	6,05037E-07	7,44780E-03	1,45386E-02
$(\boldsymbol{P}_T)^4 * (\boldsymbol{L}_d)^2$	1,45072E-04	-9,94927E-06	-9,54410E-02	2,64065E-02
$(\boldsymbol{P}_T)^5$	-7,10007E-03	5,26611E-04	5,15649E+00	-1,18710E+02
$(\boldsymbol{P}_T)^5 * (\boldsymbol{RE})$	-7,50099E-06	6,02035E-07	7,10129E-03	1,45313E-02
$(\boldsymbol{P}_T)^5 * (\boldsymbol{L}_d)$	1,61861E-04	-1,22230E-05	-1,12167E-01	-1,69805E+00
$\boldsymbol{X}0$	2,16449E+00	-1,31516E-01	-1,08207E+03	-1,09881E+03
$(\boldsymbol{P}_T)^6$	2,01523E-04	-1,50380E-05	-1,50226E-01	4,25434E+00
$(\boldsymbol{L}_d)^6$	6,12608E-07	-3,11098E-08	-3,21376E-04	-1,03787E-03
$(\boldsymbol{RE})^6$	1,34539E-07	-1,74595E-09	-5,00745E-05	-1,57101E-06

B.2.3 Line Capacity

Regarding the line capacity, this results in the coefficients in Table B.5 and Table B.6.

Table B.5: List of generated coefficients from $\boldsymbol{TS}_{lc}$ (1 of 2)

	TRAIN		TPS	
	voltage	current	active power	reactive power
$(\boldsymbol{LC})$	-2,34185E-03	2,48711E-04	1,99419E+00	3,14582E+02
$(\boldsymbol{LC})^2$	-1,10130E-03	8,62501E-05	1,26235E+00	-5,43689E+01
$(\boldsymbol{LC})^3$	8,14875E-05	-6,51409E-06	-9,58520E-02	5,44468E+00
$(\boldsymbol{LC})^4$	-2,80181E-06	2,25314E-07	3,32162E-03	-1,96696E-01
$(\boldsymbol{LC})^5$	4,59262E-08	-3,69271E-09	-5,44784E-05	3,16165E-03
$(\boldsymbol{L}_d)$	-9,02513E-01	5,76946E-02	2,92692E+02	2,36892E+03
$(\boldsymbol{L}_d) * (\boldsymbol{LC})$	4,56109E-03	-4,27650E-04	-5,33818E+00	-3,73136E+02
$(\boldsymbol{L}_d) * (\boldsymbol{LC})^2$	-1,15293E-05	1,33131E-06	2,15544E-02	6,83385E+00
$(\boldsymbol{L}_d) * (\boldsymbol{LC})^3$	-1,06712E-06	8,04656E-08	1,16019E-03	-4,86767E-02
$(\boldsymbol{L}_d) * (\boldsymbol{LC})^4$	2,36204E-08	-1,92278E-09	-2,81554E-05	-4,25901E-04
$(\boldsymbol{L}_d) * (\boldsymbol{LC})^5$	-1,61108E-10	1,37831E-11	2,03674E-07	7,10723E-06
$(\boldsymbol{L}_d)^2$	1,36201E-01	-1,16376E-02	-4,21324E+01	-5,87396E+02
$(\boldsymbol{L}_d)^2 * (\boldsymbol{LC})$	8,00103E-04	5,77075E-05	7,22532E-01	1,33741E+01
$(\boldsymbol{L}_d)^2 * (\boldsymbol{LC})^2$	5,00044E-06	-4,32231E-07	-6,49835E-03	2,76351E-01
$(\boldsymbol{L}_d)^2 * (\boldsymbol{LC})^3$	-1,23496E-08	1,32853E-09	2,03200E-05	-6,21105E-03
$(\boldsymbol{L}_d)^2 * (\boldsymbol{LC})^4$	-2,41650E-11	-5,98686E-13	-1,51335E-08	4,42123E-05
$(\boldsymbol{L}_d)^3$	-8,17350E-03	1,15315E-03	2,58065E+00	6,46659E+01
$(\boldsymbol{L}_d)^3 * (\boldsymbol{LC})$	3,56268E-05	-2,85579E-06	-3,47755E-02	-4,51091E-01
$(\boldsymbol{L}_d)^3 * (\boldsymbol{LC})^2$	-2,25408E-07	1,90136E-08	2,88350E-04	-5,88692E-03
$(\boldsymbol{L}_d)^3 * (\boldsymbol{LC})^3$	3,52779E-10	-2,95133E-11	-4,35270E-07	6,33482E-05
$(\boldsymbol{L}_d)^4$	2,00780E-04	-6,10506E-05	-7,36226E-02	-3,56900E+00
$(\boldsymbol{L}_d)^4 * (\boldsymbol{LC})$	-7,55146E-07	5,69511E-08	6,49641E-04	1,25369E-02
$(\boldsymbol{L}_d)^4 * (\boldsymbol{LC})^2$	3,23395E-09	-2,67068E-10	-4,00743E-06	3,00771E-05
$(\boldsymbol{L}_d)^5$	-1,04154E-06	1,62925E-06	8,27478E-04	9,76355E-02
$(\boldsymbol{L}_d)^5 * (\boldsymbol{LC})$	5,08439E-09	-3,48707E-10	-3,28380E-06	-1,46939E-04
$(\boldsymbol{P}_T)$	-2,95100E+00	1,54115E-01	1,05974E+03	1,35840E+03
$(\boldsymbol{P}_T) * (\boldsymbol{LC})$	8,29337E-03	-7,57692E-04	-8,58388E+00	-3,51535E+02
$(\boldsymbol{P}_T) * (\boldsymbol{LC})^2$	1,07047E-04	-7,05915E-06	-9,93874E-02	-6,87093E+01
$(\boldsymbol{P}_T) * (\boldsymbol{LC})^3$	-5,00884E-06	3,76601E-07	5,46243E-03	7,05088E-01
$(\boldsymbol{P}_T) * (\boldsymbol{LC})^4$	7,35779E-08	-5,85199E-09	-8,53756E-05	7,17568E-04
$(\boldsymbol{P}_T) * (\boldsymbol{LC})^5$	-3,86866E-10	3,28613E-11	4,83135E-07	-5,39519E-05
$(\boldsymbol{P}_T) * (\boldsymbol{L}_d)$	1,03384E+00	-6,02857E-02	-3,92642E+02	-8,50099E+02
$(\boldsymbol{P}_T) * (\boldsymbol{L}_d) * (\boldsymbol{LC})$	-3,51747E-03	2,80274E-04	3,30691E+00	-7,47526E+01
$(\boldsymbol{P}_T) * (\boldsymbol{L}_d) * (\boldsymbol{LC})^2$	1,47848E-06	-1,54518E-07	-2,60304E-03	-4,14706E+00
$(\boldsymbol{P}_T) * (\boldsymbol{L}_d) * (\boldsymbol{LC})^3$	9,17776E-09	-3,35829E-10	-2,20820E-06	4,17021E-02
$(\boldsymbol{P}_T) * (\boldsymbol{L}_d) * (\boldsymbol{LC})^4$	1,89176E-11	-4,30931E-12	-9,03908E-08	-2,45232E-04
$(\boldsymbol{P}_T) * (\boldsymbol{L}_d)^2$	-8,83234E-02	5,66964E-03	3,93533E+01	7,54916E+00
$(\boldsymbol{P}_T) * (\boldsymbol{L}_d)^2 * (\boldsymbol{LC})$	3,05081E-04	-2,50394E-05	-2,85196E-01	-7,11252E+00
$(\boldsymbol{P}_T) * (\boldsymbol{L}_d)^2 * (\boldsymbol{LC})^2$	-1,32397E-07	1,15045E-08	1,84271E-04	1,91988E-02
$(\boldsymbol{P}_T) * (\boldsymbol{L}_d)^2 * (\boldsymbol{LC})^3$	-3,37414E-12	-4,78102E-13	-3,59393E-09	-2,16132E-04
$(\boldsymbol{P}_T) * (\boldsymbol{L}_d)^3$	3,79514E-03	-2,08468E-04	-1,67691E+00	-1,58693E+00
$(\boldsymbol{P}_T) * (\boldsymbol{L}_d)^3 * (\boldsymbol{LC})$	-9,54207E-06	6,39455E-07	7,19234E-03	8,63198E-02

Table B.6: List of generated coefficients from $\boldsymbol{TS}_{lc}$ (2 of 2)

	TRAIN		TPS	
	voltage	current	active power	reactive power
$(\boldsymbol{P}_T) * (\boldsymbol{L}_d)^3 * (\boldsymbol{LC})^2$	3,21602E-09	-2,72021E-10	-4,38569E-06	-1,88856E-04
$(\boldsymbol{P}_T) * (\boldsymbol{L}_d)^4$	-6,77542E-05	3,00787E-06	3,47390E-02	-3,86353E-02
$(\boldsymbol{P}_T) * (\boldsymbol{L}_d)^4 * (\boldsymbol{LC})$	9,88682E-08	-5,65848E-09	-5,87538E-05	-4,70776E-04
$(\boldsymbol{P}_T) * (\boldsymbol{L}_d)^5$	4,00961E-07	-1,13535E-08	-3,15143E-04	1,25457E-03
$(\boldsymbol{P}_T)^2$	1,68993E+00	-1,07145E-01	-7,65814E+02	6,72708E+03
$(\boldsymbol{P}_T)^2 * (\boldsymbol{LC})$	-2,67421E-03	2,63770E-04	2,86290E+00	1,22340E+03
$(\boldsymbol{P}_T)^2 * (\boldsymbol{LC})^2$	4,99057E-06	-7,02183E-07	-1,11999E-02	2,23544E+01
$(\boldsymbol{P}_T)^2 * (\boldsymbol{LC})^3$	2,60557E-07	-1,72338E-08	-2,47575E-04	-1,75336E-01
$(\boldsymbol{P}_T)^2 * (\boldsymbol{LC})^4$	-2,03939E-09	1,38022E-10	1,98199E-06	8,14707E-04
$(\boldsymbol{P}_T)^2 * (\boldsymbol{L}_d)$	-4,07014E-01	2,30878E-02	1,56026E+02	1,33555E+03
$(\boldsymbol{P}_T)^2 * (\boldsymbol{L}_d) * (\boldsymbol{LC})$	6,58148E-04	-5,60399E-05	-6,44313E-01	7,78479E+01
$(\boldsymbol{P}_T)^2 * (\boldsymbol{L}_d) * (\boldsymbol{LC})^2$	-1,43095E-07	1,34111E-08	2,23297E-04	4,31968E-01
$(\boldsymbol{P}_T)^2 * (\boldsymbol{L}_d) * (\boldsymbol{LC})^3$	-1,47535E-09	1,15174E-10	1,71753E-06	-6,34759E-04
$(\boldsymbol{P}_T)^2 * (\boldsymbol{L}_d)^2$	3,18477E-02	-1,68193E-03	-1,10696E+01	3,59551E+00
$(\boldsymbol{P}_T)^2 * (\boldsymbol{L}_d)^2 * (\boldsymbol{LC})$	-3,53249E-05	2,84927E-06	3,33498E-02	9,22191E-01
$(\boldsymbol{P}_T)^2 * (\boldsymbol{L}_d)^2 * (\boldsymbol{LC})^2$	-2,25145E-09	1,76762E-10	2,19001E-06	5,15719E-04
$(\boldsymbol{P}_T)^2 * (\boldsymbol{L}_d)^3$	-8,88293E-04	4,41597E-05	2,76944E-01	8,98249E-01
$(\boldsymbol{P}_T)^2 * (\boldsymbol{L}_d)^3 * (\boldsymbol{LC})$	5,86783E-07	-4,54655E-08	-5,49549E-04	-4,30837E-03
$(\boldsymbol{P}_T)^2 * (\boldsymbol{L}_d)^4$	8,54196E-06	-3,79579E-07	-2,08838E-03	-9,96710E-03
$(\boldsymbol{P}_T)^3$	-4,35476E-01	2,87440E-02	2,13557E+02	-8,09568E+03
$(\boldsymbol{P}_T)^3 * (\boldsymbol{LC})$	2,86797E-04	-3,26168E-05	-3,02830E-01	-4,89519E+02
$(\boldsymbol{P}_T)^3 * (\boldsymbol{LC})^2$	-2,21053E-06	2,01970E-07	3,06200E-03	-2,38826E+00
$(\boldsymbol{P}_T)^3 * (\boldsymbol{LC})^3$	-1,06268E-09	3,13285E-11	4,15879E-07	5,47441E-03
$(\boldsymbol{P}_T)^3 * (\boldsymbol{L}_d)$	5,54291E-02	-3,52918E-03	-2,33094E+01	-5,36920E+02
$(\boldsymbol{P}_T)^3 * (\boldsymbol{L}_d) * (\boldsymbol{LC})$	-4,53808E-05	4,08165E-06	4,49026E-02	-1,35568E+01
$(\boldsymbol{P}_T)^3 * (\boldsymbol{L}_d) * (\boldsymbol{LC})^2$	2,14201E-08	-1,79235E-09	-2,77126E-05	-2,13479E-02
$(\boldsymbol{P}_T)^3 * (\boldsymbol{L}_d)^2$	-2,61398E-03	1,54640E-04	1,12317E+00	-2,30702E+00
$(\boldsymbol{P}_T)^3 * (\boldsymbol{L}_d)^2 * (\boldsymbol{LC})$	1,14255E-06	-1,03302E-07	-1,19889E-03	-4,22213E-02
$(\boldsymbol{P}_T)^3 * (\boldsymbol{L}_d)^3$	3,71293E-05	-2,03162E-06	-1,47351E-02	-3,59939E-02
$(\boldsymbol{P}_T)^4$	5,96644E-02	-3,98418E-03	-3,10442E+01	2,52955E+03
$(\boldsymbol{P}_T)^4 * (\boldsymbol{LC})$	-7,14022E-06	1,40031E-06	6,06004E-03	6,58984E+01
$(\boldsymbol{P}_T)^4 * (\boldsymbol{LC})^2$	1,08298E-07	-9,64609E-09	-1,45778E-04	9,53506E-02
$(\boldsymbol{P}_T)^4 * (\boldsymbol{L}_d)$	-3,40675E-03	2,33784E-04	1,51074E+00	7,41745E+01
$(\boldsymbol{P}_T)^4 * (\boldsymbol{L}_d) * (\boldsymbol{LC})$	9,61827E-07	-8,91011E-08	-8,66580E-04	6,92180E-01
$(\boldsymbol{P}_T)^4 * (\boldsymbol{L}_d)^2$	7,41120E-05	-4,80672E-06	-3,34504E-02	1,43328E-01
$(\boldsymbol{P}_T)^5$	-4,20868E-03	2,80095E-04	2,28620E+00	-3,01721E+02
$(\boldsymbol{P}_T)^5 * (\boldsymbol{LC})$	-2,53588E-07	-6,51917E-09	3,64888E-04	-2,90381E+00
$(\boldsymbol{P}_T)^5 * (\boldsymbol{L}_d)$	7,79171E-05	-5,70167E-06	-3,58640E-02	-3,34571E+00
$\boldsymbol{X}0$	1,46988E+00	-8,51228E-02	-5,22166E+02	-3,00541E+03
$(\boldsymbol{P}_T)^6$	1,19915E-04	-7,90274E-06	-6,72587E-02	1,22995E+01
$(\boldsymbol{L}_d)^6$	-1,87929E-08	-1,70745E-08	-5,79708E-07	-1,04014E-03
$(\boldsymbol{LC})^6$	-2,84400E-10	2,28042E-11	3,36471E-07	-1,87722E-05

APPENDIX C

Train Dynamic Model Validation Results

In chapter 4 is presented a multi-train simulation tool to generate the information of each train dynamic movement and energy consumption.

The extensive validation through real measurements provided by a partner company of a railway main operator, of the train **dynamic** model is presented in this appendix.

C.1 Introduction

The validation of the dynamic model is made with a dataset of measurements for randomly selected 8 journeys, with the validation methodology presented in Fig. C.1.

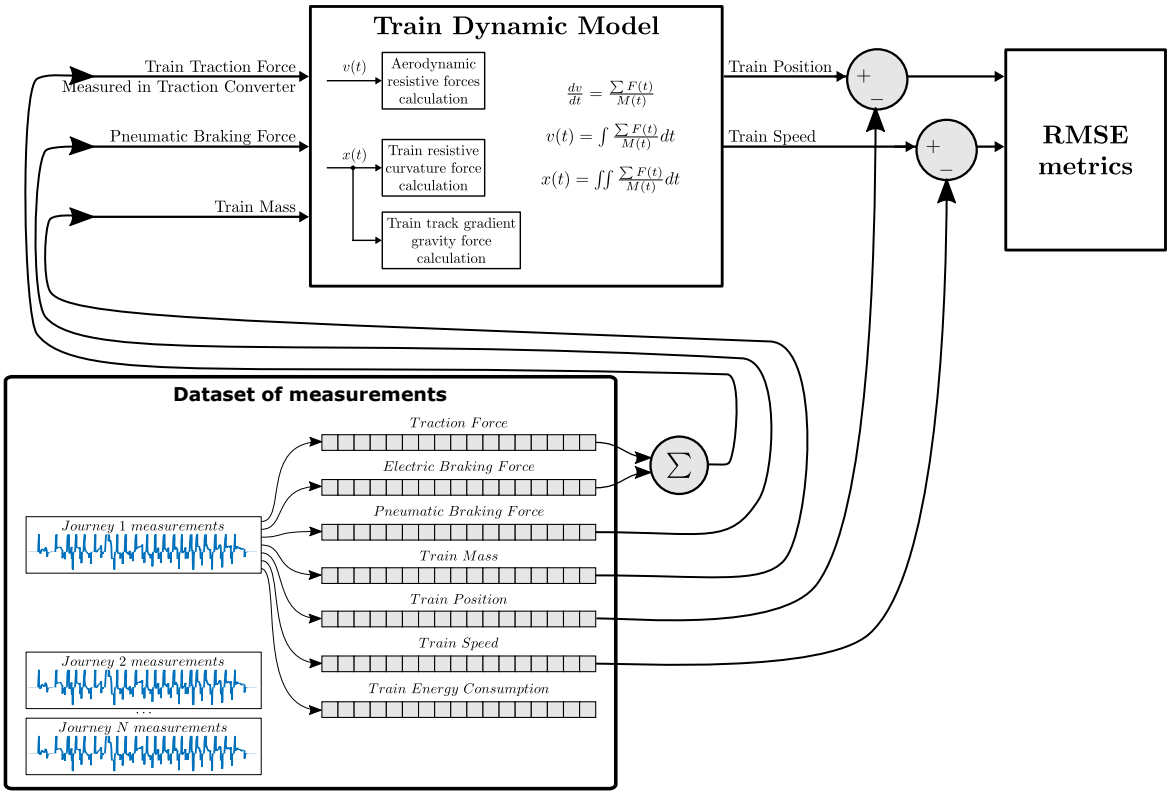

Figure C.1: Illustration of the methodology for the model evaluation.

From the equation in (C.1), the train dynamic model of the Fig. C.1 can be evaluated by feeding the known variables — $\mu_f\ F_T$, $\mu_b\ F_B$ and M — and compare it with the unknown variables — $^{dv}/_{dt}$, $v(t)$, $x(t)$ of the dynamic model.

$$\frac{dv}{dt} = \frac{\mu_f\ F_T(v) - \mu_b\ F_B(v) - w(v) - g_1(x) - g_2(x)}{M} \tag{C.1}$$

Then, the uncertainty of the system lies in the estimation of the track gradient and the resistive curvature forces.

C.2 Validation of the Dynamic Train Model

In this appendix, the validation of the dynamic train model starts with a baseline situation, where the track gradient and the resistive curvature forces are not properly estimated.

As illustrated in Fig. C.1, the real measurements are compared with the result from the model. These comparisons are presented in forms of graphs and, from the differences between models, a metric is obtained. This Root Mean Square Error (RMSE) metric comprises absolute and relative values, for the three estimated values of the model.

C.2.1 Basic Dynamic Train Model

The basic model is evaluated without the curving resistive force and with a constant gravity force (obtained by the slope between the starting and final stations and the overall distance).

In Fig. C.2 and in Fig. C.3 is presented the difference between the measurements and the model results regarding the train speed.

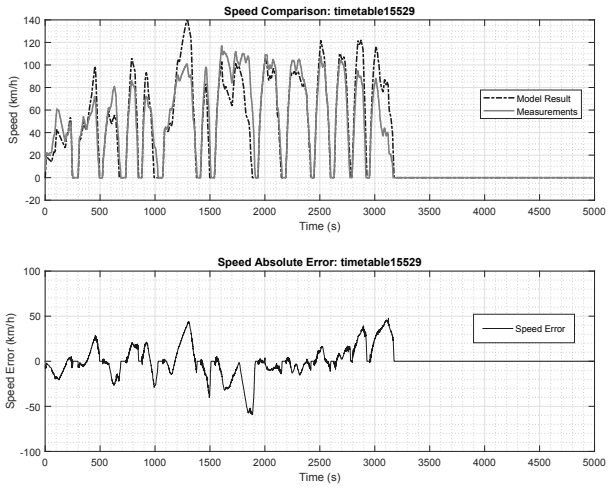

Figure C.2: Speed comparison of timetable with best position difference.

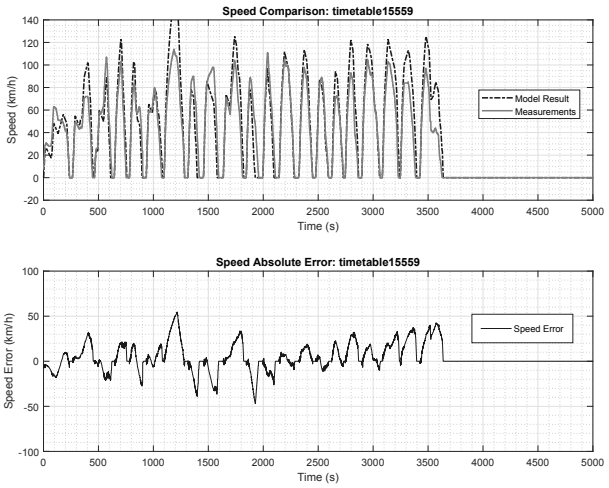

Figure C.3: Speed comparison of timetable with worst position difference.

Specifically, the modelled speed of the train can reach values above the maximum speed (since the model does not consider steep grades or closed curves).

Furthermore, in Fig.C.4 and in Fig. C.5 are presented the differences between the measurements and the model results regarding the train position.

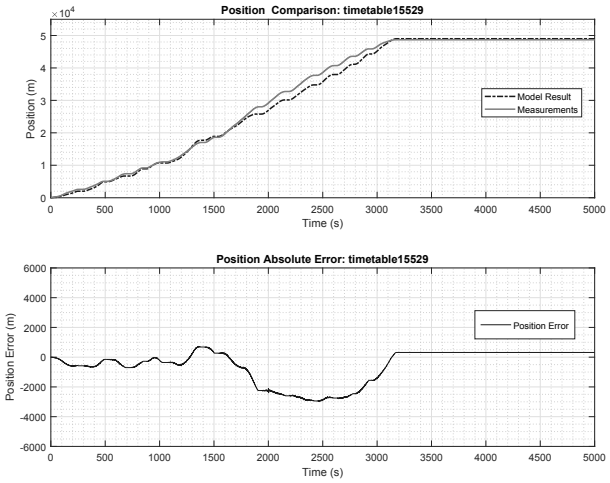

Figure C.4: Position comparison of timetable with best position difference.

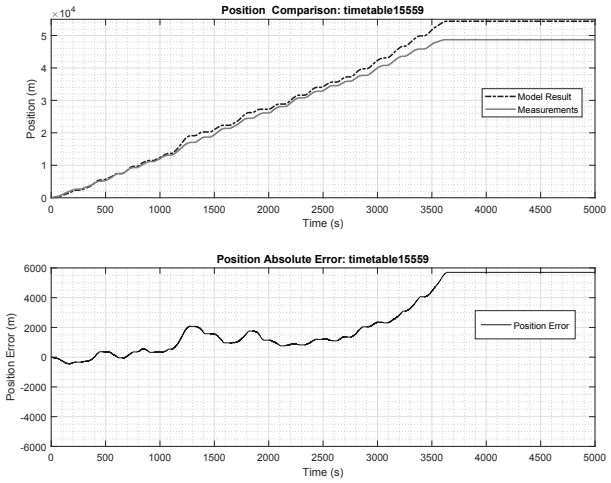

Figure C.5: Position comparison of timetable with worst position error.

In addition, in the train position errors presented above is shown that, by wrongly estimating the speed profile, the train can stop further away from the last station, as visible in Fig. C.5. As already described, it was performed a statistic evaluation of the RMSE on the difference between (i) the speed; and (ii) the position. Specifically, the train speed only has absolute RMSE value; The train position relative error is a percentage of the absolute value and length of the line;

From the Table C.1 it was obtained 5.30 km/h average in absolute RMSE for the speed difference and 3.48 % average for the position difference in relative RMSE.

Table C.1: Evaluation of basic dynamic train model

timetable number	**Speed difference** rmse (km/h)	**Position difference** rmse (m)	rmse (%)
15513	4,96	1172	2,4
15527	6,21	2691	5,5
15529	5,00	651	1,3
15533	6,07	1344	2,8
15535	4,90	904	1,9
15549	4,64	1110	2,3
15557	4,98	1904	3,9
15559	5,66	3779	7,8
Average	**5,30**	**1694**	**3,48**

C.2.2 Variable Gravity Force Dynamic Train Model

In the previously evaluated basic model, the gravity force was fixed to be constant. In this second train dynamic model, the gravity force in train is variable and function of the track gradient, where each position of the train has a specific force.

In Fig. C.6 is illustrated the gravity force that affects a train, as function of the line absolute position (where the force is given in Newton per tonne unit).

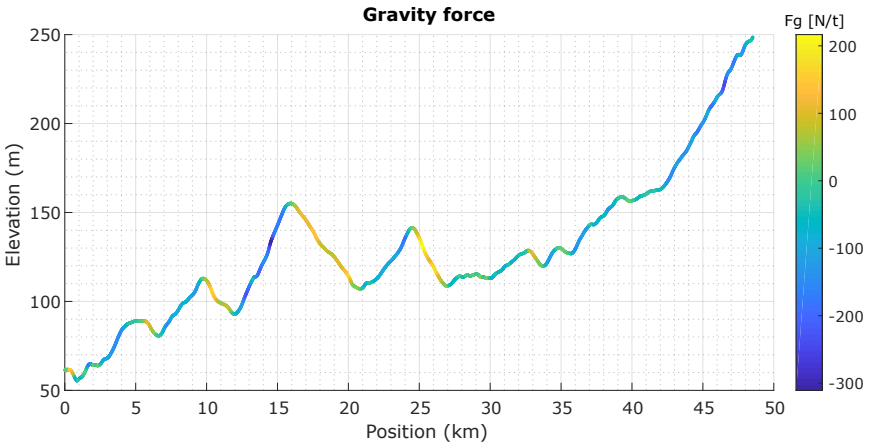

Figure C.6: Elevation and gravity force as function of the line distance.

In Fig. C.7 and in Fig. C.8 are presented the differences between the measurements and the model results regarding the train speed for this second model.

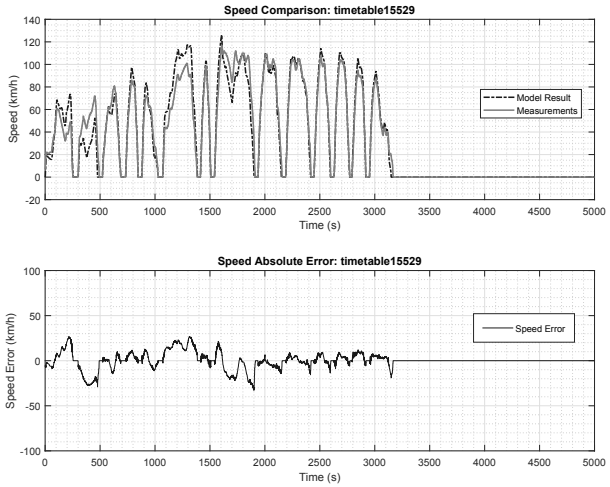

Figure C.7: Speed comparison of timetable with best position difference.

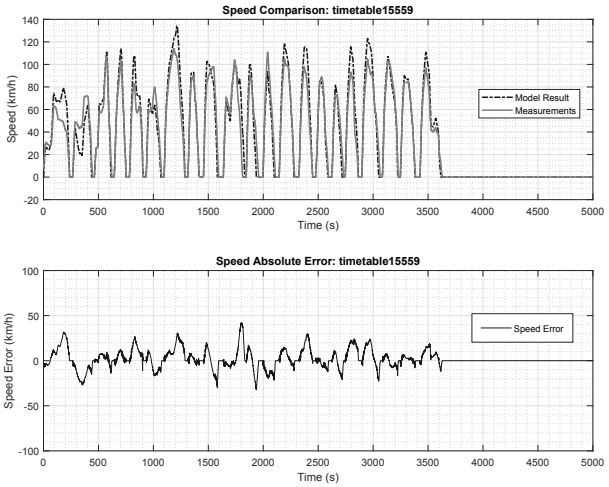

Figure C.8: Speed comparison of timetable with worst position difference.

Specifically, it is visible a reduction of the error when compared to the Fig. C.2 and Fig. C.3. This will contribute to a reduction of the position errors, as illustrated in Fig. C.9 and in Fig. C.10.

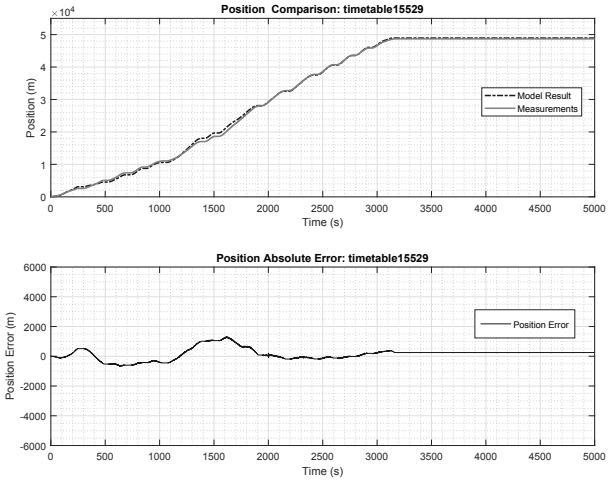

Figure C.9: Position comparison of timetable with best position difference.

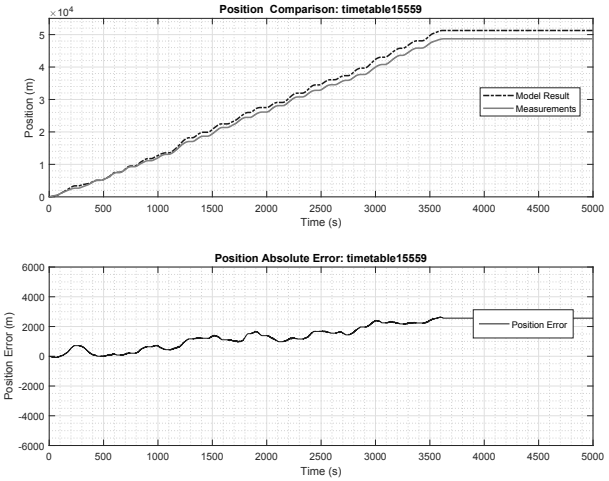

Figure C.10: Position comparison of timetable with worst position difference.

A statistical evaluation is performed, similarly to previous subsection. From the Table C.2 is obtained 3,25 km/h average in absolute RMSE for the speed difference and 1,72 % average in relative RMSE for the position difference.

Table C.2: Evaluation of the variable gravity force dynamic train model

timetable number	**Speed difference** rmse (km/h)	**Position difference** rmse (m)	rmse (%)
15513	3,32	430	0,9
15527	4,80	1342	2,8
15529	3,03	297	0,6
15533	2,39	491	1,0
15535	3,59	828	1,7
15549	2,52	497	1,0
15557	2,57	869	1,8
15559	3,79	1951	4,0
Average	**3,25**	**838**	**1,72**

C.2.3 Variable Gravity and Resistive Curvature Forces Dynamic Train Model

The final enhancement on the train dynamic model is in the estimation of the forces affecting the train movement related to the track curvature.

In Fig. C.11 is illustrated the variation of this force as function of the geographic characteristics of the line.

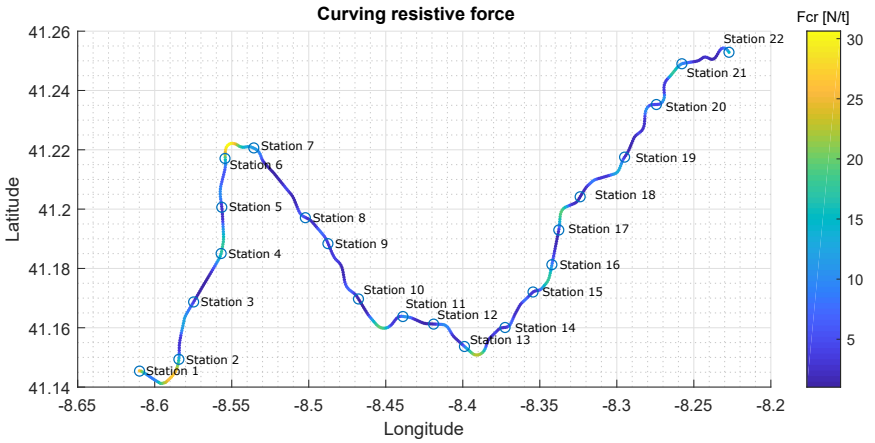

Figure C.11: Absolute position and curvature resistive force.

Therefore, this force of Fig. C.11 is also function of the train position (given in Newton per tonne unit).

In Fig. C.12 and in Fig. C.13 is presented the difference between the measurements and the model results regarding the train speed for this last model.

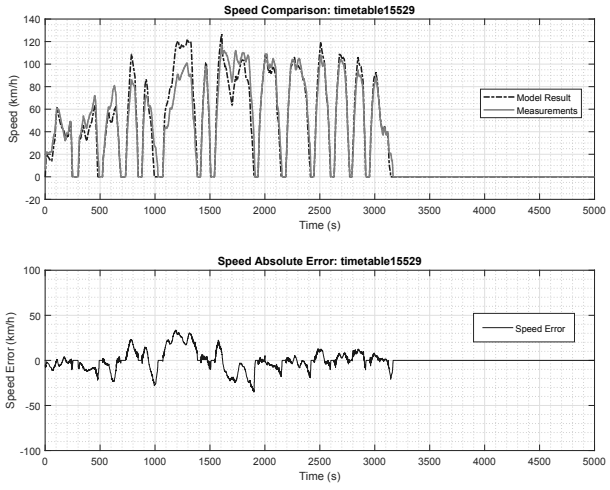

Figure C.12: Speed comparison of timetable with best position difference.

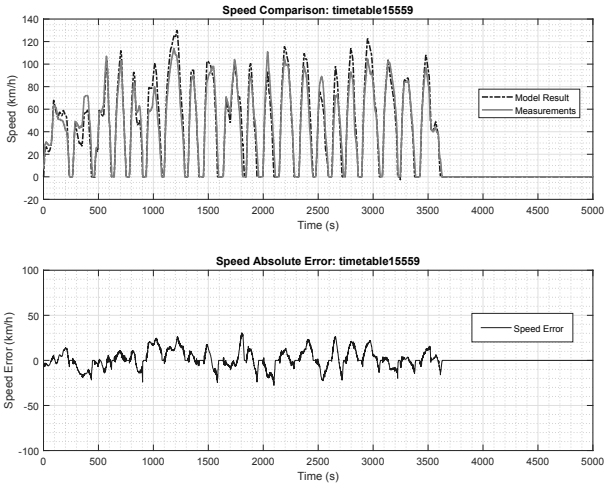

Figure C.13: Speed comparison of timetable with worst position difference.

Furthermore, in Fig. C.14 and in Fig. C.15 is presented the difference between the

measurements and the model results regarding the train position.

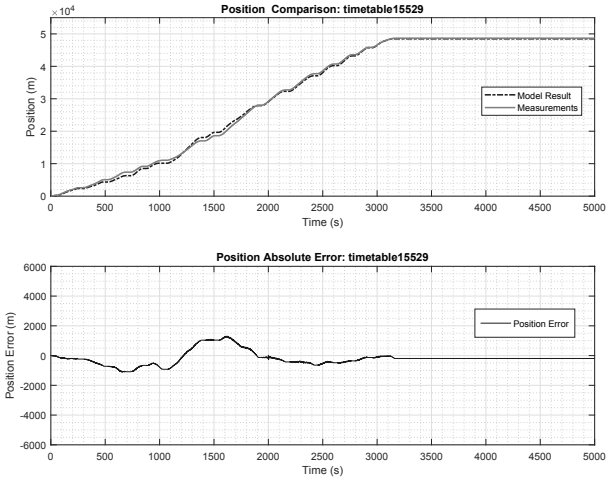

Figure C.14: Position comparison of timetable with best position difference.

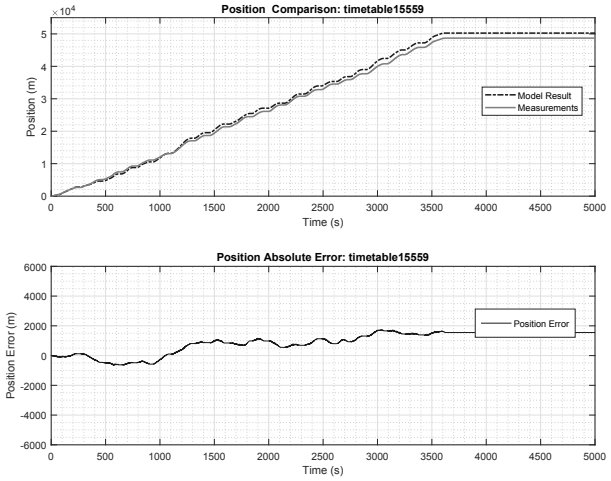

Figure C.15: Position comparison of timetable with worst position difference.

A statistical evaluation is performed, similarly to previous section. From the Table C.3 was obtained 3,04 km/h average in absolute RMSE for the speed difference and 1,03 % average in relative RMSE for the position difference.

Table C.3: Evaluation of the variable gravity and curvature resistive force dynamic train model

timetable number	**Speed difference** rmse (km/h)	**Position difference** rmse (m)	rmse (%)
15513	2,68	366	0,8
15527	3,89	559	1,2
15529	3,26	318	0,7
15533	3,25	477	1,0
15535	2,90	292	0,6
15549	2,69	445	0,9
15557	2,26	319	0,7
15559	3,38	1224	2,5
Average	**3,04**	**500**	**1,03**

APPENDIX D

Train Energy Model Validation Results

In chapter 4 is presented a multi-train simulation tool to generate the information of each train dynamic movement and energy consumption.

In this appendix is presented an extensive validation through real measurements provided by a partner company of a railway main operator, of the train **energy** model.

D.1 Introduction

The validation of the energy model is made with a dataset of measurements for randomly selected 8 journeys, with the validation methodology presented in Fig. D.1.

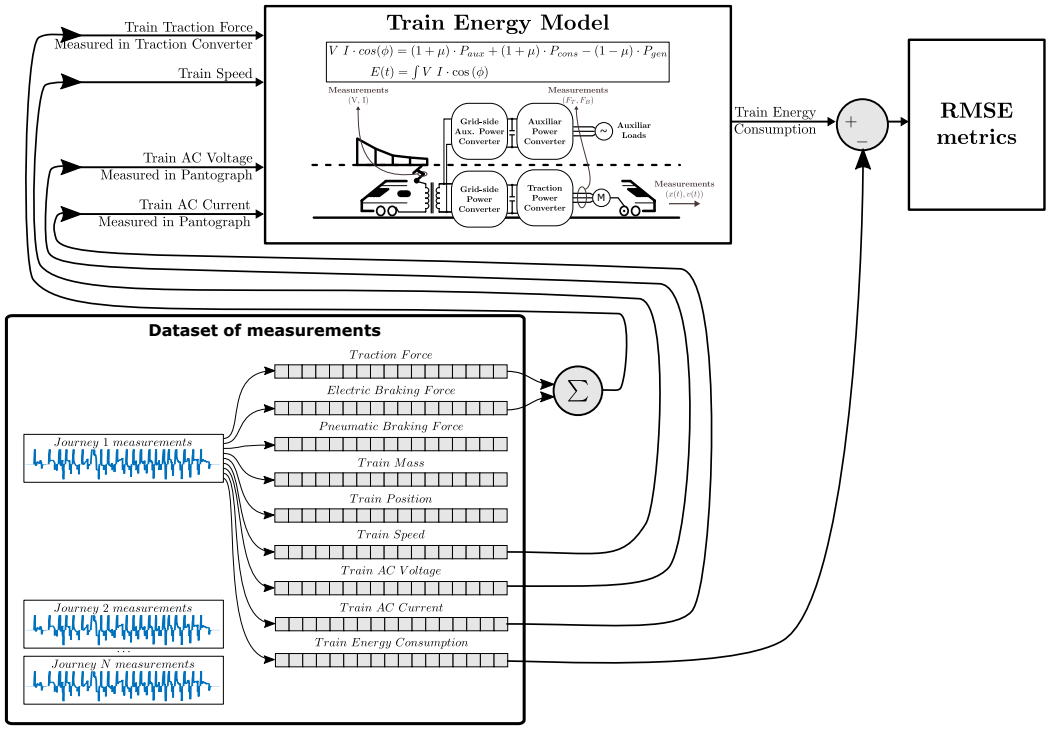

Figure D.1: Illustration of the methodology for the energy model evaluation.

Similarly to the validation methodology presented in the appendix C, in this model,

firstly is started to estimate the power consumption associated to the auxiliary services and then, based on the comparison error, the train efficiency is better estimated.

Therefore, two energy models will be evaluated: (i) the comparison of an energy model with and without auxiliary systems; and (ii), the inclusion of a non-unitary power efficiency.

D.2 Methodology to Obtain an Energy Model with Unitary Efficiency

In this section is evaluated the inclusion of auxiliary systems in a energy model with unitary efficiency.

From the specification of the case study train, the auxiliary power system is composed by a three-phase output power converter of 210 kVA and is responsible for powering the auxiliary loads such as: air-conditioning, heating system, lighting, doors, control systems, backup battery, among others.

However, this power consumption is not constant: it depends on several operation conditions and requirements. Therefore, due to this uncertainty, the power consumption associated to the auxiliary systems needs to be estimated.

One approach to obtain a good estimate of the power consumption of auxiliary systems is with the evaluation of the train total power consumption when no forces are applied to the motors. In Fig. D.2 is evaluated the train power for different traction forces and different train speeds.

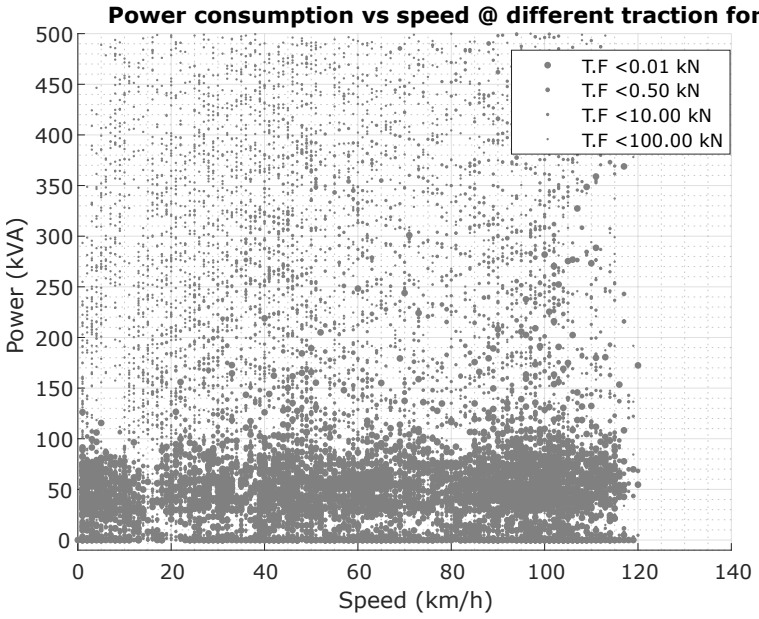

Figure D.2: Relation of power consumption and train speed with different traction forces.

The train total power of Fig. D.2 was obtained from the product of the voltage and current measurements (it was considered an unitary power factor for simplicity). This has

resulted of a total power consumption associated to the auxiliary systems to be invariant with the train speed, and limited to a maximum of 100 kVA when there is no traction (or braking) forces.

Furthermore, with this unitary efficiency model, it was evaluated the inclusion of the auxiliary systems in the train energy model, with a fixed power consumption of 100 kW. This results in Table D.1, where the RMSE error of the energy consumption has reduced from 23,52 % to 4,78 %.

Table D.1: Comparison of energy consumption (with and without auxiliary services)

timetable number	**Consumption difference without auxiliary power**		**Consumption difference with auxiliary power**	
	rmse (kWh)	rmse (%)	rmse (kWh)	rmse (%)
15513	76,78	26,85	14,99	5,24
15527	67,43	26,7	11,15	4,4
15529	42,08	18,5	25,84	11,3
15533	55,68	21,2	11,64	4,4
15535	54,80	20,8	11,46	4,3
15549	57,37	21,1	15,29	5,6
15557	64,26	25,2	3,63	1,4
15559	76,30	27,9	3,88	1,4
Average	**61,84**	**23,52**	**12,23**	**4,78**

In Fig. D.3 and in Fig. D.4 are presented two examples of the evaluation of the energy model.

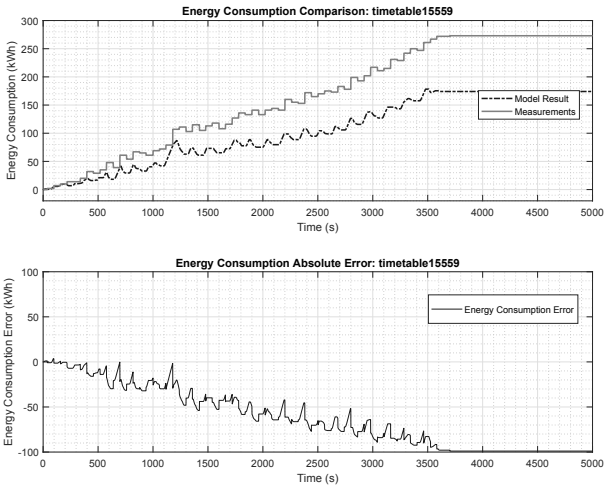

Figure D.3: Energy consumption comparison without auxiliary services.

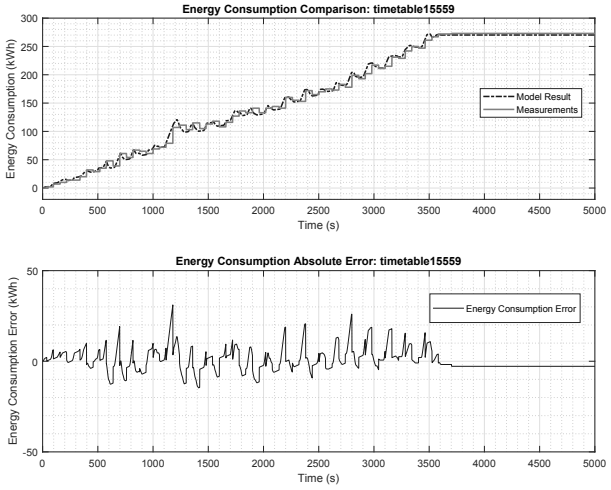

Figure D.4: Energy consumption comparison with auxiliary services.

D.3 Methodology to Obtain an Energy Model that Includes Efficiency

Similarly to the previous evaluation, in this section is proposed a methodology to obtain the value for the train efficiency. The first step is to use the measurements of the dataset, as illustrated in Fig. D.1, to evaluate the RMSE for different efficiency values. Then, the μ factor corresponding to the lower value of RMSE is selected to enhance the train electric model.

As presented in Fig. D.5, when considering non-unitary efficiency, the electric schematic of the train must be taken into consideration. Despite the efficiency of the system can be separated — the traction transformer efficiency, η_1, the traction/auxiliary power converters, (η_2 and η_3) — a generic η factor for the efficiency was established. In addition, the power factor was considered to be unitary.

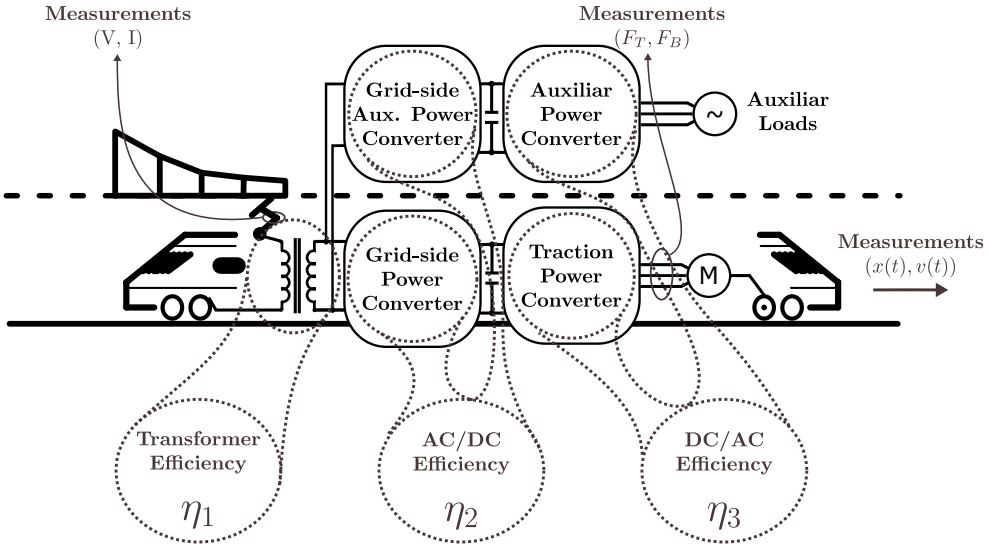

Figure D.5: Train energy model.

Considering the above issues, the overall losses factor can be obtained using the equation in (D.1):

$$V\ I \cdot cos(\phi) = (1+\xi) \cdot P_{cons} - (1-\xi) \cdot P_{gen} + (1+\xi) \cdot P_{aux} \tag{D.1}$$

where

$$P_{cons} = \begin{cases} F_T \cdot v & F_T > 0 \\ 0 & otherwise \end{cases} \tag{D.2}$$

$$P_{gen} = \begin{cases} F_T \cdot v & F_T < 0 \\ 0 & otherwise \end{cases} \tag{D.3}$$

$$P_{aux} = \sum_{a=1}^{N} P_a \approx 100\ kW \tag{D.4}$$

In Fig. D.6 is presented the variation of the RMSE value for the active power, where is compared the left and right sides of the equation in (D.1).

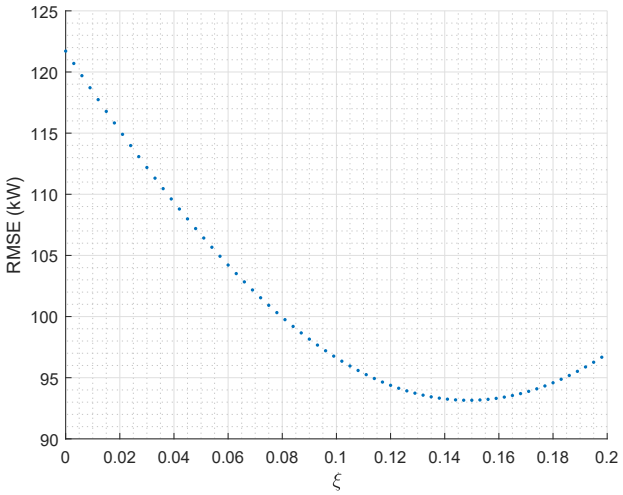

Figure D.6: Absolute train power consumption RMSE for different ξ.

Specifically, for a $\xi = 0.15$, the global efficiency is $\eta \approx 87\%$ and the difference between the product of the voltage and current is smaller when compared to the estimated power.

Furthermore, the final optimization of the train energy model will include a non-unitary energy efficiency. In Table D.2 is presented the final validation of the compliance of the energy model with the field measurements. It can be verified that a slightly global reduction of the RMSE between the unitary and the non-unitary efficiency models from 4.78 % to 4.31 %.

Table D.2: Comparison of energy consumption (with and without auxiliary services and efficiency)

timetable number	**Consumption difference without aux**		**Consumption difference with aux**		**Consumption difference with aux and μ**	
	rmse (kWh)	rmse (%)	rmse (kWh)	rmse (%)	rmse (kWh)	rmse (%)
15513	76,78	26,85	14,99	5,24	30,37	10,62
15527	67,43	26,7	11,15	4,4	12,76	5,0
15529	42,08	18,5	25,84	11,3	9,28	4,1
15533	55,68	21,2	11,64	4,4	5,61	2,1
15535	54,80	20,8	11,46	4,3	6,56	2,5
15549	57,37	21,1	15,29	5,6	6,40	2,4
15557	64,26	25,2	3,63	1,4	8,87	3,5
15559	76,30	27,9	3,88	1,4	11,79	4,3
Average	**61,84**	**23,52**	**12,23**	**4,78**	**11,45**	**4,31**

APPENDIX E

PSSA-rail Results for Case Study Line II

In chapter 5 was presented the power system state analyser (PSSA-rail) tool. To highlight the flexibility and capabilities of the proposed tool, the PSSA-rail was adapted to contemplate the data from a second case study railway line, in addition to the demonstration of PSSA-rail in chapter 5, with the energy information data generated by the MTS tool of chapter 4.

This second case study, presented in this appendix, uses the energy information data that was generated by a proprietary research and planning tool, provided by one railway undertaking company.

In this appendix are presented the relevant output results of the PSSA-rail tool, for this second case study.

E.1 Introduction

Similarly to the case study line I, in chapter 5, the first step for this second case study line is to prepare the input data for all 252 train journeys, following:

$$Info\ T_{1,..,252} = \begin{cases} Dynamics\ Data = \begin{cases} x(t),\ v(t) \\ F_T(t),\ F_B(t) \end{cases} \\ Energy\ Data = \begin{cases} P(t),\ Q(t) \\ E(t) \end{cases} \end{cases} \tag{E.1}$$

The $Info\ T_{1,..,252}$ database used in this appendix was provided by the proprietary research and planning tool, as well as the geographical architecture of the infrastructure power system.

Thus, this demonstration of the PSSA-rail in this appendix will use the train information generated by the proprietary research and planning tool in combination with the parameters of the respective railway line, as illustrated in Fig. E.1.

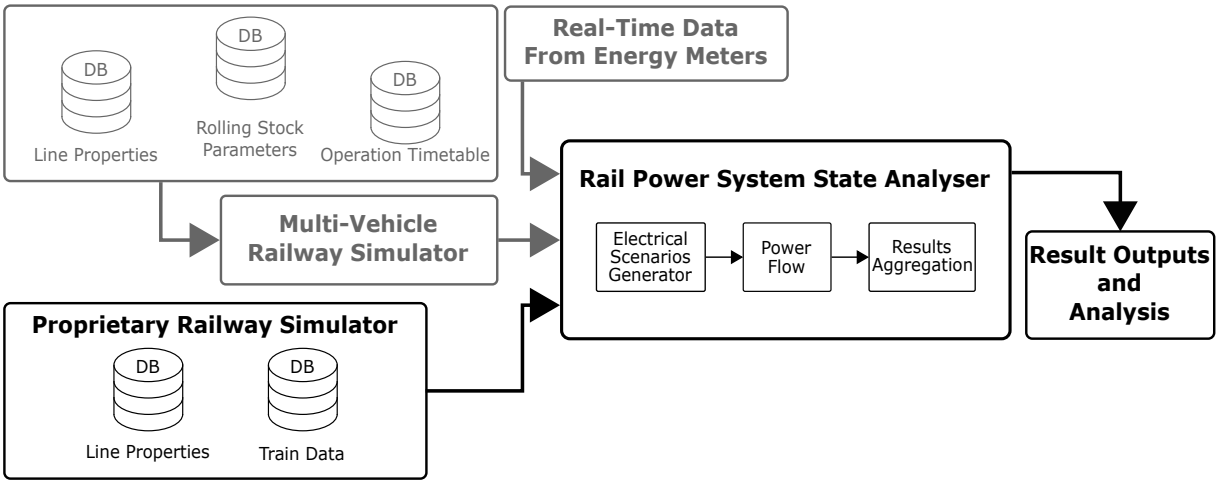

Figure E.1: Structure of a railway power system state analyser adapted to case study line II.

With all train data adapted for the PSSA-rail tool, the second step is to adapt the line properties and parameters. In particular, the line in consideration has 7 substations and approximately 250 km length (and three side lines that will not be subject of simulation in this appendix). Furthermore, the position departures and arrivals of each train journey as well as all the TPS absolute positions and neutral zones are used to generate the points of interest.

Being all the parameters of the railway line in accordance to the PSSA-rail, then the Fig. E.2 and Fig. E.3 are automatically generated by the proposed tool.

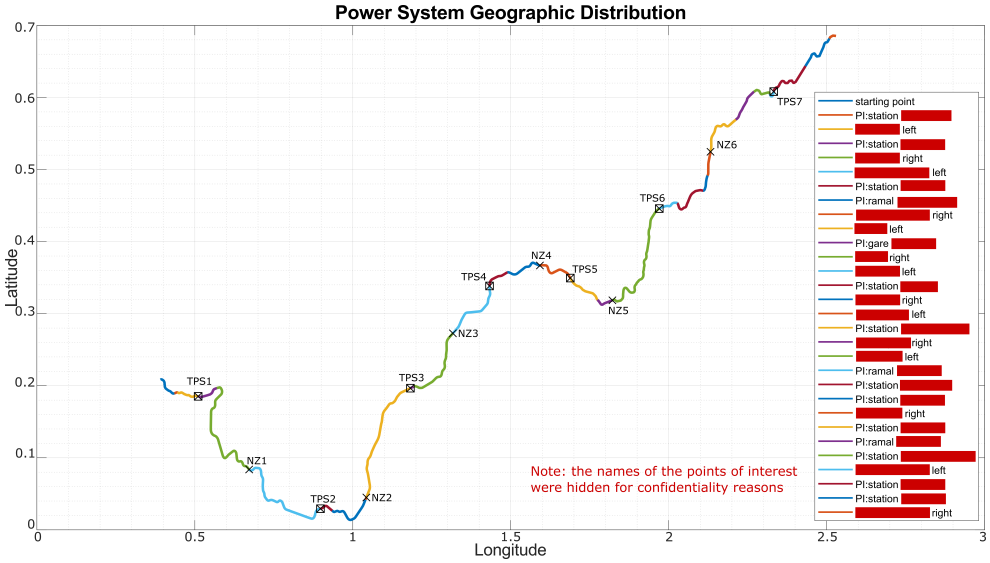

Figure E.2: Geographic distribution of the railway line under analysis. Note: the 3 degree longitude window corresponds to around 333 km; the 0.7 degree latitude window corresponds to around 78 km.

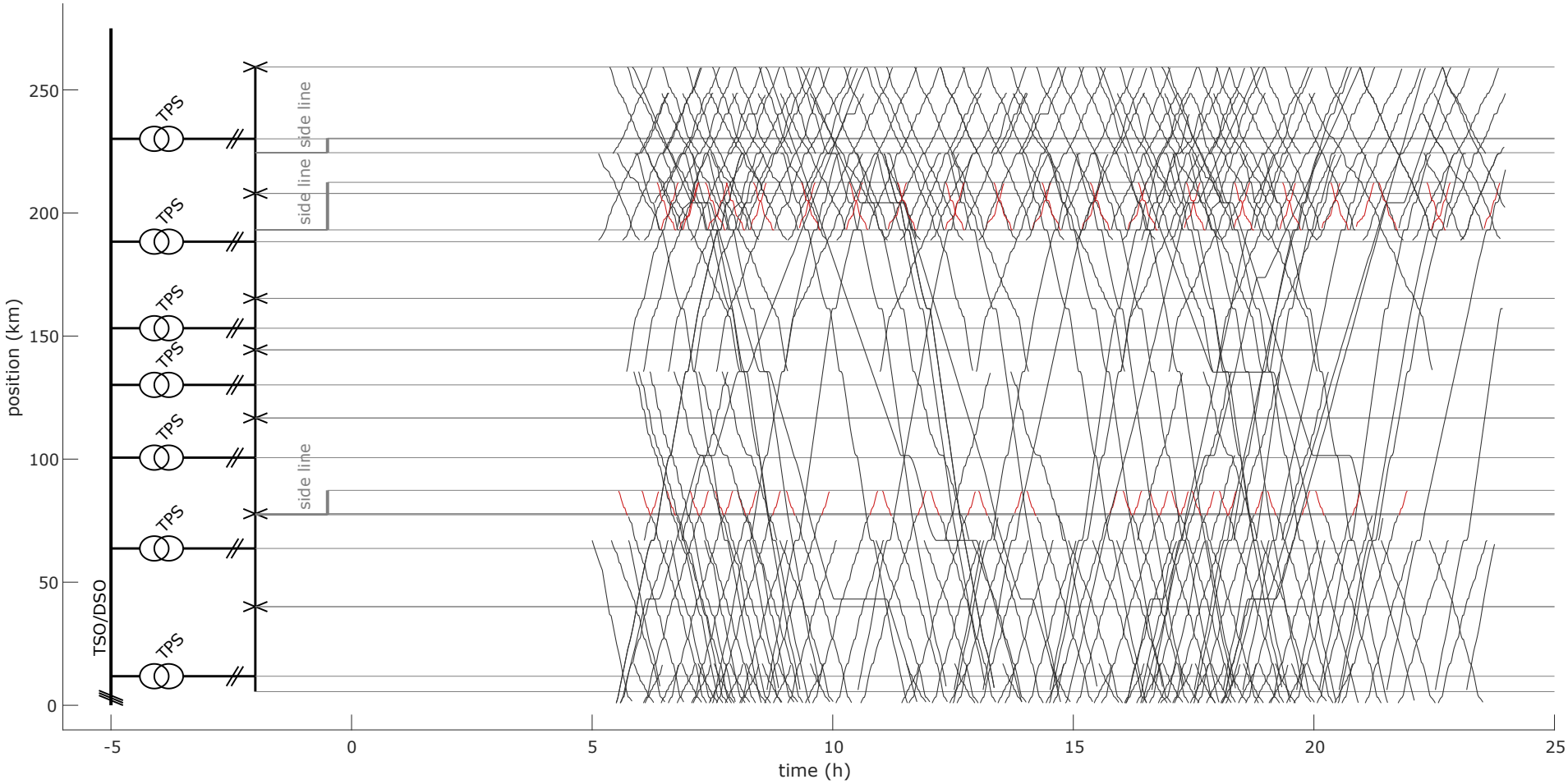

Figure E.3: Geographic distribution of the railway line under analysis. Note: the red lines are side lines not analysed in this appendix.

Furthermore, in the following diagrams are presented the automatically generated electrical equivalent diagrams for each of the seven substations, from Fig. E.4 to Fig. E.10.

To demonstrate the capabilities of the proposed tool, only the results for the TPS 7 will be presented in the following section. However, it should be highlighted that the PSSA-tool automatically generates the result graphs for any of the TPS. The TPS 7 was chosen since it is the TPS with the higher number of nodes (623 bus nodes).

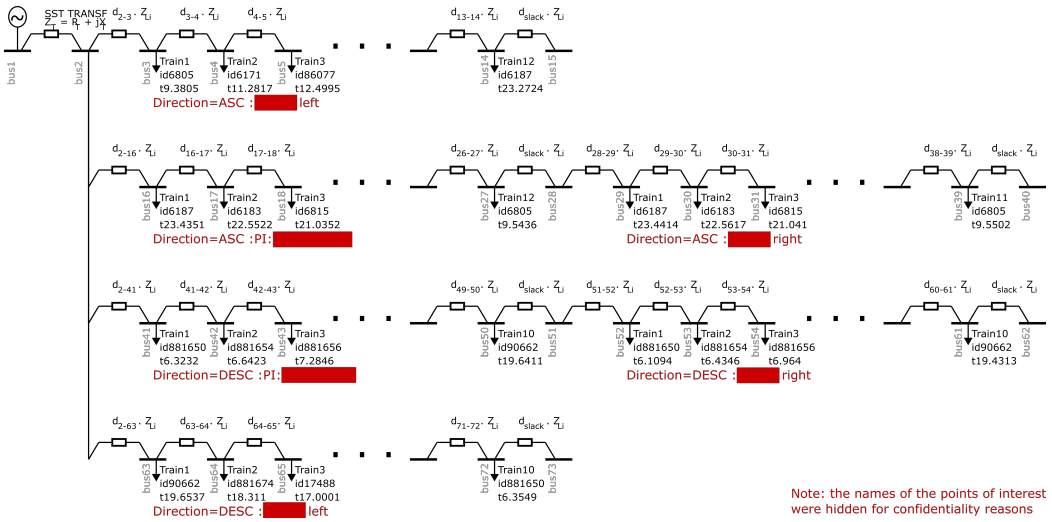

Figure E.4: Electrical equivalent diagram for TPS number 1.

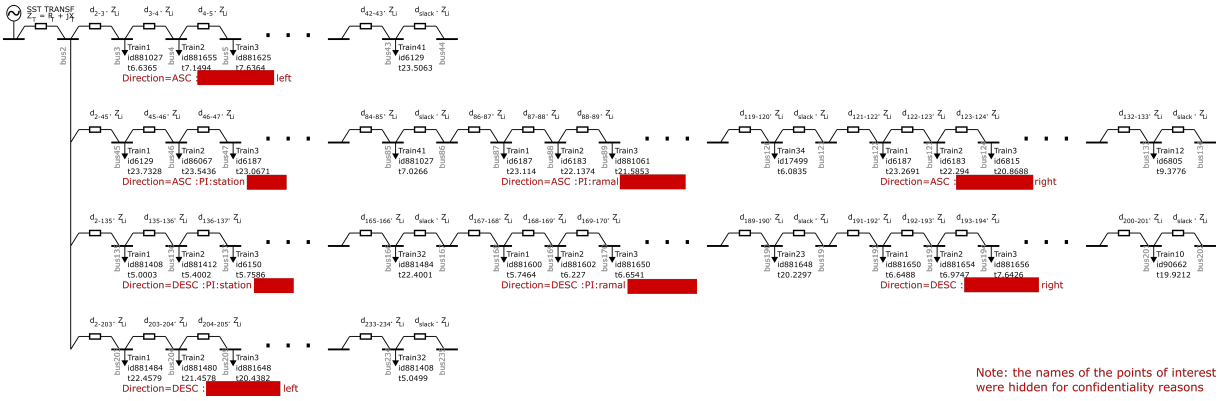

Figure E.5: Electrical equivalent diagram for TPS number 2.

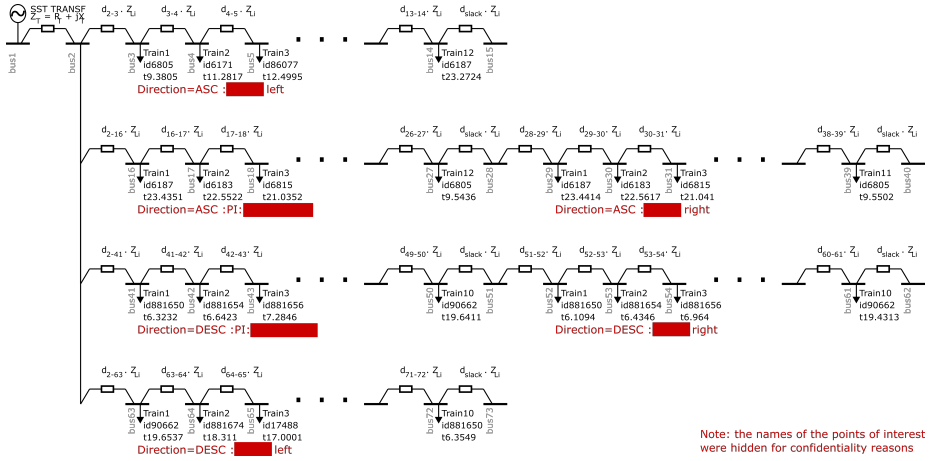

Figure E.6: Electrical equivalent diagram for TPS number 3.

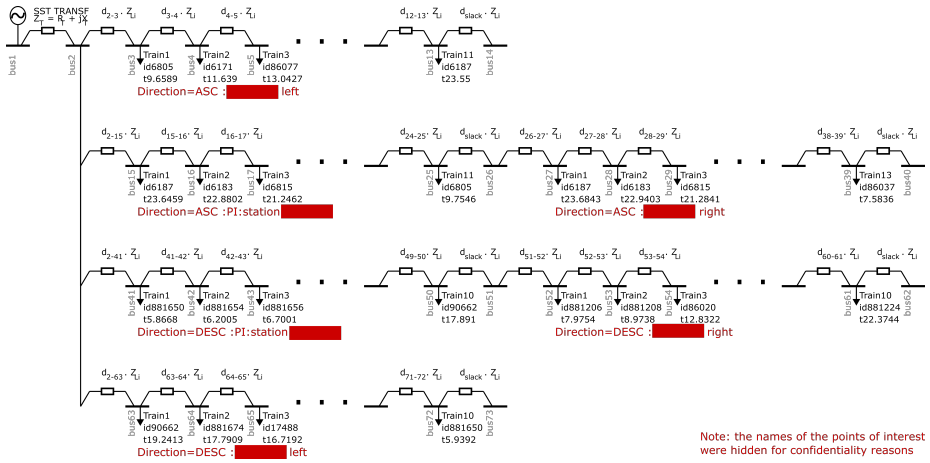

Figure E.7: Electrical equivalent diagram for TPS number 4.

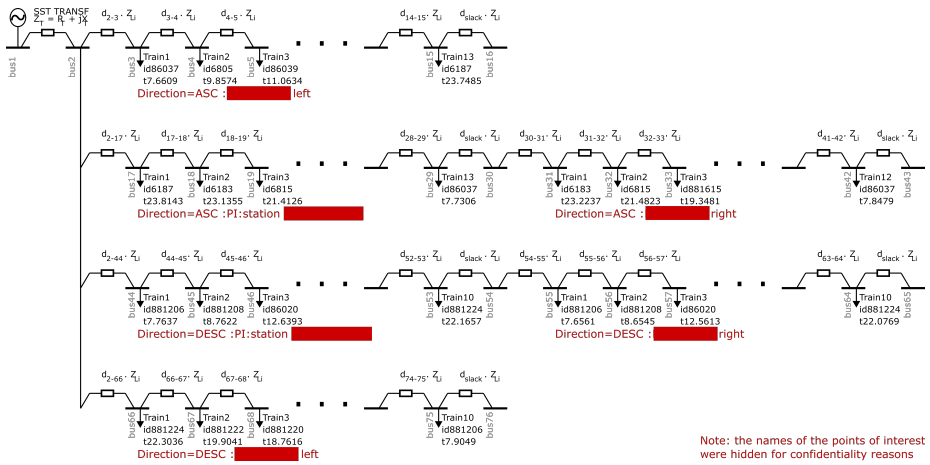

Figure E.8: Electrical equivalent diagram for TPS number 5.

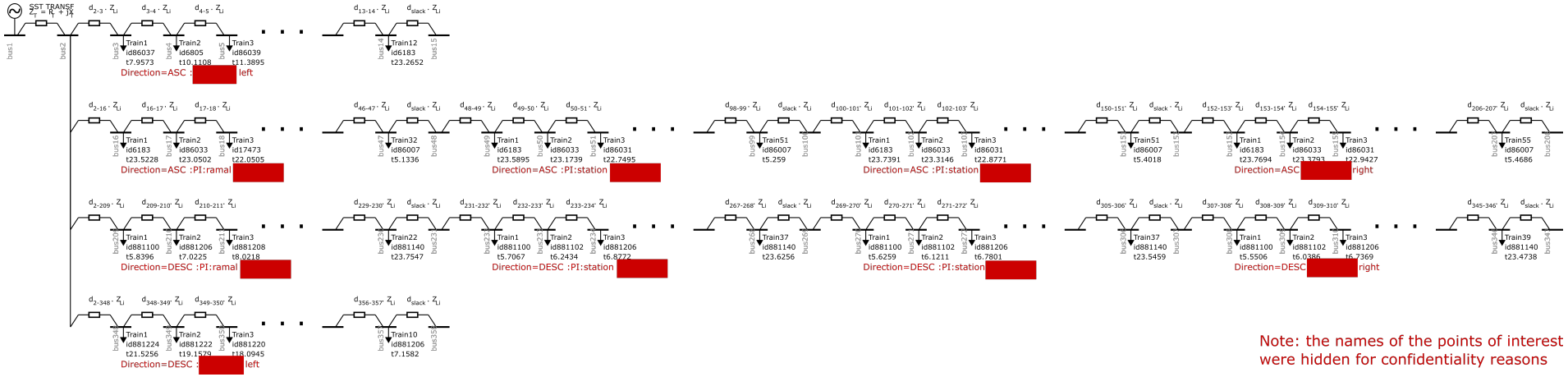

Figure E.9: Electrical equivalent diagram for TPS number 6.

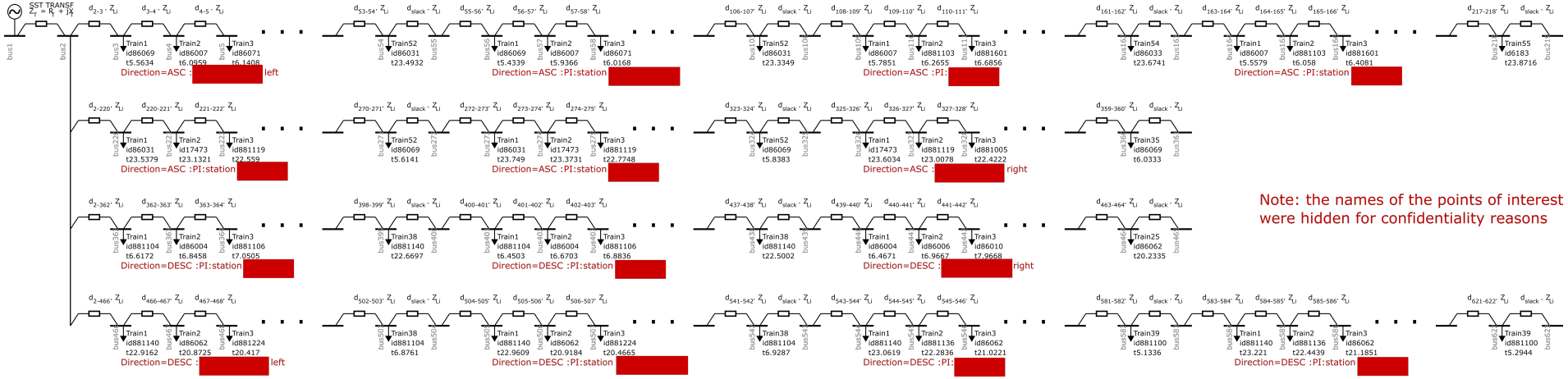

Figure E.10: Electrical equivalent diagram for TPS number 7.

E.2 Output Results

From an adequate preparation of the input train information data, then the generation of the results is automatic. In this section will be presented some of the results automatically generated by the PSSA-rail tool.

As illustrated in Fig. 5.5 of the implementation of PSSA-rail, with adequate input data on the *Prepare Simulation Module*, then the next step is to iteratively generate the knowledge on the energy at each traction substations[1]. For a given time-window and for all substations, this knowledge on the power flow for the railway line is given by the expression in (E.2).

$$PF\ Knowl\ TPS_{1,..,7} = \begin{cases} Energy\ Info = \begin{cases} P(t),\ Q(t) \\ E(t) \end{cases} \\ \\ Train\ Info = \begin{cases} V_{T_1,...,T_n}(t) \\ I_{T_1,...,T_n}(t) \end{cases} \end{cases} \tag{E.2}$$

E.2.1 Traction Substation Power Consumption

The first set of graphs will illustrate the power flow in the traction substation, as illustrated in Fig. E.11.

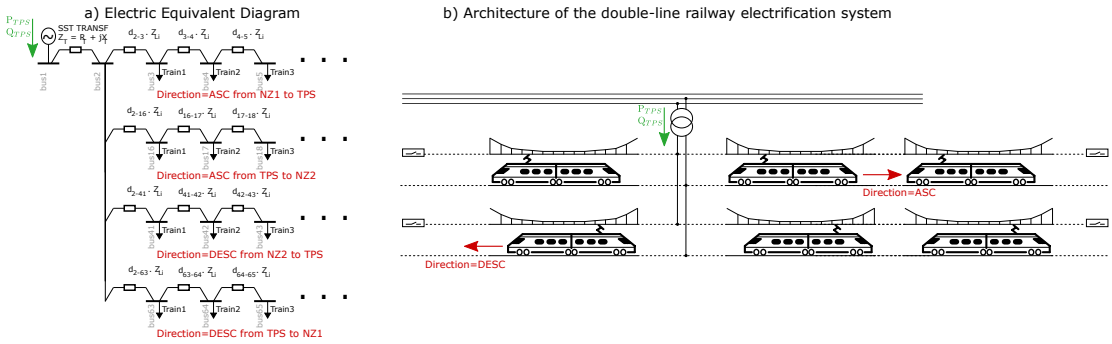

Figure E.11: Illustration of the TPS active and reactive power in each of the following graphs.

Specifically, the active and reactive power in the TPS #7 is presented in Fig. E.12, for the simulation time-window.

[1]Note: In this appendix, none of the proposed optimization strategies in chapter 5 were demonstrated. Then, only the *Execute Simulation Module* was used.

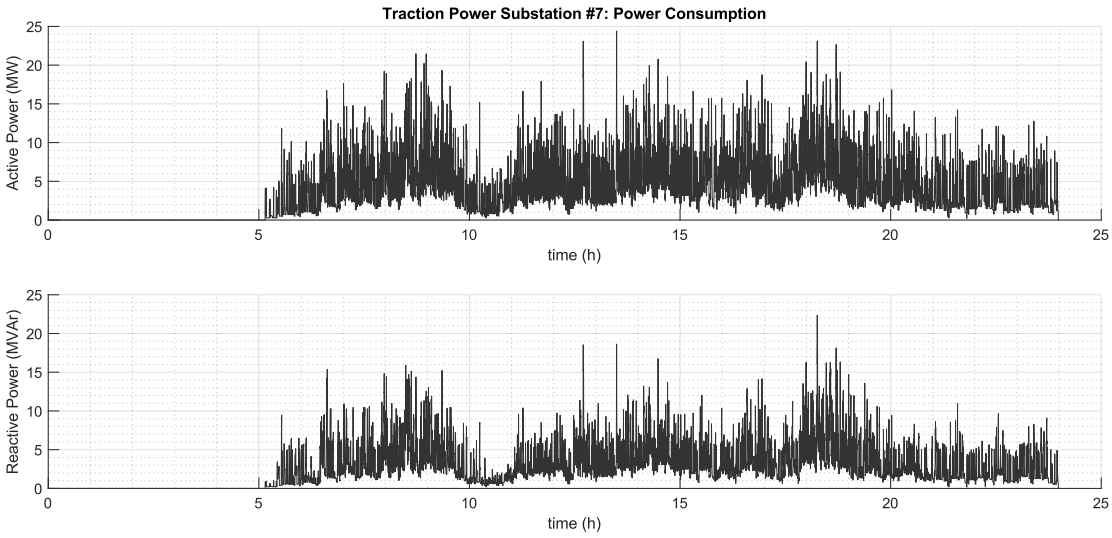

Figure E.12: Power consumption for TPS number 7, generated by PSSA-rail.

The PSSA-rail is also capable of the simulation of the active and reactive power in each branch of the traction substation, as illustrated in Fig. E.13.

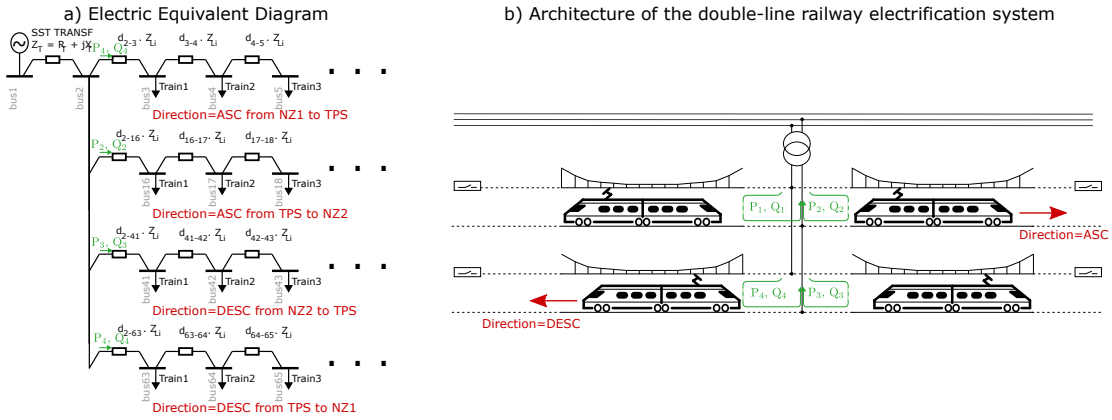

Figure E.13: Illustration of the power flow in each of the following graphs.

For the TPS #7, this result is visible in Fig. E.14.

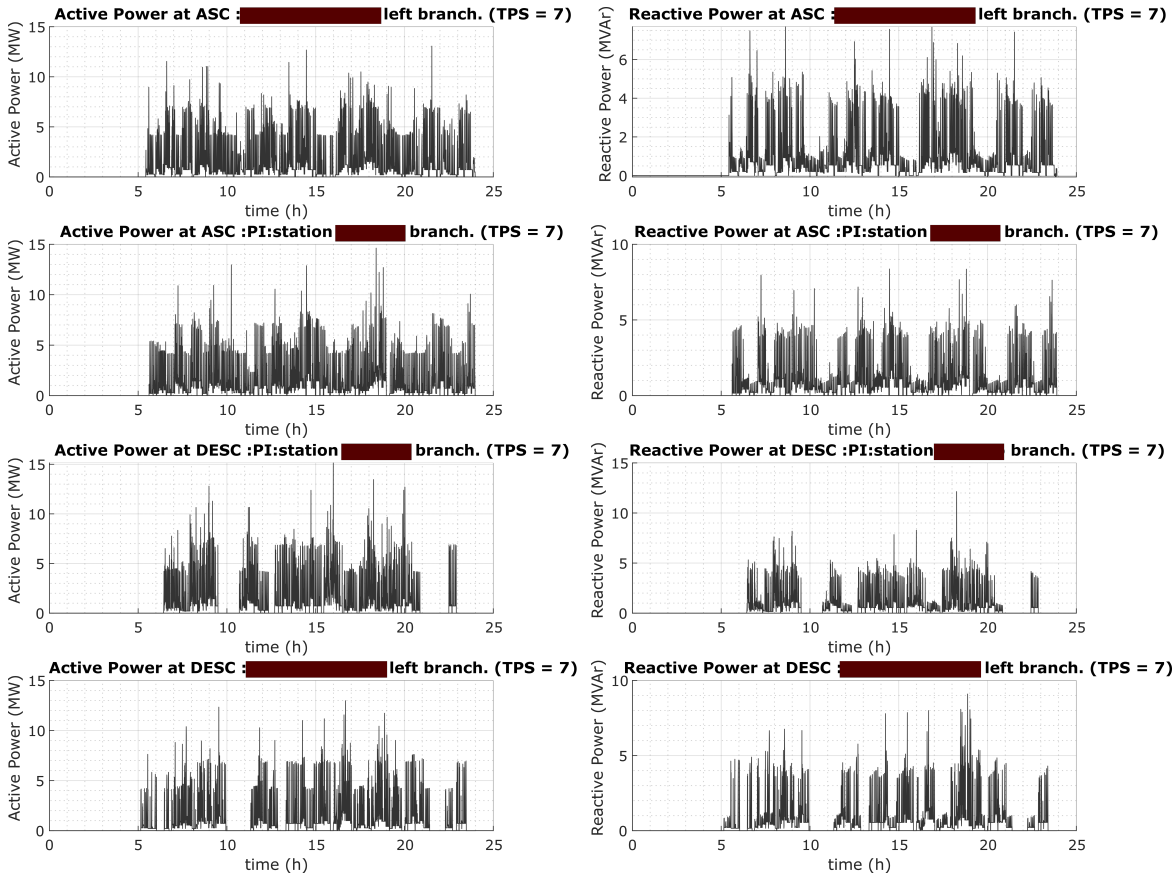

Figure E.14: Supply power in each out branch of TPS, for TPS number 7, generated by PSSA-rail. Note: the names of the branches points of interest were hidden for confidentiality reasons.

In addition to the power, the proposed tool can also simulate the current magnitude in each branch, following the illustration of Fig. E.15.

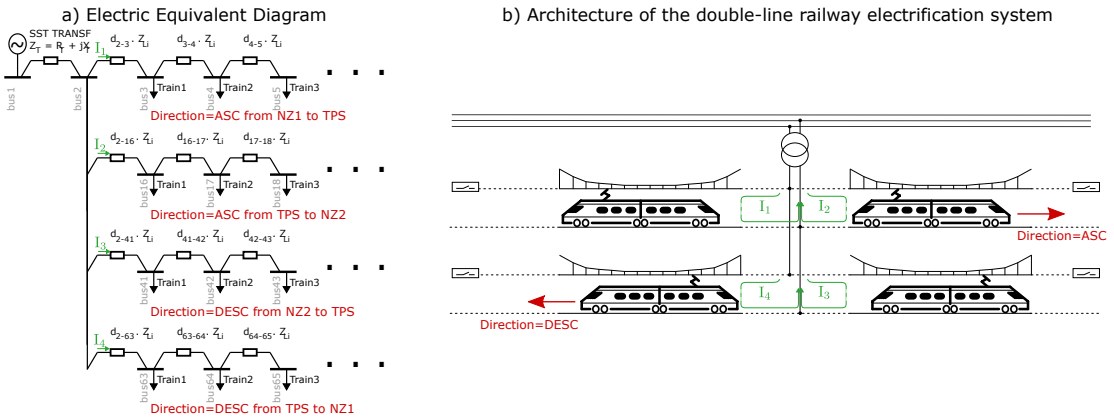

Figure E.15: Illustration of the flow of current for each of the following graphs.

The current magnitude of each of the branches of TPS #7 is visible in Fig. E.16.

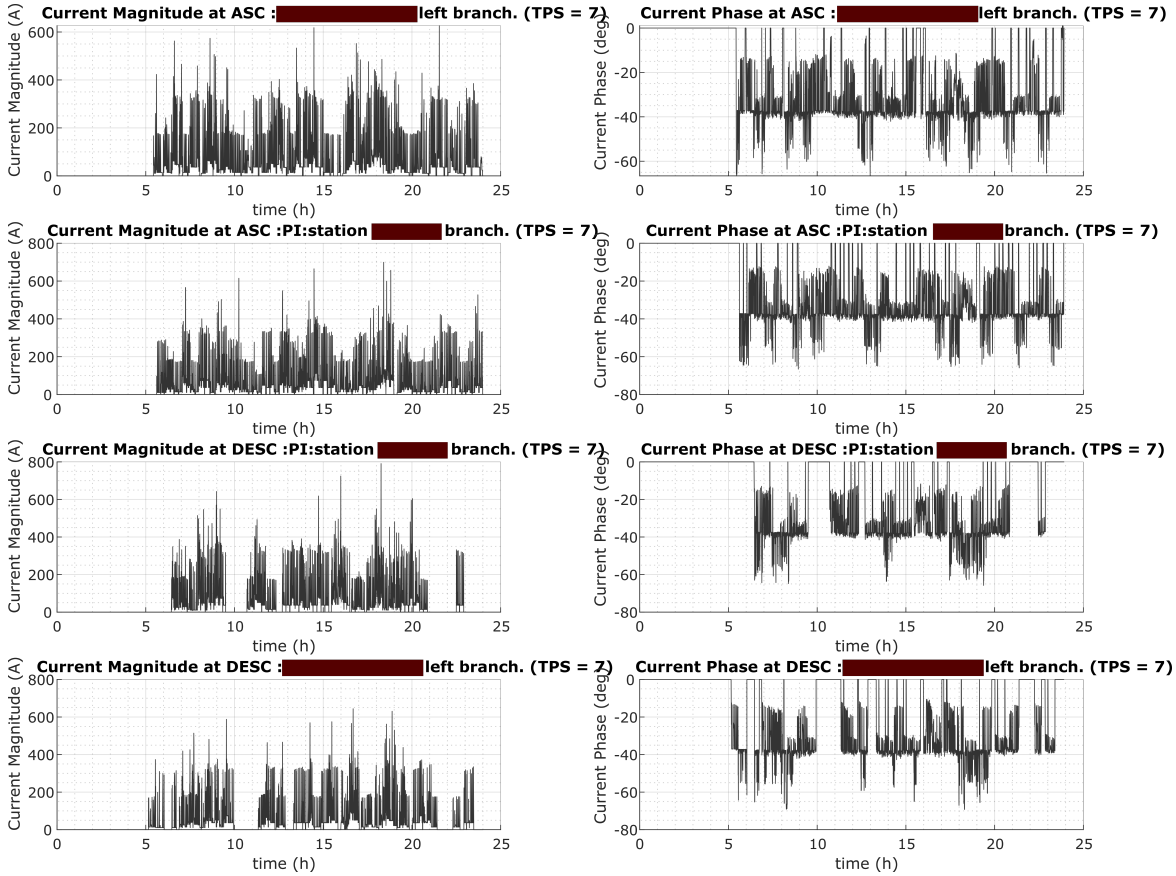

Figure E.16: Supply current in each out branch of TPS, for TPS number 7, generated by PSSA-rail. Note: the names of the branches points of interest were hidden for confidentiality reasons.

Finally, from the power in the branches, the global power in TPS #7 and the losses in the catenary, an energy evaluation can also be performed for the simulation time-window, as visible in Fig. E.17

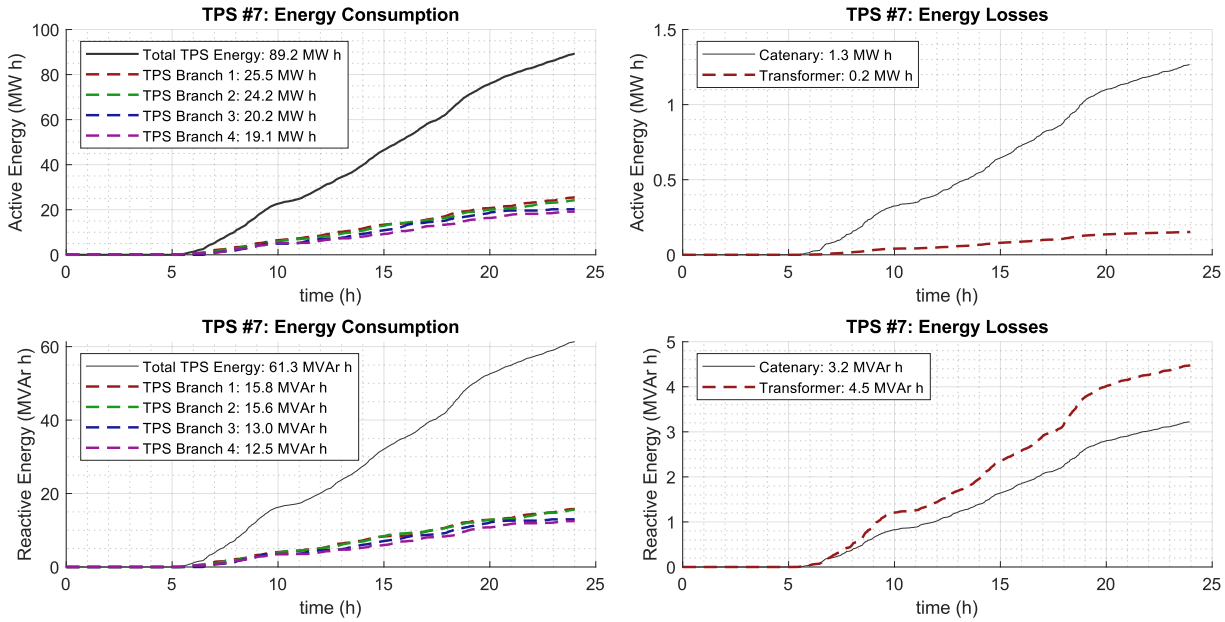

Figure E.17: Energy flow for TPS number 7, generated by PSSA-rail.

E.2.2 Train Power Consumption and Power Factor

In these set of graphs (Fig. E.18 and Fig. E.19) are presented the power consumption for each train as well as the power factor evaluation.

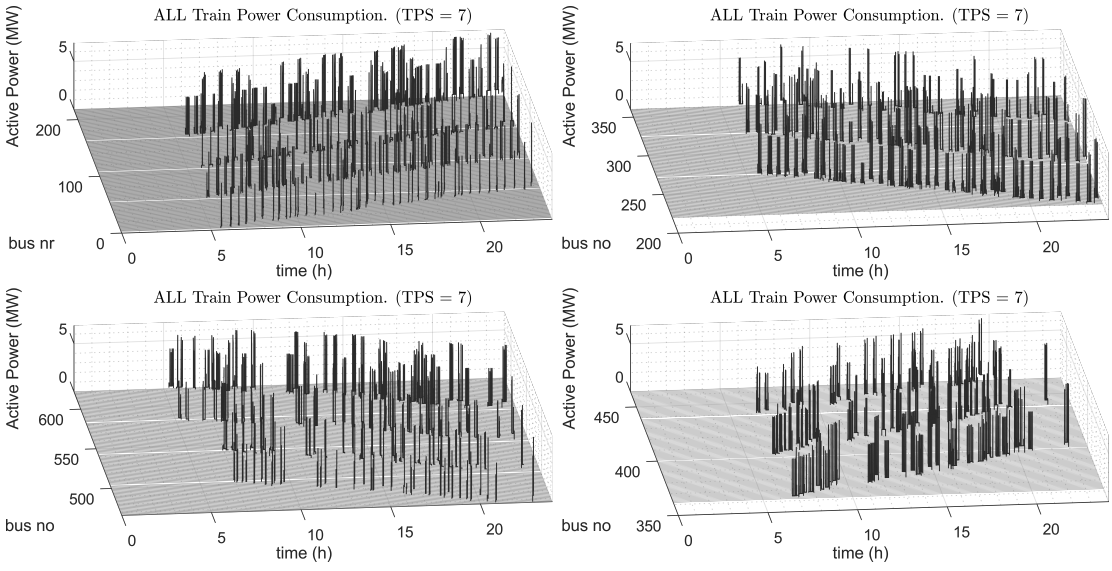

Figure E.18: Train Power consumption for TPS number 7, generated by PSSA-rail.

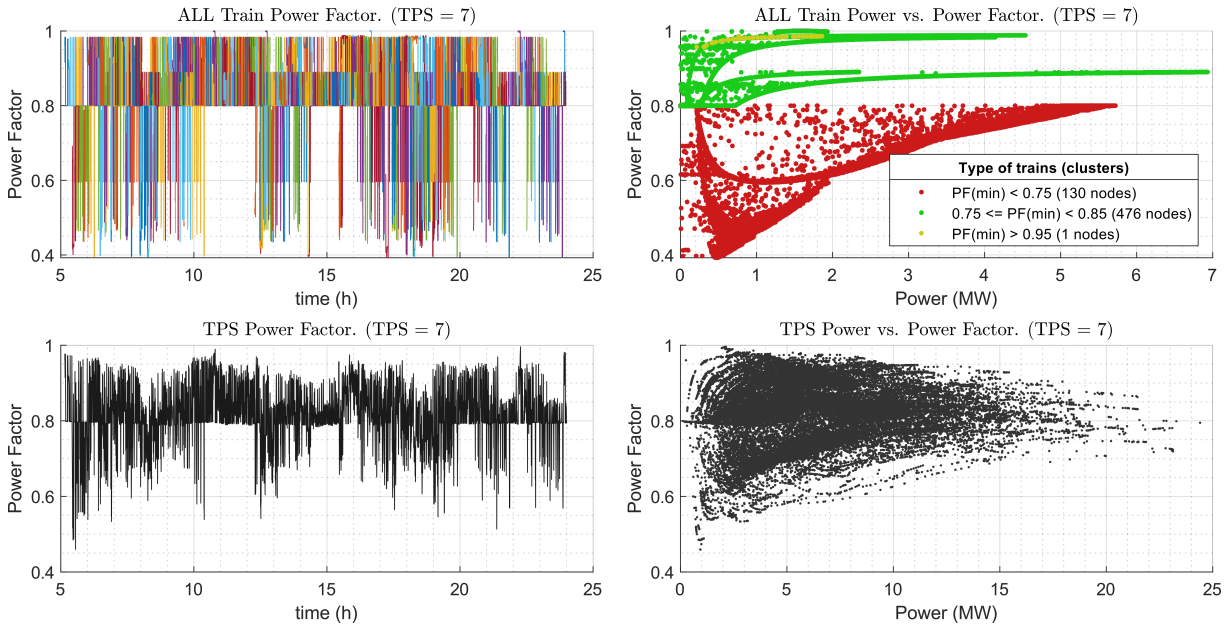

Figure E.19: Power Factor for TPS number 7, generated by PSSA-rail.

The evaluation of the power factor presented in Fig. E.19 illustrates the type of trains that are in operation in the considered railway line. It was defined three clusters of trains based on the minimum power factor, being these clusters arbitrary chosen. It is visible in the number of nodes, that the majority of trains (78 %) operates with a power factor limited to 0.8 (approximately, for small power consumptions), and higher power factor values for higher power consumption values.

However, it should be highlighted that even if the green cluster is above 0.8 for higher power consumption values, where a non-despicable quantity of trains operates at a near-unitary power factor, this does not mean that the TPS power factor can be easily estimated. Fig. E.19 shows in the graph TPS Power vs. Power Factor, that the maximum power factor in TPS will decrease with the increase of TPS power consumption (for example, in the TPS power consumption interval between 0 and 5 MW, the maximum power factor in near-unitary; for a value higher than 3 MW, the maximum power factor slightly decreases linearly until a $PF = 0.95$ *ind.* at 15 MW TPS consumption). One reason for not having unitary TPS power factor values at higher TPS power consumptions is due to the highly inductive catenary lines used in the PSSA-rail simulation, where the $^{X}/_{R_L}$ ratio is 3.

E.2.3 Voltages in Train buses and in Traction Substation

The following graphs (Fig. E.21 and Fig. E.22) will present another of the output results of the tool presented in chapter 5. Specifically, the voltage in each train node is presented as well as the TPS maximum, average and minimum voltages. Thus, these results follows the illustration in Fig. E.20.

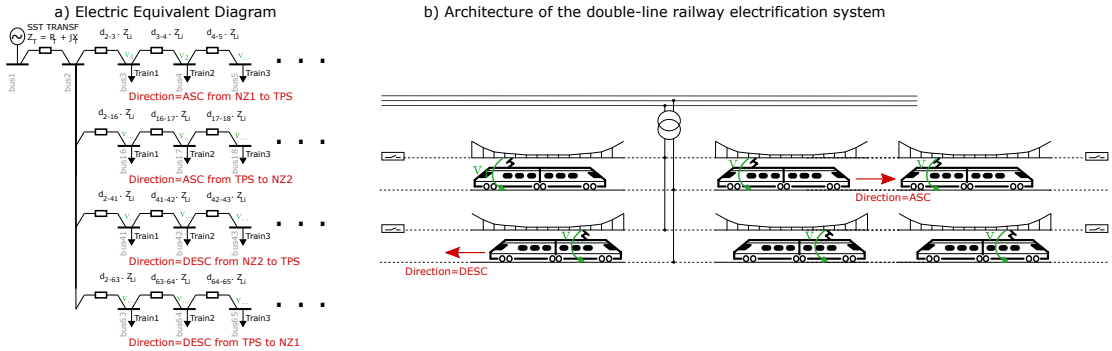

Figure E.20: Illustration of the train voltage in each of the following graphs.

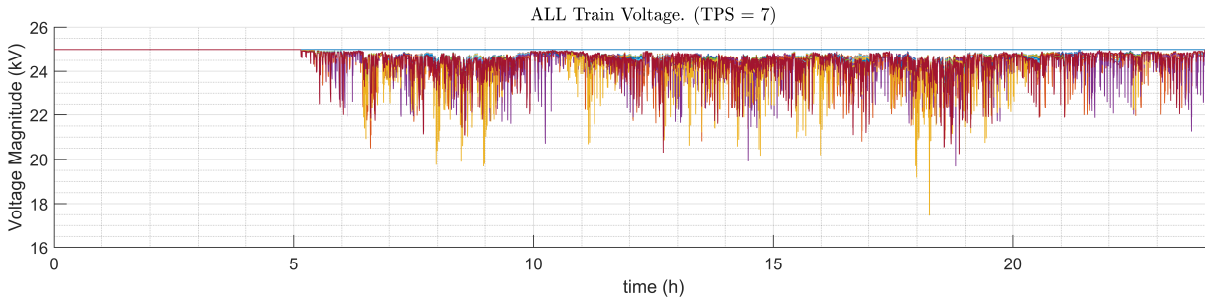

Figure E.21: Bus voltage from all nodes for TPS number 7, generated by PSSA-rail.

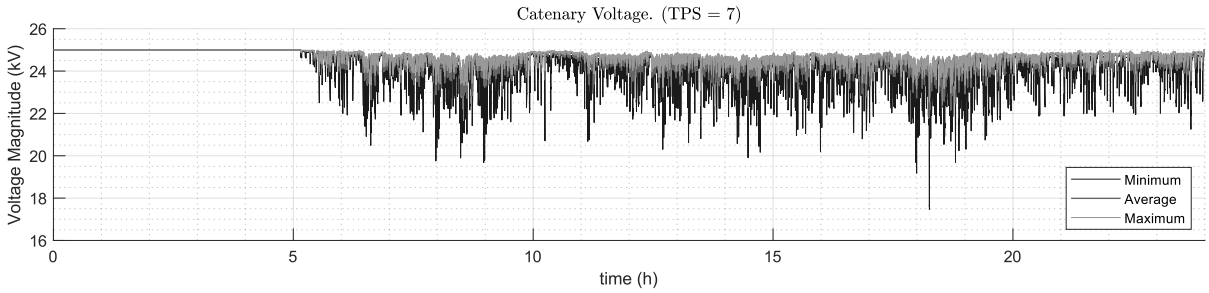

Figure E.22: Minimum bus voltage for TPS number 7, generated by PSSA-rail.

The TPS maximum, average and minimum voltages are obtained as the application of the metrics throughout all the train nodes, for the simulation time-window.

Furthermore, one other result is the voltage drops in the branches, as illustrated in Fig. E.23, with results in Fig. E.24 for the TPS #7 .

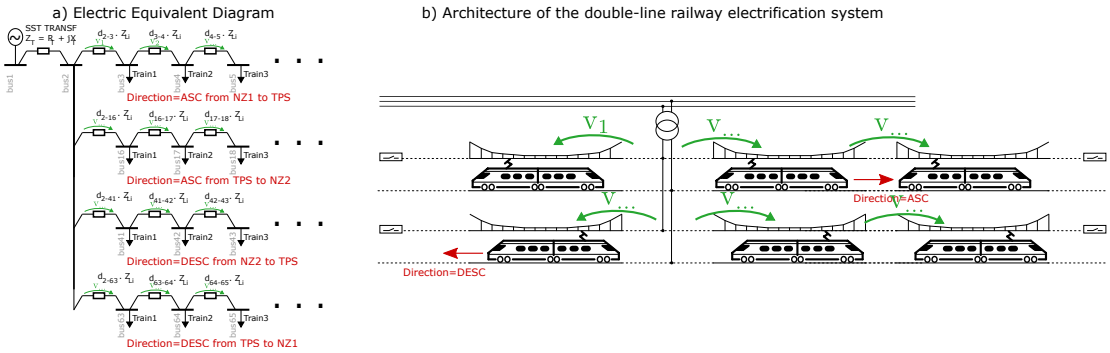

Figure E.23: Illustration of the voltage drop in each of the following graphs.

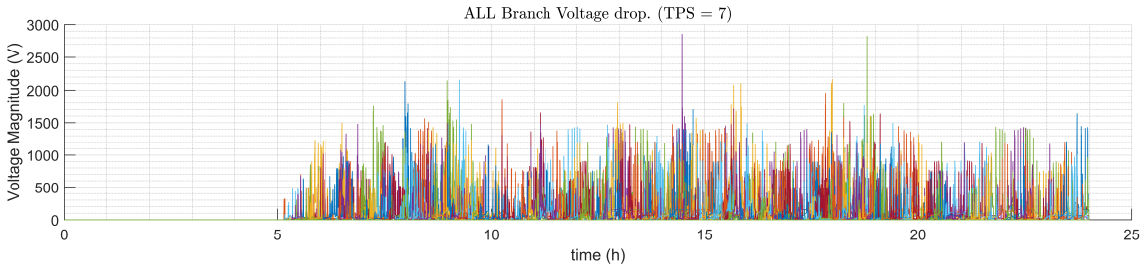

Figure E.24: Catenary branch voltage drop for TPS number 7, generated by PSSA-rail.

It should be highlighted that the results of Fig. E.24 present all the voltage drops of the 622 branches of Fig. E.10.

E.2.4 Losses in Catenary for each Traction Substation

The final result that is automatically generated by the PSSA-rail tool concerns the power losses, as illustrated in Fig. E.25.

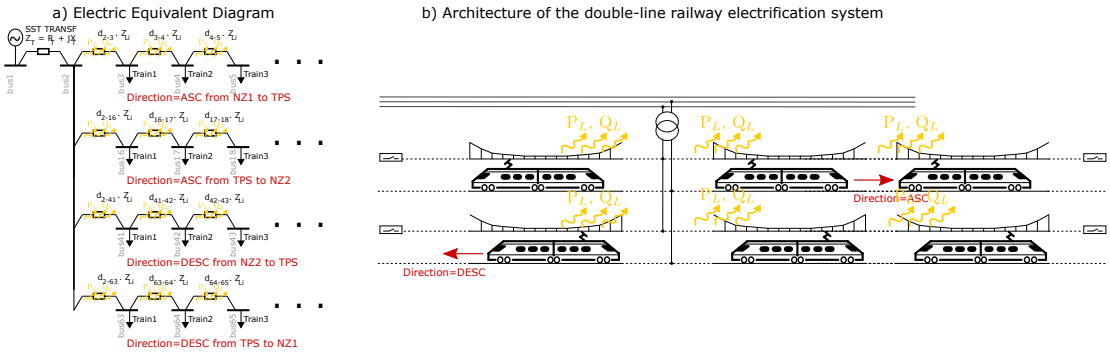

Figure E.25: Illustration of the catenary branch losses in each of the following graphs.

The active and reactive power losses in the catenary branches for the TPS #7 are presented in Fig. E.26. Furthermore, from these results, by adding all power losses, the Fig. E.27 can also be produced for the same TPS.

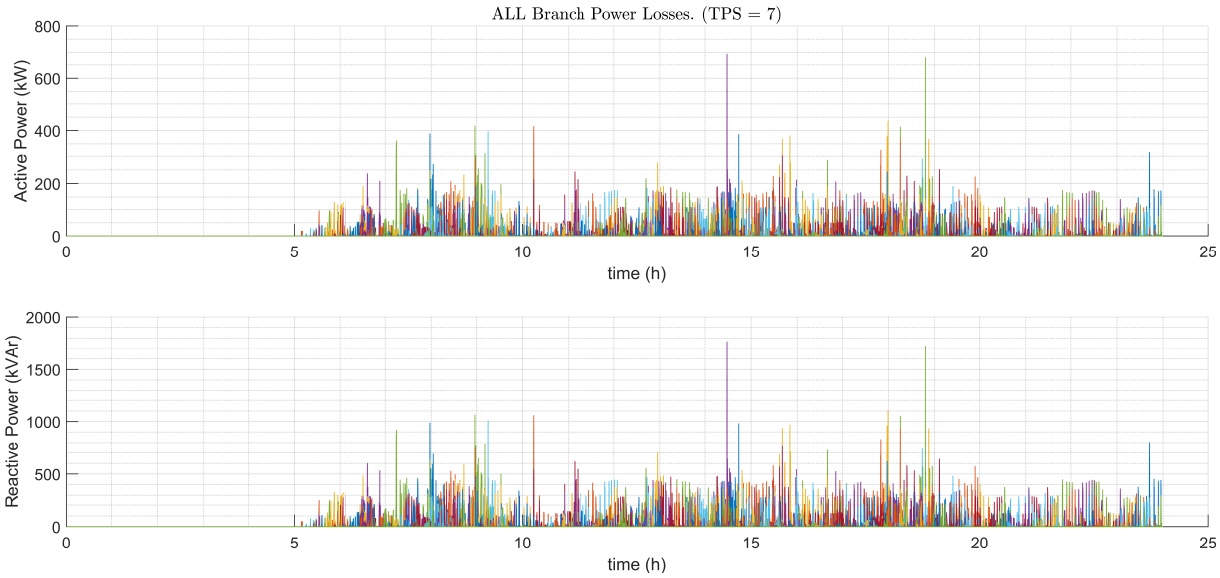

Figure E.26: Catenary branch losses for TPS number 7, generated by PSSA-rail.

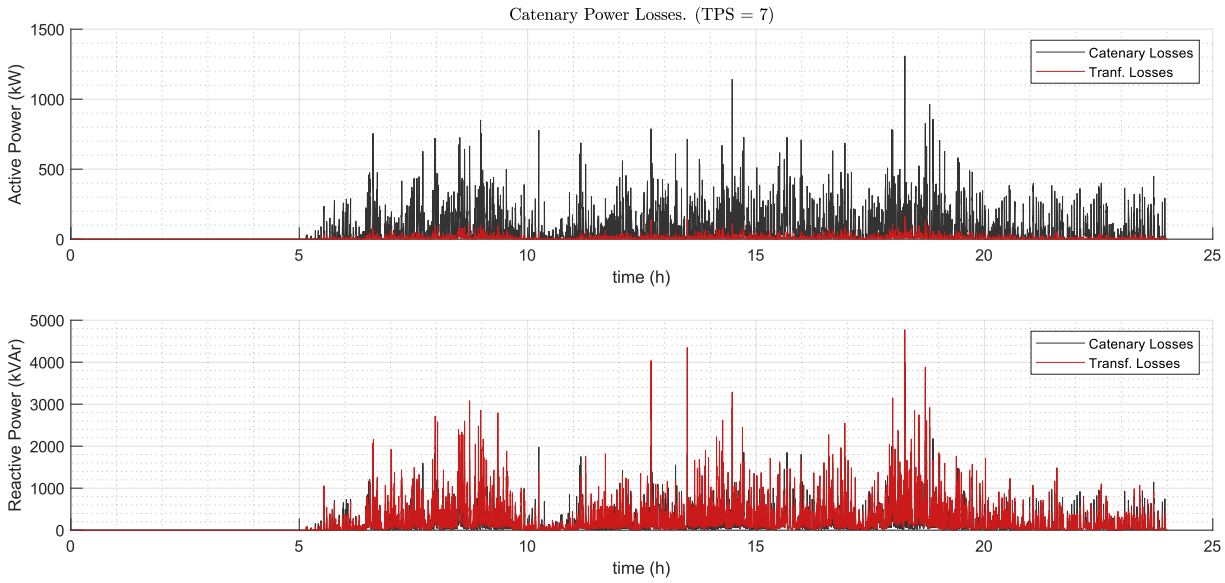

Figure E.27: Comparison of catenary and transformer losses for TPS number 7, generated by PSSA-rail.

E.3 Comparison voltage-power-position and Final Discussion

The final result presented in this demonstration is related to the capability of the tool to generate knowledge on the voltage at each train. Then, by combining the train absolute position, power consumption and voltage magnitude, the results of Fig. E.28 can be produced.

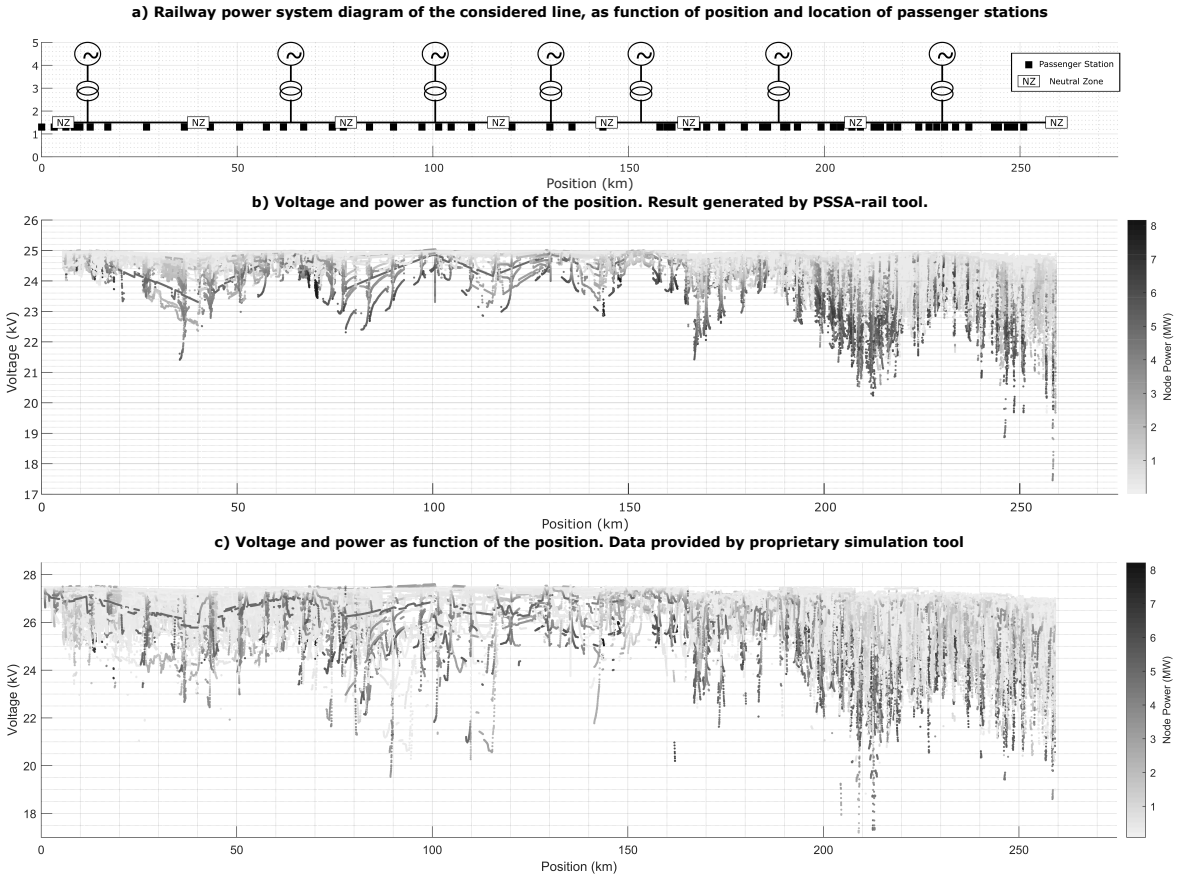

Figure E.28: Evaluation of train voltage and power, as function of the position: a) Power system diagram and passenger station localization; b) Results produced by the PSSA-rail tool; c) Results provided by proprietary simulation tool.

Furthermore, the same analysis was made with the data provided by the proprietary simulation tool. A preliminary comparison shows strong similarities in the results. The voltage drop is lower closer to the traction substation than near the neutral zones, as expected. Also, the lower voltage values are within the same range.

The obvious difference is in the maximum voltage. In the PSSA-rail simulation, it was considered that the substations are supplied with a fixed 25 kV voltage source. However, according to the IEC 60850 standard [113] where the highest permanent voltage is 27.5

kV, the infrastructure managers can adapt the voltage of the TPS traction transformers to the most suitable value for the expected train operation so that the voltage at no-load condition is lower than the highest permanent voltage.

In the results presented for the proprietary simulation tool, it is visible that the voltage at no-load condition is near 27 kV. This interesting point of operation is only possible since the results also show that the trains do not operate in regenerative mode, and the power factor is inductive.

Besides the voltage levels, the differences between the results are also caused by the current limitation of the PSSA-rail, where it is not possible to simulate train overtaking. Then, from all 334 train journeys provided by the proprietary simulation tool, the PSSA-rail only have simulated 252 journeys (75 %).

Finally, the used line model is the one presented in chapter 3, which is the major cause of differences in the comparison, where the PSSA-rail uses a $^{X}/_{R_L}$ ratio is 3 and the real line of this appendix has a $^{X}/_{R_L}$ ratio around 5. Besides, the transformers in each TPS have different short-circuit parameters among themselves and the ones used in PSSA-rail. Thus, the usage of different line parameters and transformer short-circuit values, together with different no-load condition voltage values and the simulation of only 75 % of the train journeys are the main reasons for the difference in results.

E.4 Summary

In this appendix was presented the demonstration of the adequate results generation of PSSA-rail tool for the second case study line. The results presented covers a broad diversity of graphs automatically generated by PSSA-rail.

In addition to the demonstration, in this appendix, the comparison of the PSSA-rail outputs with the ones provided by the proprietary simulation tool shows strong similarities with the proposed tool.

APPENDIX F

Data Transmission Strategy for Smart Railways

This thesis addresses tools and strategies that enable better knowledge on the state of the railway electrification. One requirement on the proposed framework for smart railways, illustrated in Fig. 1.1, is the obvious need for a communication link for the interconnection between the needed subsystems.

In this appendix, is described a strategy that was preliminary considered for the communication between trains and ground stations. It could be further extended to address the communication between moving smart railway agents and stationary ones.

Nevertheless, this strategy is of advanced interest if the real-time requirements are not essential for the communication between agents of smart railways.

This appendix starts to present a communication architecture for data transmission from onboard energy meters to a remote database. This communication strategy follows a methodology in which the majority of the gathered data is transferred via Wi-Fi, with the access points placed in every passenger stations; The remaining real-time data is transferred via LTE, constrained to limited bandwidth to keep the cost of communication low. This methodology is illustrated in the graphical abstract of the Fig. F.1.

The objective of these two communication approaches is to increase the bandwidth of the communication link, while keeping the transmission costs controlled. This strategy will be validated by the train position data of a complete journey, obtained by the Train Simulator Tool presented in chapter 4.

F.1 Introduction

Until a few years ago, trains did not have an energy metering system installed onboard. In almost all countries, railways operators and the infrastructure manager were a single company [8].

In order to ensure interoperability between different railways operators and infrastructure managers, the ERA proposes an on-ground energy data collecting system, i.e. a system to receive, store and export the Compiled Energy Billing Data (CEBD) from trains, and an onboard energy measurement system, i.e. a system responsible for the generation of the CEBD, [9]. In addition, this part of the TSI must comply with the EN 50463 standard,

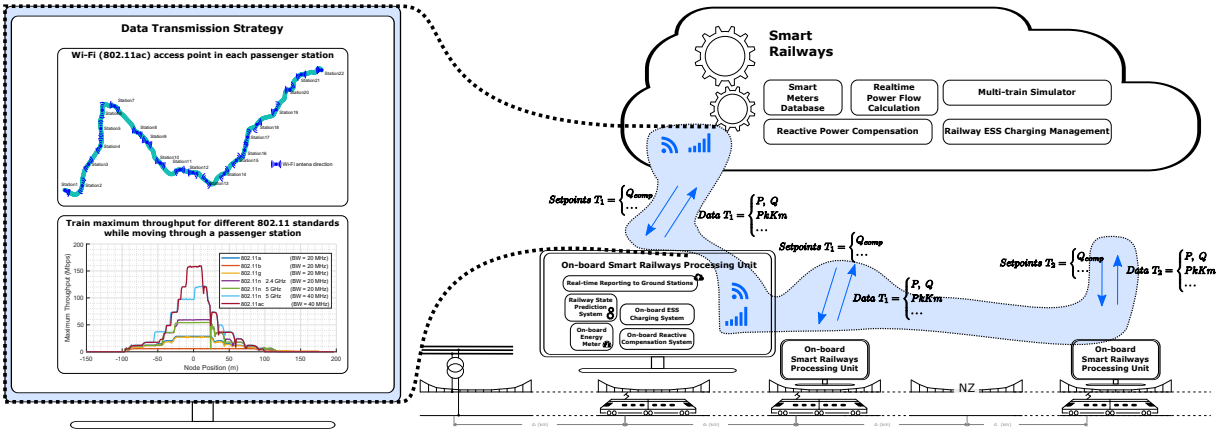

Figure F.1: Graphical abstract of appendix F — Inclusion of data transmission strategy in smart railway framework.

which regulates the energy measurement on board trains.

According to the EN 50463 standard, the maximum period of the energy data is 5 minutes. This means that at each 5 minutes, the trains must collect energy data and, after 128 energy data registers, a CEBD file is generated and transferred to a ground station. However higher frequency rates have advantages and should be endorsed.

In this work, this increase in the CEBD frequency rate is proposed, to comply with the need of energy metering system for billing purposes. Complementarily, this increase is an added value measure, since with a detailed information collection of the energy flows in the railways, it is possible to generate new knowledge and, with this knowledge, it is possible to adjust operation set-points and take measures that increase the energy efficiency [172].

Due to the nature of trains, the communication between trains and ground stations needs to be a radio communication. Initial implementations of such communication has been based on analog technology dedicated to voice and not adapted to carry data, [173]. Therefore, the communication of CEBD to ground stations is a recent topic and was not covered in the initial implementations of train-to-ground communication. The initial implementations of the transmission of CEBD to ground stations were made using a Global System for Mobile communications (GSM) modem [174]. From the conclusions of [173], the next generation of railway and metro wireless communication systems is pulled by the demand of new services, requiring much higher bandwidth than Global System for Mobile communications for Railways (GSM-R). Other publications also suggest the increase of bandwidth by using IEEE 802.11 standard solutions [175]. In current high speed railway applications, the GSM-R is transitioning to Long-Term Evolution for Railways (LTE-R) to support this increase of bandwidth [176]. The main disadvantage of this technology is the increase of the global cost, with the increase of the amount of data. Some solutions has been proposed to tackle this issue, for example, the dynamic management and reconfiguration of end-to-end networks using software defined networking [177].

The communication of CEBD data is inserted in the Vehicle-to-Infrastructure (V2I) research, despite the main focus of vehicular networks research is the increase of the road

safety and the reduction of traffic congestion. Currently, the vehicular network most investigated system is the IEEE 802.11p (working in 5.9 GHz frequency band and with 10 MHz bandwidth) and in [178] the authors suggest the usage of mmWave bands (24 GHz and 77 GHz) using narrow beam directional antennas. However, this frequency bands are suggested due to the Gbps data rates required for the increase of the road safety and the reduction of traffic congestion.

The comparison of different V2I communication systems in the railway domain is presented in Fig. F.2. As an example for the lower data rate is the energy meters communication of CEBD data to ground stations. The focus of this work is in the medium data rate, with the example of the bi-directional data transfer of detailed energy measurements. The high bandwidth data rate is suggested in the Virtual Coupling Train Sets (VCTS) concept to increase the capacity of railway lines by having closer to each other trains. VCTS requires reliable and fast real-time wireless communication, [179], and also is suggested the use of Fifth Generation Communication (5G), [180].

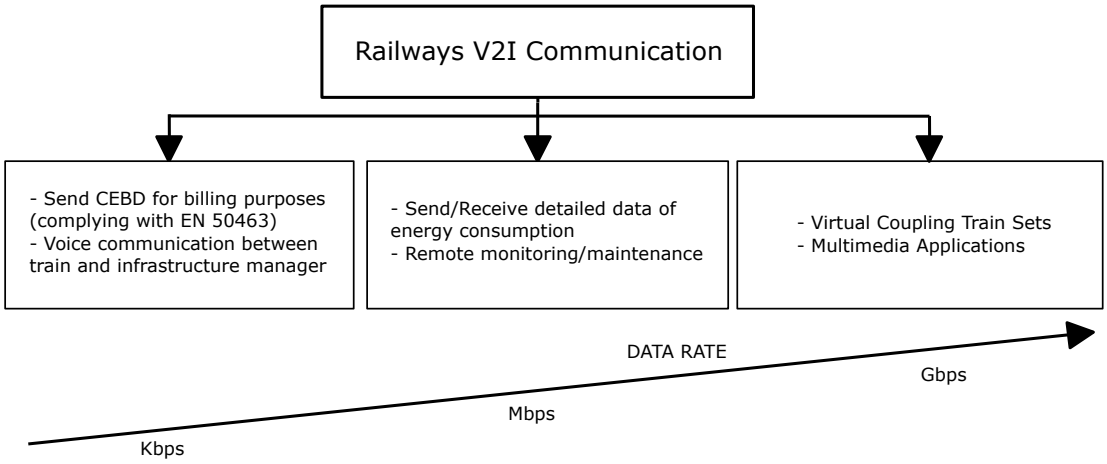

Figure F.2: Vehicle-to-Infrastructure communication: examples of systems.

For the communication of CEBD data, the annex A of EN 50463-4 standard suggests Kbps data-rates as a minimum. However, as previously referred, the increase in the detail of information of energy consumptions results, at end, in better energy efficiency operation. Therefore, the focus of this work is an evaluation of the application of a commercial IEEE 802.11 standard to fulfil the transmission requirements, in Mbps data rates, without considering currently-in-research technologies (such as IEEE 802.11p or mmWave).

Complementarily, with a detailed knowledge of the energy consumption, all the measures to reduce the energy consumption will have an online feedback. As an example, if a train enters in a regenerative braking mode, all other trains in the same line could have the real-time knowledge of this situation. An interesting opportunity to increase energy efficiency in railways is using the regenerative energy to support the increase of power consumption by other trains.

Based on the annex A of EN 50463-4 standard, the energy data can be transferred via Internet Protocol (IP), using the File Transfer Protocol (FTP) as the application level to

Table F.1: Illustration of the data requirements for an increase of the CEBD frequency rate.

CEBD aggregation period	Number of seconds covered by a record file	Number of equivalent '5 minute' record file	Size of equivalent '5 minute' record file (in kilobytes)	Minimum throughput for real-time broadcast (kilobytes/s)
5min	38400	1	18,59	0,00048
1min	7680	5	92,93	0,00242
30s	3840	10	185,85	0,0048
10s	1280	30	557,55	0,015
1s	128	300	5 575,5	0,15
100ms	12,8	3000	55 755,0	1,45
20ms	2,56	15000	278 775	7,26

transfer the CEBD as a eXtensible Markup Language (XML) file. This file has a header size of 2201 bytes and a maximum of 128 records, where each record has 128 bytes. In Table F.1 is illustrated an example of the data requirements of an increase of a CEBD frequency rate.

As example, in fact it is considered the maximum CEBD aggregation period of 5 minutes, each XML file will cover around a 10-hour period (38400 seconds) and requires 18.6 kilobytes to be transferred to ground stations. If we consider the 20 ms grid cycle, the equivalent 10-hour period will require 278.7 MB to be transferred.

F.2 Solution Proposal and Methodology

A possible solution to collect the maximum amount of data, while keeping the costs low is studied with this work. It is proposed the usage of the most recent IEEE 802.11 Wi-Fi technologies to exchange the CEBD between the trains and certain passenger stations. Fig. F.3 is an illustration of the solution proposal where each passenger station will have Wi-Fi access points with railways intranet/internet connection.

On the train side, with this proposal, the onboard energy meter generates two types of energy data; one of them with a low frequency (enough to fulfil the EN 50463 requirements, specifically 5 minute between samples) and the other energy data will be of higher sample rate. The first energy data will be transferred by LTE and the other more detailed energy data will be transferred via Wi-Fi, when the train has Wi-Fi connectivity near the stations.

The methodology covered with this work starts to identify the best Wi-Fi technology for this purpose. The ns-3 network simulator was used in other works for train-to-train communication [181]. Using the ns-3 simulator, by evaluating the maximum throughput of existent IEEE 802.11 Wi-Fi protocols, and by simulating the movement of a wireless device that crosses an access point, the obtained results are given in Fig. F.4.

With the usage of a train simulator, the journey of a train can be simulated, [13]. Then, the simulator output train position vector is included in the ns-3. As a simplification to the network simulator, only two nodes are considered and the train movement will consider the distance between the train and a passenger station.

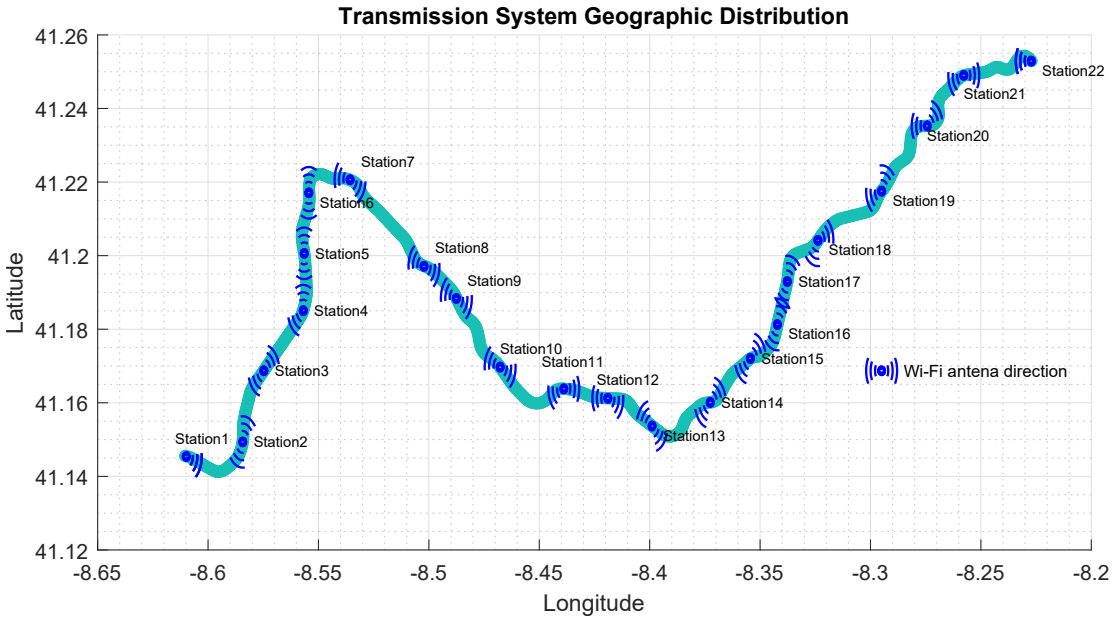

Figure F.3: Illustration of the solution proposal.

F.3 Major Findings and Results

Two case studies were considered in this work using the scenario given in Fig. F.5, specifically the case where the train will stop in every station and the case where the train will not stop in any station. This work is supported on the outcomes of the multi-train simulator [13] where all the train positions on a railway line can be obtained for one day. Having the train positions and the absolute position of passenger stations, it is possible to obtain the distance of each train to the closest passenger station.

For the case study 1, it was considered that each passenger station will have an Access Point (AP). To simulate that the train will not stop in any passenger station, a simple solution is to move the AP a couple of meters (500 m) away from each passenger station, in order to have the AP in between each passenger station. By moving the AP, it was ensured that the maximum and minimum speed that the train passes the AP is, respectively, 96.6 km/h and 49.8 km/h. Later on, using these distances between train and AP, the two cases were simulated using the ns-3 simulator.

For demonstration purposes it was simulated an User Datagram Protocol (UDP) application in ns-3 and the Wi-Fi standard used was IEEE 802.11g. (Note: as presented in Fig. F.4, by using the IEEE 802.11ac standard it is expected to have higher throughput; however, the difficulty level to implement this standard in ns-3 led to choosing a more conservative standard protocol).

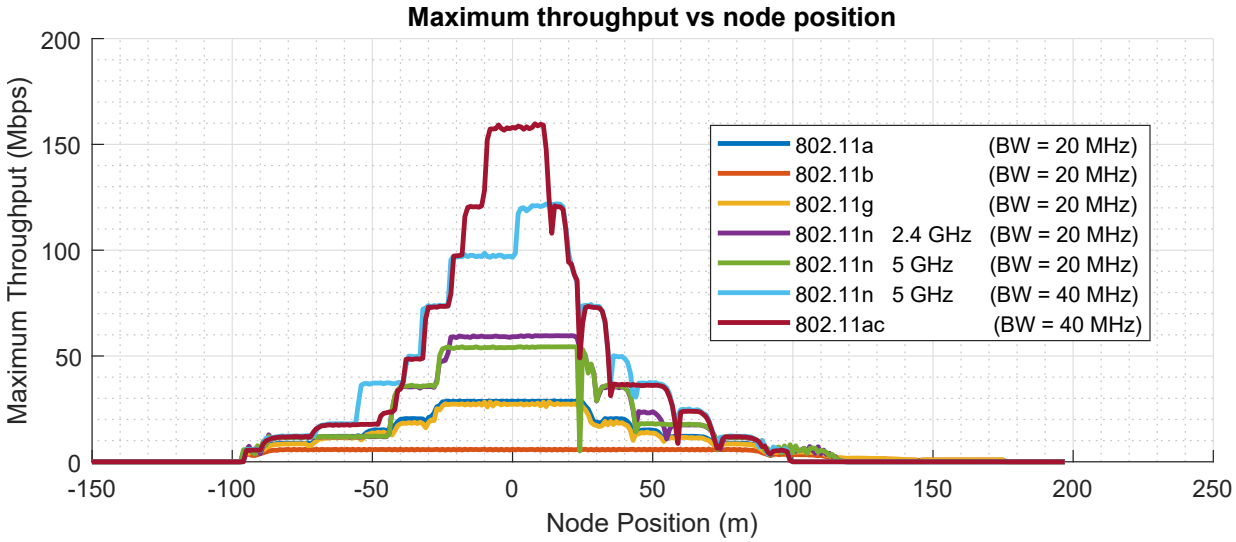

Figure F.4: Evaluation of a moving node for different IEEE 802.11 standards.

F.3.1 Case Study 1

In this case, the train will stop in every passenger station. The results related to the time evolution of the train status (on and offline), transmitted data throughput, and buffer status are presented in Fig. F.5.

In Fig. F.5 is presented in the top graph the time evolution of the train status, where the train is in online status 41.4 % of the time. In the middle graph, it is visible that it is possible to transmit around 2.5 GB of data and in the lower graph is presented the evolution of train data buffer, as the buffer that stores data when train is in offline mode. By ensuring that, when the train reaches an AP, all data present in buffer is transferred, it is possible to have applications generating data onboard trains with a maximum of 5 Mbps.

F.3.2 Case Study 2

In Fig. F.6, the results of case study 2, where the train will not stop in any passenger station, are presented, following the same sequence as in Fig. F.5.

The top graph of Fig. F.6 shows the time evolution of the train status, where the train is in online status 11.9 % of the journey time. In the middle graph, it is visible that it is possible to transmit around 180 MB of data and in the lower graph is presented the evolution of train data buffer, as the buffer stores data when train is in offline mode. In this case study, it is possible to have applications generating data at 375 kbps.

F.4 Discussion

With this solution, the transmission cost will be fixed and only dependent on the cost of installation and operation of the infrastructure: train Wi-Fi nodes and stations Wi-Fi

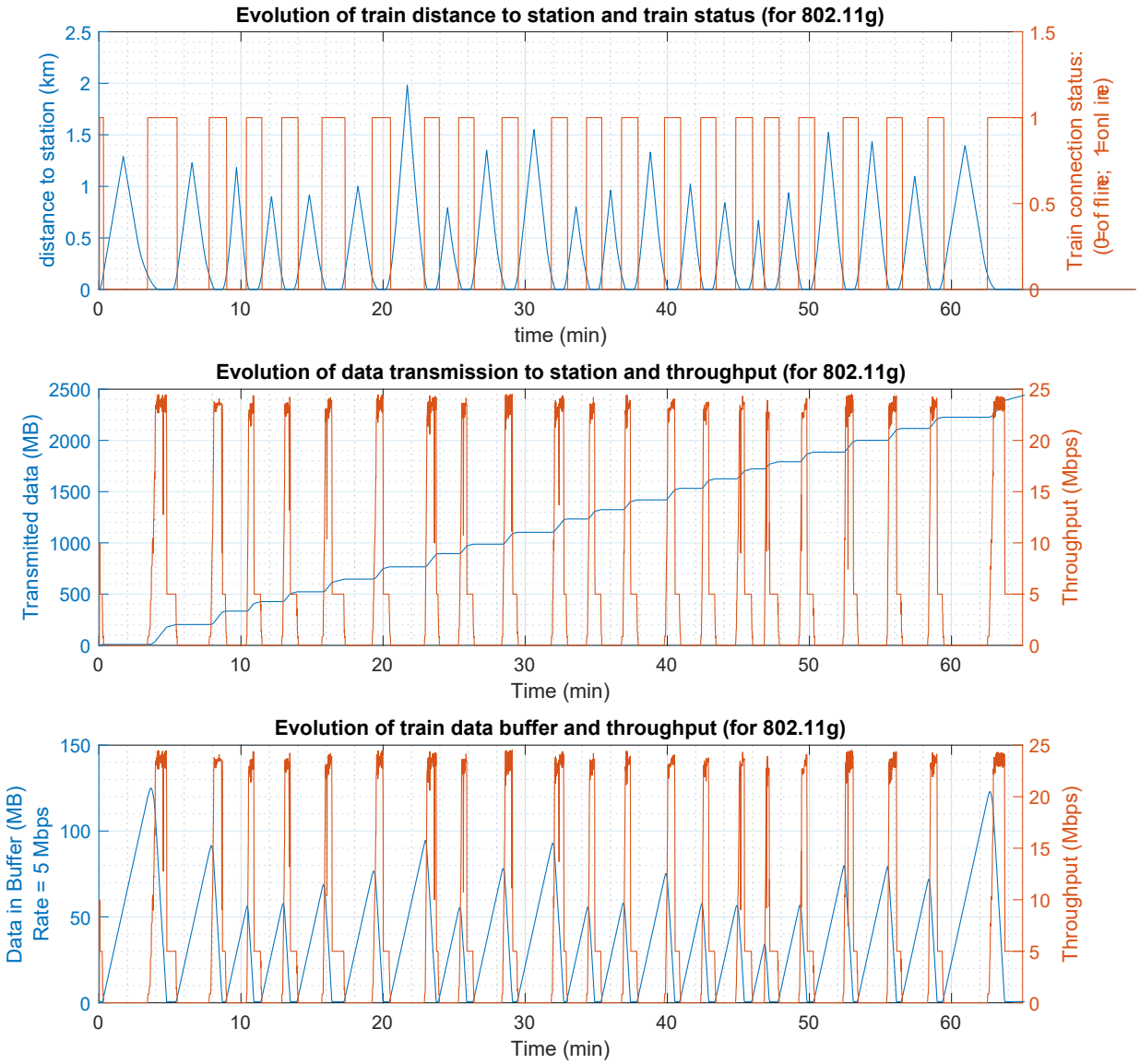

Figure F.5: Results for the case study 1.

Access Point (AP). Therefore, with the increase of the detail in energy data acquisition, the cost will remain constant, differently to the LTE-based solution. As an hypothetical example, if each GB costs € 0.5 and considering the case study 2 results, each train journey will cost € 0.09 (to transfer 180 MB). Considering the railway line in study [13], the cost to maintain all 45 daily trains and transfer 8.1 GB will be € 4.05. By extending this logic to the best case, where the train will transfer 2.5 GB in each journey, the daily cost will increase to € 56.3.

A similar example to obtain the cost of the solution proposed in this work can be discussed. Considering the cost equipment acquisition and three year operation and maintenance being, respectively, € 500 and € 250, considering the same cost for the station

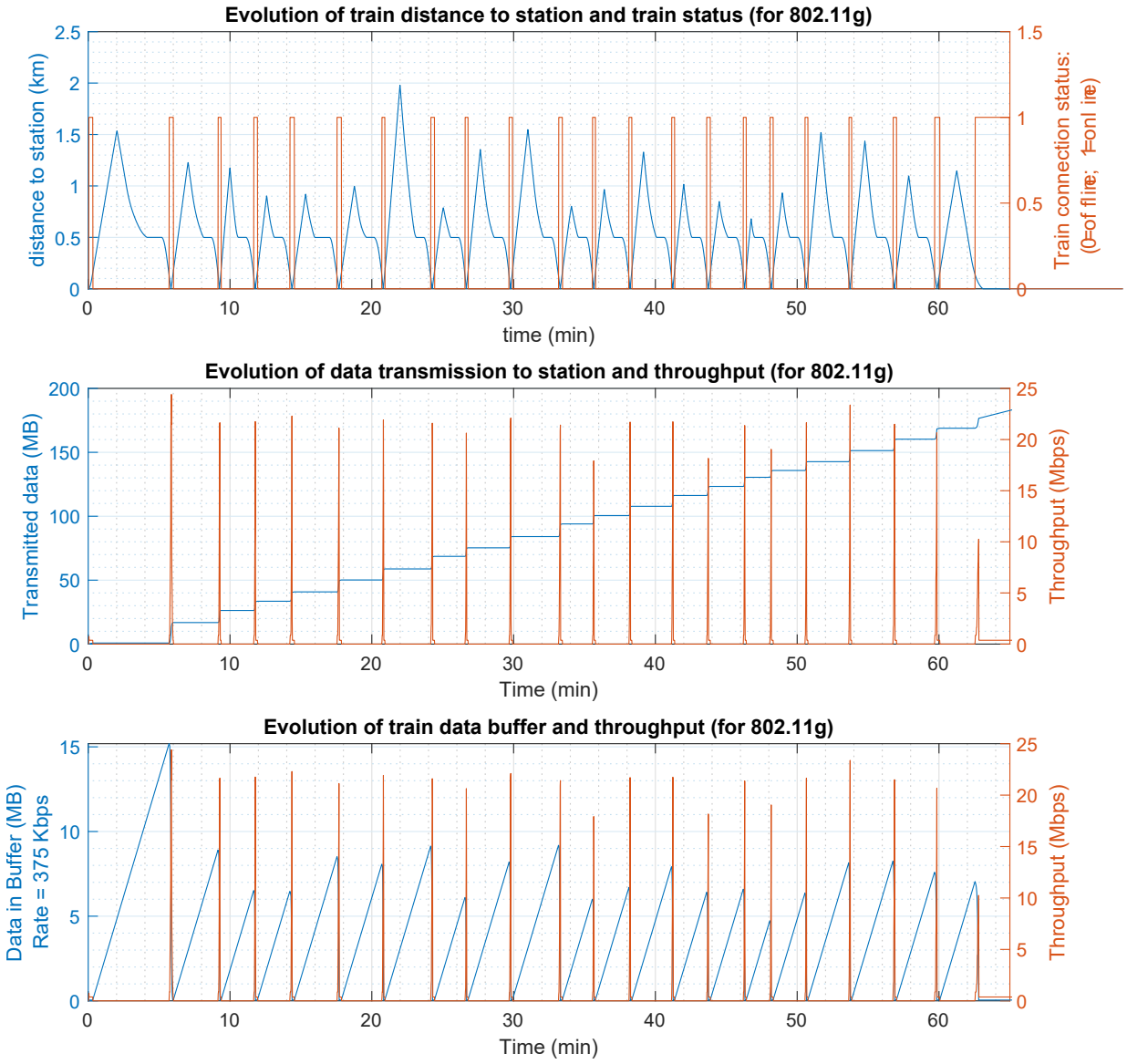

Figure F.6: Results for the case study 2.

AP and train nodes, and considering 22 station APs and 25 trains, the total cost of infrastructure will be € 35 250 (with a daily cost, for three year analysis, of € 32.2). Based on the data presented, in Fig. F.7 is illustrated a possible relation of the cost of technology for the LTE and the Wi-Fi solutions.

The crossing point value depends on the details in LTE cost and the Wi-fi infrastructure cost. From the examples previously considered, the crossing point value will be 2.9 Mbps, which leads to the conclusion that, if the train will not stop in any station, the LTE-only solution suggests to be more cost-effective. The usage of LTE + Wi-Fi is justifiable for rates higher that 2.9 Mbps.

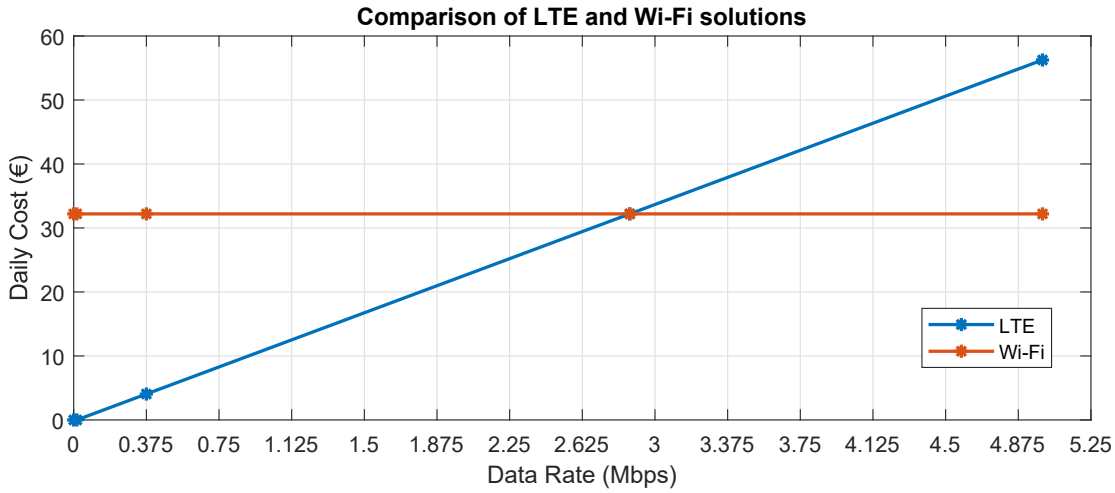

Figure F.7: Relation between the transmission cost and CEBD frequency rate.

F.5 Conclusions

In railway systems, the increase of the Compiled Energy Billing Data frequency rate results in increased detail on the knowledge that can be generated. Later on, with this expanded energy knowledge and mapping, it is possible to adjust set-points in train operations or to take measures on the infrastructure towards the increase of the energy efficiency. In addition, with this incremented knowledge, possible measures to improve the railway capacity can be evaluated. Consequently, the increase of CEBD frequency rate will result in a rise of the communication costs.

As a practical evaluation of a sub-urban railway line, in this work were considered two case studies. In the first, the train stops in every station. In the second, the train does not stop in any station. If all passenger stations are equipped with ordinary Wi-Fi access points, in the first case study, the train will be online 41 % of the journey time, which allows 5 Mbps of continuous data-rate generation, which is enough for transmitting all the data gathered during a journey. In the case where the train does not stop in any station, the train will be online only 12 % of the journey time, imposing a maximum a 375 kbps of continuous data-rate generation.

This limited work concluded that there is a threshold (throughput higher than 2.9 Mbps, in the presented cases) where the cost of the Wi-Fi solution in combination with the LTE will result in lower communication costs.

References

[1] International Energy Agency, "The Future of Rail – Opportunities for energy and the environment," *International Energy Agency*, 2019. [Online]. Available: https://www.iea.org/reports/the-future-of-rail

[2] International Energy Agency (IEA) and International Union of Railways (UIC), "Energy consumption and CO2 emissions focus on passenger rail services. International Energy Agency (IEA) and International Union of Railways (UIC)," 2017. [Online]. Available: https://uic.org/IMG/pdf/handbook_iea-uic_2017_web3.pdf

[3] Shift2Rail Joint Undertaking, "Multi-Anual Action Plan (amended version: November 2019)," Shift2Rail Joint Undertaking, Tech. Rep., 2019. [Online]. Available: https://shift2rail.org/wp-content/uploads/2020/09/MAAP-Part-A-and-B.pdf

[4] E. Pilo, S. Mazumder, and I. Franco, "Railway Electrical Smart Grids: An introduction to next-generation railway power systems and their operation," *IEEE Electrification Magazine*, vol. 2, no. 3, pp. 49–55, sep 2014, doi:10.1109/mele.2014.2338411.

[5] C. Zins, "Conceptual approaches for defining data, information, and knowledge," *Journal of the American Society for Information Science and Technology*, vol. 58, no. 4, pp. 479–493, 2007, doi:10.1002/asi.20508.

[6] Y. Duan, L. Shao, G. Hu, Z. Zhou, Q. Zou, and Z. Lin, "Specifying architecture of knowledge graph with data graph, information graph, knowledge graph and wisdom graph," in *2017 IEEE 15th International Conference on Software Engineering Research, Management and Applications (SERA)*. IEEE, jun 2017, doi:10.1109/sera.2017.7965747.

[7] CENELEC EN50463, "Railway applications - energy measurement on board trains," European Committee for Electrotechnical Standardization, Brussels, Belgium, Standard, 2012.

[8] European Commission, "Council Directive 91/440/EEC of 29 July 1991 on the development of the Community's railways," European Commission., Jul. 1991. [Online]. Available: http://data.europa.eu/eli/dir/1991/440/oj

[9] EU Agency for Railways, "Guide for the application of the energy technical specifications for interoperability," Tech. Rep., 2010. [Online]. Available: https://www.era.europa.eu/sites/default/files/activities/docs/iu_tsi_guide_annex01_inf_tsi_en.pdf

[10] M. Zasiadko, "New stage of energy measuring for European rail sector," online: https://www.railtech.com/policy/2019/10/28/new-stage-of-energy-measuring-for-european-rail-sector/ (accessed Jul 2020), Oct. 2019. [Online]. Available: https://www.railtech.com/policy/2019/10/28/new-stage-of-energy-measuring-for-european-rail-sector/?gdpr=accept

[11] B. Paltridge, "Thesis and dissertation writing: an examination of published advice and actual practice," *English for Specific Purposes*, vol. 21, no. 2, pp. 125–143, jan 2002, doi:10.1016/s0889-4906(00)00025-9.

[12] V. A. Morais, J. L. Afonso, and A. P. Martins, "Modeling and validation of the dynamics and energy consumption for train simulation," in *2018 International Conference on Intelligent Systems (IS)*. IEEE, sep 2018, doi:10.1109/is.2018.8710569.

[13] V. A. Morais, A. A. Rocha, J. L. Afonso, and A. P. Martins, "Heuristic-based speed profile generation for multi-train simulator," in *2018 International Conference on Intelligent Systems (IS)*. IEEE, sep 2018, doi:10.1109/is.2018.8710483.

[14] V. A. Morais, J. L. Afonso, A. S. Carvalho, and A. P. Martins, "New reactive power compensation strategies for railway infrastructure capacity increasing," *Energies*, vol. 13, no. 17, p. 4379, aug 2020, doi:10.3390/en13174379.

[15] V. A. Morais, J. L. Afonso, and A. P. Martins, "Towards smart railways: A charging strategy for on-board energy storage systems," in *Lecture Notes of the Institute for Computer Sciences, Social Informatics and Telecommunications Engineering*. Springer International Publishing, 2020, doi:10.1007/978-3-030-45694-8_3. pp. 33–46.

[16] V. A. Morais, J. L. Afonso, and A. P. Martins, "Towards Smart Railways: A Charging Strategy for Railway Energy Storage Systems," *EAI Endorsed Transactions on Energy Web*, vol. 18, no. 41, Jan. 2021, doi:10.4108/eai.14-1-2021.168136.

[17] A. Steimel, *Electric Traction — Motive Power and Energy Supply: Basics and Practical Experience*. Oldenbourg Industrieverlag, 2008. ISBN 9783835631328

[18] G. Abad and X. Agirre, *Power Electronics and Electric Drives for Traction Applications*, G. Abad, Ed. John Wiley & Sons, Ltd., 2016. ISBN 9781118954454

[19] B.-K. Chen and B.-S. Guo, "Three phase models of specially connected transformers," *IEEE Transactions on Power Delivery*, vol. 11, no. 1, pp. 323–330, 1996, doi:10.1109/61.484031.

[20] United States Department of Energy, "A National Vision For Electricity's Second 100 Years," Online. [Accessed Nov. 2020], 2003. [Online]. Available: http://energy.gov/sites/prod/files/oeprod/DocumentsandMedia/Electric_Vision_Document.pdf

[21] European Technology Platform: Smart Grids, "Vision and Strategy for Europe's Electricity Networks of the Future," Online. [Accessed Nov. 2020], 2006. [Online]. Available: https://ec.europa.eu/research/energy/pdf/smartgrids_en.pdf

[22] Cisco Systems, Inc., "Why Cisco And Smart Grid?" Online. [Accessed Nov. 2020], 2009. [Online]. Available: https://www.cisco.com/c/dam/en_us/about/citizenship/environment/docs/sGrid_qa_c67_532319.pdf

[23] International Electrotechnical Commission, "IEC Smart Grid Standardization Roadmap," Online. [Accessed Nov. 2020], 2009. [Online]. Available: https://www.iec.ch/smartgrid/downloads/sg3_roadmap.pdf

[24] Institute of Electrical and Electronics Engineers, "About IEEE Smart Grid," Online. [Accessed Nov. 2020], 2011. [Online]. Available: https://smartgrid.ieee.org/about-ieee-smart-grid

[25] H. Hayashiya, H. Yoshizumi, T. Suzuki, T. Furukawa, T. Kondoh, M. Kitano, T. Aoki, T. Ishii, N. Kurosawa, and T. Miyagawa, "Necessity and possibility of smart grid technology application on railway power supply system," in *Proceedings of the 2011 14th European Conference on Power Electronics and Applications*. IEEE, 2011, pp. 1–10.

[26] E. Pilo, S. K. Mazumder, and I. Gonzalez-Franco, "Smart Electrical Infrastructure for AC-Fed Railways With Neutral Zones," *IEEE Transactions on Intelligent Transportation Systems*, pp. 1–11, 2015, doi:10.1109/tits.2014.2336535.

[27] S. Nasr, M. Iordache, and M. Petit, "Smart micro-grid integration in DC railway systems," in *IEEE PES Innovative Smart Grid Technologies, Europe*. IEEE, oct 2014, doi:10.1109/isgteurope.2014.7028913.

[28] S. Nasr, "Optimization of railway network using smart-grid solutions," PhD Thesis, Université Paris Saclay (COmUE), 2016.

[29] P. Pankovits, J. Pouget, B. Robyns, F. Delhaye, and S. Brisset, "Towards railway-smartgrid: Energy management optimization for hybrid railway power substations," in *IEEE PES Innovative Smart Grid Technologies, Europe*. IEEE, oct 2014, doi:10.1109/isgteurope.2014.7028816.

[30] S. Khayyam, F. Ponci, H. Lakhdar, and A. Monti, "Agent-based energy management in railways," in *2015 International Conference on Electrical Systems for Aircraft, Railway, Ship Propulsion and Road Vehicles (ESARS)*. IEEE, mar 2015, doi:10.1109/esars.2015.7101445.

[31] S. Khayyam, F. Ponci, J. Goikoetxea, V. Recagno, V. Bagliano, and A. Monti, "Railway Energy Management System: Centralized-Decentralized Automation Architecture," *IEEE Transactions on Smart Grid*, vol. 7, no. 2, pp. 1164–1175, mar 2016, doi:10.1109/TSG.2015.2421644.

[32] Smart Grid Coordination Group, "Smart Grid Reference Architecture," CEN-CENELEC, Tech. Rep., 2012. [Online]. Available: https://ec.europa.eu/energy/sites/ener/files/documents/xpert_group1_reference_architecture.pdf

[33] I. H. Sánchez, "Application of a Smart Grid to the Spanish Electrical Railway," *Vía Libre Railway Research*, no. 11, 2016. [Online]. Available: https://www.tecnica-vialibre.es/en/ficharticulo_en.asp?item=144

[34] M. Fleck, S. Khayyam, and A. Monti, "Day-ahead optimization for railway energy management system," in *2016 International Conference on Electrical Systems for Aircraft, Railway, Ship Propulsion and Road Vehicles & International Transportation Electrification Conference (ESARS-ITEC)*. IEEE, nov 2016, doi:10.1109/esars-itec.2016.7841381.

[35] S. Khayyam, N. Berr, L. Razik, M. Fleck, F. Ponci, and A. Monti, "Railway System Energy Management Optimization Demonstrated at Offline and Online Case Studies," *IEEE Transactions on Intelligent Transportation Systems*, vol. 19, no. 11, pp. 3570–3583, nov 2018, doi:10.1109/tits.2018.2855748.

[36] L. Razik, N. Berr, S. Khayyam, F. Ponci, and A. Monti, "REM-S–Railway Energy Management in Real Rail Operation," *IEEE Transactions on Vehicular Technology*, vol. 68, no. 2, pp. 1266–1277, feb 2019, doi:10.1109/tvt.2018.2885007.

[37] D. Serrano-Jiménez, L. Abrahamsson, S. Castaño-Solís, and J. Sanz-Feito, "Electrical railway power supply systems: Current situation and future trends," *International Journal of Electrical Power & Energy Systems*, vol. 92, pp. 181–192, nov 2017, doi:10.1016/j.ijepes.2017.05.008.

[38] H. Steele, C. Roberts, and S. Hillmansen, "Railway smart grids: Drivers, benefits and challenges," *Proceedings of the Institution of Mechanical Engineers, Part F: Journal of Rail and Rapid Transit*, vol. 233, no. 5, pp. 526–536, sep 2018, doi:10.1177/0954409718800523.

[39] M. Khodaparastan, A. Mohamed, and W. Brandauer, "Recuperation of regenerative braking energy in electric rail transit systems," *IEEE Transactions on Intelligent Transportation Systems*, vol. 20, no. 8, pp. 2831–2847, aug 2019, doi:10.1109/TITS.2018.2886809.

[40] M. Brenna, V. Bucci, M. C. Falvo, F. Foiadelli, A. Ruvio, G. Sulligoi, and A. Vicenzutti, "A Review on Energy Efficiency in Three Transportation Sectors: Railways, Electrical Vehicles and Marine," *Energies*, vol. 13, no. 9, p. 2378, may 2020, doi:10.3390/en13092378.

[41] L. A. M. Barros, M. Tanta, A. P. Martins, J. L. Afonso, and J. G. Pinto, "Opportunities and Challenges of Power Electronics Systems in Future Railway Electrification," in *2020 IEEE 14th International Conference on Compatibility, Power Electronics*

and Power Engineering (CPE-POWERENG). IEEE, jul 2020, doi:10.1109/cpe-powereng48600.2020.9161695.

[42] P. Arboleya, C. Mayet, B. Mohamed, J. A. Aguado, and S. de la Torre, "A review of railway feeding infrastructures: Mathematical models for planning and operation," *eTransportation*, vol. 5, p. 100063, aug 2020, doi:10.1016/j.etran.2020.100063.

[43] H. Novak, M. Vasak, and V. Lesic, "Hierarchical energy management of multi-train railway transport system with energy storages," in *2016 IEEE International Conference on Intelligent Rail Transportation (ICIRT)*. IEEE, aug 2016, doi:10.1109/icirt.2016.7588722.

[44] H. Novak, V. Lesic, and M. Vasak, "Hierarchical coordination of trains and traction substation storages for energy cost optimization," in *2017 IEEE 20th International Conference on Intelligent Transportation Systems (ITSC)*. IEEE, oct 2017, doi:10.1109/itsc.2017.8317787.

[45] H. Novak, M. Vasak, and V. Lesic, "Hierarchical Model Predictive Control for Coordinated Electric Railway Traction System Energy Management," *IEEE Transactions on Intelligent Transportation Systems*, vol. 20, no. 7, pp. 2715–2727, 2019, doi:10.1109/tits.2018.2882087.

[46] J. A. Aguado, A. J. S. Racero, and S. de la Torre, "Optimal Operation of Electric Railways With Renewable Energy and Electric Storage Systems," *IEEE Transactions on Smart Grid*, vol. 9, no. 2, pp. 993–1001, mar 2018, doi:10.1109/tsg.2016.2574200.

[47] I. Sengor, H. C. Kilickiran, H. Akdemir, B. Kekezoglu, O. Erdinc, and J. P. S. Catalao, "Energy Management of a Smart Railway Station Considering Regenerative Braking and Stochastic Behaviour of ESS and PV Generation," *IEEE Transactions on Sustainable Energy*, vol. 9, no. 3, pp. 1041–1050, jul 2018, doi:10.1109/tste.2017.2759105.

[48] F. Ciccarelli, L. D. Noia, and R. Rizzo, "Integration of Photovoltaic Plants and Supercapacitors in Tramway Power Systems," *Energies*, vol. 11, no. 2, p. 410, feb 2018, doi:10.3390/en11020410.

[49] A. Fernández-Rodríguez, A. Fernández-Cardador, A. Cucala, and M. Falvo, "Energy Efficiency and Integration of Urban Electrical Transport Systems: EVs and Metro-Trains of Two Real European Lines," *Energies*, vol. 12, no. 3, p. 366, jan 2019, doi:10.3390/en12030366.

[50] M. Chen, Z. Cheng, Y. Liu, Y. Cheng, and Z. Tian, "Multitime-Scale Optimal Dispatch of Railway FTPSS Based on Model Predictive Control," *IEEE Transactions on Transportation Electrification*, vol. 6, no. 2, pp. 808–820, jun 2020, doi:10.1109/tte.2020.2992693.

[51] Q. Lu, Z. Gao, B. He, C. Che, and C. Wang, "Centralized-Decentralized Control for Regenerative Braking Energy Utilization and Power Quality Improvement in Modified AC-Fed Railways," *Energies*, vol. 13, no. 10, p. 2582, may 2020, doi:10.3390/en13102582.

[52] D. R. Dupré, "Improving the electrical infrastructure of dc-electrified railway systems to increase energy efficiency, taking into account complex topologies and representative traffic scenarios," PhD Thesis, Universidad Pontificia Comillas. Madrid (Spain), 2020.

[53] D. I. Fletcher, R. F. Harrison, and S. Nallaperuma, "TransEnergy – a tool for energy storage optimization, peak power and energy consumption reduction in DC electric railway systems," *Journal of Energy Storage*, vol. 30, p. 101425, aug 2020, doi:10.1016/j.est.2020.101425.

[54] A. Zahedmanesh, K. M. Muttaqi, and D. Sutanto, "A Sequential Decision-Making Process for Optimal Technoeconomic Operation of a Grid-Connected Electrical Traction Substation Integrated With Solar PV and BESS," *IEEE Transactions on Industrial Electronics*, vol. 68, no. 2, pp. 1353–1364, feb 2021, doi:10.1109/tie.2020.2969128.

[55] E. Pilo, "Diseño óptimo de la electrificación de ferrocarriles de alta velocidad," PhD Thesis, Universidad Pontificia Comillas. Madrid (Spain), 2003.

[56] H. Hu, Y. Shao, L. Tang, J. Ma, Z. He, and S. Gao, "Overview of harmonic and resonance in railway electrification systems," *IEEE Transactions on Industry Applications*, vol. 54, no. 5, pp. 5227–5245, sep 2018, doi:10.1109/tia.2018.2813967.

[57] H. Lee, C. Lee, G. Jang, and S. Kwon, "Harmonic analysis of the korean high-speed railway using the eight-port representation model," *IEEE Transactions on Power Delivery*, vol. 21, no. 2, pp. 979–986, apr 2006, doi:10.1109/tpwrd.2006.870985.

[58] P. Rodrigues, V. A. Morais, A. Martins, and A. Carvalho, "STATCOM simulation models for analysis of electrified railways," in *IECON 2019 - 45th Annual Conference of the IEEE Industrial Electronics Society*. IEEE, oct 2019, doi:10.1109/iecon.2019.8927256.

[59] S.-L. Chen, R.-J. Li, and P.-H. Hsi, "Traction system unbalance problem—analysis methodologies," *IEEE Transactions on Power Delivery*, vol. 19, no. 4, pp. 1877–1883, oct 2004, doi:10.1109/tpwrd.2004.829920.

[60] S. Xie, "Study on methods to reducing rail potential of high-speed railway," in *IECON 2006 - 32nd Annual Conference on IEEE Industrial Electronics*. IEEE, nov 2006, doi:10.1109/iecon.2006.347355.

[61] H. Lee, S. Oh, G. Kim, and C. An, "A study on the equivalent conductor representation of AC electric railway system," in *Information and Multimedia Technology, 2009. ICIMT'09. International Conference on.* IEEE, 2009, doi:10.1109/ICIMT.2009.40. pp. 33–37.

[62] J. de Dios Sanz-Bobi, J. Garzon-Nunez, R. Loiero, and J. Felez, "Electrical Disturbances from High Speed Railway Environment to Existing Services," in *Electrical Generation and Distribution Systems and Power Quality Disturbances.* InTech, nov 2011.

[63] I. Abdulaziz, "Mathematical modelling and computer simulations of induced voltage calculations in AC electric traction." phdthesis, Edinburgh Napier University, Apr. 2003.

[64] J. Jimenez-Octavio, E. Pilo, O. Lopez-Garcia, and A. Carnicero, "Coupled electromechanical cost optimization of high speed railway overheads," in *ASME/IEEE 2006 Joint Rail Conference.* American Society of Mechanical Engineers, 2006, doi:10.1109/RRCON.2006.215314. pp. 231–240.

[65] E. Pilo, L. Rouco, and A. Fernández, "Catenary and autotransformer coupled optimization for 2x25kv systems planning," in *Power Supply, Energy Management and Catenary Problems.* WIT Press, mar 2010, pp. 113–122.

[66] C. J. Goodman and T. Kulworawanichpong, "Sequential Linear Power Flow Solution For AC Electric Railway Power Supply Systems," *WIT Transactions on the Built Environment*, vol. 61, p. 10, 2002.

[67] S. V. Raygani, A. Tahavorgar, S. S. Fazel, and B. Moaveni, "Load flow analysis and future development study for an AC electric railway," *IET Electrical Systems in Transportation*, vol. 2, no. 3, pp. 139–147, 2012, doi:10.1049/iet-est.2011.0052.

[68] J. Zhang, M. Wu, and Q. Liu, "A novel power flow algorithm for traction power supply systems based on the thévenin equivalent," *Energies*, vol. 11, no. 1, p. 126, jan 2018, doi:10.3390/en11010126.

[69] R. D. Zimmerman, C. E. Murillo-Sanchez, and R. J. Thomas, "MATPOWER: Steady-State Operations, Planning, and Analysis Tools for Power Systems Research and Education," *IEEE Transactions on Power Systems*, vol. 26, no. 1, pp. 12–19, feb 2011, doi:10.1109/tpwrs.2010.2051168.

[70] R. D. Zimmerman and C. E. Murillo-Sánchez, "Matpower user's manual," 2019, doi:10.5281/ZENODO.3251118.

[71] C. Cole, *Handbook of railway vehicle dynamics - Chapter 9*, Taylor and F. Group, Eds. CRC press, 2006.

[72] Q. Wu, M. Spiryagin, and C. Cole, "Longitudinal train dynamics: an overview," *Vehicle System Dynamics*, vol. 54, no. 12, pp. 1688–1714, sep 2016, doi:10.1080/00423114.2016.1228988.

[73] C. Cole, M. Spiryagin, Q. Wu, and Y. Q. Sun, "Modelling, simulation and applications of longitudinal train dynamics," *Vehicle System Dynamics*, vol. 55, no. 10, pp. 1498–1571, jun 2017, doi:10.1080/00423114.2017.1330484.

[74] Q. Wu, B. Wang, M. Spiryagin, and C. Cole, "Curving resistance from wheel-rail interface," *Vehicle System Dynamics*, pp. 1–19, nov 2020, doi:10.1080/00423114.2020.1843689.

[75] R. Conti, E. Galardi, E. Meli, D. Nocciolini, L. Pugi, and A. Rindi, "Energy and wear optimisation of train longitudinal dynamics and of traction and braking systems," *Vehicle System Dynamics*, vol. 53, no. 5, pp. 651–671, jan 2015, doi:10.1080/00423114.2014.990466.

[76] P.-H. Hsi and S.-L. Chen, "Electric load estimation techniques for high-speed railway (hsr) traction power systems," *IEEE transactions on vehicular technology*, vol. 50, no. 5, pp. 1260–1266, 2001, doi:10.1109/25.950327.

[77] G. M. Scheepmaker, R. M. Goverde, and L. G. Kroon, "Review of energy-efficient train control and timetabling," *European Journal of Operational Research*, vol. 257, no. 2, pp. 355–376, 2017, doi:10.1016/j.ejor.2016.09.044.

[78] R. E. Kopp, "Pontryagin maximum principle," in *Mathematics in Science and Engineering*. Elsevier, 1962, vol. 5, pp. 255–279.

[79] L. S. Pontryagin, *Mathematical theory of optimal processes*, Taylor and F. Group, Eds. Routledge, 2018.

[80] I. P. Milroy, "Aspects of automatic train control," Ph.D. dissertation, Loughborough University, 1980. [Online]. Available: https://repository.lboro.ac.uk/articles/thesis/Aspects_of_automatic_train_control/9537395

[81] P. G. Howlett and P. J. Pudney, *Energy-Efficient Train Control*. Springer London, 1995.

[82] R. R. Liu and I. M. Golovitcher, "Energy-efficient operation of rail vehicles," *Transportation Research Part A: Policy and Practice*, vol. 37, no. 10, pp. 917 – 932, 2003, doi:https://doi.org/10.1016/j.tra.2003.07.001.

[83] M. Dominguez, A. Fernandez-Cardador, A. P. Cucala, and R. R. Pecharroman, "Energy savings in metropolitan railway substations through regenerative energy recovery and optimal design of ATO speed profiles," *IEEE Transactions on Automation Science and Engineering*, vol. 9, no. 3, pp. 496–504, jul 2012, doi:10.1109/tase.2012.2201148.

[84] M. Domínguez, A. Fernández, A. P. Cucala, and P. Lukaszewicz, "Optimal design of metro automatic train operation speed profiles for reducing energy consumption," *Proceedings of the Institution of Mechanical Engineers, Part F: Journal of Rail and Rapid Transit*, vol. 225, no. 5, pp. 463–474, aug 2011, doi:10.1177/09544097jrrt420.

[85] C. Chang and S. Sim, "Optimising train movements through coast control using genetic algorithms," *IEE Proceedings-Electric Power Applications*, vol. 144, no. 1, pp. 65–73, 1997, doi:10.1049/ip-epa:19970797.

[86] S. Lechelle and Z. Mouneimne, "Optidrive: a practical approach for the calculation of energy-optimised operating speed profiles," *Rail traction Systems (RTS 2010), IET Conference on*, 2010, doi:10.1049/ic.2010.0029.

[87] C. M. Sicre Vara del Rey, M. A. Cucala García, and A. Fernández Cardador, "Real time regulation of efficient driving of high speed trains based on a genetic algorithm and a fuzzy model of manual driving," *Engineering Applications of Artificial Intelligence*, pp. 79–92, 2014, doi:10.1016/j.engappai.2013.07.015.

[88] S. Lu, S. Hillmansen, T. K. Ho, and C. Roberts, "Single-train trajectory optimization," *IEEE Transactions on Intelligent Transportation Systems*, vol. 14, no. 2, pp. 743–750, 2013, doi:10.1109/TITS.2012.2234118.

[89] R. Chevrier, P. Pellegrini, and J. Rodriguez, "Energy saving in railway timetabling: A bi-objective evolutionary approach for computing alternative running times," *Transportation Research Part C: Emerging Technologies*, vol. 37, pp. 20–41, 2013, doi:10.1016/j.trc.2013.09.007.

[90] K. Keskin and A. Karamancioglu, "Application of firefly algorithm to train operation," in *2016 IEEE 8th International Conference on Intelligent Systems (IS)*, Sept 2016, doi:10.1109/IS.2016.7737386. pp. 692–697.

[91] C. Goodman, L. K. Siu, and T. K. Ho, "A review of simulation models for railway systems," in *Proc. of International Conference on Developments in Mass Transit Systems, 20 - 23 April 1998.* IEE, 1998, doi:10.1049/cp:19980101.

[92] B. Mellitt, C. J. Goodman, and R. I. M. Arthurton, "Simulator for studying operational and power-supply conditions in rapid-transit railways," in *Proceedings of the Institution of Electrical Engineers*, vol. 125, no. 4, 1978, doi:10.1049/piee.1978.0075. pp. 298–303.

[93] Z. Tian, "System Energy Optimisation Strategies for DC Railway Traction Power Networks," phdthesis, University of Birmingham, 2017.

[94] SNCF Réseau, "Appendix 6.1.3 — Principles for the Charges Related to the Use of Electric Traction," Network Statement 2020 Timetable, Sep. 2018. [Online]. Available: https://www.sncf-reseau.com/sites/default/files/drr_horaires/drr_2020/en/DRR2020-appendix6.1.3.pdf

[95] A. Nash and D. Huerlimann, "Railroad simulation using opentrack," in *Proc. of the Int. Conf. on Computers in Railways, COMPRAIL'IX, May 2004*.

[96] A. Stephan, "Openpowernet – simulation of railway power supply systems," in *Proc of the Int. Conf. on Computer System Design and Operation in the Railway and Other Transit Systems, COMPRAIL 2008*, doi:10.2495/CR080441.

[97] Siemens AG, "System design with Sitras Sidytrac and Sitras EMF — Simulation of AC and DC traction power supply," 2016. [Online]. Available: https://www.downloads.siemens.com/download-center/download?DLA14_74

[98] R. A. Uher, *Program Manual for the Train Operations Model / Rail Systems Center*, 3rd ed., Rail Systems Center, Sep. 2020. [Online]. Available: http://www.railsystemscenter.com/TOM-MAN.pdf

[99] T. Kulworawanichpong, "Multi-train modeling and simulation integrated with traction power supply solver using simplified newton–raphson method," *Journal of Modern Transportation*, vol. 23, no. 4, pp. 241–251, oct 2015, doi:10.1007/s40534-015-0086-y.

[100] C. Roberts, "Talk at Portugal Railway Summit 2021: Railway Activities at the University of Birmingham and UK Railway Research and Innovation Network (UKRRIN)," Feb. 2021, video: youtu.be/pDmuPMTEZMo?t=24867. [Online]. Available: https://www.ferrovia2021.eventovirtual.pt/

[101] T. Kulworawanichpong, "Optimizing AC electric railway power flows with power electronic control," Ph.D. dissertation, University of Birmingham, 2003.

[102] M. Abril, F. Barber, L. Ingolotti, M. Salido, P. Tormos, and A. Lova, "An assessment of railway capacity," *Transportation Research Part E: Logistics and Transportation Review*, vol. 44, no. 5, pp. 774–806, sep 2008, doi:10.1016/j.tre.2007.04.001.

[103] J. Geischberger and M. Moesters, "Impact of faster freight trains on railway capacity and operational quality," *International Journal of Transport Development and Integration*, vol. 4, no. 3, pp. 274–285, jul 2020, doi:10.2495/tdi-v4-n3-274-285.

[104] M. Aeberhard, C. Courtois, and P. Ladoux, "Railway traction power supply from the state of the art to future trends," in *SPEEDAM 2010*. IEEE, jun 2010, doi:10.1109/speedam.2010.5542093.

[105] A. T. Langerudy, A. Mariscotti, and M. A. Abolhassani, "Power Quality Conditioning in Railway Electrification: A Comparative Study," *IEEE Transactions on Vehicular Technology*, vol. 66, no. 8, pp. 6653–6662, Aug. 2017, doi:10.1109/TVT.2017.2661820.

[106] M. Tanta, J. G. Pinto, V. Monteiro, A. P. Martins, A. S. Carvalho, and J. L. Afonso, "Topologies and Operation Modes of Rail Power Conditioners in AC Traction Grids: Review and Comprehensive Comparison," *Energies*, vol. 13, no. 9, p. 2151, may 2020, doi:10.3390/en13092151.

[107] A. Luo, C. Wu, J. Shen, Z. Shuai, and F. Ma, "Railway static power conditioners for high-speed train traction power supply systems using three-phase V/V transformers," *IEEE Transactions on Power Electronics*, vol. 26, no. 10, pp. 2844–2856, 2011, doi:10.1109/TPEL.2011.2128888.

[108] N. Dai, M. Wong, K. Lao, and C. Wong, "Modelling and control of a railway power conditioner in co-phase traction power system under partial compensation," *IET Power Electronics*, vol. 7, no. 5, pp. 1044–1054, May 2014, doi:10.1049/iet-pel.2013.0396.

[109] Z. Sun, X. Jiang, D. Zhu, and G. Zhang, "A novel active power quality compensator topology for electrified railway," *IEEE Transactions on power electronics*, vol. 19, no. 4, pp. 1036–1042, 2004, doi:10.1109/TPEL.2004.830032.

[110] K. Lao, N. Dai, W. Liu, and M. Wong, "Hybrid Power Quality Compensator With Minimum DC Operation Voltage Design for High-Speed Traction Power Systems," *IEEE Transactions on Power Electronics*, vol. 28, no. 4, pp. 2024–2036, 2013, doi:10.1109/TPEL.2012.2200909.

[111] K. Lao, M. Wong, N. Y. Dai, C. Wong, and C. Lam, "Analysis of DC-Link Operation Voltage of a Hybrid Railway Power Quality Conditioner and Its PQ Compensation Capability in High-Speed Cophase Traction Power Supply," *IEEE Transactions on Power Electronics*, vol. 31, no. 2, pp. 1643–1656, Feb. 2016, doi:10.1109/TPEL.2015.2417356.

[112] M. Tanta, J. G. Pinto, V. Monteiro, A. P. Martins, A. S. Carvalho, and J. L. Afonso, "Deadbeat Predictive Current Control for Circulating Currents Reduction in a Modular Multilevel Converter Based Rail Power Conditioner," *Applied Sciences*, vol. 10, no. 5, p. 1849, mar 2020, doi:10.3390/app10051849.

[113] International Electrotechnical Commission, "IEC 60850: "Railway Applications — Supply Voltages of Traction Systems"," International Electrotechnical Commission (IEC), 2007.

[114] G. Celli, F. Pilo, and S. B. Tennakoon, "Voltage regulation on 25 kV AC railway systems by using thyristor switched capacitor," in *Proc. (Cat. No.00EX441) Ninth Int Conf. Harmonics and Quality of Power*, vol. 2, Oct. 2000, doi:10.1109/ICHQP.2000.897752. pp. 633–638 vol.2.

[115] P.-C. Tan, P. C. Loh, and D. G. Holmes, "A Robust Multilevel Hybrid Compensation System for 25-kV Electrified Railway Applications," *IEEE Transactions on Power Electronics*, vol. 19, no. 4, pp. 1043–1052, jul 2004, doi:10.1109/tpel.2004.830038.

[116] M. Fracchia, C. Courtois, A. Talibart, P. Bordignon, T. Consani, E. Merli, S. Bacha, M. Stuart, K. Zoeter, G. G. Burrarini, and M. Renglet, "High voltage booster for railway applications," in *World Congress on Railway Research.*, 2001, [Online]. [Online]. Available: http://www.railway-research.org/IMG/pdf/278.pdf

[117] L. Zanotto, R. Piovan, V. Toigo, E. Gaio, P. Bordignon, T. Consani, and M. Fracchia, "Filter Design for Harmonic Reduction in High-Voltage Booster for Railway Applications," *IEEE Transactions on Power Delivery*, vol. 20, no. 1, pp. 258–263, jan 2005, doi:10.1109/tpwrd.2004.835054.

[118] S. V. Raygani, B. Moaveni, S. S. Fazel, and A. Tahavorgar, "SVC implementation using neural networks for an AC electrical railway," *WSEAS Transactions on Circuits and Systems*, vol. 10, no. 5, pp. 173–183, 2011.

[119] T. Kulworawanichpong and C. J. Goodman, "Optimal area control of AC railway systems via PWM traction drives," *IEE Proceedings - Electric Power Applications*, vol. 152, no. 1, pp. 33–70, 2005, doi:10.1049/ip-epa:20040979.

[120] A. Tahavorgar, S. V. Raygani, and S. Fazel, "Power quality improvement at the point of common coupling using on-board PWM drives in an electrical railway network," in *2010 1st Power Electronic & Drive Systems & Technologies Conference (PEDSTC)*, IEEE. IEEE, 2010, doi:10.1109/PEDSTC.2010.5471781. pp. 412–417.

[121] J. Han and K. Zhou, "Interference research and analysis of LTE-R," in *2013 5th IEEE International Symposium on Microwave, Antenna, Propagation and EMC Technologies for Wireless Communications*. IEEE, oct 2013, doi:10.1109/mape.2013.6689858.

[122] R. He, B. Ai, G. Wang, K. Guan, Z. Zhong, A. F. Molisch, C. Briso-Rodriguez, and C. P. Oestges, "High-Speed Railway Communications: From GSM-R to LTE-R," *IEEE Vehicular Technology Magazine*, vol. 11, no. 3, pp. 49–58, sep 2016, doi:10.1109/mvt.2016.2564446.

[123] M. Sneps-Sneppe and D. Namiot, "Digital railway and how to move from GSM-r to LTE-r and 5g," in *Convergent Cognitive Information Technologies*. Springer International Publishing, 2020, pp. 392–402.

[124] V. Gelman, "Energy storage that may be too good to be true: Comparison between wayside storage and reversible thyristor controlled rectifiers for heavy rail," *IEEE Vehicular Technology Magazine*, vol. 8, no. 4, pp. 70–80, dec 2013, doi:10.1109/mvt.2013.2283350.

[125] P. Arboleya, I. El-Sayed, B. Mohamed, and C. Mayet, "Modeling, simulationand analysis of on-board hybrid energy storage systems for railway applications," *Energies*, vol. 12, no. 11, p. 2199, jun 2019, doi:10.3390/en12112199.

[126] N. Ghaviha, J. Campillo, M. Bohlin, and E. Dahlquist, "Review of application of energy storage devices in railway transportation," *Energy Procedia*, vol. 105, pp. 4561–4568, may 2017, doi:10.1016/j.egypro.2017.03.980.

[127] V. Gelman, "Braking energy recuperation," *IEEE Vehicular Technology Magazine*, vol. 4, no. 3, pp. 82–89, sep 2009, doi:10.1109/mvt.2009.933480.

[128] P. Arboleya, P. Bidaguren, and U. Armendariz, "Energy is on board: Energy storage and other alternatives in modern light railways," *IEEE Electrification Magazine*, vol. 4, no. 3, pp. 30–41, sep 2016, doi:10.1109/mele.2016.2584938.

[129] Y. Zheng, J. Zhao, Y. Song, F. Luo, K. Meng, J. Qiu, and D. J. Hill, "Optimal operation of battery energy storage system considering distribution system uncertainty," *IEEE Transactions on Sustainable Energy*, vol. 9, no. 3, pp. 1051–1060, jul 2017, doi:10.1109/TSTE.2017.2762364.

[130] S. Leonori, E. D. Santis, A. Rizzi, and F. M. F. Mascioli, "Multi objective optimization of a fuzzy logic controller for energy management in microgrids," in *2016 IEEE Congress on Evolutionary Computation (CEC)*. IEEE, jul 2016, doi:10.1109/cec.2016.7743811.

[131] E. D. Santis, A. Rizzi, A. Sadeghiany, and F. M. F. Mascioli, "Genetic optimization of a fuzzy control system for energy flow management in micro-grids," in *2013 Joint IFSA World Congress and NAFIPS Annual Meeting (IFSA/NAFIPS)*. IEEE, jun 2013, doi:10.1109/ifsa-nafips.2013.6608437.

[132] S. Leonori, M. Paschero, A. Rizzi, and F. M. F. Mascioli, "An optimized microgrid energy management system based on FIS-MO-GA paradigm," in *2017 IEEE International Conference on Fuzzy Systems (FUZZ-IEEE)*. IEEE, jul 2017, doi:10.1109/fuzz-ieee.2017.8015438.

[133] M. R. Akbarzadeh-T and A. H. Meghdadi, *Evolutionary fuzzy systems. In Intelligent Control Systems Using Soft Computing Methodologies. 434-461.*, A. Zilouchian and M. Jamshidi, Eds. CRC Press LLC, 2001.

[134] A. Kropp and R. Torre, "Docker: containerize your application," in *Computing in Communication Networks*, F. Fitzek, F. Granelli, and P. Seeling, Eds. Elsevier, 2020, ch. 12, pp. 231–244.

[135] M. Reta-Hernández, *"Transmission Line Parameters", in "Electric Power Generation, Transmission, and Distribution"*, 2nd ed., L. Grigsby, Ed. CRC Press, 2007.

[136] E. Pilo, L. Rouco, and A. Fernández-Cardador, "A reduced representation of 2x25 kV electrical systems for high-speed railways." in *Proceedings of the 2003 IEEE/ASME Joint Rail Conference*, 2003, doi:10.1109/RRCON.2003.1204665.

[137] J. Holtz and J. O. Krah, "On-line identification of the resonance conditions in the overhead supply line of electric railways," *Archiv für Elektrotechnik*, vol. 74, no. 1, pp. 99–106, jan 1990, doi:10.1007/bf01573236.

[138] M. Brenna, F. Foiadelli, and D. Zaninelli, *Electrical Railway Transportation Systems*, John Wiley & Sons, Ed. IEEE Press Series on Power Engineering, 2018.

[139] J. R. Carson, "Wave Propagation in Overhead Wires with Ground Return," *Bell System Technical Journal*, vol. 5, no. 4, pp. 539–554, oct 1926, doi:10.1002/j.1538-7305.1926.tb00122.x.

[140] C. Alexander and M. Sadiku, "Chapter 13: Magnetically Coupled Circuits," in *Fundamentals of Electric Circuits*, fifth edition ed. The McGraw-Hill Companies, Inc., 2013, pp. 555–563. ISBN 978-0-07-338057-5

[141] R. Cella, G. Giangaspero, A. Mariscotti, A. Montepagano, P. Pozzobon, M. Ruscelli, and M. Vanti, "Measurement of AT Electric Railway System Currents at Power-Supply Frequency and Validation of a Multiconductor Transmission-Line Model," *IEEE Transactions on Power Delivery*, vol. 21, no. 3, pp. 1721–1726, jul 2006, doi:10.1109/tpwrd.2006.874109.

[142] A. Mariscotti, P. Pozzobon, and M. Vanti, "Distribution of the traction return current in AT electric railway systems," *IEEE Transactions on Power Delivery*, vol. 20, no. 3, pp. 2119–2128, jul 2005, doi:10.1109/tpwrd.2005.848721.

[143] H. Klein, "Entstehung, ausbreitung und wirkung der störströme von pulsstromrichtern auf bahnfahrzeugen mit wechselspannungseinspeisung," doctoralthesis, Wuppertal, 1987, phD dissertation. [Online]. Available: https://books.google.pt/books?id=Dp_xtgAACAAJ

[144] K. Würflinger, "Aktive bedämpfung von niederfrequenten störströmen in bahnstromnetzen mittels der umrichterregelung," doctoralthesis, Ruhr-Universität Bochum, Universitätsbibliothek, 2007, phD dissertation. pp: 124.

[145] A. Cecen, "Multivariate Polynomial Regression," GitHub: ahmetcecen/MultiPolyRegress-MatlabCentral, 2020.

[146] A. Agrawal, P. D. Deshpande, A. Cecen, G. P. Basavarsu, A. N. Choudhary, and S. R. Kalidindi, "Exploration of data science techniques to predict fatigue strength of steel from composition and processing parameters," *Integrating Materials and Manufacturing Innovation*, vol. 3, no. 1, pp. 90–108, apr 2014, doi:10.1186/2193-9772-3-8.

[147] A. Cecen, H. Dai, Y. C. Yabansu, S. R. Kalidindi, and L. Song, "Material structure-property linkages using three-dimensional convolutional neural networks," *Acta Materialia*, vol. 146, pp. 76–84, mar 2018, doi:10.1016/j.actamat.2017.11.053.

[148] P. Howlett, "The optimal control of a train," *Annals of Operations Research*, vol. 98, no. 1, pp. 65–87, Dec 2000, doi:10.1023/A:1019235819716.

[149] CENELEC EN 50463-2, "Railway applications - energy measurement on board trains," 2017.

[150] A. L. López, R. Pecharromán, E. Pilo, A. Cucala, and A. Fernández-Cardador, "Analysis of energy-saving strategies in railway power supply systems," in *9th World Congress on Railway Research-WCRR*, 2011, pp. 22–26.

[151] D. Roch-Dupré, A. P. Cucala, R. R. Pecharromán, Á. J. López-López, and A. Fernández-Cardador, "Simulation-based assessment of the installation of a reversible substation in a railway line, including a realistic model of large traffic perturbations," *International Journal of Electrical Power & Energy Systems*, vol. 115, p. 105476, feb 2020, doi:10.1016/j.ijepes.2019.105476.

[152] C. Anjos, *A catenaria e as outras instalações fixas de tracção elétrica*. Ferbritas, Empreendimentos Indústrias e Comerciais, 2007. ISBN 978-989-20-0534-8

[153] H. Pouryousef and P. Lautala, "Hybrid simulation approach for improving railway capacity and train schedules," *Journal of Rail Transport Planning & Management*, vol. 5, no. 4, pp. 211–224, dec 2015, doi:10.1016/j.jrtpm.2015.10.001.

[154] S. Bruni, G. Bucca, A. Collina, and A. Facchinetti, *Dynamics of the Pantograph Catenary System, In Handbook of Railway Vehicle Dynamics*, S. Iwnicki, M. Spiryagin, C. Cole, and T. McSweeney, Eds. CRC Press, nov 2019.

[155] Y. Song, Z. Liu, A. Rxnnquist, P. Navik, and Z. Liu, "Contact Wire Irregularity Stochastics and Effect on High-speed Railway Pantograph-Catenary Interactions," *IEEE Transactions on Instrumentation and Measurement*, pp. 1–1, 2020, doi:10.1109/tim.2020.2987457.

[156] Z. Wang, Y. Cheng, G. Mei, W. Zhang, G. Huang, and Z. Yin, "Torsional vibration analysis of the gear transmission system of high-speed trains with wheel defects," *Proceedings of the Institution of Mechanical Engineers, Part F: Journal of Rail and Rapid Transit*, vol. 234, no. 2, pp. 123–133, mar 2019, doi:10.1177/0954409719833791.

[157] CENELEC EN 50388-1, "Railway Applications – Fixed Installations and Rolling Stock – Technical Criteria for the Coordination between Traction Power Supply and Rolling Stock to Achieve Interoperability – Part 1: General," 2007.

[158] A. Mariscotti, "Impact of Harmonic Power Terms on the Energy Measurement in AC Railways," *IEEE Transactions on Instrumentation and Measurement*, pp. 6731–6738, 2020, doi:10.1109/tim.2020.2992167.

[159] Y. Xu, "Latency and Bandwidth Analysis of LTE for a Smart Grid," Master's thesis, KTH Royal Institute of Technology, 2011, pp: 22. [Online]. Available: http://www.diva-portal.org/smash/get/diva2:472305/FULLTEXT01.pdf

[160] H. Ibaiondo and A. Romo, "Kinetic energy recovery on railway systems with feedback to the grid," in *Proceedings of 14th International Power Electronics and Motion Control Conference EPE-PEMC 2010*. IEEE, sep 2010, doi:10.1109/epepemc.2010.5606545.

[161] F. Zhu, Z. Yang, F. Lin, and Y. Xin, "Decentralized Cooperative Control of Multiple Energy Storage Systems in Urban Railway Based on Multiagent Deep Reinforcement Learning," *IEEE Transactions on Power Electronics*, vol. 35, no. 9, pp. 9368–9379, sep 2020, doi:10.1109/tpel.2020.2971637.

[162] E. H. Mamdani and S. Assilian, "An experiment in linguistic synthesis with a fuzzy logic controller," *International Journal of Man-Machine Studies*, vol. 7, pp. 1–13, 1975, doi:10.1016/s0020-7373(75)80002-2.

[163] V. A. Morais, J. L. Afonso, and A. P. Martins, "Innovative communication system for railways smart metering towards system efficiency improvement," in *Proceedings of the 4th International Conference on Energy and Environment: bringing together Engineering and Economics*, 2019, pp. 191–196.

[164] B. Ai, C. Briso-Rodriguez, X. Cheng, T. Kurner, Z.-D. Zhong, K. Guan, R.-S. He, L. Xiong, D. W. Matolak, and D. G. Michelson, "Challenges toward wireless communications for high-speed railway," *IEEE Transactions on Intelligent Transportation Systems*, vol. 15, no. 5, pp. 2143–2158, oct 2014, doi:10.1109/tits.2014.2310771.

[165] T. Zhou, C. Tao, S. Salous, and L. Liu, "Geometry-based multi-link channel modeling for high-speed train communication networks," *IEEE Transactions on Intelligent Transportation Systems*, vol. 21, no. 3, pp. 1229–1238, mar 2020, doi:10.1109/tits.2019.2905036.

[166] J. Foust, "SpaceX's space-internet woes: Despite technical glitches, the company plans to launch the first of nearly 12,000 satellites in 2019," *IEEE Spectrum*, vol. 56, no. 1, pp. 50–51, jan 2019, doi:10.1109/mspec.2019.8594798.

[167] Z. Tang, H. Yin, C. Yang, J. Yu, and H. Guo, "Predicting the electricity consumption of urban rail transit based on binary nonlinear fitting regression and support vector regression," *Sustainable Cities and Society*, vol. 66, p. 102690, mar 2021, doi:10.1016/j.scs.2020.102690.

[168] M. Centra, "Hourly Electricity Load Forecasting: An Empirical Application To The Italian Railways," *World Academy of Science, Engineering and Technology*, 2011, doi:10.5281/ZENODO.1082583.

[169] MATLAB, *version 9.4.0 (R2018a)*. Natick, Massachusetts: The MathWorks Inc., 2018.

[170] S. Golestan, J. M. Guerrero, and J. C. Vasquez, "Three-phase plls: A review of recent advances," *IEEE Transactions on Power Electronics*, vol. 32, no. 3, pp. 1894–1907, March 2017, doi:10.1109/TPEL.2016.2565642.

[171] R. Teodorescu, F. Blaabjerg, M. Liserre, and P. C. Loh, "Proportional-resonant controllers and filters for grid-connected voltage-source converters," *IEE Proceedings - Electric Power Applications*, vol. 153, no. 5, pp. 750–762, Sep. 2006, doi:10.1049/ip-epa:20060008.

[172] A. Gatti and A. Ghelardini, "The European Energy Measurement System on board of trains," in *Procedings of World Congres on Railway Research*, 2011.

[173] A. Bertout and E. Bernard, "Next generation of railways and metros wireless communication systems," *ASPECT, Institution of Railways Signal Engineers*, 2012.

[174] K. Weiland, "Electric traction energy metering on German Railways and the impact of European standardisation on the energy billing process in Germany," in *Power Supply, Energy Management and Catenary Problems*. WIT Press, mar 2010, pp. 95–100. [Online]. Available: https://www.witpress.com/elibrary/wit-transactions-on-the-built-environment/74/12118

[175] P. Hsu, "WLAN: the future for railway communications networks," May 2011.

[176] S. Banerjee, M. Hempel, and H. Sharif, "A Survey of Wireless Communication Technologies & Their Performance for High Speed Railways," *Journal of Transportation Technologies*, vol. 06, no. 01, pp. 15–29, 2016, doi:10.4236/jtts.2016.61003.

[177] A. Gopalasingham, Q. P. Van, L. Roullet, C. S. Chen, E. Renault, L. Natarianni, S. D. Marchi, and E. Hamman, "Software-Defined mobile backhaul for future Train to ground Communication services," in *2016 9th IFIP Wireless and Mobile Networking Conference (WMNC)*. IEEE, jul 2016, doi:10.1109/wmnc.2016.7543984.

[178] T. S. Rappaport, Y. Xing, G. R. MacCartney, A. F. Molisch, E. Mellios, and J. Zhang, "Overview of Millimeter Wave Communications for Fifth-Generation (5G) Wireless Networks—With a Focus on Propagation Models," *IEEE Transactions on Antennas and Propagation*, vol. 65, no. 12, pp. 6213–6230, dec 2017, doi:10.1109/tap.2017.2734243.

[179] A. Homay, M. de Sousa, L. Almeida, A. Martins, and E. Oliveira, "Multi-agent Based Uncoordinated Channel Hopping in the IEEE 802.15.4e," in *Advances in Intelligent Systems and Computing*. Springer International Publishing, jul 2017, pp. 287–296.

[180] F. Flammini, S. Marrone, R. Nardone, A. Petrillo, S. Santini, and V. Vittorini, "Towards Railway Virtual Coupling," *Proc. of the 5th International Conference on Electrical Systems for Aircraft, Railway, Ship Propulsion and Road Vehicles (ESARS) and International Transportation Electrification Conference (ITEC), Nottingham, UK,*, 2018, doi:10.1109/ESARS-ITEC.2018.8607523.

[181] A. Dandoush, A. Tuholukova, S. Alouf, G. Neglia, S. Simoens, P. Derouet, and P. Dersin, "ns-3 Based Framework for Simulating Communication Based Train Control (CBTC) Systems," in *Proceedings of the Workshop on ns-3 - WNS3 2016*. ACM Press, 2016, doi:10.1145/2915371.2915378.